Dual-Responsive Polymer and Hybrid Systems: Applications for Gene Delivery and Hydrogels

DISSERTATION

zur Erlangung des akademischen Grades eines

Doktors der Naturwissenschaften (Dr. rer. nat.)

an der Bayreuther Graduiertenschule für Mathematik und

Naturwissenschaften der Universität Bayreuth

vorgelegt von

Alexander P. Majewski

Geboren in Coburg

Bayreuth 2013

Die vorliegende Arbeit wurde in der Zeit von Dezember 2009 bis Mai 2013 in Bayreuth am Lehrstuhl Makromolekulare Chemie II unter Betreuung von Herrn Prof. Dr. Axel H.E. Müller angefertigt.

Vollständiger Abdruck der von der Bayreuther Graduiertenschule für Mathematik und Naturwissenschaften (BayNAT) der Universität Bayreuth genehmigten Dissertation zur Erlangung des akademischen Grades eines Doktors der Naturwissenschaften (Dr. rer. Nat.).

Dissertation eingereicht am: 14.06.2013
Zulassung durch das Leitungsgremium: 03.07.2013
Wissenschaftliches Kolloquium: 13.09.2013

Amtierender Direktor: Prof. Dr. Franz Xaver Schmid

Prüfungsausschuss:

Prof. Dr. Axel H. E. Müller	(Erstgutachter)
Prof. Dr. Thomas Hellweg	(Zweitgutachter)
Prof. Dr. Ruth Freitag	(Vorsitz)
Prof. Dr. Birgit Weber	

Dedicated to my wife Songyi & son Aaron

and my family

Table of Contents

Summary

This thesis focused on the synthesis of functional materials based on water-soluble and responsive polymers, in particular poly((2-dimethylamino)ethyl methacrylate) (PDMAEMA). The dual-responsive behavior and polycationic character at physiological pH of PDMAEMA lead to outstanding properties and thus, to a versatile component for water-based applications. The main concept of the thesis was to combine the ability for gene delivery of PDMAEMA with the magnetic properties of iron oxide nanoparticles to enable an activity of the gene vector in an applied external magnetic field. Another point was to apply the dual-responsive behavior of PDMAEMA (temperature and pH) for physically cross-linked hydrogels.

Initial studies on magnetic dual-responsive gene vectors revealed a facile synthesis of PDMAEMA-grafted iron oxide nanoparticles utilizing dopamine as physically binding anchor group for the polymer chains. Here, a dopamine-based ATRP initiator was applied for the surface modification of the nanoparticles, which enabled a controlled polymerization technique *via* the "grafting-from" approach. Gene transfection experiments with CHO-K1 cells show that the transfection efficiency is significantly higher than for poly(ethyleneimine) (PEI), which is regarded as the "gold standard" among the polycationic gene vectors. Although the hybrid particles show a considerably high molecular weight (4.3 MDa), which should lead to a significant increase of the cytotoxicity as observed for linear PDMAEMA their cytotoxicity is remarkably low, lower than that of PEI. Thus, the excellent performance in gene delivery experiments can be attributed to the star-like architecture of the PDMAEMA. Moreover, the uptake of our superparamagnetic gene vector into the cells enables a magnetic cell separation by applying an external magnetic field.

However, due to the non-covalent bonds of dopamine to the iron oxide nanoparticles, the PDMAEMA chains undergo a detachment with time from the nanoparticle surface. This led to the synthesis of PDMAEMA-based magnetic core-shell-corona nanoparticles. Here, the iron oxide nanoparticles were covered with a thin silica shell in order to link the PDMAEMA chains covalently to the inorganic core *via* silane chemistry. This approach revealed stable dual-responsive hybrid nanoparticles with irreversible binding of the polymer chains and a high long-term stability in aqueous media. These hybrid star-like particles also show excellent gene delivery. The inter-polyelectrolyte complex formation between the PDMAEMA corona of the core-shell-corona particles and pDNA showed that the pDNA molecules are

individually complexed with single nanoparticles at N/P ratios (polymer nitrogen / pDNA phosphorous) where the best transfection results are obtained. The magnetic cell separation was further improved by using a Magnetic Activated Cell Sorting system (MACS^{TM}). The magnetically separated cells maintain a high transfection efficiency as well as viability and could even be further cultivated.

Another aspect of this thesis was to include PDMAEMA as stimuli-responsive block in a double switchable block copolymer-based hydrogel. For this purpose, we chose a physically cross-linked ABCBA pentablock terpolymer system, which was polymerized via sequential ATRP and consist of a water-soluble PEO middle block, two dual-responsive (temperature/pH) PDMAEMA B-blocks as well as two thermo-responsive poly(di(ethylene glycol) methyl ether methacrylate) (PDEGMA) A-blocks (PDEGMA-*b*-PDMAEMA-*b*-PEO-*b*-PDMAEMA-*b*-PDEGMA). The aggregation behavior in dilute solution was investigated *via* temperature-dependent Dynamic Light Scattering (DLS) revealing that both stimuli-responsive blocks can be triggered separately and the coil-to-globule transition temperatures of the stimuli-responsive blocks were found to be strongly dependent on the block lengths for low molecular weights. In concentrated solutions, however, rheology studies did not show a further change in the mechanical properties after gelation for the investigated ABCBA pentablock terpolymer compositions. As a result, the principle of our complex system points towards a successful synthesis of a dual-responsive ABCBA pentablock terpolymer hydrogel system, which may show two distinct phase transition even for the gel state, if longer block lengths of the outer A- and B-blocks would be applied.

Zusammenfassung

Die vorliegende Dissertation basiert vorwiegend auf der Synthese funktioneller, wasserlöslicher und stimuli-sensitiven Polymeren unter der Verwendung von Poly((2-dimethylamino)ethylmethacrylat) (PDMAEMA). PDMAEMA zeigt ein doppelt stimuli-sensitives Verhalten und besitzt polykationischen Charakter unter physiologischen Bedingungen. Dies führt zu herausragenden Eigenschaften und einer vielseitig einsetzbaren Komponente für wasserbasierende Anwendungen. Der Hauptaspekt dieser Dissertation war es die Fähigkeiten des PDMAEMAs für den Gentransfer mit den magnetischen Eigenschaften von Eisenoxid-Nanopartikeln zu kombinieren, um dadurch einen Genvektor zu erhalten, der auf ein externes magnetisches Feld anspricht. Ein weiteres Ziel war es die doppelte Sensitivität zu äußeren Reizen (Temperatur und pH) von PDMAEMA für physikalisch vernetzte Gele anzuwenden.

Erste Ergebnisse auf dem Gebiet der magnetischen doppelt stimuli-sensitiven Genvektoren führten zu einer vergleichsweise einfachen Synthese von Eisenoxid-Nanopartikeln mit aufgepfropften PDMAEMA unter der Verwendung von Dopamin als physikalisch adsorbierende Ankergruppe der Polymerketten. Hierfür wurde ein Dopamin-Derivat für die Oberflächenmodifikation der Eisenoxid-Nanopartikel verwendet, welches eine ATRP-Initiatorgruppe trägt. Dadurch war es möglich DMAEMA kontrolliert radikalisch von der Oberfläche aus („grafting-from“) zu polymerisieren. Gentransfer-Experimente mit CHO-K1 Zellen zeigten, dass die Transfektionseffizienz wesentlich höher ist als bei Polyethylenimin (PEI), das als der „goldene Standard“ unter den polykationischen Polymeren gehandelt wird. Die Hybrid-Partikel besitzen ein relativ hohes Molekulargewicht (4,3 MDa), was eine hohe Zytotoxizität schlussfolgern lässt, wie es bei linearen PDMAEMA der Fall ist. Jedoch ist die Zytotoxizität auffallend gering, sogar geringer als die von PEI. Dadurch kann die exzellente Darbietung in den Gentransfer-Experimenten der sternähnlichen Struktur des PDMAEMAs zugeschrieben werden. Des Weiteren ermöglichte die Aufnahme unseres superparamagnetischen Genvektors in die Zellen eine magnetische Zelltrennung unter der Verwendung eines externen magnetischen Felds.

Aufgrund der nicht kovalenten Bindung der Dopamin-Ankergruppe an die Eisenoxid-Nanopartikel löst sich ein Teil der PDMAEMA-Ketten mit der Zeit von der Oberfläche ab. Daher wurden in einem nächsten Schritt magnetische Kern-Schale-Korona Nanopartikel

synthetisiert, wobei die Korona wiederum aus PDMAEMA besteht. Um Zugang zu dieser komplexeren Struktur zu erhalten, wurden die Nanopartikel mit einer dünnen Silica-Schale ummantelt, auf die in einem folgenden Schritt mittels Silan-Chemie die PDMAEMA-Ketten kovalent angebunden werden konnten. Dadurch entstanden dauerhaft stabile doppelt stimuli-sensitive Hybrid-Nanopartikel, welche keine Freisetzung der PDMAEMA-Ketten von der Nanopartikeloberfläche mehr aufwiesen und zudem auch eine hohe Langzeitstabilität in wässrigem Medium besitzen. Diese sternähnlichen Hybridpartikel zeigten exzellente Ergebnisse bei Gentransfer-Experimenten. Die Entstehung von Inter-Polyelektrolyt-Komplexen zwischen der PDMAEMA-Korona der Kern-Schale-Korona Partikel und pDNA zeigten, dass bei den N/P-Verhältnissen (Polymer Stickstoff / pDNA Phosphor), bei denen die besten Transfektionsergebnisse erzielt worden sind, jeweils ein pDNA Molekül pro Nanopartikel komplexiert wird. Die magnetische Zelltrennung wurde weiterentwickelt, indem ein magnetisch aktiviertes Zelltrennungssystem (Magnetic Activated Cell Sorting system (MACS^{TM})) angewendet wurde. Die magnetisch abgetrennten Zellen behielten ihre hohe Transfektionseffizienz, sowie hohe Viabilität. Zudem war eine weitere Kultivierung dieser Zellen möglich.

Ein weiterer Bestandteil der Dissertation war es PDMAEMA als stimuli-sensitiven Block in ein doppelt schaltbares Blockcopolymer-Hydrogel zu integrieren. Für diesen Zweck hatten wir uns für ein physikalisch vernetztes ABCBA Pentablockterpolymer-System entschieden. Dieses wurde mittels sequentieller ATRP polymerisiert und besteht aus einem wasserlöslichen Polyethylenoxid (PEO) Mittelblock, zwei doppelt stimuli-sensitiven (Temperatur/pH) PDMAEMA B-Blöcken, sowie zwei thermo-sensitiven Poly((diethylenglycol)methylethermethacrylat) (PDEGMA) A-Blöcken (PDEGMA-*b*-PDMAEMA-*b*-PEO-*b*-PDMAEMA-*b*-PDEGMA). Das Aggregationsverhalten wurde in verdünnten Lösungen durch temperaturabhängige dynamische Lichtstreu-Experimente (DLS) bestimmt, wobei gezeigt werden konnte, dass beide stimuli-sensitive Blöcke unabhängig voneinander geschalten werden können und dass die Knäuel-Globulus-Übergangstemperaturen dieser Blöcke stark von der Blocklänge für niedrige Molekulargewichte abhängig ist. Rheologieuntersuchungen von konzentrierten Lösungen konnten jedoch keine weitere Änderung der mechanischen Eigenschaften des Hydrogels nach dem Gelieren für die untersuchten ABCBA Pentablockterpolymer-Zusammensetzungen ermitteln. Dies führt zum Ergebnis, dass das Prinzip unseres komplexen Systems auf eine erfolgreiche Synthese von doppelt stimuli-sensitiven ABCBA Pentablockterpolymer-Hydrogelen hindeutet, welche sogar zwei deutliche Phasenübergänge für den Gelzustand

zeigen könnten, wenn größere Blocklängen für die äußeren A- und B-Blöcke verwendet würden.

Glossary

°C	degree Celsius
^{1}H-NMR	proton nuclear magnetic resonance
A_{NP}	surface area of one single nanoparticle
AF4/AF-FFF	asymmetric flow field-flow fractionation
alt	alternating
ATRP	atom transfer radical polymerization
b	block
BIBDA	2-bromoisobutyryl dopamide
BIBSI	6-(trichlorosilyl)hexyl 2-bromoisobutyrate
c	concentration
c_{cgc}	critical gelation concentration
cm^{-1}	wavenumber
cm^3	cubic centimeter
$CoFe_2O_4$	cobalt ferrite
CROP	cationic ring-opening polymerization
DCC	*N,N*'-dicyclohexylcarbodiimide
DCM	dichloromethane
DLS	dynamic light scattering
DMAc	dimethylacetamide
DMAP	4-(dimethylamino)pyridine
DP_n	degree of polymerization
e.g.	for example (exempli gratia)
EDX	Energy Dispersive X-Ray Spectroscopy
EGFP	enhanced green fluorescent protein
et al.	et alii
etc.	et cetera
f_{DEGMA}	molar fraction of DEGMA units
f_{DMAEMA}	molar fraction of DMAEMA units
$Fe(CO)_5$	iron pentacarbonyl
γ-Fe_2O_3	maghemite
Fe_3O_4	magnetite

FT-IR	fourier transform infrared spectroscopy
g	gram
G'	storage modulus
G''	loss modulus
h	hour
HFMS	high gradient magnetic separations
HMTETA	1,1,4,7,10,10-hexamethyl triethylenetetramine
Hz	hertz
i.e.	that is (id est)
kg	kilogram
kDa	kilodalton
L	liter
LCST	lower critical solution temperature
MDa	megadalton
MRI	magnetic resonance imaging
MTC	magnetically targeted carriers
mL	milliliter
mg	milligram
µDSC	micro-differential scanning calorimetry
m	mass
M	molecular weight
M_n	number average molecular weight
MACS™	magnetic activated cell sorting
min	minute
mM	millimolar
mmol	millimol
MTT	3-(4,5-dimethylthyazolyl-2)-2,5-diphenyl tetrazolium bromide
MWCO	molecular weight cut off
N_A	Avogadro's number
nm	nanometer
nm²	square nanometer
NMP	nitroxide-mediated polymerization
NP	nanoparticle
N/P	polymer nitrogen / pDNA phosphorous

OSM	oligomeric sulfomethazine
P2VP/P4VP	poly(2/4-vinylpyridine)
PAA	poly(acrylic acid)
PAAm	poly(acrylamide)
PAMAM	poly(amidoamine)
PAN	poly(acrylonitrile)
PCGA	poly(ε-caprolactone-*co*-glycolide)
PCLA	poly(ε-caprolactone-*co*-lactide)
PDAMA	poly(2-methyl-acrylic acid 2-[(2-dimethylamino) ethyl] methylamino) ethyl ester
PDEAEMA	poly(2-(diethylaminoethyl) methacrylate)
PDEGMA	poly(di(ethylene glycol) methyl ether methacrylate)
PDI	polydispersity index
PDMAEAm	poly(2-(dimethylaminoethyl) acrylamide)
PDMAEMA	poly((2-dimethylamino)ethyl methacrylate)
pDNA	plasmid-deoxyribonucleic acid
PEI	poly(ethyleneimine)
PEO	poly(ethylene oxide)
P(GME-*co*-EGE)	poly(glycidyl methyl ether-*co*-ethyl glycidyl ether)
PHEMA	poly(2-hydroxyethyl methacrylate)
PLL	poly(L-lysine)
PMDETA	1,1,4,7,7-pentamethyldiethylenetriamine
PMMA	poly(methyl methacrylate)
PNAGA	poly(N-acryloyl glycinamide)
PNIPAAm	poly(N-isopropylacrylamide)
POEGMA	poly(oligo(ethylene glycol) methyl ether methacrylate)
PPI	poly(propylenimine)
ppm	parts per million
PPO	poly(propylene oxide)
PS	poly(styrene)
PSSS	poly(sodium 4-styrenesulfonate)
RAFT	reversible addition fragmentation chain transfer polymerization
ROMP	ring-opening metathesis polymerization
sec	second

SiO_2	silicon dioxide, silica
SI	supporting information
SEC	size exclusion chromatography
T_{CP}	cloud point
T_{SG}	sol-gel transition temperature
T_{tr}	coil-to-globule transition temperature
TEM	transmission electron microscopy
TEOS	tetraethyl orthosilicate
TGA	thermogravimetric analysis
THF	tetrahydrofuran
UCST	upper critical solution temperature
UV-/Vis	ultraviolet/visible
VSM	vibrating sample magnetometry
wt-%	weight percent
XRD	x-ray powder diffraction

Chapter 1 – Introduction

1.1. Iron Oxide Nanoparticles

1.1.1. Synthesis and Magnetic Properties

Magnetic nanoparticles, particularly iron oxide nanoparticles (either in the form of magnetite (Fe_3O_4) or maghemite (γ-Fe_2O_3)), represent an attractive and intensively studied class of materials in the nanotechnology. In addition to their responsiveness to an external magnetic field (superparamagnetism), they are also considered to be biocompatible, depending on their physicochemical properties and routes of administration.[1] The improvement and development of new synthetic techniques and functionalization strategies is crucial to gain control of the size, shape and surface properties, leading to potential applications in many different fields.[2]

Iron oxide nanoparticles with a diameter below 15 nm consist of a single magnetic domain and, thus, show superparamagnetic behavior.[3, 4] In superparamagnetic materials the magnetic orientation is strongly influenced by thermal excitations (Néel relaxation), causing a statistical distribution of the magnetic moments. As a result, without an external magnetic field these particles show an average magnetization of zero, and a magnetization measurement of superparamagnetic material reveals a typical sigmoidal curve showing no hysteresis (Figure 1A). Notably, superparamagnetic nanoparticles show a significantly higher magnetic moment in comparison to conventional paramagnetism. Even though there is no exactly defined range, it can be assumed that the Néel relaxation dominates for magnetic nanoparticles with a diameter of less than 20 nm, and by Brownian relaxation, which describes the particle relaxation by rotational reorientation of the particle, above 20 nm.[5] Besides the phenomenon of superparamagnetism of nanoparticles, magnetic materials such as cobalt ferrite ($CoFe_2O_4$) exhibit a "blocked" Neél relaxation,[6] in which the nanoparticles exclusively follow the Brownian mechanism in a magnetic field, which results in a hysteresis within the magnetization curve.

In general, many synthetic routes were established for magnetic nanoparticles, leading to a wide range of magnetic nanomaterials from a large variety of different compounds, which were recently comprehensively reviewed by Behrens.[7] The synthesis of iron oxide nanoparticles in particular is well investigated, from a variety of different synthetic routes which allows precise adjustment of the size, size distribution and shape of the nanoparticles as

well as the surface chemistry, giving the potential for stabilization of the particles with, for example, hydrophilic or hydrophobic surfactants. Since nanoparticles have an extremely high surface-to-volume ratio and thus show a strong tendency to agglomerate in order to reduce their surface energy, surfactants are necessary to counter these forces and enable stabilisation of the nanoparticles.[8] Stabilization agents are commonly adsorbed on the particle surface and use either electrostatic forces or steric hindrance to avoid particle agglomeration.[9-11] Typical surfactants include carboxylic acids, amines, ionic surfactants or polysaccharides.[11-15]

Probably the most common method of synthesizing iron oxide nanoparticles is the co-precipitation method. This method offers a simple way to generate nanoparticles with a rather small polydispersity, via the reaction of a Fe^{2+}/Fe^{3+} salt solution under basic conditions (Figure 1B).[16, 17] The nanoparticle suspension is further stabilized by subsequent addition of hydrophilic or hydrophobic surfactants, which are typically citric acid or oleic acid, respectively.[18, 19] The size of the nanoparticles (typically < 20 nm) can be controlled by the pH and ionic strength of the reaction solution.[20, 21] Alternatively, narrowly distributed iron oxide nanoparticles can be prepared *via* thermal decomposition of iron pentacarbonyl ($Fe(CO)_5$) in high boiling solvents using oleic acid as a stabilizer.[22, 23] The size of the particles can be easily adjusted by varying the oleic acid / $Fe(CO)_5$ ratio, yielding iron oxide particles in the dimensions of 3 – 15 nm (Figure 1C and 1D). Furthermore, there is a wide range of other synthetic routes available for iron oxide nanoparticles, such as sol-gel synthesis,[24, 25] hydrothermal reactions,[26, 27] flow injection synthesis,[28] electrochemical methods,[29, 30] aerosol/vapour-phase method,[31, 32] sonochemical decomposition,[33, 34] supercritical fluid method,[35] synthesis using nanoreactors and microbial methods.[36-40]

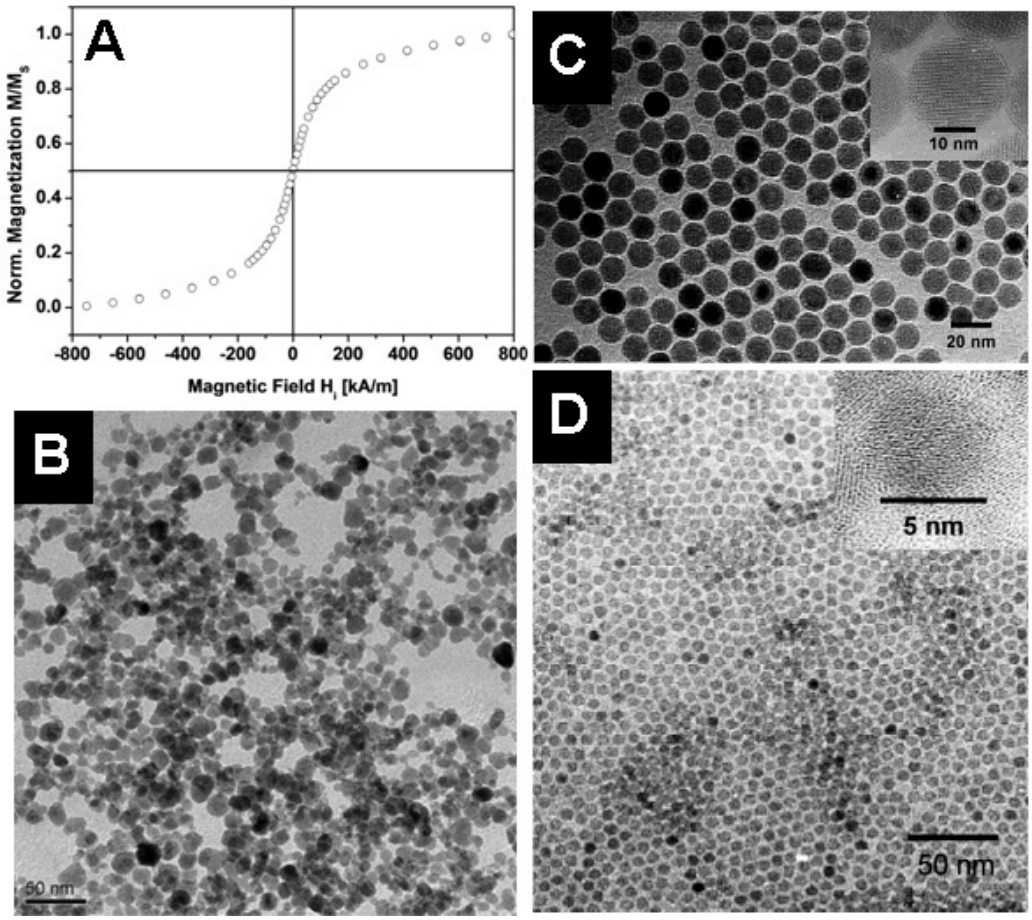

Figure 1. (A) Typical magnetization curve of superparamagnetic iron oxide nanoparticles. (B) TEM micrograph of iron oxide nanoparticles synthesized *via* co-precipitation method. (C) and (D) High (inset) and low resolution TEM micrographs of maghemite nanoparticles synthesized *via* thermal decomposition. Reprinted with permission from refs. 22 and 72. Copyright 2001 and 2010 American Chemical Society.

1.1.2. Applications in Pharmacy, Biomedicine and Technics

Iron oxide is one of the most investigated materials as a nanoparticle for synthesis and surface modification. This large body of knowledge results in an interesting magnetic multi-purpose tool for a large variety of different applications. The high biocompatibility of iron oxide makes this material interesting for potential applications in the biotechnical/medical field (Figure 2), such as magnetic resonance imaging (MRI),[41] cell sorting,[42, 43] anti-cancer agents (hyperthermia),[44-46] magnetically targeted carriers (MTC) and drug/gene delivery (Figure 2).[1, 47-50] In terms of gene delivery, magnetic nanoparticles are frequently applied for enhancing the transfection efficiency *via* magnetofection, in which magnetic force is used to pull non-viral gene vector grafted magnetic nanoparticles (polyplexes) into targeted cells. This causes a rapid uptake of the magnetic polyplexes, resulting in a fast and efficient method of transfecting cells.[51] Iron oxide nanoparticles are already established carrier systems for gene

vectors. All frequently used polymers for gene transfer, including PEI, PDMAEMA, chitosan and dendrimers, have already been successfully grafted onto magnetic nanoparticles for magnetofection,.[52-56]

Further applications, beyond the scope of this thesis, include High Gradient Magnetic Separations (HFMS) for wastewater treatment,[57] catalysis,[58] magnetic gels,[59-62] magnetically triggered sealings, loudspeaker membranes, and dampers and additives in polishing agents.[63, 64]

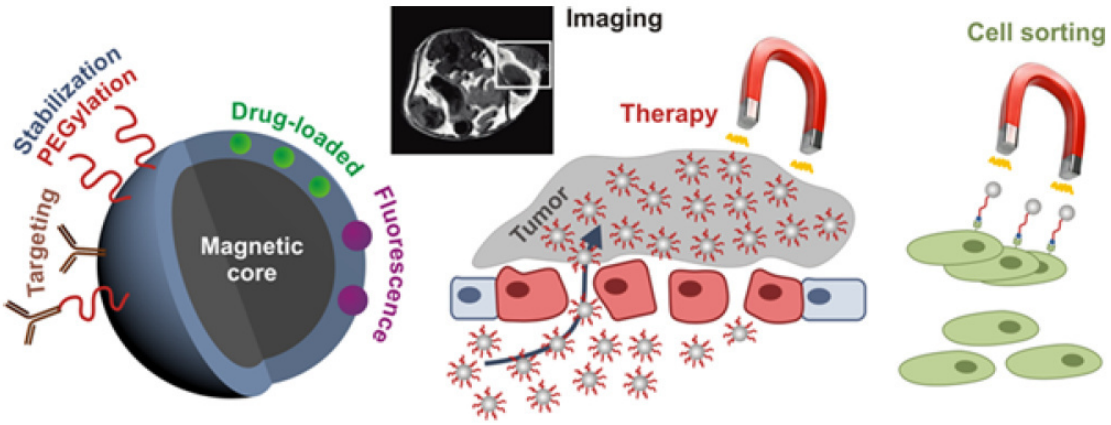

Figure 2. Pharmaceutical and biomedical applications of magnetic nanoparticles. Reprinted with permission from ref. 1. Copyright 2012 American Chemical Society.

1.1.3. Functional Iron Oxide Nanoparticles

1.1.3.1. Surface Modification Methods

The surface chemistry of iron oxide nanoparticles plays a key role in tuning their specific properties. Surfactants serve not only as stabilizers, but can also offer the possibility of adding functional groups. Surfactant molecules are usually physically adsorbed on the nanoparticle surface, providing a flexible system for a further ligand exchange, for example exchange of the surfactant with molecules bearing additional functional sites (Figure 3). A ligand exchange reaction is performed by taking advantage of anchoring groups in the additional molecule, which show a higher affinity to attach to the iron oxide surface than the surfactant. Phosphate esters and dopamine derivatives are considered to bind strongly onto the iron oxide surface, showing excellent stability even in aqueous media.[56, 65, 66] Dopamine especially is a frequently used biomimetic candidate for such exchange reactions.[67, 68]

Another elegant method for modification of iron oxide nanoparticles is the use of silanes which carry an additional functional group. In this approach the silanes coordinate onto the nanoparticle surface, where they undergo a self-condensation reaction forming a thin polysiloxane layer around the particle, offering a permanent immobilization of a choice of functionalities on the nanoparticle.[69-72]

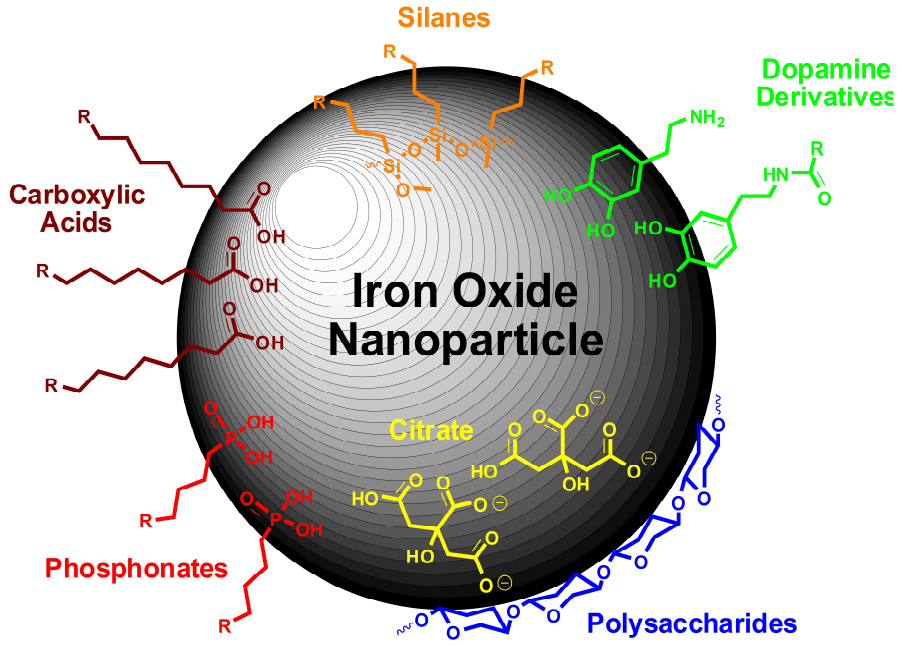

Figure 3. Schematic illustration of different anchor groups for the functionalization of iron oxide nanoparticles

A closely related method is first completely covering the iron oxide nanoparticle with a protective silica shell. The silica surface can then be modified to yield stable core-shell nanostructures. Besides the well-known Stöber method other interesting synthesis routes were developed, even successfully encapsulating single iron oxide nanoparticles.[73-75] A recent approach which attracted considerable attention is the use of oleic acid-stabilized iron oxide nanoparticles dispersed in a reverse microemulsion with Igepal® as surfactant. This method gives singly encapsulated nanoparticles with a perfectly round shape, as well as simultaneously allowing control of the size of the silica shell in a range below 50 nm.[76-78] This nucleation process was described by the La Mer theory (Figure 4),[78] in which a certain solubility concentration of the tetraethyl orthosilicate (TEOS) monomer (denoted as C_s) must be exceeded in order to initiate the heterogeneous nucleation of silica around the iron oxide nanoparticles. As long as the concentration stays below the critical concentration for the

homogeneous nucleation (C_{homo}), individually encapsulated iron oxide nanoparticles can be obtained. The increase of monomer concentration above C_s triggers the formation of two different species, consisting of silica covered nanoparticles and pure silica nanoparticles, respectively.

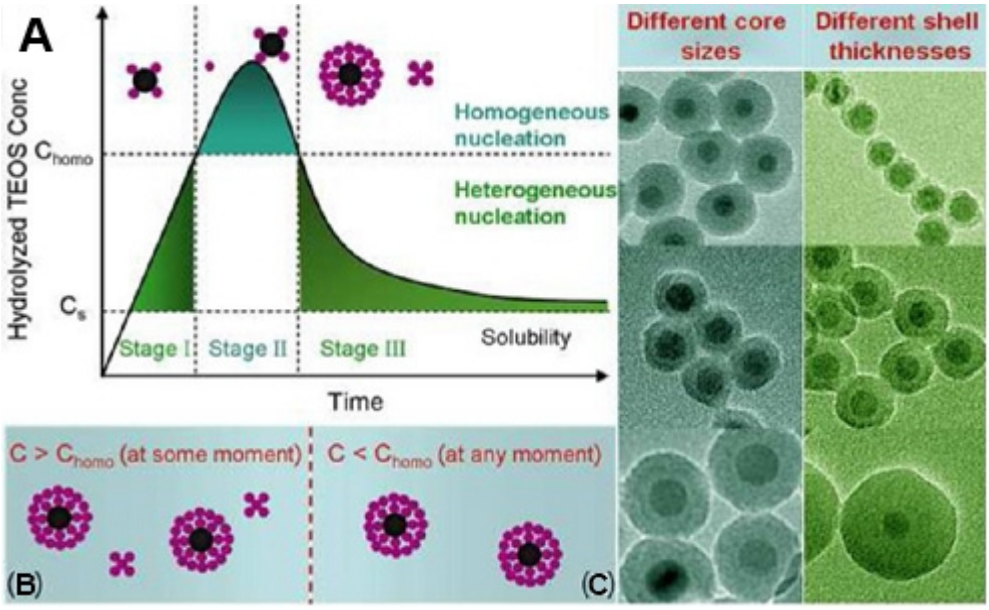

Figure 4. (A) La Mer-like diagram: hydrolyzed TEOS (monomer) concentration against time, showing homogeneous and heterogeneous nucleation. (B) The existence of both, Fe_3O_4@SiO_2 core/shell nanoparticles and SiO_2 nanoparticles when $C > C_{homo}$ at some moment. (C) Only the existence of Fe_3O_4@SiO_2 core/shell nanoparticles when $C < C_{homo}$ at any moment. (right) Synthesis of Fe_3O_4@SiO_2 core/shell nanoparticles using different core sizes and varying the shell thickness. Reprinted with permission from ref. 78. Copyright 2012 American Chemical Society.

1.1.3.2. Functional Magnetic Nanoparticle-Polymer Hybrids

A further increase of functionality can be obtained by decorating magnetic nanoparticles with an organic polymer corona. This results in an interesting class of hybrid nanomaterials combining the advantages of the magnetic properties of the inorganic core and the functionality/responsiveness of the attached polymer. Different methods of anchoring organic compounds on the surface have already been demonstrated in the previous chapter. Here, a small overview of the variety of polymer-grafted nanoparticles will be shown.

There are two common routes to couple polymer chains with nanoparticles. In the first, the "grafting-onto" approach, the polymer is prepared separately from the nano-object and bears an additional anchor group which shows a high binding affinity to the nanoparticle. This

enables a versatile grafting method for attaching tailor-made polymers onto the nanoparticle *via* a ligand exchange reaction.[66, 79, 80] In addition, "click chemistry" has also become a powerful method. Potential synthetic routes use either the thiol-ene "click" reaction to couple a thiolene end-functionalized polymer on a vinyl-grafted nanoparticle, or the well-known Cu(I) catalyzed azide-alkyne cycloaddition to couple azide-functionalized polymer chains onto alkyne pre-functionalized nanoparticles.[68, 76] An advantage of the grafting-onto method is the possibility of simultaneously grafting two different homopolymers onto the particle surface, which is an easy route to nanoparticles carrying a mixed polymer corona.[81-84] The grafting-onto approach is frequently based on physically strong binding anchor groups, such as dopamine. Even though dopamine is a generally accepted to be an effective agent for introducing functionality to iron oxide nanoparticles, a reversible binding of catechol end-functionalized PEO was discovered by the group of Reimhult.[85] This disadvantage can be compensated, however, by adding electron-withdrawing groups such as NO_2 to the catechol ring. This enhances drastically the electronic interactions with Fe^{2+}/Fe^{3+} ions in solution and thus with iron oxide nanoparticles.[86]

Conversely, the "grafting-from" approach provides facile methods for the permanent attachment of the polymer chains. Here, pre-functionalized nanoparticles are used to initiate polymerization directly from the particle surface.[87, 88] Permanent bonding of the initiator molecules is easily possible in this step, leading to stable polymer-grafted nanoparticles. For instance, the group of Schmidt utilized silane-functionalized Atom Transfer Radical Polymerization (ATRP) initiators which form a thin cross-linked initiator shell around the nanoparticles.[69, 72, 89] Due to the denser packing of the small initiator molecules on the nanoparticle surface, higher grafting densities can be achieved compared to the attachment of whole polymer chains *via* the grafting-onto method. Thus, the grafting-from method is typically preferred for grafting dense polymer brushes, as shown by the group of Barner-Kowollik. They confirmed this trend by a direct comparison of grafting-from vs. grafting-onto methods, utilizing cellulose as a substrate.[90] A better control of the polymeric content distribution and higher grafting densities could be achieved by applying the grafting-from concept. In addition, there are generally almost no limitations in the possible polymerization techniques for surface-initiated polymerizations; all common controlled polymerization methods, such as ATRP,[91-93] Reversible Addition Fragmentation chain Transfer polymerization (RAFT),[94-96] Nitroxide-Mediated Polymerization (NMP),[97-99] as well as Cationic Ring-Opening Polymerization (CROP), may be utilised in this approach.[100]

The incorporation of magnetic nanoparticles within a micellar core is also a versatile tool for the preparation of hybrid structures. The drawback of this method is the lack of control over the amount of nanoparticles incorporated during the micelle formation process, leading to magnetic core-shell hybrid micelles (magnetomicelles) carrying multiple nanoparticles per micelle, and thus leading to bigger dimensions of the core.[101-104] In some applications, such as MRI using iron oxide nanoparticles, this may be even an advantage due to increased response in a magnetic field resulting in a significant boost of the transverse relaxivity compared to singly encapsulated nanoparticles.[105] One key parameter is the surface chemistry of the nanoparticle, which must match with the micelle-core building block in order to avoid rejection of the nanoparticles. Typical driving forces for the formation of these micelles are either compatibility of non-ionic surfactants of the nanoparticles, or electrostatic interactions.[102, 106]

The attached polymer corona of the nanoparticles can be used for a wide variety of different applications. Since superparamagnetic particles can be inductively heated in an AC magnetic field, they provide attractive properties if combined with a thermo-responsive polymer corona. The thermo-responsive colloids can be remotely heated via applyication of an external magnetic field, causing a phase transition of the polymer, which may be a useful mechanism for magnetically driven drug release or shape transitions.[107] Chanana *et al.* investigated the reversible agglomeration of PDEGMA/PEOGMA-grafted magnetite nanoparticles in aqueous conditions, as well as the influence of these magnetic hybrids inside red blood cells with respect to a contrast enhancement for MRI (Figure 5A).[108] The magnetism of the nanoparticles can be efficiently used to design magnetically recoverable systems. Gelbrich *et al.* demonstrated a colloidal system consisting of iron oxide nanoparticles covered by a water-soluble thermosensitive polymer corona. Within the polymer corona, functional molecules (trypsin) were introduced as biocatalysts. This system showed a high catalytic activity, and due to the magnetic core the catalyst could be easily separated after use.[72] The group of Matyjaszewski synthesized recyclable antibacterial magnetic nanoparticles grafted with quaternized PDMAEMA. The antibacterial effect could be kept constant over several cycles by magnetically recovering the particles before each use (Figure 5B).[66] In addition, positively charged polymers have the ability to bind other noble metallate anions and to act as an electron donator for reduction, as successfully applied for amphiphilic poly(2-(dimethylaminoethyl) acrylamide)-*b*-poly(N-isopropylacrylamide) (PDMAEAm-*b*-PNIPAAm) diblock copolymer grafted maghemite nanoparticles. The positively charged PDMAEAm inner block was loaded with $[AuCl_4]^-$ ions. A subsequent reduction of these ions

produced a gold layer around the magnetic core while still retaining the temperature-sensitivity of the PNIPAAm (Figure 5C).[109] Since magnetic nanoparticles show great potential in biomedical applications, PEO-grafted magnetic nanoparticles are frequently used for reducing *in vivo* interactions with other proteins. Thus, nanoparticles with a biocompatible PEO polymer corona show a "stealth effect" contributing to longer retention periods in the body.[48]

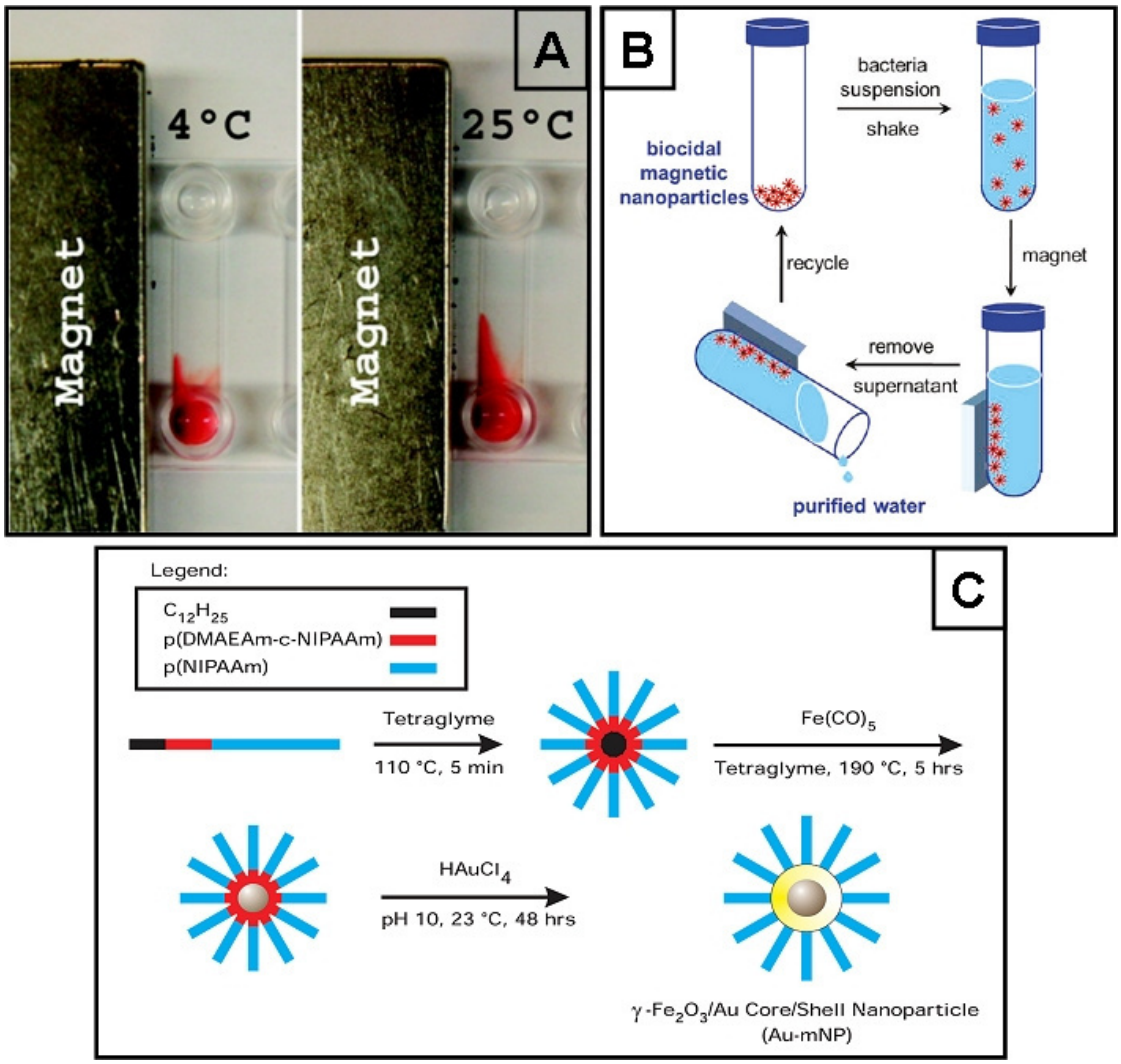

Figure 5. (A) Photographs of using a magnet to manipulate red blood cells loaded with PDEGMA grafted magnetite nanoparticles at 4 °C (left panel) and 25 °C (right panel). (B) Schematic illustration of recycling magnetic nanoparticles modified with quaternized PDMAEMA for antibacterial application and (C) Synthesis of nanoparticles consisting of a magnetic core, gold shell and an amphiphilic corona. Reprinted with permission from ref. 66, 108 and 109. Copyright 2009 and 2011 American Chemical Society.

1.2. Non-Viral Gene Delivery Mediated by Polycationic Polymers

1.2.1. Mechanism

The mechanism of delivery of nucleic acids into a cell, particularly the delivery of the pDNA to the nucleus utilizing polycations, is still not completely understood (Figure 6). Thus, a general prediction on the best polycationic delivery system is up to date not possible. Poly(ethyleneimine) (PEI) is one of the most popular polycationic gene vectors. Since the first successful transfection utilizing PEI as gene vector in 1995, PEI has rapidly developed to a well-studied delivery system,[110, 111] with linear and branched PEI the most commonly used structures for gene delivery. For linear polycations such as PEI and PDMAEMA, an increase of the transfection efficiency can be achieved by applying higher molecular weights of the polymer for gene delivery experiments, however, this in turn increases the cytotoxicity of the gene vector.[112, 113] As a result, there is still much potential for progress in new delivery systems via the development of polymers with different architectures.[114]

A typical procedure starts with the complexation of the polyanionic DNA with the polycationic gene vector to for form positively charged "polyplexes". The polyplex assembly takes place in the absence of the cells and is driven by the increase in entropy due to the release the respective counterions of the DNA and the gene vector.[115] This complexation step is crucial since both the cell membrane and the DNA are negatively charged, and would electrostatically repulse each other without the incorporation of a polycationic gene vector. An excess of positive charges is therefore necessary in order to bind to the cell membrane, resulting in N/P ratios (N: amount of nitrogen units of the gene vector; P: phosphate groups of the DNA) much higher than unity; best results are typically achieved with a N/P ratio of 10.[116] The generally accepted mechanism for the cell uptake is *via* endocytosis, followed by the endosomal escape of the polyplexes and the subsequent migration of these polyplexes in the cytoplasma and their uptake into the nucleus. The exact mechanisms, however, are still not fully understood, particularly the intracellular trafficking mechanisms.[117, 118] Several questions remain unanswered, namely: (1) How exactly the trapped polyplexes escape from the endosomes and what the driving force is which causes the polyplexes to be set free in the cytosol; (2) How do the polyplexes travel through the cytosol to the nucleus considering a concentrated protein solution and a fairly high viscosity; and (3) Whether the DNA is released in the cytosol or inside the nucleus and how does the released DNA or the whole polyplex pass through the nuclear membrane (here, the common consensus is that the

polyplexes/pDNA access the nuclei during the cell division when the nuclear membrane breaks down).[116]

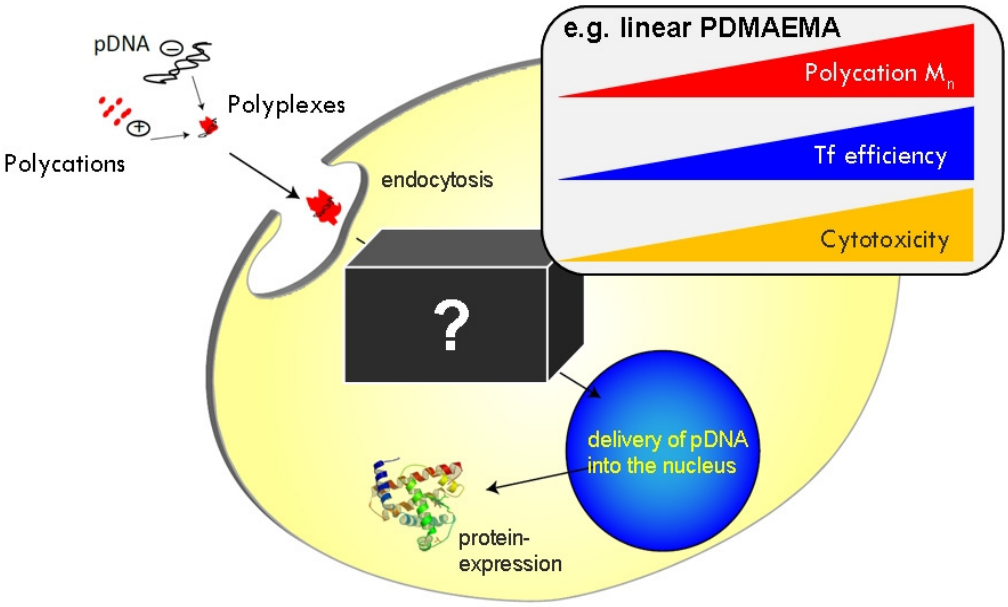

Figure 6. Schematic illustration of non-viral gene delivery utilizing polycationic systems. Reprinted with permission from Dr. Valérie Jérôme.

Several important issues also arise from the N/P ratio, which has a particularly large effect on the success of the transfection. Because of the high N/P ratios, which are necessary for an efficient transfection, the excess of the cationic gene vector appears to play an important role in the transfection efficiency. PEI, for example, complexes the DNA molecules completely at an N/P ratio of 3, independent of the chain length.[119, 120] This results in a considerably large amount of free polymer chains, which is problematic because the free PEI chains are even more toxic than the PEI bound to the DNA.[121, 122] Especially long polycationic polymers can easily penetrate and destabilize cell membranes, which typically consist of anionic phospholipid bilayers.[119, 120] These free cationic polymer chains are thought to play a key role in the transfection by improving the release of the polyplexes from the endosomes. Another mechanism leading to a release of the polyplexes from the endosomes is the "proton sponge" concept. Since a pH decrease takes place within the endosomal development, a further protonation of the amines of the gene vector is induced, causing an increase of counter-ions in the endosomes. This generates a high osmotic pressure promoting a disruption of the endosomes. Even though this model enjoys great acceptance in non-viral gene delivery it can still not be confirmed as major driving force for endosomes disruption.[123] Interestingly, a

comparison of transfection using low and high molecular weight polymers at same N/P ratios shows a significantly better overall transfection efficiency for the larger polycations, although a higher osmotic pressure for smaller molecules would be expected.[120] Hennink *et al.* tried to improve the transfection efficiency by applying the "proton sponge" concept and increasing the buffer capacity by synthesizing a polymer bearing two tertiary amine groups in the side chain (poly(2-methyl-acrylic acid 2-[(2-dimethylamino) ethyl] methylamino) ethyl ester (PDAMA) resulting in an even less potential gene vector.[124] Contradictory results were achieved by decreasing the buffer capacities of the polycations *via* partial acetylation of PEI, which gives a significantly higher transfection efficiency.[125] These results indicate an inconsistent relation between the buffering capacity of the polycation and transfection efficiency. Furthermore, theoretical calculations for an endosomally captured PEI-DNA polyplex with an N/P ratio of 7 showed that when the pH is decreased from 7.4 to 5.0, the generated osmotic pressure is insufficient to fracture a lipid vesicle.[123] These findings indicate that while the "proton sponge" effect may certainly not be the dominant driving force for the intracellular trafficking of the polyplexes, it should still not be underestimated. An even more detailed review of progress and perspectives for polymeric gene delivery is given in a recent paper by Yue and Wu.[116]

1.2.2. Polycationic Polymers for Gene Delivery

Besides the electroporation method[126] and physical methods such as microinjection and biobalisitc (gene gun),[127] there exist two other common ways for delivering nucleic acids into mammalian cells, namely viral and non-viral gene delivery.[128, 129] In viral gene delivery systems, viruses are modified, carrying for example a therapeutic gene for transfection.[130] Viruses are experts in delivering nucleic acids into cells showing excellent delivery efficiencies. However, the quantity of foreign DNA that can be accommodated in the viral genome is much less than the one that can be incorporated in a plasmid. Furthermore, these systems can cause strong immune reactions, which make viruses unpredictable and therefore potentially dangerous candidates for gene delivery.[131] This drawback can be avoided by using non-viral gene vectors, which can be divided further into lipid-based and polymer-based gene vectors.[111] Due to their large potential variety and individual tenability, polymeric vectors offer great potential and flexibility for non-viral gene delivery, even though they are less efficient than their viral equivalents.[123] It should be mentioned, however, that the new generation of non-viral gene delivery agents show transfection efficiencies close to those of

viral delivery agents (except for some restrictions in the field of transfection of primary cells).[113]

All the well-studied polymeric gene delivery systems have one major factor in common: namely, primary, secondary or tertiary protonatable amine groups, leading to a polycationic character in aqueous media. Nature already provides some potential candidates based on carbohydrates, such as chitosan and poly(glycoamidoamines) or polypeptides.[132-134] In contrast, well-studied synthetic representatives include dendrimers, poly(L-lysine) (PLL), PEI, and PDMAEMA.

The sophisticated "star-like" architecture of dendrimers shows potential properties for gene delivery. Poly(amidoamine) (PAMAM) dendrimers were the first introduced to the field of gene delivery in 1993 by Haensler and Szoka.[135] Due to their better transfection efficiency and lower cytotoxicity compared to unmodified PEI, PAMAM dendrimers are a frequently used tool for gene delivery studies.[136-138] Other dendrimeric vectors useful for gene delivery consist of poly(propylenimine) (PPI),[139-141] PLL and carbosilanes.[142-146]

Gene vectors from linear synthetic polymers, such as PLL, can also deliver nucleic acids sufficiently. PLL is synthesized *via* ring-opening polymerization of the protected *N*-carboxy-(*N*-benzyloxycarbonyl)-L-lysine anhydride, and the molecular weight can be adjusted by specific monomer-to-initiator feed ratios.[147] The resulting PLL, with molecular weight greater than 3000 Da, is able to form stable polyplexes with DNA for gene delivery. Although the high molecular weight PLL shows excellent condensing capacities with DNA, a considerably high cytotoxicity is observed.[148] Thus, the group of Kataoka introduced a second PEO-block to the PLL (PLL-*b*-PEO) in order to enhance the biocompatibility.[149, 150] This PLL-*b*-PEO system complexes the DNA by forming polyplexes consisting of a PLL/DNA core and a PEO corona, resulting in promising results for *in vitro* and *in vivo* gene transfection.[151] The transfection efficiency could be further improved by utilizing crosslinkable thiolated PLL-*b*-PEO block copolymers; cross-linking the polyplexes showed an even greater transfection efficiency compared to the unmodified PLL-*b*-PEO.[152]

PEI and PDMAEMA in their linear form show a moderate performance in transfection efficiency.[153, 154] As mentioned previously, an increase in molecular weight causes an increase in transfection efficiency, as well as a simultaneous increase of the cytotoxicity.[155, 156] Since polymer chemistry is a very versatile tool for creating new structures and architectures, many different delivery systems based on PEI and PDMAEMA were developed in an attempt to resolve the dilemma between transfection efficiency and cytotoxicity.[111, 157]

Linear PEI is difficult to synthesize; thus typically the branched 25kDa PEI is applied, consisting of a mixture of primary, secondary and tertiary amino groups. It is probably the best-studied polymer for gene delivery and sometimes called the "gold standard".[116] Thus, PEI as a gene delivery agent has been studied *in vivo* as well as *in vitro*.[158, 159] The biocompatibility and retention times of the polyplexes for *in vivo* experiments were enhanced by grafting poly(ethylene oxide) (PEO) chains onto PEI, but this technique shows a lower transfection efficiency than unmodified PEI.[160] The synthesis of an alternating copolymer of PEI and PEO (PEI-*alt*-PEO), however, showed both increased transfection efficiency and reduced cytotoxicity compared to branched PEI with a molecular weight of 25 kDa.[161]

Similarly to PEI, PDMAEMA-based gene vectors have also been modified with PEO.[162-166] The use of bioreducable disulfide bonds between PDMAEMA and PEO in an ABA block copolymer (PDMAEMA-*b*-PEO-*b*-PDMAEMA) showed a higher transfection efficiency than the usual covalently linked counterpart.[167] The groups of Hennink and Armes/Stolnik pioneered the use of PDMAEMA as gene vector.[168-173] Since then the architectural development of PDMAEMA gene vectors has further proceeded, with particularly branched and star-shaped PDMAEMA gaining significant attention as gene delivery agents.[174-176] The superior transfection abilities of PDMAEMA stars compared to conventional linear PDMAEMA were established by the groups of Müller and Freitag. A progressive improvement of the gene vector by increasing the arm number regarding to the cytotoxicity could be shown.[154] The idea of implementing even more arms led to the synthesis of a PDMAEMA star carrying 20 chains, resulting in an immense boost in the transfection efficiency and a simultaneous reduction in cytotoxicity.[113] The concept of high molecular weight stars was further confirmed by identical architectures showing excellent transfection results for block copolymer micelles with a PDMAEMA corona.[113, 177]

1.3. Water-Soluble Stimuli-Responsive Polymers

This chapter deals with the most frequently used water-soluble stimuli-responsive polymers. The group of temperature-responsive polymers typically consists of non-ionic polymers. These polymers, however, can be further divided in two classes, showing either a lower critical solution temperature (LCST) or an upper critical solution temperature (UCST), showing a partial solubility within a certain temperature range. The LCST behaviour is based on the unfavorable entropy of mixing, which is usually driven by the destruction of hydrogen bonds between the polymer and water at elevated temperatures, inducing phase separation.

Conversely, the destruction of strong intra- and intermolecular interactions of a polymer lead to an improved solubility with an increase in temperature, causing UCST behavior.[178, 179] Here, an important indicative property is the cloud point, which describes the moment the polymer becomes water-insoluble causing turbidity of the polymer solution. Since no exact definition of the cloud point exists, the determination of the cloud point differs depending on the experimenter. Two frequently used methods for determining cloud point are the onset or the turning point of the turbidity curve.[180, 181]

Studies of water-soluble UCST polymers such as poly(*N*-acryloyl glycinamide) (PNAGA) and copolymers of poly(acrylamide-*co*-acrylonitrile) (PAAm-*co*-PAN) are rare and play a minor role in the field of responsive polymers, as recently reviewed by Seuring and Agarwal.[182] The probably most well-known and investigated thermo-responsive polymer is poly(*N*-isopropylacrylamide) (PNIPAAm). PNIPAAm is a LCST polymer and shows a sharp coil-to-globule transition at approximately 32 °C. Above this temperature the polymer becomes insoluble due to the entropic gain caused by favorable formation of inter- and intramolecular hydrogen bonds between the amide groups, leading to a release of water molecules. The cloud point around body temperature (37 °C) attracted considerable attention for biomedical applications, and the structural similarity to poly(leucine) makes it comparable to a simple protein model.[183, 184] Additionally, copolymerization with other acrylamide derviatives can be used to vary the LCST.[185] These properties result in PNIPAAm being an attractive candidate for stimuli-responsive block copolymers as well as for the formation of hydrogels and microgels.[186-189] Poly(oligo(ethylene glycol) methyl ether methacrylate)s (POEGMA), with 2 to 10 ethylene glycol units in the polymer side chains, also show LCST behavior and biocompatibility.[108] Poly((diethylene glycol) methyl ether methacrylate) (PDEGMA), a polymer with side chains containing 2 polyethylene oxide units, shows a relatively low cloud point around room temperature (25 – 28 °C), compared to POEGMA (carrying side chains with 8 – 9 ethylene oxide units) which has a cloud point around 90 °C.[190-192] A copolymerization of both polymers at different ratios enables the adjustment of the cloud point in the temperature range of 25 – 90 °C, which covers almost the whole temperature range of interest for aqueous applications.[192-194]

Another interesting group of stimuli-responsive polymers is sensitive to pH, in which the solubility of a polymer can be controlled by changing the degree of protonation. These polymers carry a protonable/deprotonable group in the side chain and are only soluble within a certain pH range, in which the polymer carries a sufficient amount of positive or negative charges. Due to the polyelectrolytic character the polymer is well hydrated, which in turn

enhances the solubility. Conversely, a decrease of the charges within the polymer by changing the pH and therefore the protonation, reduces the solubility. Generally, there exist two classes of pH-responsive polymers, which can be divided in polycationic and polyanionic polymer systems. A typical polyanionic polymer is poly(acrylic acid) (PAA). At low pH PAA is completely protonated, and thus becomes poorly water-soluble. An increase of pH causes a progressive deprotonation of the carboxylic groups resulting in an anionic polyelectrolyte with an excellent water-solubility.[195-197] A common pH-responsive polycationic polymer is poly(2/4-vinylpyridine) (P2VP/P4VP), which is insoluble above pH 5. This polymer can be converted into a water-soluble polyelectrolyte by protonating the nitrogen of the pyridine at pH < 5.[198, 199] A conversion into a permanent polyelectrolyte is possible *via* quaternization of the nitrogen.[102, 200]

Poly(2-(dimethylamino)ethyl methacrylate) (PDMAEMA) and poly(2-(diethylaminoethyl) methacrylate) (PDEAEMA) polymers show outstanding behaviour in aqueous systems. These polymers, containing a tertiary amine group on the side chain, exhibit dual responsive behavior in water.[201-203] Since the tertiary nitrogen group of the methacrylate can be protonated it undergoes a coil-to-globule phase transition depending on pH. PDMAEMA, for instance, is highly charged at low pH resulting in an excellent water-solubility (pH 7; cloud point $T_{CP} \approx 80$ °C). An increase of the pH causes a progressive deprotonation of the polymer leading to a cloud point which decreases to around room temperature at pH 10. In addition, Plamper *et al.* showed that the cloud point is also strongly dependent on the molecular weight at high pH values.[181]

1.4. "Smart" Hydrogels

1.4.1. Definition

As the term "Hydrogel" suggests, this special class of soft matter materials consists mainly of water, with a minor fraction consisting of an infinite three-dimensional network. This network is generally based on water-soluble polymers, which are cross-linked either by covalent bonds or physical junctions.[204, 205] Here, the term "smart" refers to polymers which respond to external stimuli by undergoing sharp, reversible phase transitions (*e.g.* coil-to-globule).[206, 207] This means that even small changes of external parameters can cause a swelling or contraction of the hydrogel. The unique properties of hydrogel systems lead to a variety of different applications for cosmetics, biomaterials or coatings.[207-210]

Common synthetic polymers used in chemically cross-linked hydrogels are poly(2-hydroxyethyl methacrylate) (PHEMA), PEO and PNIPAAm.[211, 212] PNIPAAm especially has attracted considerable attention as a hydrogel, due to the coil-to-globule phase transition (at 32 °C) being close to body temperature.[189, 213]

Physically cross-linked hydrogels have the advantage of full reversibility back to the liquid state. The cross-linking points of this structure result from self-assembly mechanisms driven by hydrogen bonding,[214, 215] partial crystallization,[216-218] or hydrophobic or electrostatic interactions.[204, 205, 219] For this purpose, a variety of hydrogels were developed based on functional polymers which can be triggered by outer stimuli such as temperature,[207, 220, 221] pH,[222-224] or light.[221, 225] There still exist, however, physical hydrogels which also contain irreversible cross-link junctions. For instance, hydrogel networks consisting of an ABA block copolymer can be permanently cross-linked by utilizing hydrophobic polymers, *i.e.* poly(styrene) (PS) or poly(methyl methacrylate) PMMA.[223, 226] In general, block copolymers of synthetic polymers are versatile systems for achieving hydrogels with different topologies (linear-, star-shape) and sensitivities depending on the polymer composition. A short overview of the diversity of block copolymer systems is given in the next section.

1.4.2. Hydrogels Based on Block Copolymer Systems

The most frequently investigated block copolymer structures are illustrated in Figure 7A-C. Here, the A-block symbolizes the hydrophilic block and the B-block indicates the stimuli-responsive block of the polymer.

In AB/ABA block copolymer hydrogels, the B-block is first triggered by an outer stimulus (*i.e.* temperature, pH, etc.) causing micelle formation (Figure 7A). At low concentrations the micelles are freely dispersed in the medium. Exceeding the critical gelation concentration (c_{cgc}) of the solution results in a hydrogel consisting of closely packed micelles.[227-231] However, a relatively high c_{cgc} is necessary leading to the hydrogel containing polymer at concentrations above 20 wt-%. Well-known and intensively studied hydrogels can be built from closely packed PEO-*b*-PPO-*b*-PEO Pluronics® micelles consisting, at ambient temperatures, of a PPO micellar core and a hydrated PEO corona.[232]

The hydrogel formation in BAB systems takes place via the phase transition of the B-blocks, leading to flower-like micelles with a backfolded hydrophilic middle block (Figure 7B). At the c_{cgc} the “bridging effect” causes crosslinking of the micelles, in which the B-blocks of the

terpolymer are integrated in different micelles, which are linked by the hydrophilic middle block, which stabilises the hydrogel network. PEO is typically chosen as hydrophilic middle block.[233, 234] The group of Armes have even introduced an ionic biocompatible poly(2-methacryloyloxyethyl phosphorylcholine) middle block for different gelator systems.[235-237] In his recent review a detailed summary of various different BAB-type hydrogels is given.[238]

Star polymers represent another promising group of hydrogel gelators (Figure 7C). Due to their star-like architecture, each molecule can provide multiple connection sites. $(AB)_x$ diblock copolymer stars especially show a high potential for formation of physically cross-linked hydrogels.[202, 203, 239-243] In addition, star polymers can be used as gelators *via* host-guest systems. Recent studies showed β-cyclodextrin end-functionalized PEO star polymers interacting with their guest molecule-modified counterparts and forming a hydrogel.[244]

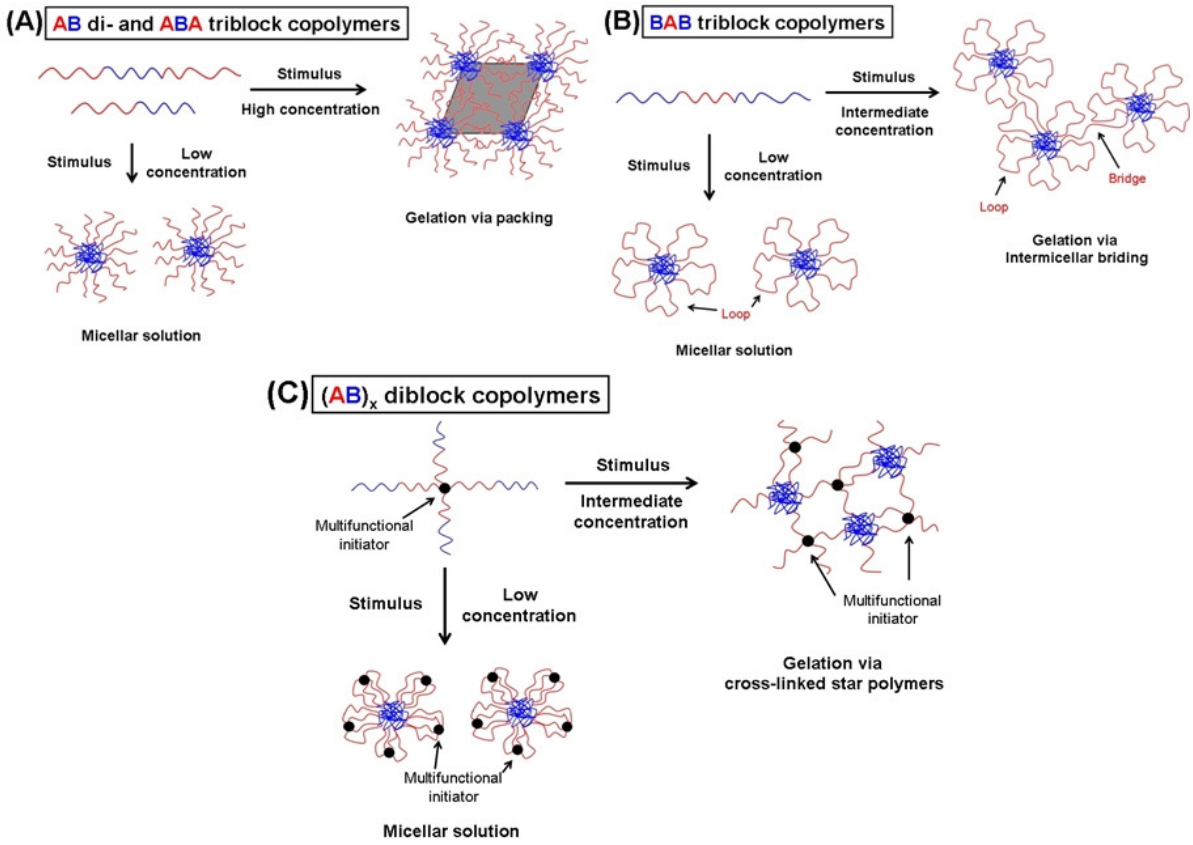

Figure 7. Aggregation and gelation mechanisms for stimulus-responsive AB/ABA diblock/triblock (A) and BAB triblock (B) and $(AB)_x$ diblock star (C) copolymers, in which A is the hydrophilic block and B is the stimulus-responisve block.

Multi-responsive systems, such as ABC triblock terpolymers, undergo an interesting gelation mechanism. Here, the middle block (B-block) resembles the hydrophilic part (Figure 8). The

A- and C-block are stimuli-responsive blocks, each sensitive to different environmental effects. Thus, these two blocks can be triggered separately, leading first to micelle formation before the insolubilization of the second responsive block causes physical cross-linking and hydrogel formation. This is similar to the bridging effect in the BAB mechanism, but this time whole micelles are involved in building the hydrogel network at the c_{cgc}, and the middle block serves as the connection between the micellar cores and the hydrogel junctions of the collapsed second stimuli-responsive block. Such ABC-systems were intensively studied by Reinicke *et al.*[194, 199] For instance, a hydrogel consisting of P2VP-*b*-PEO-*b*-poly(glycidyl methyl ether-*co*-ethyl glycidyl ether) (P(GME-*co*-EGE)) triblock terpolymer was synthesized showing both a pH-responsive P2VP block and a temperature-responsive P(GME-*co*-EGE) block. Other dual-responsive ABC systems with different compositions were also shown to undergo hydrogel formation.[235, 245, 246]

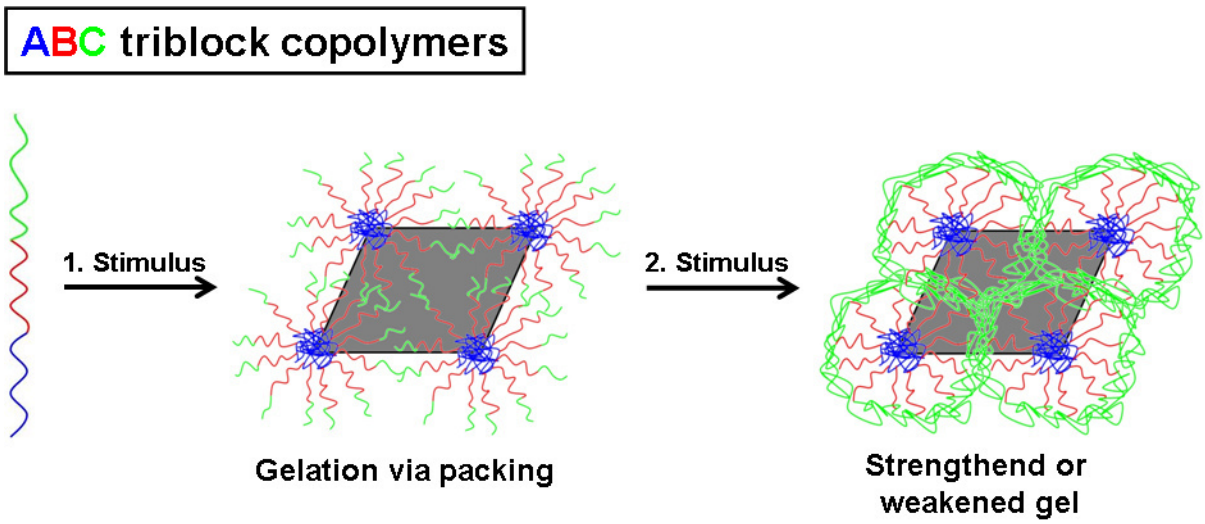

Figure 8. Gelation mechanism for ABC triblock terpolymers, where B is the hydrophilic block; A and C are the independently switchable stimuli-responsive blocks.

Another method of introducing a second stimulus within a hydrogel network is through ABCBA pentablock terpolymers. Studies on dual-responsive hydrogels are rare and there exist even less examples of completely hydrophilic switchable dual-responsive pentablock copolymers used in hydrogels. This is certainly due to the difficulties in synthesis of such polymers and their resulting rather complex structures. A simple way to create an ABCBA pentablock terpolymers, however, is by taking advantage of a PEO-*b*-PPO-*b*-PEO Pluronic® terpolymer functionalized with initiating sites on both ends for further polymerization.[247, 248] This approach was used by Determan *et al.* for copolymerization of DMAEMA and

DEAEMA, respectively. The micellar assembly and hydrogen properties of the resulting modified Pluronics® polymers were investigated, showing an increased functionality for biomedical applications.[249] Other possibilities were shown by Beheshti *et al.*,[250] who investigated an ABCBA hydrogel system consisting of two anionic poly(sodium 4-styrenesulfonate) (PSSS) A-blocks, two thermosensitive PNIPAAm B-blocks and a PEO middle block; or the group of Lee, who intensively investigated a dual-responsive ABCBA pentablock terpolymer consisting of a thermo-responsive biodegradable polyester block copolymer BCB inner segment (poly(ε-caprolactone-*co*-lactide)-*b*-PEO-*b*-poly(ε-caprolactone-*co*-lactide) (PCLA-PEO-PCLA) or poly(ε-caprolactone-*co*-glycolide)-*b*-PEO-*b*-poly(ε-caprolactone-*co*-glycolide) (PCGA-PEO-PCGA)), with pH-sensitive oligomeric sulfomethazine (OSM) A-blocks.[251-253] Another example with interesting gelation behavior is given by Tsitsilianis *et. al*., who synthesized an ABCBA pentablock terpolymer with two permanently hydrophobic PMMA A-blocks and a polyampholyte triblock as potential bridging middle chain (PMMA-*b*-PAA-*b*-P2VP-*b*-PAA-*b*-PMMA).[254]

1.5. Aim of the Thesis

The design of functional (nano)materials based on responsive polymers is a fast developing and interesting field of research. These materials exhibit either ionic and/or non-ionic functionalities, which can respond to a large variety of outer stimuli such as temperature, pH, light, etc. This in turn provides the access to applications ranging from biomedicine to coatings and switchable membranes.

The motivation of this work was combining water-soluble functional polymers, in particular PDMAEMA, with either inorganic components or other water-soluble and/or stimuli-responsive polymers to develop systems, which would lead to potential applications in aqueous media.

Since PDMAEMA reveals polycationic character at physiological pH, it is regarded as a potential nonviral gene vector. PDMAEMA applied as a star-like architecture shows superior properties (higher transfection efficiency, lower cytotoxicity) in gene delivery in comparison to its linear counterpart. Thus, one focus of this thesis was the development of star-like PDMAEMA-based gene vectors, which show additional response to an applied magnetic field for enhancing the application range, *i.e.* magnetic cell separation. For this purpose, PDMAEMA grafted superparamagnetic iron oxide nanoparticles can be obtained *via* different surface modification methods of the nanoparticles' surface and controlled polymerization

techniques (*e.g.*, ATRP). The developed approach should result in well-defined nanohybrid gene vectors, which have to be investigated with respect to their stability and complexation behavior with pDNA, but particularly as gene vector for transfection of eukaryotic cells and moreover, the response of the transfected cells within an applied magnetic field for enabling a magnetically driven cell separation.

Another goal of this thesis was to apply the dual-responsive character of PDMAEMA for hydrogels, which include two independently switchable responsive water-soluble polymers. Such challenging systems are commonly based on ABC or ABCBA block copolymers and are hard to achieve as well as to characterize resulting in a field of research, which still lacks diversity. Here, the intention is the synthesis of double-switchable amphiphilic ABCBA pentablock terpolymers containing a water-soluble C middle block, and separately switchable pH and/or temperature responsive A- and B-blocks. The target is the investigation of the aggregation and gelation behavior of these systems in dilute and concentrated solutions.

1.6. References

(1) Reddy, L. H.; Arias, J. L.; Nicolas, J.; Couvreur, P. *Chem. Rev.* **2012**, *112*, 5818-5878.

(2) Laurent, S.; Forge, D.; Port, M.; Roch, A.; Robic, C.; Vander Elst, L.; Muller, R. N. *Chem. Rev.* **2008**, *108*, 2064-2110.

(3) Odenbach, S., *Colloidal magnetic fluids: basics, development and application of ferrofluids*. Springer: Berlin Heidelberg, 2009; Vol. 763, p 430.

(4) Fortin, J.-P.; Wilhelm, C.; Servais, J.; Ménager, C.; Bacri, J.-C.; Gazeau, F. *J. Am. Chem. Soc.* **2007**, *129*, 2628-2635.

(5) Lévy, M.; Wilhelm, C.; Siaugue, J.-M.; Horner, O.; Bacri, J.-C.; Gazeau, F. *J. Phys.: Condens. Matter* **2008**, *20*, 204133.

(6) Messing, R.; Frickel, N.; Belkoura, L.; Strey, R.; Rahn, H.; Odenbach, S.; Schmidt, A. M. *Macromolecules* **2011**, *44*, 2990-2999.

(7) Behrens, S. *Nanoscale* **2011**, *3*, 877-892.

(8) Kim, D. K.; Zhang, Y.; Voit, W.; Rao, K. V.; Muhammed, M. *J. Magn. Magn. Mater.* **2001**, *225*, 30-36.

(9) Kim, D. K.; Mikhaylova, M.; Zhang, Y.; Muhammed, M. *Chem. Mater.* **2003**, *15*, 1617-1627.

(10) Lin, C.-L.; Lee, C.-F.; Chiu, W.-Y. *J. Colloid Interface Sci.* **2005**, *291*, 411-420.

(11) Kim, D. K.; Mikhaylova, M.; Wang, F. H.; Kehr, J.; Bjelke, B. r.; Zhang, Y.; Tsakalakos, T.; Muhammed, M. *Chem. Mater.* **2003**, *15*, 4343-4351.

(12) Yuan, Y.; Rende, D.; Altan, C. L.; Bucak, S.; Ozisik, R.; Borca-Tasciuc, D.-A. *Langmuir* **2012**, *28*, 13051-13059.

(13) Kotsmar, C.; Yoon, K. Y.; Yu, H.; Ryoo, S. Y.; Barth, J.; Shao, S.; Prodanović , M.; Milner, T. E.; Bryant, S. L.; Huh, C.; Johnston, K. P. *Ind. Eng. Chem. Res.* **2010**, *49*, 12435-12443.

(14) Kaittanis, C.; Banerjee, T.; Santra, S.; Santiesteban, O. J.; Teter, K.; Perez, J. M. *Bioconjugate Chem.* **2011**, *22*, 307-314.

(15) Gelbrich, T.; Feyen, M.; Schmidt, A. M. *Macromolecules* **2006**, *39*, 3469-3472.

(16) Bacri, J. C.; Perzynski, R.; Salin, D.; Cabuil, V.; Massart, R. *J. Magn. Magn. Mater.* **1986**, *62*, 36-46.

(17) Massart, R. *IEEE Trans. Magn.* **1981**, *17*, 1247-1248.

(18) Viota, J. L.; Durán, J. D. G.; González-Caballero, F.; Delgado, A. V. *J. Magn. Magn. Mater.* **2007**, *314*, 80-86.

(19) López-López, M. T.; Durán, J. D. G.; Delgado, A. V.; González-Caballero, F. *J. Colloid Interface Sci.* **2005**, *291*, 144-151.

(20) Gribanov, N. M.; Bibik, E. E.; Buzunov, O. V.; Naumov, V. N. *J. Magn. Magn. Mater.* **1990**, *85*, 7-10.

(21) Li, L.; Mak, K. Y.; Leung, C. W.; Chan, K. Y.; Chan, W. K.; Zhong, W.; Pong, P. W. T. *Microelectron. Eng.* **2013**, in press.

(22) Hyeon, T.; Lee, S. S.; Park, J.; Chung, Y.; Na, H. B. *J. Am. Chem. Soc.* **2001**, *123*, 12798-12801.

(23) Park, J.; An, K.; Hwang, Y.; Park, J.-G.; Noh, H.-J.; Kim, J.-Y.; Park, J.-H.; Hwang, N.-M.; Hyeon, T. *Nat. Mater.* **2004**, *3*, 891-895.

(24) da Costa, G. M.; De Grave, E.; de Bakker, P. M. A.; Vandenberghe, R. E. *J. Solid State Chem.* **1994**, *113*, 405-412.

(25) Itoh, H.; Sugimoto, T. *J. Colloid Interface Sci.* **2003**, *265*, 283-295.

(26) Khollam, Y. B.; Dhage, S. R.; Potdar, H. S.; Deshpande, S. B.; Bakare, P. P.; Kulkarni, S. D.; Date, S. K. *Mater. Lett.* **2002**, *56*, 571-577.

(27) Chen, F.; Gao, Q.; Hong, G.; Ni, J. *J. Magn. Magn. Mater.* **2008**, *320*, 1775-1780.

(28) Salazar-Alvarez, G.; Muhammed, M.; Zagorodni, A. A. *Chem. Eng. Sci.* **2006**, *61*, 4625-4633.

(29) Cabrera, L.; Gutierrez, S.; Menendez, N.; Morales, M. P.; Herrasti, P. *Electrochim. Acta* **2008**, *53*, 3436-3441.

(30) Marques, R. F. C.; Garcia, C.; Lecante, P.; Ribeiro, S. J. L.; Noé, L.; Silva, N. J. O.; Amaral, V. S.; Millán, A.; Verelst, M. *J. Magn. Magn. Mater.* **2008**, *320*, 2311-2315.

(31) Strobel, R.; Pratsinis, S. E. *Adv. Powder Technol.* **2009**, *20*, 190-194.

(32) González-Carreño, T.; Morales, M. P.; Gracia, M.; Serna, C. J. *Mater. Lett.* **1993**, *18*, 151-155.

(33) Enomoto, N.; Akagi, J.; Nakagawa, Z. *Ultrason. Sonochem.* **1996**, *3*, S97-S103.

(34) Dang, F.; Enomoto, N.; Hojo, J.; Enpuku, K. *Ultrason. Sonochem.* **2009**, *16*, 649-654.

(35) Lam, U. T.; Mammucari, R.; Suzuki, K.; Foster, N. R. *Ind. Eng. Chem. Res.* **2008**, *47*, 599-614.

(36) Breulmann, M.; Cölfen, H.; Hentze, H.-P.; Antonietti, M.; Walsh, D.; Mann, S. *Adv. Mater.* **1998**, *10*, 237-241.

(37)Abu Bakar, M.; Tan, W. L.; Abu Bakar, N. H. H. *J. Magn. Magn. Mater.* **2007**, *314*, 1-6.

(38) Narayanan, K. B.; Sakthivel, N. *Adv. Colloid Interface Sci.* **2010**, *156*, 1-13.

(39) Moon, J.-W.; Roh, Y.; Lauf, R. J.; Vali, H.; Yeary, L. W.; Phelps, T. J. *J. Microbiol. Methods* **2007**, *70*, 150-158.

(40) Moon, J.-W.; Rawn, C.; Rondinone, A.; Love, L.; Roh, Y.; Everett, S. M.; Lauf, R.; Phelps, T. *J. Ind. Microbiol. Biotechnol.* **2010**, *37*, 1023-1031.

(41) Qiao, R.; Yang, C.; Gao, M. *J. Mater. Chem.* **2009**, *19*, 6274-6293.

(42) Ansari, F.; Grigoriev, P.; Libor, S.; Tothill, I. E.; Ramsden, J. J. *Biotechnol. Bioeng.* **2009**, *102*, 1505-1512.

(43) Di Corato, R.; Piacenza, P.; Musarò, M.; Buonsanti, R.; Cozzoli, P. D.; Zambianchi, M.; Barbarella, G.; Cingolani, R.; Manna, L.; Pellegrino, T. *Macromol. Biosci.* **2009**, *9*, 952-958.

(44) Hou, C.-H.; Hou, S.-M.; Hsueh, Y.-S.; Lin, J.; Wu, H.-C.; Lin, F.-H. *Biomaterials* **2009**, *30*, 3956-3960.

(45) Kievit, F. M.; Zhang, M. *Acc. Chem. Res.* **2011**, *44*, 853-862.

(46) Day, E. S.; Morton, J. G.; West, J. L. *J. Biomech. Eng.* **2009**, *131*, 074001-5.

(47) Hao, R.; Xing, R.; Xu, Z.; Hou, Y.; Gao, S.; Sun, S. *Adv. Mater.* **2010**, *22*, 2729-2742.

(48) Gupta, A. K.; Gupta, M. *Biomaterials* **2005**, *26*, 3995-4021.

(49) Quan, Q.; Xie, J.; Gao, H.; Yang, M.; Zhang, F.; Liu, G.; Lin, X.; Wang, A.; Eden, H. S.; Lee, S.; Zhang, G.; Chen, X. *Mol. Pharm.* **2011**, *8*, 1669-1676.

(50) Mahmoudi, M.; Simchi, A.; Imani, M.; Häfeli, U. O. *J. Phys. Chem. C* **2009**, *113*, 8124-8131.

(51) Plank, C.; Zelphati, O.; Mykhaylyk, O. *Adv. Drug Delivery Rev.* **2011**, *63*, 1300-1331.

(52) Corchero, J. L.; Villaverde, A. *Trends Biotechnol.* **2009**, *27*, 468-476.

(53) Kami, D.; Takeda, S.; Itakura, Y.; Gojo, S.; Watanabe, M.; Toyoda, M. *Int. J. Mol. Sci.* **2011**, *12*, 3705-3722.

(54) Liu, W.-M.; Xue, Y.-N.; Peng, N.; He, W.-T.; Zhuo, R.-X.; Huang, S.-W. *J. Mater. Chem.* **2011**, *21*, 13306-13315.

(55) Bhattarai, S. R.; Kim, S. Y.; Jang, K. Y.; Lee, K. C.; Yi, H. K.; Lee, D. Y.; Kim, H. Y.; Hwang, P. H. *Nanomedicine: NBM* **2008**, *4*, 146-154.

(56) Majewski, A. P.; Schallon, A.; Jérôme, V.; Freitag, R.; Müller, A. H. E.; Schmalz, H. *Biomacromolecules* **2012**, *13*, 857-866.

(57) Hasany, S. F.; Rehman, A.; Jose, R.; Ahmed, I. *AIP Conf. Proc.* **2012**, *1502*, 298-321.

(58) Mou, X.; Wei, X.; Li, Y.; Shen, W. *CrystEngComm* **2012**, *14*, 5107-5120.

(59) Nagireddy, N.; Yallapu, M.; Kokkarachedu, V.; Sakey, R.; Kanikireddy, V.; Pattayil Alias, J.; Konduru, M. *J. Polym. Res.* **2011**, *18*, 2285-2294.

(60) Zhang, Y.; Yang, B.; Zhang, X.; Xu, L.; Tao, L.; Li, S.; Wei, Y. *Chem. Commun.* **2012**, *48*, 9305-9307.

(61) Ilg, P. *Soft Matter* **2013**, *9*, 3465-3468.

(62) Caykara, T.; Yörük, D.; Demirci, S. *J. Appl. Polym. Sci.* **2009**, *112*, 800-804.

(63) Berkovsky, B. M.; Bashtovoy, V. G., *Magnetic Fluids and Applications Handbook*. Begell House: New York, 1996.

(64) Zahn, M. *J. Nanopart. Res.* **2001**, *3*, 73-78.

(65) Xu, C.; Xu, K.; Gu, H.; Zheng, R.; Liu, H.; Zhang, X.; Guo, Z.; Xu, B. *J. Am. Chem. Soc.* **2004**, *126*, 9938-9939.

(66) Dong, H.; Huang, J.; Koepsel, R. R.; Ye, P.; Russell, A. J.; Matyjaszewski, K. *Biomacromolecules* **2011**, *12*, 1305-1311.

(67) Marcelo, G.; Munoz-Bonilla, A.; Rodriguez-Hernandez, J.; Fernandez-Garcia, M. *Polym. Chem.* **2013**, *4*, 558-567.

(68) Goldmann, A. S.; Schödel, C.; Walther, A.; Yuan, J.; Loos, K.; Müller, A. H. E. *Macromol. Rapid Commun.* **2010**, *31*, 1608-1615.

(69) Frickel, N.; Messing, R.; Gelbrich, T.; Schmidt, A. M. *Langmuir* **2009**, *26*, 2839-2846.

(70) Flesch, C.; Delaite, C.; Dumas, P.; Bourgeat-Lami, E.; Duguet, E. *J. Polym. Sci., Part A: Polym. Chem.* **2004**, *42*, 6011-6020.

(71) Frickel, N.; Messing, R.; Gelbrich, T.; Schmidt, A. M. *Langmuir* **2010**, *26*, 2839-2846.

(72) Gelbrich, T.; Reinartz, M.; Schmidt, A. M. *Biomacromolecules* **2010**, *11*, 635-642.

(73) Graf, C.; Vossen, D. L. J.; Imhof, A.; van Blaaderen, A. *Langmuir* **2003**, *19*, 6693-6700.

(74) Hartlen, K. D.; Athanasopoulos, A. P. T.; Kitaev, V. *Langmuir* **2008**, *24*, 1714-1720.

(75) Stöber, W.; Fink, A.; Bohn, E. *J. Colloid Interface Sci.* **1968**, *26*, 62-69.

(76) Pfaff, A.; Schallon, A.; Ruhland, T. M.; Majewski, A. P.; Schmalz, H.; Freitag, R.; Müller, A. H. E. *Biomacromolecules* **2011**, *12*, 3805-3811.

(77) Ruhland, T. M.; Reichstein, P. M.; Majewski, A. P.; Walther, A.; Müller, A. H. E. *J. Colloid Interface Sci.* **2012**, *374*, 45-53.

(78)Ding, H. L.; Zhang, Y. X.; Wang, S.; Xu, J. M.; Xu, S. C.; Li, G. H. *Chem. Mater.* **2012**, *24*, 4572-4580.

(79) Nikolic, M. S.; Krack, M.; Aleksandrovic, V.; Kornowski, A.; Förster, S.; Weller, H. *Angew. Chem., Int. Ed.* **2006**, *45*, 6577-6580.

(80) Xu, C.; Sun, S. *Polym. Int.* **2007**, *56*, 821-826.

(81) Boyer, C.; Priyanto, P.; Davis, T. P.; Pissuwan, D.; Bulmus, V.; Kavallaris, M.; Teoh, W. Y.; Amal, R.; Carroll, M.; Woodward, R.; St Pierre, T. *J. Mater. Chem.* **2010**, *20*, 255-265.

(82) Gravano, S. M.; Dumas, R.; Liu, K.; Patten, T. E. *J. Polym. Sci., Part A: Polym. Chem.* **2005**, *43*, 3675-3688.

(83) Zhao, B.; Brittain, W. J. *Prog. Polym. Sci.* **2000**, *25*, 677-710.

(84)Saleh, N.; Phenrat, T.; Sirk, K.; Dufour, B.; Ok, J.; Sarbu, T.; Matyjaszewski, K.; Tilton, R. D.; Lowry, G. V. *Nano Lett.* **2005**, *5*, 2489-2494.

(85) Amstad, E.; Gillich, T.; Bilecka, I.; Textor, M.; Reimhult, E. *Nano Lett.* **2009**, *9*, 4042-4048.

(86) Amstad, E.; Gehring, A. U.; Fischer, H.; Nagaiyanallur, V. V.; Hähner, G.; Textor, M.; Reimhult, E. *J. Phys. Chem. C* **2011**, *115*, 683-691.

(87) Tchoul, M. N.; Dalton, M.; Tan, L.-S.; Dong, H.; Hui, C. M.; Matyjaszewski, K.; Vaia, R. A. *Polymer* **2012**, *53*, 79-86.

(88) Vestal, C. R.; Zhang, Z. J. *J. Am. Chem. Soc.* **2002**, *124*, 14312-14313.

(89) Frickel, N.; Gottlieb, M.; Schmidt, A. M. *Polymer* **2011**, *52*, 1781-1787.

(90) Hansson, S.; Trouillet, V.; Tischer, T.; Goldmann, A. S.; Carlmark, A.; Barner-Kowollik, C.; Malmström, E. *Biomacromolecules* **2013**, *14*, 64-74.

(91) Garcia, I.; Zafeiropoulos, N. E.; Janke, A.; Tercjak, A.; Eceiza, A.; Stamm, M.; Mondragon, I. *J. Polym. Sci., Part A: Polym. Chem.* **2007**, *45*, 925-932.

(92)Guo, Z.; Chen, Y.; Zhou, W.; Huang, Z.; Hu, Y.; Wan, M.; Bai, F. *Mater. Lett.* **2008**, *62*, 4542-4544.

(93) Liu, B.; Zhang, D.; Wang, J.; Chen, C.; Yang, X.; Li, C. *J. Phys. Chem. C* **2013**, *117*, 6363-6372.

(94)Huynh, V. T.; Pearson, S.; Noy, J.-M.; Abboud, A.; Utama, R. H.; Lu, H.; Stenzel, M. H. *ACS Macro Letters* **2013**, *2*, 246-250.

(95) Tastet, D.; Save, M.; Charrier, F.; Charrier, B.; Ledeuil, J.-B.; Dupin, J.-C.; Billon, L. *Polymer* **2011**, *52*, 606-616.

(96) Huang, Y.; Liu, Q.; Zhou, X.; Perrier, S. b.; Zhao, Y. *Macromolecules* **2009**, *42*, 5509-5517.

(97) Chevigny, C.; Gigmes, D.; Bertin, D.; Jestin, J.; Boué, F. *Soft Matter* **2009**, *5*, 3741-3753.

(98) Blas, H.; Save, M.; Boissière, C.; Sanchez, C.; Charleux, B. *Macromolecules* **2011**, *44*, 2577-2588.

(99) Chevigny, C.; Gigmes, D.; Bertin, D.; Schweins, R.; Jestin, J.; Boué, F. *Polym. Chem.* **2011**, *2*, 567-571.

(100) Jordan, R.; West, N.; Ulman, A.; Chou, Y.-M.; Nuyken, O. *Macromolecules* **2001**, *34*, 1606-1611.

(101) Talelli, M.; Rijcken, C. J. F.; Lammers, T.; Seevinck, P. R.; Storm, G.; van Nostrum, C. F.; Hennink, W. E. *Langmuir* **2009**, *25*, 2060-2067.

(102) Reinicke, S.; Döhler, S.; Tea, S.; Krekhova, M.; Messing, R.; Schmidt, A. M.; Schmalz, H. *Soft Matter* **2010**, *6*, 2760-2773.

(103) Mistlberger, G.; Koren, K.; Scheucher, E.; Aigner, D.; Borisov, S. M.; Zankel, A.; Pölt, P.; Klimant, I. *Adv. Funct. Mater.* **2010**, *20*, 1842-1851.

(104) Niu, D.; Li, Y.; Ma, Z.; Diao, H.; Gu, J.; Chen, H.; Zhao, W.; Ruan, M.; Zhang, Y.; Shi, J. *Adv. Funct. Mater.* **2010**, *20*, 773-780.

(105) Qiu, P.; Jensen, C.; Charity, N.; Towner, R.; Mao, C. *J. Am. Chem. Soc.* **2010**, *132*, 17724-17732.

(106) Kim, G.-C.; Li, Y.-Y.; Chu, Y.-F.; Cheng, S.-X.; Zhang, X.-Z.; Zhuo, R.-X. *J. Biomater. Sci., Polym. Ed.* **2008**, *19*, 1249-1259.

(107) Schmidt, A. M. *Colloid Polym. Sci.* **2007**, *285*, 953-966.

(108) Chanana, M.; Jahn, S.; Georgieva, R.; Lutz, J.-F.; Bäumler, H.; Wang, D. *Chem. Mater.* **2009**, *21*, 1906-1914.

(109) Nash, M. A.; Lai, J. J.; Hoffman, A. S.; Yager, P.; Stayton, P. S. *Nano Lett.* **2010**, *10*, 85-91.

(110) Boussif, O.; Lezoualc'h, F.; Zanta, M. A.; Mergny, M. D.; Scherman, D.; Demeneix, B.; Behr, J. P. *Proc. Natl. Acad. Sci. U.S.A.* **1995**, *92*, 7297-7301.

(111) Mintzer, M. A.; Simanek, E. E. *Chem. Rev.* **2008**, *109*, 259-302.

(112) Kim, Y.-K.; Kwon, J.-T.; Jiang, H.-L.; Choi, Y.-J.; Cho, M.-H.; Cho, C.-S. *J. Nanosci. Nanotechnol.* **2012**, *12*, 5149-5154.

(113) Schallon, A.; Synatschke, C. V.; Jérôme, V.; Müller, A. H. E.; Freitag, R. *Biomacromolecules* **2012**, *13*, 3463-3474.

(114) Uchida, E.; Mizuguchi, H.; Ishii-Watabe, A.; Hayakawa, T. *Biol. Pharm. Bull.* **2002**, *25*, 891-897.

(115) Bloomfield, V. A. *Biopolymers* **1997**, *44*, 269-282.

(116) Yue, Y.; Wu, C. *Biomater. Sci.* **2013**, *1*, 152-170.

(117) Xiang, S.; Tong, H.; Shi, Q.; Fernandes, J. C.; Jin, T.; Dai, K.; Zhang, X. *J. Control. Release* **2012**, *158*, 371-378.

(118) Pichon, C.; Billiet, L.; Midoux, P. *Curr. Opin. Biotechnol.* **2010**, *21*, 640-645.

(119) Yue, Y.; Jin, F.; Deng, R.; Cai, J.; Chen, Y.; Lin, M. C. M.; Kung, H.-F.; Wu, C. *J. Control. Release* **2011**, *155*, 67-76.

(120) Yue, Y.; Jin, F.; Deng, R.; Cai, J.; Dai, Z.; Lin, M. C. M.; Kung, H.-F.; Mattebjerg, M. A.; Andresen, T. L.; Wu, C. *J. Control. Release* **2011**, *152*, 143-151.

(121) Boeckle, S.; von Gersdorff, K.; van der Piepen, S.; Culmsee, C.; Wagner, E.; Ogris, M. *J. Gene Med.* **2004**, *6*, 1102-1111.

(122) Fahrmeir, J.; Gunther, M.; Tietze, N.; Wagner, E.; Ogris, M. *J. Control. Release* **2007**, *122*, 236-245.

(123) Won, Y.-Y.; Sharma, R.; Konieczny, S. F. *J. Control. Release* **2009**, *139*, 88-93.

(124) Funhoff, A. M.; van Nostrum, C. F.; Koning, G. A.; Schuurmans-Nieuwenbroek, N. M. E.; Crommelin, D. J. A.; Hennink, W. E. *Biomacromolecules* **2003**, *5*, 32-39.

(125) Forrest, M. L.; Meister, G.; Koerber, J.; Pack, D. *Pharm. Res.* **2004**, *21*, 365-371.

(126) Sundararajan, R. *Mol. Biotechnol.* **2009**, *41*, 69-82.

(127) Chou, T.-h. W.; Biswas, S.; Lu, S., In *Gene Delivery to Mammalian Cells: Volume 1: Nonviral Gene Transfer Techniques*, Heiser, W. C., Ed. Humana Press Inc.: Totowa, 2003; Vol. 245, pp 147-165.

(128) Park, T. G.; Jeong, J. H.; Kim, S. W. *Adv. Drug Delivery Rev.* **2006**, *58*, 467-486.

(129) Elsabahy, M.; Nazarali, A.; Foldvari, M. *Curr. Drug Delivery* **2011**, *8*, 235-244.

(130) During, M. J. *Adv. Drug Delivery Rev.* **1997**, *27*, 83-94.

(131) Hacein-Bey-Abina, S.; Von Kalle, C.; Schmidt, M.; McCormack, M. P.; Wulffraat, N.; Leboulch, P.; Lim, A.; Osborne, C. S.; Pawliuk, R.; Morillon, E.; Sorensen, R.; Forster, A.; Fraser, P.; Cohen, J. I.; de Saint Basile, G.; Alexander, I.; Wintergerst, U.; Frebourg, T.; Aurias, A.; Stoppa-Lyonnet, D.; Romana, S.; Radford-Weiss, I.; Gross, F.; Valensi, F.; Delabesse, E.; Macintyre, E.; Sigaux, F.; Soulier, J.; Leiva, L. E.; Wissler, M.; Prinz, C.; Rabbitts, T. H.; Le Deist, F.; Fischer, A.; Cavazzana-Calvo, M. *Science* **2003**, *302*, 415-419.

(132) Borchard, G. *Adv. Drug Delivery Rev.* **2001**, *52*, 145-150.

(133) Liu, Y.; Wenning, L.; Lynch, M.; Reineke, T. M. *J. Am. Chem. Soc.* **2004**, *126*, 7422-7423.

(134) Ignatovich, I. A.; Dizhe, E. B.; Pavlotskaya, A. V.; Akifiev, B. N.; Burov, S. V.; Orlov, S. V.; Perevozchikov, A. P. *J. Biol. Chem.* **2003**, *278*, 42625-42636.

(135) Haensler, J.; Szoka, F. C. *Bioconjugate Chem.* **1993**, *4*, 372-379.

(136) Lee, J. H.; Lim, Y.-B.; Choi, J. S.; Lee, Y.; Kim, T.-I.; Kim, H. J.; Yoon, J. K.; Kim, K.; Park, J.-S. *Bioconjugate Chem.* **2003**, *14*, 1214-1221.

(137) Kim, T.-I.; Seo, H. J.; Choi, J. S.; Jang, H.-S.; Baek, J.-U.; Kim, K.; Park, J.-S. *Biomacromolecules* **2004**, *5*, 2487-2492.

(138) Luo, D.; Haverstick, K.; Belcheva, N.; Han, E.; Saltzman, W. M. *Macromolecules* **2002**, *35*, 3456-3462.

(139) Kabanov, V. A.; Zezin, A. B.; Rogacheva, V. B.; Gulyaeva, Z. G.; Zansochova, M. F.; Joosten, J. G. H.; Brackman, J. *Macromolecules* **1999**, *32*, 1904-1909.

(140) Schatzlein, A. G.; Zinselmeyer, B. H.; Elouzi, A.; Dufes, C.; Chim, Y. T. A.; Roberts, C. J.; Davies, M. C.; Munro, A.; Gray, A. I.; Uchegbu, I. F. *J. Control. Release* **2005**, *101*, 247-258.

(141) Kim, T.-I.; Baek, J.-U.; Zhe Bai, C.; Park, J.-S. *Biomaterials* **2007**, *28*, 2061-2067.

(142) Krska, S. W.; Seyferth, D. *J. Am. Chem. Soc.* **1998**, *120*, 3604-3612.

(143) Ortega, P.; Bermejo, J. F.; Chonco, L.; de Jesus, E.; de la Mata, F. J.; Fernández, G.; Flores, J. C.; Gómez, R.; Serramía, M. J.; Muñoz-Fernandez, M. A. *Eur. J. Inorg. Chem.* **2006**, *2006*, 1388-1396.

(144) Bermejo, J. F.; Ortega, P.; Chonco, L.; Eritja, R.; Samaniego, R.; Müllner, M.; de Jesus, E.; de la Mata, F. J.; Flores, J. C.; Gomez, R.; Muñoz-Fernandez, A. *Chemistry – A European Journal* **2007**, *13*, 483-495.

(145) Kaneshiro, T. L.; Wang, X.; Lu, Z.-R. *Mol. Pharm.* **2007**, *4*, 759-768.

(146) Inoue, Y.; Kurihara, R.; Tsuchida, A.; Hasegawa, M.; Nagashima, T.; Mori, T.; Niidome, T.; Katayama, Y.; Okitsu, O. *J. Control. Release* **2008**, *126*, 59-66.

(147) Fuller, W. D.; Verlander, M. S.; Goodman, M. *Biopolymers* **1976**, *15*, 1869-1871.

(148) Choi, Y. H.; Liu, F.; Kim, J.-S.; Choi, Y. K.; Jong Sang, P.; Kim, S. W. *J. Control. Release* **1998**, *54*, 39-48.

(149) Harada, A.; Togawa, H.; Kataoka, K. *Eur. J. Pharm. Sci.* **2001**, *13*, 35-42.

(150) Katayose, S.; Kataoka, K. *Bioconjugate Chem.* **1997**, *8*, 702-707.

(151) Lee, M.; Han, S.-O.; Ko, K. S.; Koh, J. J.; Park, J.-S.; Yoon, J.-W.; Kim, S. W. *Mol. Ther.* **2001**, *4*, 339-346.

(152) Kakizawa, Y.; Harada, A.; Kataoka, K. *Biomacromolecules* **2001**, *2*, 491-497.

(153) Parhamifar, L.; Larsen, A. K.; Hunter, A. C.; Andresen, T. L.; Moghimi, S. M. *Soft Matter* **2010**, *6*, 4001-4009.

(154) Synatschke, C. V.; Schallon, A.; Jérôme, V.; Freitag, R.; Müller, A. H. E. *Biomacromolecules* **2011**, *12*, 4247-4255.

(155) Fischer, D.; Li, Y.; Ahlemeyer, B.; Krieglstein, J.; Kissel, T. *Biomaterials* **2003**, *24*, 1121-1131.

(156) Hunter, A. C. *Adv. Drug Delivery Rev.* **2006**, *58*, 1523-1531.

(157) Agarwal, S.; Zhang, Y.; Maji, S.; Greiner, A. *Mater. Today* **2012**, *15*, 388-393.

(158) Chollet, P.; Favrot, M. C.; Hurbin, A.; Coll, J.-L. *J. Gene Med.* **2002**, *4*, 84-91.

(159) Ogris, M.; Brunner, S.; Schüller, S.; Kircheis, R.; Wagner, E. *Gene Ther.* **1999**, *6*, 595-605.

(160) Merdan, T.; Kunath, K.; Petersen, H.; Bakowsky, U.; Voigt, K. H.; Kopecek, J.; Kissel, T. *Bioconjugate Chem.* **2005**, *16*, 785-792.

(161) Park, M. R.; Han, K. O.; Han, I. K.; Cho, M. H.; Nah, J. W.; Choi, Y. J.; Cho, C. S. *J. Control. Release* **2005**, *105*, 367-380.

(162) Funhoff, A. M.; Monge, S.; Teeuwen, R.; Koning, G. A.; Schuurmans-Nieuwenbroek, N. M. E.; Crommelin, D. J. A.; Haddleton, D. M.; Hennink, W. E.; van Nostrum, C. F. *J. Control. Release* **2005**, *102*, 711-724.

(163) Qian, Y.; Zha, Y.; Feng, B.; Pang, Z.; Zhang, B.; Sun, X.; Ren, J.; Zhang, C.; Shao, X.; Zhang, Q.; Jiang, X. *Biomaterials* **2013**, *34*, 2117-2129.

(164) Laus, M.; Sparnacci, K.; Ensoli, B.; Buttò, S.; Caputo, A.; Mantovani, I.; Zuccheri, G.; Samorì, B.; Tondelli, L. *J. Biomater. Sci., Polym. Ed.* **2001**, *12*, 209-228.

(165) Mathew, A.; Cao, H.; Collin, E.; Wang, W.; Pandit, A. *Int. J. Pharm.* **2012**, *434*, 99-105.

(166) Lin, S.; Du, F.; Wang, Y.; Ji, S.; Liang, D.; Yu, L.; Li, Z. *Biomacromolecules* **2008**, *9*, 109-115.

(167) Zhu, C.; Zheng, M.; Meng, F.; Mickler, F. M.; Ruthardt, N.; Zhu, X.; Zhong, Z. *Biomacromolecules* **2012**, *13*, 769-778.

(168) van de Wetering, P.; Cherng, J.-Y.; Talsma, H.; Crommelin, D. J. A.; Hennink, W. E. *J. Control. Release* **1998**, *53*, 145-153.

(169) Cherng, J.-Y.; van de Wetering, P.; Talsma, H.; Crommelin, D. J. A.; Hennink, W. E. *Pharm. Res.* **1996**, *13*, 1038-1042.

(170) van de Wetering, P.; Cherng, J.-Y.; Talsma, H.; Hennink, W. E. *J. Control. Release* **1997**, *49*, 59-69.

(171) Deshpande, M. C.; Davies, M. C.; Garnett, M. C.; Williams, P. M.; Armitage, D.; Bailey, L.; Vamvakaki, M.; Armes, S. P.; Stolnik, S. *J. Control. Release* **2004**, *97*, 143-156.

(172) Deshpande, M. C.; Garnett, M. C.; Vamvakaki, M.; Bailey, L.; Armes, S. P.; Stolnik, S. *J. Control. Release* **2002**, *81*, 185-199.

(173) Rungsardthong, U.; Deshpande, M.; Bailey, L.; Vamvakaki, M.; Armes, S. P.; Garnett, M. C.; Stolnik, S. *J. Control. Release* **2001**, *73*, 359-380.

(174) Schallon, A.; Jérôme, V.; Walther, A.; Synatschke, C. V.; Müller, A. H. E.; Freitag, R. *React. Funct. Polym.* **2010**, *70*, 1-10.

(175) Georgiou, T. K.; Vamvakaki, M.; Patrickios, C. S.; Yamasaki, E. N.; Phylactou, L. A. *Biomacromolecules* **2004**, *5*, 2221-2229.

(176) Xu, F. J.; Zhang, Z. X.; Ping, Y.; Li, J.; Kang, E. T.; Neoh, K. G. *Biomacromolecules* **2009**, *10*, 285-293.

(177) Gary, D. J.; Lee, H.; Sharma, R.; Lee, J.-S.; Kim, Y.; Cui, Z. Y.; Jia, D.; Bowman, V. D.; Chipman, P. R.; Wan, L.; Zou, Y.; Mao, G.; Park, K.; Herbert, B.-S.; Konieczny, S. F.; Won, Y.-Y. *ACS Nano* **2011**, *5*, 3493-3505.

(178) Sanchez, I. C.; Stone, M. T., *Polymer Blends Volume 1: Formulation*. John Wiley & Sons, Inc.: New York, 2000.

(179) Kuckling, D.; Urban, M. W., In *Handbook of Stimuli-Responsive Materials*, Urban, M. W., Ed. Wiley-VCH Verlag GmbH & Co. KGaA: Weinheim, 2011.

(180) Seuring, J.; Agarwal, S. *Macromol. Chem. Phys.* **2010**, *211*, 2109-2117.

(181) Plamper, F. A.; Ruppel, M.; Schmalz, A.; Borisov, O.; Ballauff, M.; Müller, A. H. E. *Macromolecules* **2007**, *40*, 8361-8366.

(182) Seuring, J.; Agarwal, S. *Macromol. Rapid Commun.* **2012**, *33*, 1898-1920.

(183) Wei, H.; Cheng, S.-X.; Zhang, X.-Z.; Zhuo, R.-X. *Prog. Polym. Sci.* **2009**, *34*, 893-910.

(184) Dimitrov, I.; Trzebicka, B.; Müller, A. H. E.; Dworak, A.; Tsvetanov, C. B. *Prog. Polym. Sci.* **2007**, *32*, 1275-1343.

(185) Šťastná, J.; Hanyková, L.; Spěváček, J. *Colloid Polym. Sci.* **2012**, *290*, 1811-1817.

(186) Cong, H.; Li, L.; Zheng, S. *Polymer* **2013**, *54*, 1370-1380.

(187) Schwartz, V. B.; Thétiot, F.; Ritz, S.; Pütz, S.; Choritz, L.; Lappas, A.; Förch, R.; Landfester, K.; Jonas, U. *Adv. Funct. Mater.* **2012**, *22*, 2376-2386.

(188) Zheng, Q.; Zheng, S. *J. Polym. Sci., Part A: Polym. Chem.* **2012**, *50*, 1717-1727.

(189) Guan, Y.; Zhang, Y. *Soft Matter* **2011**, *7*, 6375-6384.

(190) Munoz-Bonilla, A.; Fernandez-Garcia, M.; Haddleton, D. M. *Soft Matter* **2007**, *3*, 725-731.

(191) Han, D.; Tong, X.; Boissière, O.; Zhao, Y. *ACS Macro Letters* **2011**, *1*, 57-61.

(192) Lutz, J.-F.; Hoth, A. *Macromolecules* **2005**, *39*, 893-896.

(193) Ge, Z.; Zhou, Y.; Xu, J.; Liu, H.; Chen, D.; Liu, S. *J. Am. Chem. Soc.* **2009**, *131*, 1628-1629.

(194) Reinicke, S.; Schmalz, H. *Colloid Polym. Sci.* **2011**, *289*, 497-512.

(195) Pergushov, D. V.; Babin, I. A.; Plamper, F. A.; Schmalz, H.; Müller, A. H. E.; Zezin, A. B. *Dokl. Phys. Chem.* **2009**, *425*, 57-61.

(196) Schumacher, M.; Ruppel, M.; Kohlbrecher, J.; Burkhardt, M.; Plamper, F.; Drechsler, M.; Müller, A. H. E. *Polymer* **2009**, *50*, 1908-1917.

(197) Plamper, F. A.; Becker, H.; Lanzendörfer, M.; Patel, M.; Wittemann, A.; Ballauff, M.; Müller, A. H. E. *Macromol. Chem. Phys.* **2005**, *206*, 1813-1825.

(198) Reinicke, S.; Schmelz, J.; Lapp, A.; Karg, M.; Hellweg, T.; Schmalz, H. *Soft Matter* **2009**, *5*, 2648-2657.

(199) Reinicke, S.; Karg, M.; Lapp, A.; Heymann, L.; Hellweg, T.; Schmalz, H. *Macromolecules* **2010**, *43*, 10045-10054.

(200) Synatschke, C. V.; Schacher, F. H.; Fortsch, M.; Drechsler, M.; Müller, A. H. E. *Soft Matter* **2010**, *7*, 1714-1725.

(201) Schmalz, A.; Hanisch, M.; Schmalz, H.; Müller, A. H. E. *Polymer* **2010**, *51*, 1213-1217.

(202) Schmalz, A.; Schmalz, H.; Müller, A. H. E. *Soft Matter* **2012**, *8*, 9436-9445.

(203) Schmalz, A.; Schmalz, H.; Müller, A. H. E. *Z. Phys. Chem.* **2012**, *226*, 695-709.

(204) Tsitsilianis, C. *Soft Matter* **2010**, *6*, 2372-2388.

(205) Ahn, S.-K.; Kasi, R. M.; Kim, S.-C.; Sharma, N.; Zhou, Y. *Soft Matter* **2008**, *4*, 1151-1157.

(206) Rodríguez-Hernández, J.; Chécot, F.; Gnanou, Y.; Lecommandoux, S. *Prog. Polym. Sci.* **2005**, *30*, 691-724.

(207) Gil, E. S.; Hudson, S. M. *Prog. Polym. Sci.* **2004**, *29*, 1173-1222.

(208) Peppas, N. A.; Hilt, J. Z.; Khademhosseini, A.; Langer, R. *Adv. Mater.* **2006**, *18*, 1345-1360.

(209) Winnik, M. A.; Yekta, A. *Curr. Opin. Colloid Interface Sci.* **1997**, *2*, 424-436.

(210) Patel, A.; Mequanint, K., Hydrogel Biomaterials. In *Biomedical Engineering - Frontiers and Challenges*, Fazel, R., Ed. InTech: Rijeka, 2011; pp 275-296.

(211) Zhu, J. *Biomaterials* **2010**, *31*, 4639-4656.

(212) Kopecek, J. *J. Polym. Sci., Part A: Polym. Chem.* **2009**, *47*, 5929-5946.

(213) Kikuchi, A.; Okano, T. *Prog. Polym. Sci.* **2002**, *27*, 1165-1193.

(214) Lee, K. Y.; Mooney, D. J. *Chem. Rev.* **2001**, *101*, 1869-1880.

(215) Hart, D. S.; Gehrke, S. H. *J. Pharm. Sci.* **2007**, *96*, 484-516.

(216) Bae, S. J.; Joo, M. K.; Jeong, Y.; Kim, S. W.; Lee, W.-K.; Sohn, Y. S.; Jeong, B. *Macromolecules* **2006**, *39*, 4873-4879.

(217) Bae, S. J.; Suh, J. M.; Sohn, Y. S.; Bae, Y. H.; Kim, S. W.; Jeong, B. *Macromolecules* **2005**, *38*, 5260-5265.

(218) Gong, C.; Shi, S.; Dong, P.; Kan, B.; Gou, M.; Wang, X.; Li, X.; Luo, F.; Zhao, X.; Wei, Y.; Qian, Z. *Int. J. Pharm.* **2009**, *365*, 89-99.

(219) Song, S.; Dong, R.; Wang, D.; Song, A.; Hao, J. *Soft Matter* **2013**, *9*, 4209-4218.

(220) Chen, G.; Hoffman, A. S. *Nature* **1995**, *373*, 49-52.

(221) Dai, S.; Ravi, P.; Tam, K. C. *Soft Matter* **2009**, *5*, 2513-2533.

(222) Gotzamanis, G. T.; Tsitsilianis, C.; Hadjiyannakou, S. C.; Patrickios, C. S.; Lupitskyy, R.; Minko, S. *Macromolecules* **2005**, *39*, 678-683.

(223) Topham, P. D.; Howse, J. R.; Mykhaylyk, O. O.; Armes, S. P.; Jones, R. A. L.; Ryan, A. J. *Macromolecules* **2006**, *39*, 5573-5576.

(224) Markland, P.; Zhang, Y.; Amidon, G. L.; Yang, V. C. *J. Biomed. Mater. Res.* **1999**, *47*, 595-602.

(225) Pouliquen, G.; Tribet, C. *Macromolecules* **2005**, *39*, 373-383.

(226) Hietala, S.; Strandman, S.; Järvi, P.; Torkkeli, M.; Jankova, K.; Hvilsted, S.; Tenhu, H. *Macromolecules* **2009**, *42*, 1726-1732.

(227) Choi, B. G.; Sohn, Y. S.; Jeong, B. *J. Phys. Chem. B* **2007**, *111*, 7715-7718.

(228) Tang, T.; Castelletto, V.; Parras, P.; Hamley, I. W.; King, S. M.; Roy, D.; Perrier, S.; Hoogenboom, R.; Schubert, U. S. *Macromol. Chem. Phys.* **2006**, *207*, 1718-1726.

(229) Chen, C. F.; Lin, C. T. Y.; Chu, I. M. *Polym. Int.* **2010**, *59*, 1428-1435.

(230) Scalfani, V. F.; Bailey, T. S. *Macromolecules* **2011**, *44*, 6557-6567.

(231) Hamley, I. W.; Cheng, G.; Castelletto, V. *Macromol. Biosci.* **2011**, *11*, 1068-1078.

(232) Nakashima, K.; Bahadur, P. *Adv. Colloid Interface Sci.* **2006**, *123-126*, 75-96.

(233) Fechler, N.; Badi, N.; Schade, K.; Pfeifer, S.; Lutz, J.-F. *Macromolecules* **2009**, *42*, 33-36.

(234) Vermonden, T.; Besseling, N. A. M.; van Steenbergen, M. J.; Hennink, W. E. *Langmuir* **2006**, *22*, 10180-10184.

(235) Li, C.; Buurma, N. J.; Haq, I.; Turner, C.; Armes, S. P.; Castelletto, V.; Hamley, I. W.; Lewis, A. L. *Langmuir* **2005**, *21*, 11026-11033.

(236) Ma, Y.; Tang, Y.; Billingham, N. C.; Armes, S. P.; Lewis, A. L. *Biomacromolecules* **2003**, *4*, 864-868.

(237) Castelletto, V.; Hamley, I. W.; Ma, Y.; Bories-Azeau, X.; Armes, S. P.; Lewis, A. L. *Langmuir* **2004**, *20*, 4306-4309.

(238) Madsen, J.; Armes, S. P. *Soft Matter* **2012**, *8*, 592-605.

(239) Li, Y.; Narain, R.; Ma, Y.; Lewis, A. L.; Armes, S. P. *Chem. Commun.* **2004**, *0*, 2746-2747.

(240) Lin, H.-H.; Cheng, Y.-L. *Macromolecules* **2001**, *34*, 3710-3715.

(241) Zhang, H.; Yan, Q.; Kang, Y.; Zhou, L.; Zhou, H.; Yuan, J.; Wu, S. *Polymer* **2012**, *53*, 3719-3725.

(242) Cao, Z.; Liu, W.; Ye, G.; Zhao, X.; Lin, X.; Gao, P.; Yao, K. *Macromol. Chem. Phys.* **2006**, *207*, 2329-2335.

(243) Li, Y.; Tang, Y.; Narain, R.; Lewis, A. L.; Armes, S. P. *Langmuir* **2005**, *21*, 9946-9954.

(244) van de Manakker, F.; Vermonden, T.; el Morabit, N.; van Nostrum, C. F.; Hennink, W. E. *Langmuir* **2008**, *24*, 12559-12567.

(245) Taribagil, R. R.; Hillmyer, M. A.; Lodge, T. P. *Macromolecules* **2010**, *43*, 5396-5404.

(246) Zhou, C.; Hillmyer, M. A.; Lodge, T. P. *J. Am. Chem. Soc.* **2012**, *134*, 10365-10368.

(247) Choo, E. S. G.; Yu, B.; Xue, J. *J. Colloid Interface Sci.* **2011**, *358*, 462-470.

(248) Mei, A.; Guo, X.; Ding, Y.; Zhang, X.; Xu, J.; Fan, Z.; Du, B. *Macromolecules* **2010**, *43*, 7312-7320.

(249) Determan, M. D.; Cox, J. P.; Seifert, S.; Thiyagarajan, P.; Mallapragada, S. K. *Polymer* **2005**, *46*, 6933-6946.

(250) Beheshti, N.; Zhu, K.; Kjoniksen, A.-L.; Knudsen, K. D.; Nystrom, B. *Soft Matter* **2011**, *7*, 1168-1175.

(251) Shim, W. S.; Yoo, J. S.; Bae, Y. H.; Lee, D. S. *Biomacromolecules* **2005**, *6*, 2930-2934.

(252) Shim, W. S.; Kim, S. W.; Lee, D. S. *Biomacromolecules* **2006**, *7*, 1935-1941.

(253) Huynh, D. P.; Shim, W. S.; Kim, J. H.; Lee, D. S. *Polymer* **2006**, *47*, 7918-7926.

(254) Tsitsilianis, C.; Stavrouli, N.; Bocharova, V.; Angelopoulos, S.; Kiriy, A.; Katsampas, I.; Stamm, M. *Polymer* **2008**, *49*, 2996-3006.

Chapter 2 – Overview of the Thesis

This thesis focuses on the relevance of water-soluble functional polymers for present and future technologies. Due to its weak polycationic character poly((2-dimethylamino)ethyl methacrylate) (PDMAEMA) exhibits outstanding properties, such as temperature- and pH-sensitivity, which lead to potential applications for biomedical or biotechnical use. In chapter 3-5 three publications are presented dealing with gene delivery and dual-responsive hydrogels primarily based on PDMAEMA.

Dual-responsive superparamagnetic PDMAEMA grafted iron oxide nanoparticles were synthesized *via* a "grafting-from" approach utilizing a physically adsorbed dopamine-based ATRP initiator. The pH-dependent coil-to-globule transition temperatures were investigated by turbidimetry and a reversible binding of the dopamine anchor group was shown *via* Asymmetric Flow Field-Flow Fractionation (AF4). Due to the polycationic character of PDMAEMA at physiological pH the hybrid particles were further tested for gene delivery experiments. Moreover, the uptake of the magnetic gene vector inside the cells enables a magnetically driven cell separation by applying an external magnetic field (Chapter 3).

The established system was further improved by encapsulating the iron oxide nanoparticle with silica prior to the ATRP initiator functionalization for the polymerization of DMAEMA *via* the "grafting-from" approach yielding dual-responsive core-shell-corona nanoparticles. Here, covalent bonds between the PDMAEMA chains and the inorganic core could be obtained preventing a detachment of the polymer chains. The complexation behavior of the hybrid material and pDNA was investigated by determining zeta potentials and hydrodynamic radii of the formed polyplexes as a function of the N/P ratio (polymer nitrogen / pDNA phosphorous). This system was as well tested for gene delivery and magnetic cell separation experiments (Chapter 4).

The dual-responsive behavior of PDMAEMA was applied for creating physically cross-linked hydrogels, which can undergo two separate switchable phase transitions. For this purpose ABCBA pentablock terpolymers were synthesized consisting of a PEO middle block, two dual-responsive PDMAEMA B-blocks and two temperature-responsive PDEGMA A-blocks. The temperature- and pH-dependent solution and gelation behavior of the BCB intermediates and the ABCBA block copolymers were investigated *via* dynamic light scattering (DLS) and rheology (Chapter 5).

2.1. Dual-Responsive Magnetic Core-Shell Nanoparticles for Nonviral Gene Delivery and Cell Separation

This initial project focused on the synthesis of PDMAEMA grafted iron oxide (maghemite) nanoparticles as a potential candidate for gene delivery and magnetic cell separation. The facile synthesis approach can be divided into three steps. The basis is represented by oleic acid stabilized maghemite (γ-Fe_2O_3) nanoparticles generated through thermal decomposition of $Fe(CO)_5$ in the presence of oleic acid yielding monodisperse maghemite nanoparticles. Subsequently, a physically binding dopamine-based ATRP initiator was used for surface modification, which was in a last step applied for the polymerization of DMAEMA *via* a "grafting-from" approach (Scheme 1).

Scheme 1. Synthesis of dual-responsive maghemite nanoparticles.

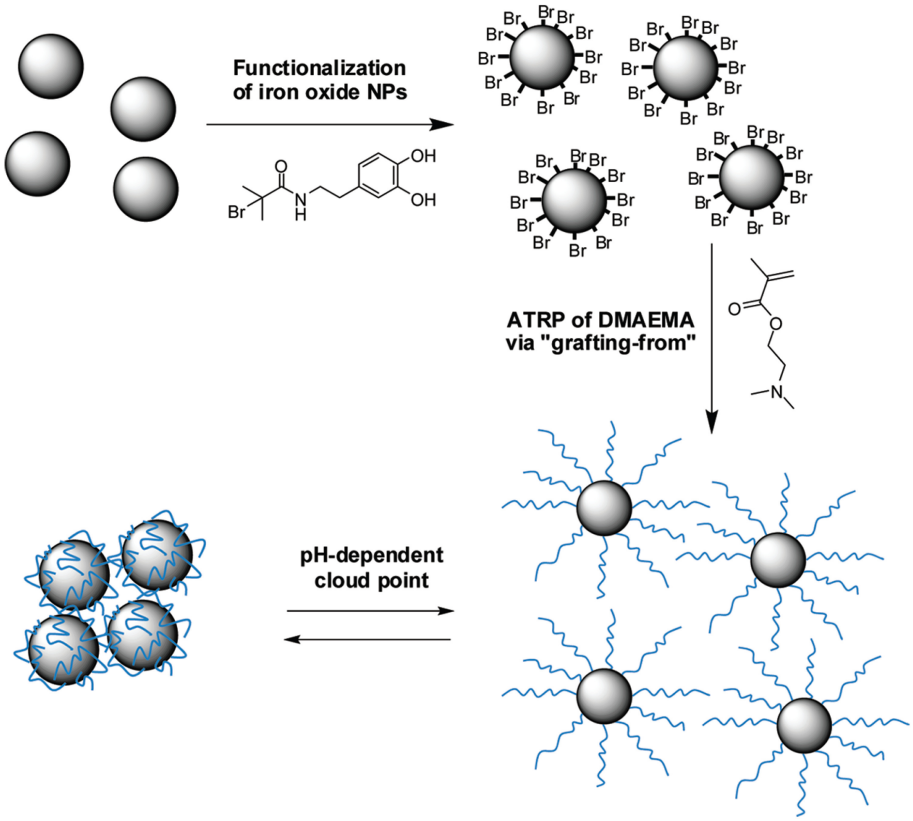

Each step of the synthesis was characterized in detail applying a variety of different analytical methods, namely, Transmission Electron Microscopy (TEM), Dynamic Light Scattering (DLS), Fourier Transform Infrared Spectroscopy (FT-IR), Thermographic Analysis (TGA), Size Exclusion Chromatography (SEC, of the cleaved-off PDMAEMA chains) and Vibrating

Sample Magnetometry (VSM). An evaluation of these data revealed, besides the indication for a successful grafting approach, a grafting density of the PDMAEMA grafted nanoparticles of 0.15 chains/nm². Thus, the polymer grafted nanoparticles bear 46 PDMAEMA chains of DP_n = 590 per particle, denoted as γ-Fe_2O_3@$(PDMAEMA_{590})_{46}$. Moreover, it could be shown that the superparamagnetic character of the maghemite nanoparticles remains after the grafting process, which is essential for its further application (magnetic cell separation).

The stability of the hybrid particles was further investigated *via* Asymmetric Flow Field-Flow Fractionation (AF4). Here, a time-dependent detachment of the polymer chains after purification was shown even though the catechol group of the dopamine-based initiator is regarded as a strong binding anchor group in aqueous media (Figure 1A and B). The reversible binding of this anchor group led to a significant increase of free PDMEAMA within the first week levelling out over approximately 100 days until an equilibrium state was reached. At this point the investigated sample contained more than 50 % free polymer chains. This effect, however, had no significant influence on the long-term stability, which is indicated by the absence of sedimentation or aggregation of the particles even after one year of storage.

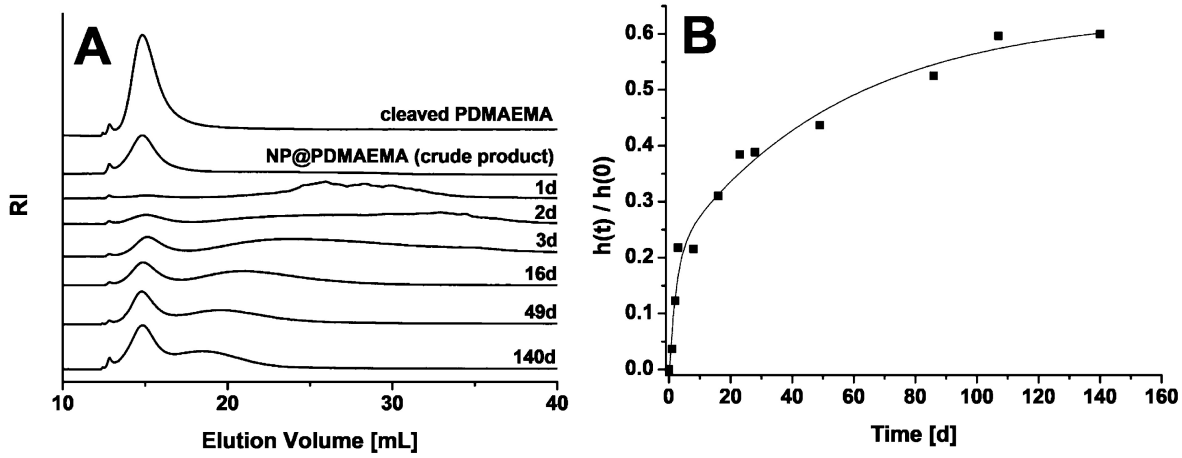

Figure 1. (A) Comparison of AF-FFF elugrams (RI signal, c = 1 g/L) of the cleaved-off PDMAEMA chains, γ-Fe_2O_3@ $(PDMAEMA_{590})_{46}$ crude product, and γ-Fe_2O_3@ $(PDMAEMA_{590})_{51}$ at various times after purification (eluent: deionized water containing 25 mM $NaNO_3$ and 200 ppm NaN_3). (B) Kinetics of the detachment of PDMAEMA chains.

In addition, freshly purified PDMAEMA grafted nanoparticles were investigated *via* turbidimetry. Due to the protonatable tertiary amine groups in the side chains of PDMAEMA it shows a pH-dependent Lower Critical Solution Temperature (LCST). Thus, at low pH the amine group is protonated, which results in a good solubility and a significant higher coil-to-

globule transition (here, denoted as cloud point) than in the deprotonated state at high pH. Since the hybrid particles resemble a star-like architecture the cloud points are similar to those of multi-arm PDMAEMA stars.

Furthermore, the polycationic character at physiological pH of PDMAEMA and thus, γ-Fe_2O_3@$(PDMAEMA_{590})_{46}$ provides suitable conditions for gene delivery experiments. The cytotoxicity was determined *via* the MTT test and the potential as transfection agent was investigated under standard conditions in CHO-K1 cells. As a result, the hybrid material showed significantly lower cytotoxicity by simultaneously almost doubling the transfection efficiency (> 50 %) in comparison to poly(ethyleneimine) (PEI), which is regarded as the "gold standard" for polycationic gene delivery systems. Notably, γ-Fe_2O_3@ $(PDMAEMA_{590})_{46}$ has an overall molecular weight of approximately 4.3 MDa, which would typically lead to a high cytotoxicity for linear PDMAEMA. These findings show the strong dependence on the architecture of PDMAEMA for gene delivery experiments.

Besides the excellent performance for the transfection of mammalian cells, the magnetic gene vector provided magnetic properties to the cells after the transfection. In a simple experiment could be shown that transfected cells can be quantitatively separated by applying a NdFeB magnet over night (Figure 2).

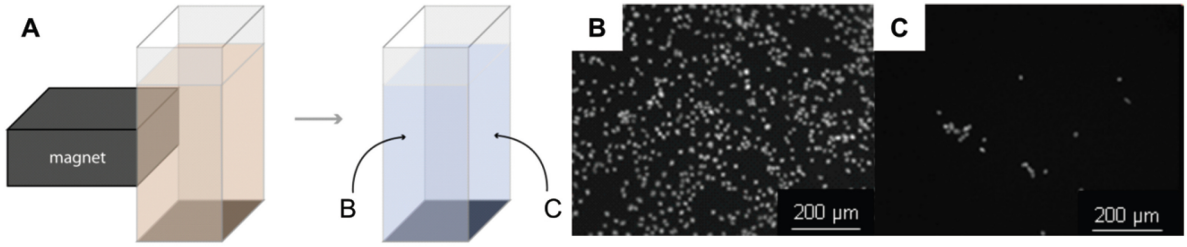

Figure 2. Magnetic separation of cells transfected with γ-Fe_2O_3@ $(PDMAEMA_{590})_{46}$/pDNA polyplexes. Separation scheme (A); Microscopy pictures of the cells grown on the wall facing the magnet (B) or on the opposite wall (C).

2.2. PDMAEMA-Grafted Core-Shell-Corona Particles for Nonviral Gene Delivery and Magnetic Cell Separation

This study is closely related to the initial work on magnetic polymer/nanoparticle hybrids as gene vectors based on dopamine as anchor group for the polymer. Even though these hybrids already showed superior properties in gene delivery in comparison to PEI and linear PDMAEMA, the free detaching polymer chains of this system have an unpredictable influence on the transfection of the cells. Here, the new concept was to connect the PDMAEMA covalently to the core to confirm that the high transfection potential results from the star-like architecture of the grafted nanoparticles (Scheme 2).

Monodisperse oleic acid stabilized nanoparticles serve again as the core of the hybrid material. A reverse microemulsion process was applied to form a thin silica shell around the nanoparticle. This shell was modified with a silane end-functionalized ATRP initiator, which was consecutively added within the same synthesis step yielding ATRP initiator functionalized individually silica-encapsulated maghemite nanoparticles. A subsequent polymerization of DMAEMA *via* a "grafting-from" approach led to magnetic covalently grafted PDMAEMA core-shell-corona nanoparticles.

Scheme 2. Synthesis of PDMAEMA grafted core-shell-corona nanoparticles.

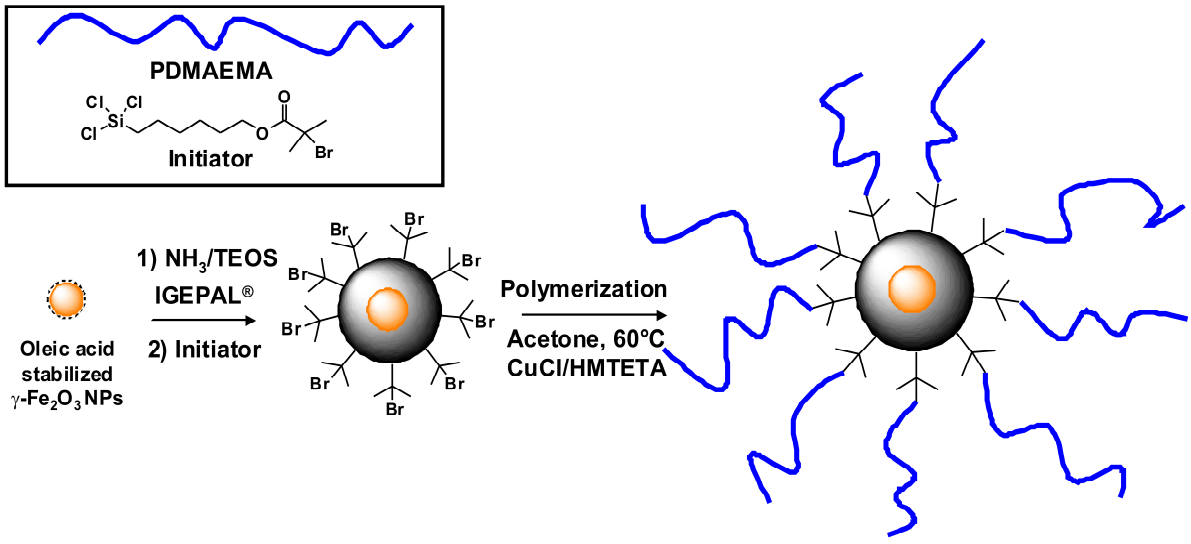

The investigation of this hybrid material revealed indeed single encapsulated nanoparticles (Figure 3A) bearing covalently bound PDMAEMA chains with a grafting density of 0.04 chains/nm², which corresponds to 91 polymer chains of DP_n = 540 per particle, denoted as γ-Fe_2O_3@silica@$(PDMAEMA_{540})_{91}$. The superparamagnetic behavior as well as the long-

term stability of more than one year in aqueous media were retained after the silica encapsulation.

The dual-responsive behavior of the PDMAEMA corona was investigated by turbidity measurements and DLS. The hybrid particles were shown to undergo the typical pH-dependent coil-to-globule transitions similar to our first approach and the effect of the degree of protonation on the corona size could be shown *via* DLS (Figure 3B). At pH 4 the corona is highly protonated, which results in almost completely stretched chains leading to a maximum in the hydrodynamic radius. On the contrary, at pH 10 a significantly lower hydrodynamic radius was observed due to the nearly deprotonated PDMAEMA corona.

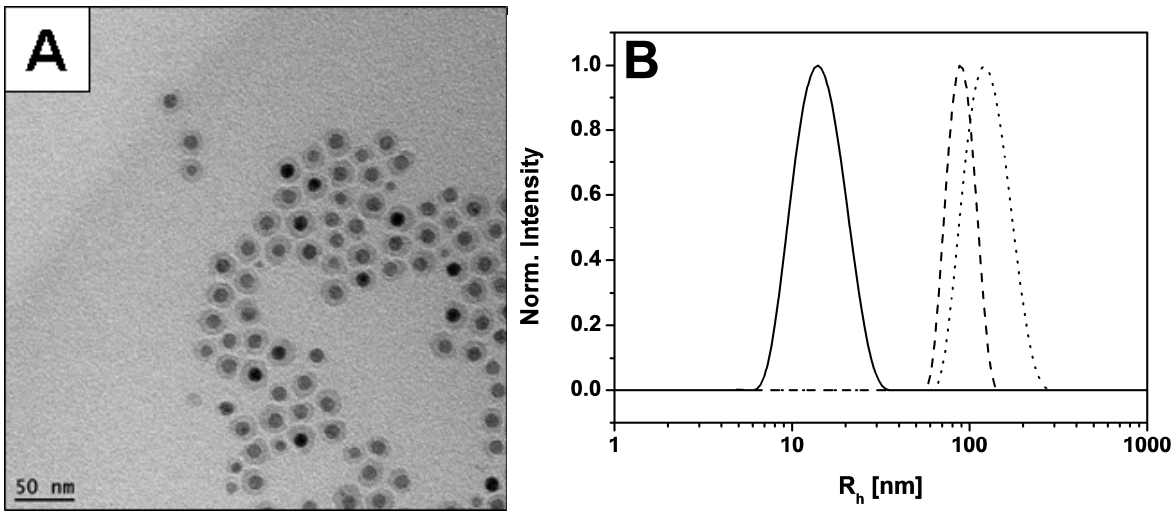

Figure 3. (A) TEM micrograph of γ-Fe_2O_3@silica@BIBSI nanoparticles. The sample was prepared by drop-coating a cyclohexane dispersion of the nanoparticles (c < 0.1 g/L) on a carbon-coated copper grid. (B) Hydrodynamic radii distribution (θ = 90°; c = 0.1 g/L) of γ-Fe_2O_3@Silica@BIBSI in cyclohexane (solid line), γ-Fe_2O_3@silica@$(PDMAEMA_{540})_{91}$ in pH 10 buffer solution (dashed line) and in pH 4 buffer solution (dotted line).

Due to the covalently bound PDMAEMA chains it was now possible to study the complexation behavior with pDNA under transfection conditions without negative side effects of detaching free polymer (Figure 4A and B). The γ-Fe_2O_3@silica@$(PDMAEMA_{540})_{91}$/pDNA inter-polyelectrolyte complexes (polyplexes) were studied with regard to their size and zeta potential at different N/P ratios. As a result, at N/P ratios ≥ 7.5 polyplexes from single complexed pDNA molecules per nanoparticle were formed. Furthermore, at N/P = 5 the highest aggregation was observed caused by the almost neutral zeta potential and thus, the lack of stabilizing charges. Further decrease of the N/P ratio leads again to a decrease of the polyplex size, but the overall size is still significant higher than for the individually complexed pDNA molecules, which may occur due to bridging effects of two hybrid particles binding to one single pDNA molecule.

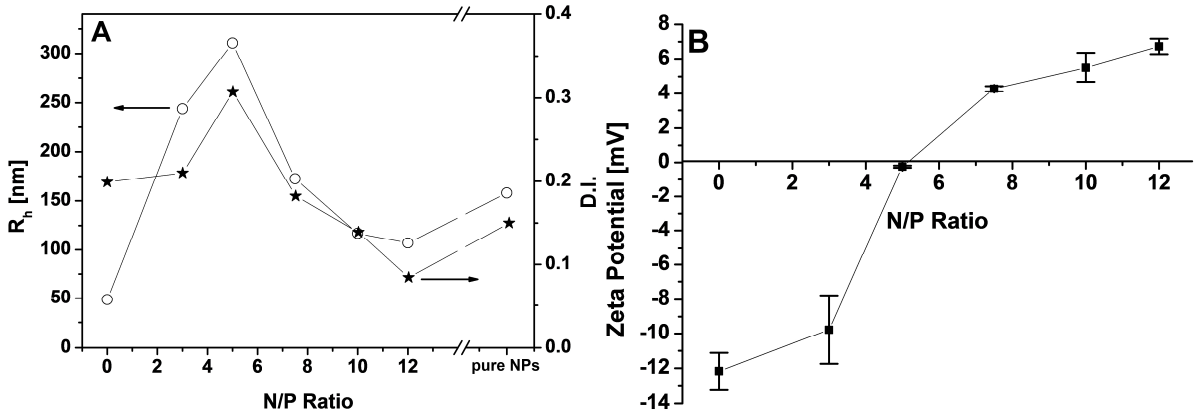

Figure 4. (A) Average hydrodynamic radii (○) and dispersity indices (★) at different N/P ratios of the γ-Fe_2O_3@silica@$(PDMAEMA_{540})_{91}$/pDNA polyplexes; pH ~ 7.8. (B) Zeta potentials of the γ-Fe_2O_3@silica@$(PDMAEMA_{540})_{91}$/pDNA polyplexes at different N/P ratios. The lines in both graphs are guides to the eye.

The γ-Fe_2O_3@silica@$(PDMAEMA_{540})_{91}$ particles performed best in transfection experiments at N/P ratios between 7.5 – 10 (positive zeta potential, CHO-K1 cells) resulting in transfection efficiencies >50 % and a low cytotoxicity. The cytotoxicity is slightly increased as compared to our previous system, which can be attributed to the almost doubled molecular weight of the PDMAEMA corona (7.7 MDa).

Instead of a simple separation experiment the magnetic separation was performed using a Magnetic Activated Cell Sorting system (MACS^{TM}). Both bound and unbound cell fractions were quantitatively determined revealing that most of the cells carry a sufficient amount of magnetic material for a successful separation. The separated cells (transfection efficiency >60 %) showed a high viability and could even be further cultivated.

The new synthesis strategy led to stable and well-defined PDMAEMA grafted hybrid particles with high potential for gene delivery experiments. Thus, this approach can be applied for investigating the impact of distinct grafting density as well as PDMAEMA chain length dependences on the transfection efficiency and cytotoxicity.

2.3. Double Responsive Pentablock Terpolymers: Self-Assembly and Gelation Behavior

This study dealt with the utilization of the dual-responsive behavior of PDMAEMA for the construction of double responsive hydrogels. Here, the synthesized hydrogels were based on ABCBA pentablock terpolymers, where dual-responsive (temperature/pH) PDMAEMA B-blocks and temperature-responsive poly(di(ethylene glycol) methyl ether methacrylate) (PDEGMA) A-blocks can be separately switched water-insoluble by applying an external stimulus, while a poly(ethylene oxide) (PEO) middle C-block is merely responsible for the stabilization of the system.

The proposed self-assembly of this system is shown in Scheme 3. In dilute solutions the ABCBA pentablock terpolymers assemble into flower-like micelles upon heating initiated by the coil-to-globule phase transition (T_{tr}) of the outer PDEGMA A-blocks, which occurs at lower temperatures as compared to the phase transition temperature of the PDMAEMA B-blocks. The resulting flower-like micelles consist of a PDEGMA core, which is stabilized by looped PDMAEMA-*b*-PEO-*b*-PDMAEMA segments of the pentablock terpolymer. Since the PDMAEMA blocks are dual-responsive the micelles can undergo a further contraction depending on pH at T_{tr}(PDMAEMA) caused by the collapse of the PDMAEMA blocks. As a result, core (PDEGMA) – shell (PDMAEMA) – corona (looped PEO) micelles are obtained. At high concentrations, the ABCBA pentablock terpolymers assemble into a physically cross-linked hydrogel network, which is induced by the collapsing PDEGMA A-blocks. The further contraction of PDMAEMA at higher temperatures should then lead to a change in the mechanical properties of the gel.

Scheme 3. Self-assembly of ABCBA pentablock terpolymers.

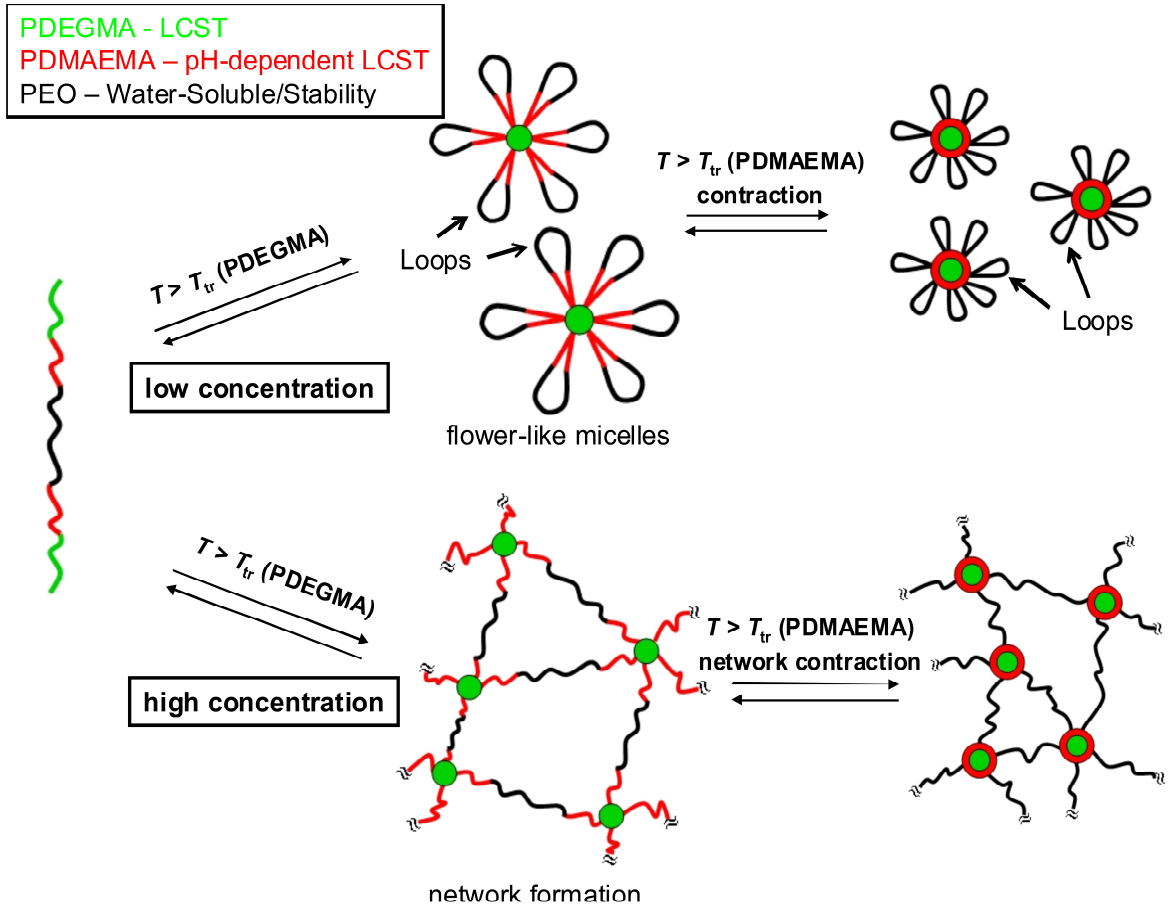

The synthesis of the PDEGMA-*b*-PDMAEMA-*b*-PEO-*b*-PDMAEMA-*b*-PDEGMA ABCBA pentablock terpolymers was performed by using a bifunctional PEO_{775} (DP_n = 775, degree of functionality = 1.66) ATRP-macroinitiator for a sequential ATRP of DMAEMA and DEGMA. This approach, however, was limited to relatively short blocks, *i.e.* $DP_n \leq 90$ and $DP_n \leq 43$ for the PDMAEMA B-blocks and the PDEGMA A-blocks, respectively. The synthesis of higher molecular weights resulted in broad molecular weight distributions caused, *e.g.*, by transfer reactions during the polymerization. The PDMAEMA-*b*-PEO-*b*-PDMAEMA triblock copolymer intermediate with DP_n(PDMAEMA) = 90 (ABA-90) revealed a reasonable PDMAEMA block length along with a low PDI and was then used for further polymerization of the ABCBA pentablock copolymers.

Temperature-dependent DLS measurements of dilute solutions (c = 2 g/L) were performed with both the PDMAEMA-*b*-PEO-*b*-PDMAEMA triblock copolymer intermediates (ABA) as well as the PDEGMA-*b*-PDMAEMA-*b*-PEO-*b*-PDMAEMA-*b*-PDEGMA pentablock terpolymers (ABCBA). The transition points for the PDMAEMA blocks in the ABA intermediates were shown to be dependent on pH and the molecular weight of the PDMAEMA blocks, revealing similar values compared to those described in literature.

Notably, no significant influence on the phase transition temperatures, which may be caused by the long hydrophilic PEO_{775} middle block, was observed. The introduction of the PDEGMA outer blocks led to a significant change in the aggregation behavior for the ABCBA pentablock terpolymers (denoted as ABCBA-x, where x = number average degree of polymerisation of PDEGMA block) in dilute solutions (Figure 5). Here, three different ABCBA pentablock terpolymers were studied *via* temperature-dependent DLS revealing two separate phase transitions upon heating, thus confirming that both responsive blocks can be triggered separately. The first transition is initiated by the pH-independent coil-to-globule phase transition of the PDEGMA outer blocks at low temperatures (T_{tr} = 29 – 33 °C) for the two systems with the highest molar fraction of DEGMA units (ABCBA-25 and ABCBA-43), and the second pH-dependent transition at higher temperatures (T_{tr} > 40 for pH < 10) corresponds to the collapse of the PDMAEMA blocks (Figure 5A-C). These transitions are indicated by a significant increase of the count rate caused by each collapse of the respective blocks, which can only be clearly observed for pH = 8 (Figure 5A) since the two separated phase transitions of PDEGMA and PDMAEMA start to merge for pH ≥ 9 (Figure 5B and C). However, short PDEGMA blocks as shown for ABCBA-11 revealed a phase transition at drastically elevated temperatures (T_{tr} = 45 °C). The collapse of these short $PDEGMA_{11}$ blocks showed a weak impact on the count rate and could only be observed for pH = 8 (Figure 5A) due to $T_{tr}(PDEGMA_{11}) > T_{tr}$ (PDMAEMA) for pH > 8 (Figure 5B and C).

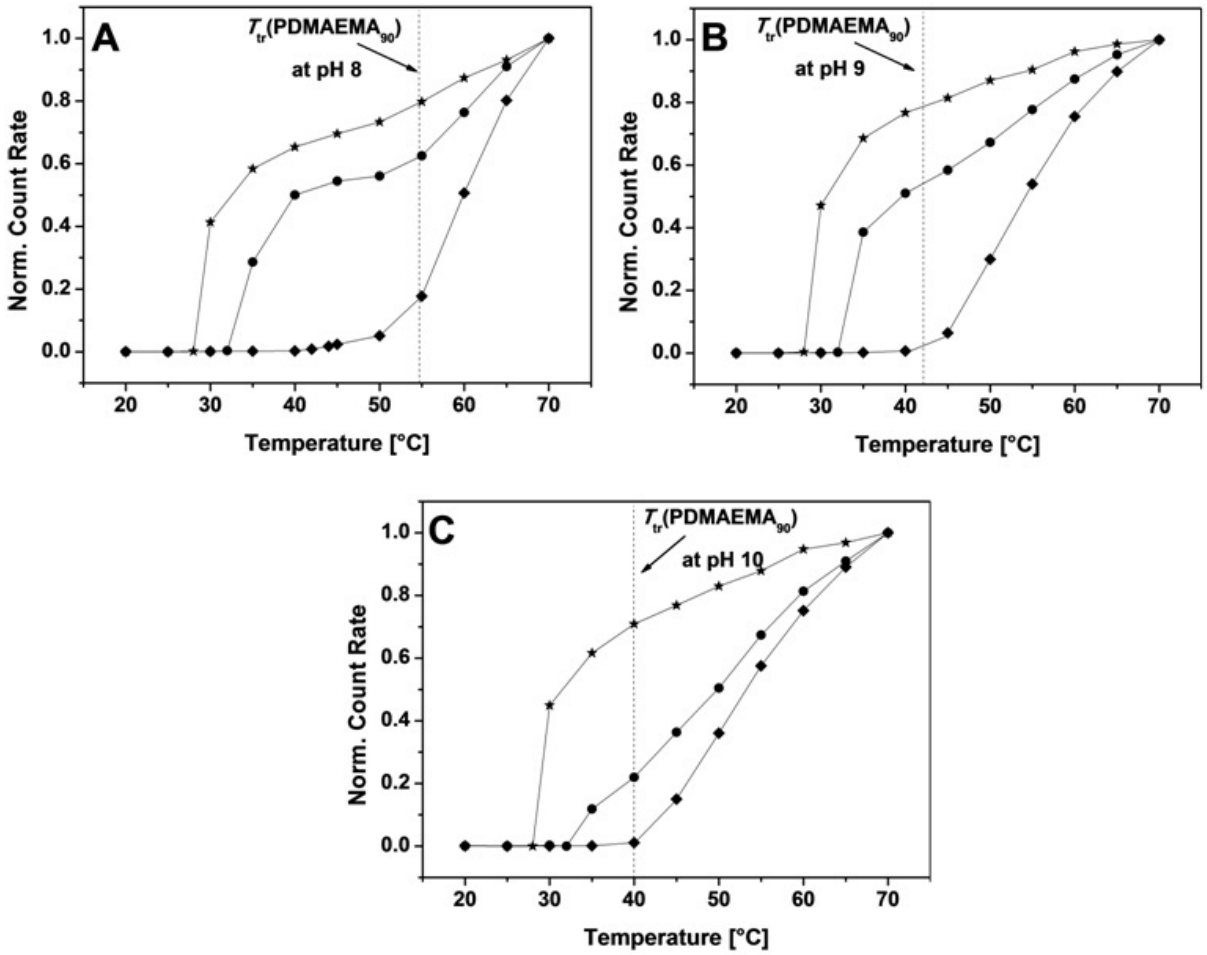

Figure 5. Temperature-dependent scattering intensities at $\theta = 90°$ for ABCBA pentablock copolymers in different buffer solutions (c = 2 g/L) at A) pH 8, B) pH 9 and C) pH 10 (ABCBA-11 (◆), ABCBA-25 (●) and ABCBA-43 (★)); the dashed line indicates the T_{tr} of the PDMAEMA block in the corresponding ABA triblock copolymer precursor (DP_n(PDMAEMA) = 90) at the respective pH.

Hydrogel formation of concentrated solutions was initially shown for the ABA triblock copolymer intermediates, which revealed that a molar fraction of DMAEMA units of $f_{DMAEMA} \geq 0.19$ is needed to form free-standing gels. Furthermore, rheology measurements of these gels indicated higher gel strengths and that the sol-gel transition temperature (T_{SG}) shifts to lower temperatures by increasing the molecular weight of the PDMAEMA blocks, concentration of the solution or pH. For instance, a 10 wt% solution of the ABA triblock copolymer carrying an average degree of polymerization of 90 (ABA-90) formed no gel at pH = 9 and a 20 wt% solution at pH = 10 was necessary to form a strong freestanding gel (Figure 6A). A doubling of the molecular weight of the PDMAEMA blocks, however, led to gelation for any investigated solution and revealed already strong gels for a 10 wt% solution at pH 10.

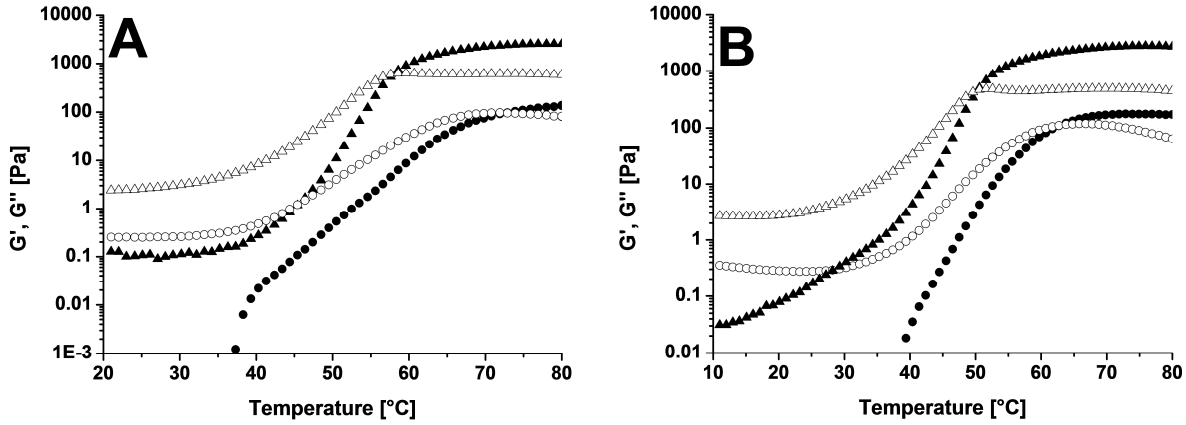

Figure 6. Temperature-dependent storage and loss moduli for A) ABA-90 at pH 10 and a concentration of 10 wt% (*G*' (●), *G*'' (○)) and 20 wt% (*G*' (▲), *G*'' (△)), respectively and B) for ABCBA-25 at pH 10 and a concentration of 10 wt% (*G*' (●), *G*'' (○)) and 20 wt% (*G*' (▲), *G*'' (△)), respectively.

Gels from 10 and 20 wt% solutions of ABCBA-25 and ABCBA-43 were only investigated at pH 10 as ABA-90, which represents the precursor for all ABCBA pentablock terpolymers, forms only very weak gels at pH = 9. Even though the PDEGMA blocks lower the T_{SG} by 8 – 10 °C, a change in the mechanical properties of the hydrogel, which could then be attributed to the second phase transition of the collapsing PDMAEMA at higher temperatures, was not observed (Scheme 3, Figure 6B). Notably, an approximately doubling of the PDEGMA block length (ABCBA-43) leads to similar results to those from the ABCBA-25. This might be attributed to the long PEO middle block, which may compensate for the second collapse of the PDMAEMA. Consequently, an increase of the molar fractions of DEGMA units above those presented in this study ($f_{DEGMA} \leq 0.08$) might be necessary to shift the sol-gel transitions of the ABCBA hydrogels to lower temperatures close to T_{tr}(PDEGMA) and, in addition, to realize two clearly separated phase transitions with a sufficient impact on the mechanical properties of the hydrogel at the point where PDMAEMA starts to collapse.

2.4. Individual Contributions to Joint Publications

The results presented in this thesis were obtained in collaboration with others and have been published or submitted to publication as indicated below. In the following, the contributions of all the co-authors to the different publications are specified. The asterisk denotes the corresponding author(s).

Chapter 3

This work is published in *Biomacromolecules* **2012**, 13, 857–866 under the title:

"Dual-Responisve Magnetic Core-Shell Nanoparticles for Non-Viral Gene Delivery and Cell Separation"

By Alexander P. Majewski, Anja Schallon, Valérie Jérôme, Ruth Freitag, Axel H. E. Müller* and Holger Schmalz*

I conducted all experiments and wrote the publication, except that:

• A. Schallon conducted all cell experiments (transfection/MTT/cell separation) and wrote the biological part of the manuscript.

• V. Jérôme, R. Freitag, A. H. E. Müller and H. Schmalz were involved in scientific discussions and correcting the manuscript.

Chapter 4

This work has been published in *Biomacromolecules* **2013**, 14, 3081-3090 under the title:

"PDMAEMA-Grafted Core-Shell-Corona Particles for Non-Viral Gene Delivery and Magnetic Cell Separation"

by Alexander P. Majewski, Ullrich Stahlschmidt, Valérie Jérôme, Ruth Freitag*, Axel H. E. Müller* and Holger Schmalz*

I conducted all experiments and wrote the publication, except that:

• U. Stahlschmidt conducted all cell experiments (transfection/MTT/cell separation).

• V. Jérôme wrote the biological part of the manuscript.

• V. Jérôme, R. Freitag, A. H. E. Müller and H. Schmalz were involved in scientific discussions and correcting the manuscript.

Chapter 5

This work will be submitted to *Colloid and Polymer Science* under the title:

"Double Responsive Pentablock Terpolymers: Self-Assembly and Gelation Behavior"

by Alexander P. Majewski, Tina Borke, Andreas Hanisch, Axel H. E. Müller* and Holger Schmalz*

I conducted all experiments and wrote the publication, except that:

• T. Borke synthesized the ABA triblock copolymer intermediates under my supervision.

• A. Hanisch supervised the synthesis and analysis of the PEO-macroinitiator.

• A. H. E. Müller and H. Schmalz were involved in scientific discussions and correcting the manuscript.

Chapter 3

Dual-Responsive Magnetic Core-Shell Nanoparticles for Non-Viral Gene Delivery and Cell Separation

Alexander P. Majewski[1], Anja Schallon[2], Valérie Jérôme[2], Ruth Freitag[2], Axel H. E. Müller[1,*] and Holger Schmalz[1,*]

[1]Makromolekulare Chemie II and [2]Bioprozesstechnik, Universität Bayreuth, 95440 Bayreuth, Germany; Fax: +49 921553393; E-Mail: holger.schmalz@uni-bayreuth.de, axel.mueller@uni-bayreuth.de

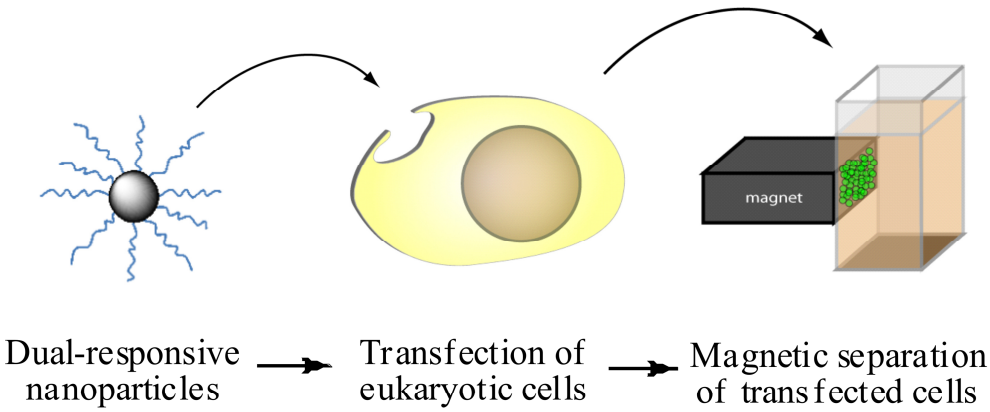

Reprinted with permission from Majewski, A.P.; Schallon, A.; Jérôme, V.; Freitag, R.; Müller, A.H.E.; Schmalz, H. *Biomacromolecules* **2012**, 13, 857-866.

3.1. Abstract

We present the synthesis of dual-responsive (pH and temperature) magnetic core-shell nanoparticles utilizing the grafting-from approach. First, oleic acid stabilized superparamagnetic maghemite (γ-Fe_2O_3) nanoparticles (NP's), prepared by thermal decomposition of iron pentacarbonyl, were surface-functionalized with ATRP initiating sites bearing a dopamine anchor group *via* ligand exchange. Subsequently, 2-(dimethylamino)ethyl methacrylate (DMAEMA) was polymerized from the surface by ATRP, yielding dual-responsive magnetic core-shell NP's (γ-Fe_2O_3@PDMAEMA). The attachment of the dopamine anchor group on the nanoparticles´ surface is shown to be reversible to a certain extent, resulting in a grafting density of 0.15 chains per nm² after purification. Nevertheless, the grafted NP´s show excellent long-term stability in water over a wide pH range, and exhibit a pH- and temperature-dependent reversible agglomeration as revealed by turbidimetry. The efficiency of γ-Fe_2O_3@PDMAEMA hybrid nanoparticles as a potential transfection agent was explored under standard conditions in CHO-K1 cells. Remarkably, γ-Fe_2O_3@PDMAEMA led to a twofold increase of the transfection efficiency without increasing the cytotoxicity as compared to poly(ethyleneimine) (PEI) and yielded on average more than 50% transfected cells. Moreover, after transfection with the hybrid nanoparticles the cells acquired magnetic properties that could be used for selective isolation of transfected cells.

3.2. Introduction

Surface modification of inorganic nanomaterials has become a rapidly developing technique in recent years. In particular, iron oxide nanoparticles (NP's) have attracted considerable interest due to well established and facile preparation routes, such as co-precipitation or thermal decomposition, availability on large scale, biocompatibility and their superparamagnetic behavior.[1-10] Attaching molecules or polymers onto the NP surface by means of post-synthesis functionalization is one key step to obtain hybrid core-shell NP's with tailored properties. Mostly, polymers are physically adsorbed on the NP surface. This is achieved by the grafting-onto method utilizing polymers with suitable functional end groups (anchor groups), which are able to bind to the surface of the particle.[10-14] Alternatively, the grafting-from approach can be used to obtain core-shell nanoparticles. In this case, the initiating moiety is immobilized on the nanoparticle surface and the polymerization takes place directly from the surface.[14-17] In recent studies dopamine was frequently used as a robust anchor for iron oxide surfaces.[18-22] The functional catechol end group of dopamine binds also very strongly to many other types of surfaces, *e.g.*, Ti, TiO_2, FePt as well as stainless steel, which enables dopamine to be used as a universal anchor group.[23-28] Zhou and co-workers used dopamine-based initiators for surface initiated atom transfer radical polymerization (ATRP) and ring-opening metathesis polymerization (ROMP) from TiO_2 nanotubes.[29, 30] Another effective route to obtain magnetic core-shell structures is based on hybrid micelle formation utilizing hydrophobic or electrostatic interactions between nanoparticles and suitable (block) copolymers as driving forces.[31-35] However, only a poor control over the number of nanoparticles immobilized in the micellar core can be achieved with this method and hence, the core sizes are significantly increased compared to the grafting-from approach using functionalized nanoparticles.

Polymer-grafted water-soluble hybrid materials exhibiting functional and/or responsive properties are considered as attractive components for biomedical applications.[36, 37] Here, thermo-responsive polymers, which show only a partial solubility, *i.e.*, they are soluble only within a certain temperature range determined by the upper critical solution temperature (UCST) and/or lower critical solution temperature (LCST), are of particular interest. One possible application was illustrated by Chanana et al. who reported biocompatible magnetite nanoparticles prepared by a grafting-onto approach using a catechol-terminated thermo-responsive copolymer.[38] They could even demonstrate a reversible agglomeration inside red blood cells as well as an utilization for contrast enhancement in magnetic resonance imaging (MRI). Another example is given by Gelbrich et al. who successfully used thermo-responsive

copolymers grafted on magnetic NP's for bioseparation and catalysis.[39] In particular, tertiary amine-containing methacrylates, like poly(2-(dimethylamino)ethyl methacrylate) (PDMAEMA), show an interesting double-responsive behavior in aqueous solution, which is manifested by a strong dependence of their cloud point on pH.[40, 41]

Besides, cationic polyelectrolytes have great potential for non-viral gene delivery and cell labeling.[42-46] Notably, several groups have shown that the above mentioned PDMAEMA-based polycations can efficiently transfect cells *in vitro*.[47-53] In the medical and biotechnological field there is continued interest in the development of non-viral vectors for transport of nucleic acids into cells.[54-56] Unfortunately, the efficiency of these delivery systems was shown to be dependent on the cell type, and so far there is no clear consensus on the best non-viral vector available.[57]

Gene delivery utilizing functionalized magnetic NPs was pioneered twelve years ago by Plank and collaborators.[58] In the meantime, as recently reviewed by Plank et al.[59] several research groups have utilized and optimized magnetic nanoparticles formulations to deliver nucleic acids into cells.[60-62] However, much less investigations have been performed on PDMAEMA-covered magnetic nanoparticles. Recent work by Boyer et al. describes the high potential of PDMAEMA grafted magnetic NP's for siRNA delivery.[43] From the combined analysis of transfection and cytotoxicity data previously collected in our group, we hypothesized that polymers with a branched architecture, in particular a star-shaped one, and high charge density are promising candidates for efficient gene delivery.[63, 64] Since our approach provides a similar architecture, which is based on PDMAEMA-grafted magnetic NP's, gene delivery experiments should confirm these studies and result in a significant higher transfection efficiency than polyethyleneimine (PEI) by simultaneously decreasing the cytotoxicity. Comparable systems utilizing PEI-grafted magnetic NP's show promising results. However, most of these experiments were based on *Magnetofection*™, *i.e.*, on improving gene delivery by controlled application of a magnetic force.[65]

Here, we provide a facile synthesis of γ-Fe_2O_3@PDMAEMA NP's combined with efficient applications in biotechnology. The synthesis of hybrid core-shell NP's by grafting PDMAEMA from the surface of maghemite nanoparticles utilizing a dopamine-based ATRP initiator, 2-bromoisobutyryl dopamide (BIBDA) (Scheme 1). These particles (γ-Fe_2O_3@PDMAEMA) are shown to undergo dual-responsive reversible agglomeration, *i. e.*, the cloud point is adjustable by pH, as depicted in Scheme 1. Furthermore, the particles were characterized with respect to the achieved grafting density, stability and magnetic response.

The cytotoxicity of the hybrid NP's and their efficiency as transfection reagent were investigated under standard conditions and transfected cells were quantitatively separated by applying a magnet.

Scheme 1. Synthesis of dual-responsive maghemite nanoparticles.

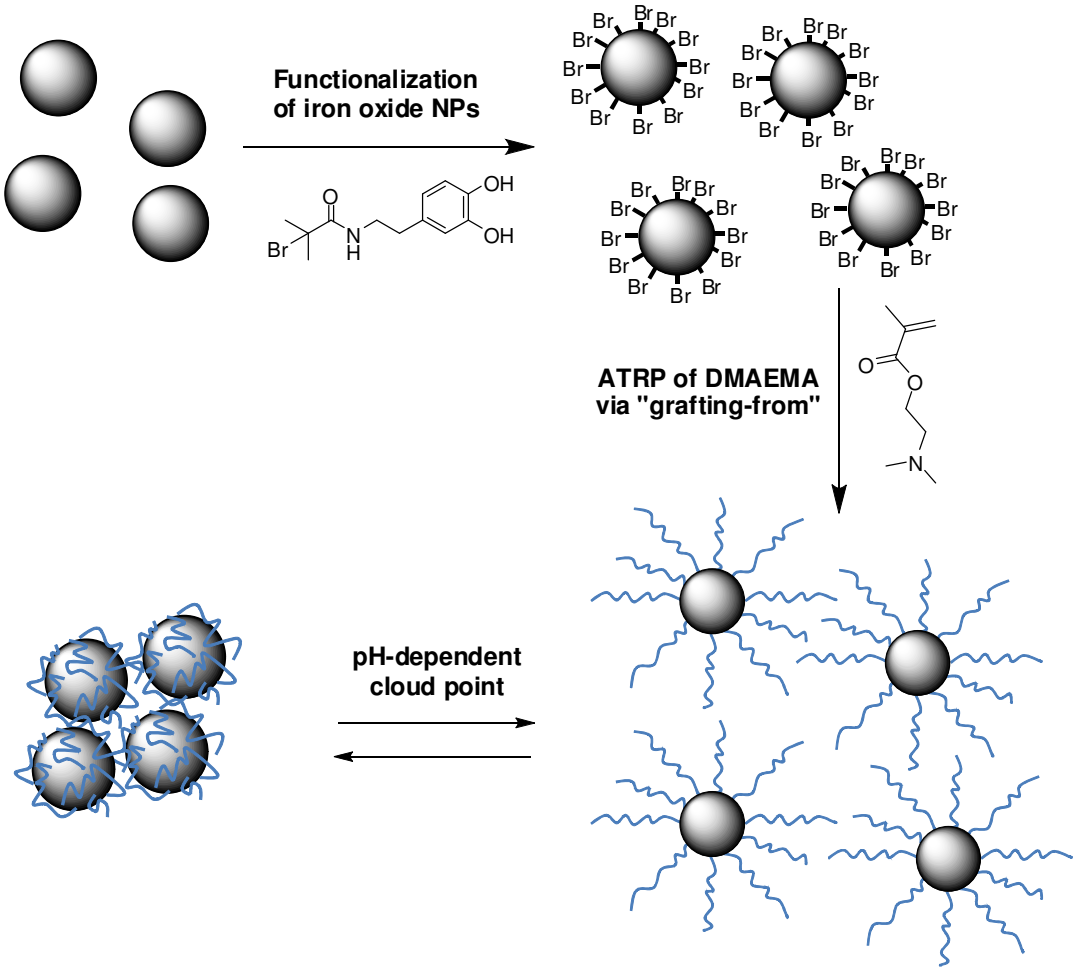

3.3. Experimental Part

Materials. AVS buffer solution pH 7-10 (Titrinorm™, VWR), 2-bromoisobutyryl bromide (98%, Sigma-Aldrich), 2-(dimethylamino)ethyl methacrylate (DMAEMA, 99%, Sigma-Aldrich), dioctyl ether (99%, Sigma-Aldrich), 1,4-dioxane (analytical reagent grade, Fisher Scientific), 1,1,4,7,10,10-hexamethyl triethylenetetramine (HMTETA, 97%, Sigma-Aldrich), 3-hydroxytyramine hydrochloride (98%, Sigma-Aldrich), Iron(0) pentacarbonyl (99.9%, Sigma-Aldrich), oleic acid (90%, Fluka), sodium carbonate monohydrate (99.5%, Sigma-Aldrich), and sodium tetraborate decahydrate (99.5%, Sigma-Aldrich) were used as received. Copper(I) chloride was purified according to literature[66] and the monomer was destabilized by passing through a basic aluminum oxide column. For dialysis a regenerated cellulose tube

(ZelluTrans, Roth) with a MWCO of 6-8 kDa was used. The used NdFeB magnets were purchased at Fehrenkemper Magnetsysteme (dimensions: D = 25 mm, H = 16 mm (disc); L = 63 mm, W = 36 mm, H = 10 mm (block)). The synthesis of the dopamine based ATRP initiator 2-bromo-N-[2-(3,4-dihydroxyphenyl)ethyl]-isobutyryl amide (2-bromoisobutyryl dopamide, BIBDA) was performed as described elsewhere.[26, 29]

3-(4,5-Dimethylthyazolyl-2)-2,5-diphenyl tetrazolium bromide (MTT), Hoechst 33258, and branched polyethyleneimine (PEI, 25 kDa) were purchased from Sigma-Aldrich. PEI was prepared as 50 μM aqueous stock solutions, all other polymers as 500 μM stock solution. Cell culture materials, media and solutions were from PAA Laboratories. Serum reduced medium OptiMEM was from Invitrogen. Plasmid DNA was prepared by using the EndoFree Plasmid Kit from Qiagen. Ultrapure deionized water was used for the preparation of all aqueous solutions and for dialysis. Plasmid pH2B-EGFP[67] (5.1 kb) encoding the nuclei localized EGFP (enhanced green fluorescent protein) driven by the cytomegalovirus immediate early promoter was used in all transfection experiments. The plasmid was amplified in *E. coli DH5 alpha* strain in LB medium to sufficient quantities by using standard molecular biology techniques, including harvesting and purification *via* Qiagen's Giga-Prep kits. Plasmid DNA (pDNA) concentration and quality were determined by $A_{260}/_{280}$ ratio and by agarose gel electrophoresis.

Synthesis of oleic acid stabilized maghemite nanoparticles. The synthesis of the γ-Fe_2O_3 nanoparticles was adapted from Hyeon et al.[4] A 500 mL two-necked round-bottom flask, connected to a reflux condenser, was charged with 250 mL dioctyl ether and 58.0 mL oleic acid (51.52 g, 182.4 mmol) and degassed with nitrogen for 15 min. The reaction mixture was heated to 100 °C under nitrogen atmosphere before adding $Fe(CO)_5$ (8 mL, 60.8 mmol). Subsequently, the mixture was heated to reflux for 1.5 h until the color of the solution turned black. After cooling down to room temperature the reaction mixture was stirred under air to initiate the oxidation process of the initially formed iron nanoparticles to γ-Fe_2O_3. The nanoparticles were precipitated with ethanol and collected by a NdFeB magnet. After decantation of the supernatant, the nanoparticles were immediately redispersed and stored in toluene.

Synthesis of ATRP initiator functionalized maghemite nanoparticles (γ-Fe_2O_3@BIBDA). First, 500 mg of the oleic acid stabilized maghemite nanoparticles dispersed in toluene were precipitated in ethanol and redispersed in THF. This purification process was repeated three times before redispersion in 30 mL THF followed by addition of

250 mg dopamine initiator (2-bromoisobutyryl dopamide (BIBDA)), which corresponds to a initiator/NP ratio of approx. 3000/1. The mixture was shaken for 3 days at room temperature to allow for an efficient ligand exchange. Subsequently, the particles were precipitated in methanol to remove the excess of non-bound initiator and dialyzed further against anisole for 4 days, the solvent applied for ATRP of DMAEMA.

Synthesis of PDMAEMA grafted maghemite nanoparticles (γ-Fe_2O_3@PDMAEMA). A 250 mL screw cap glass equipped with a septum was charged with 500 mg BIBDA-functionalized nanoparticles dispersed in 150 mL anisole, 100 mL DMAEMA (93.3 g, 594 mmol) and 82 mg CuCl (0.83 mmol). The mixture was purged with nitrogen for 30 min before adding 0.23 mL degassed HMTETA (0.19 g, 0.83 mmol) dissolved in 2 mL anisole. The reaction mixture was heated to 60 °C for 42 h. After cooling down to room temperature the reaction was terminated by exposing the mixture to air under stirring for 10 min. The crude product was purified by passing it through a silica column to remove the copper catalyst. Subsequently, the grafted NP's were precipitated in *n*-hexane, redissolved in 1,4-dioxane and freeze-dried. Finally, non-grafted PDMAEMA chains were removed by temperature-induced precipitation.

Temperature-induced precipitation. 200 mg of the grafted particles were dissolved in 20 mL of a boric acid based buffer solution (pH 10). This solution was heated until the particles started to precipitate ($T_{CP} \approx 25$ °C). The supernatant was decanted and the particles were again dissolved in 20 mL of fresh buffer solution. This temperature-induced precipitation was performed 3 times. The particles were finally dialysed against deionized water and stored as aqueous dispersion.

Cleavage of PDMAEMA from grafted γ-Fe_2O_3 nanoparticles. To characterize the grafted PDMAEMA chains, the γ-Fe_2O_3@PDMAEMA nanoparticles were dispersed in 3 M hydrochloric acid which causes the hydrolysis of the iron oxide cores. Subsequently, the resulting yellow solution was dialyzed for 3 days against deionized water to neutral pH. The detached polymer chains were characterized by DMAc-SEC using a PDMAEMA calibration, which revealed a number average molecular weight of M_n(PDMAEMA) = 93.000 g/mol and a PDI of 1.22.

Characterization. *Asymmetric Flow Field-Flow Fractionation (AF-FFF)* was performed on a Wyatt Technology Eclipse 2 separation system equipped with an RI detector. The flow channel was equipped with a 30 kDa regenerated cellulose membrane and a 490 μm thickness spacer. Degassed and filtered deionized water containing $NaNO_3$ (25 mM) and NaN_3 (200

ppm) was used as the carrier solvent. The flow profile was 1 min of an initial focusing step, 20 μL sample injection into the flow channel over 2 min, followed by a sample focusing step of 5 min. The volumetric channel flow rate was set at 1.5 mL/min and the constant cross-flow rate at 0.4 mL/min for 90 minutes. The sample concentration was 1 g/L.

The detachment of PDMAEMA chains from γ-Fe_2O_3@PDMAEMA nanoparticles with time was monitored by evaluating the height, $h(t)$, of the AF-FFF elution peak corresponding to non-bound PDMAEMA chains at V_e = 15 ml. The height of the RI signal is proportional to the mass of PDMAEMA and is thus taken as a quantitative measure for the amount of detached PDMAEMA chains. For that purpose, a freshly purified γ-Fe_2O_3@PDMAEMA sample bearing 51 $PDMAEMA_{590}$ chains per particle. γ-Fe_2O_3@$(PDMAEMA_{590})_{51}$, was measured directly after purification *via* temperature-induced precipitation and after storage for certain time intervals in aqueous dispersion. As a reference the peak height, $h(0)$, the signal of the cleaved-off PDMAEMA chains, obtained by acidic hydrolysis of the particles, was used. Due to the identical concentrations of the applied samples the signal height, $h(0)$, of the cleaved-off PDMAEMA was corrected with respect to the PDMAEMA content of the grafted nanoparticles of 72.5 wt% (determined by TGA). Thus, the corrected reference peak height, $h(0)$, corresponds to the maximum amount of free polymer chains that can be present in the hybrid nanoparticle dispersion. Consequently, the ratio $h(t)/h(0)$ was followed in dependence of time to study the kinetics of the detachment of grafted PDMAEMA chains.

Size Exclusion Chromatography (SEC) was performed on a system based on GRAM columns (7 μm particle diameter) with 10^2 and 10^3 Å pore diameter (Polymer Standards Service) equipped with a RI- and UV-detector from Agilent 1200 Series. N,N-Dimethylacetamide (DMAc) with 0.05% lithium bromide was used as eluent at a flow rate of 0.8 mL/min. The measurements were conducted at 60 °C. For data evaluation a calibration with linear PDMAEMA standards was applied.

Fourier Transform Infrared Spectroscopy (FT-IR) was carried out on a Spectrum 100 FT-IR spectrometer (Perkin Elmer) using an U-ATR unit. The measurements were performed by placing the dried samples directly on top of the U-ATR unit.

Vibrating Sample Magnetometry (VSM): Magnetization curves at room temperature were recorded with an Lake Shore Vibrating Sample Magnetometer Model 7404 applying field strengths up to 1.4 T. Samples were measured in sealed Kel-F vessels, placed on a fiber glass sample holder between two poles of an electromagnet, and vibrated at a frequency of 82 Hz.

Transmission Electron Microscopy (TEM) images were taken with a Zeiss EM922 OMEGA (EFTEM) electron microscope. Samples were prepared by placing one drop of the solution onto carbon-coated copper grids. Afterwards the remaining solvent was removed by blotting with a filter paper. Examinations were carried out at room temperature. Zero-loss filtered images (DE = 0 eV) were taken at an accelerating voltage of 200 kV. All images were registered digitally by a bottom mounted CCD camera system (Ultrascan 1000, Gatan), combined and processed with a digital imaging processing system (Gatan Digital Micrograph Suite GMS 1.8). The hydrophilization of the TEM grids was performed for 30 s under air utilizing a Solarius 950 Advance Plasma System from Gatan.

Dynamic Light Scattering (DLS) was carried out on an ALV DLS/SLS-SP 5022F compact goniometer system with an ALV 5000/E correlator and a He-Ne laser (λ = 632.8 nm). The measurement was performed for 30 min at a scattering angle of 90°. The sample (c = 0.5 g/L) was filtrated through a 0.2 μm PTFE-filter prior to the measurement. The data were analyzed using the CONTIN algorithm which yields an intensity-weighted distribution of relaxation times (τ) after an inverse Laplace transformation of the intensity auto-correlation function. These relaxation times were transformed into translational diffusion coefficients and further into hydrodynamic radii using the Stokes-Einstein equation.

Ion Chromatography was performed to determine the bromine content of the ATRP initiator functionalized particles (γ-Fe_2O_3@BIBDA) utilizing a micro combustion/absorption equipment (self-construction of Mikroanalytische Labor Pascher, Remagen/Germany) and an ion chromatograph consisting of a Metrohm IC 100 unit, CO_2-suppressor and a conductivity detector. The samples were decomposed under oxygen at 1050 °C and the resulting gases were absorbed in 5% aqueous H_2O_2 solution.

Thermogravimetric Analysis (TGA) measurements were carried out using a Mettler Toledo TGA/SDTA 85 at a heating rate of 10 K/min between 30 and 1000 °C under an air-flow of 60 mL/min. The typical sample weight was between 8 and 15 mg. For determining the grafting densities, ρ_{graft}, of the functionalized maghemite nanoparticles the weight loss determined by TGA was used to calculate the amount of molecules per nm^2 according to eq. 1:

$$\rho_{graft} = \frac{\Delta m / M}{Q \cdot A_{NP}} \cdot N_A , \qquad (1)$$

$$Q = (m_0 - \Delta m) / m_{NP} , \qquad (2)$$

where m_0, Δm and m_{NP} correspond to the initial sample weight, the weight of the grafted molecules or polymer determined by TGA, and the mass of a single nanoparticle, respectively. M is the molecular weight of BIBDA or M_n of the grafted polymer. N_A is the Avogadro's number and A_{NP} corresponds to the surface of one nanoparticle. For the calculation the NP's were assumed to be monodisperse in size with a spherical shape and an average diameter of 9.9 nm as determined by TEM. This results in an average surface area of A_{NP} = 307.9 nm² and an average NP volume of V_{NP} = 508.1 nm^3 for a single iron oxide nanoparticle. The mass of a single NP (m_{NP} = 2.5·10^{-18} g) was obtained by considering the density of maghemite (ρ = 4.9 g/cm³).[68]

Energy Dispersive X-Ray Spectroscopy (EDX) was performed on a Leo 1530 Gemini instrument equipped with a field emission cathode and a X-ray detector. The used acceleration voltage was between 0.5 kV and 3.0 kV. For preparation, the purified sample was drop-coated onto a silicon wafer and dried.

X-Ray Powder Diffraction (XRD) measurements were performed on a X'Pert Pro Powder diffractometer from PANalytical ($Cu_{K\alpha}$ radiation, 40 kV, 40 mA). For detection a X'Celerator Scientific RTMS detection unit was used. The dried samples were pestled and measured for 24 h.

Turbidity Measurements were performed using a titrator (Titrando 809, Metrohm, Herisau, Switzerland) equipped with a turbidity probe (λ_0 = 523 nm, Spectrosense, Metrohm) and a temperature sensor (Pt 1000, Metrohm). The temperature program (1 K/min) was run by a thermostat (LAUDA RE 306 and Wintherm_Plus software), using a home-made thermostatable vessel. The cloud points were determined from the intersection of the two tangents applied to the two linear regimes of the transmittance curve at the onset of turbidity.

Cell Transfection Experiments. *Mammalian Cell Lines and Culture Conditions.* The CHO-K1 (CCL-61, ATCC) and L929 (CCL-1, ATCC) cell lines were used in the transfection and cytotoxicity experiments, respectively. The cell lines were maintained in RPMI 1640 (CHO-K1) and MEM (L929) cell culture media supplemented with 10% fetal calf serum (FCS), 100 μg/mL streptomycin, 100 IU/mL penicillin, and 2 - 4 mM L-glutamine (as recommended by ATCC). Cells were cultivated at 37 °C in a humidified 5% CO_2 atmosphere.

Transfection. For transfection, the CHO-K1 cells were seeded at a density of 2 x 10^5 cells/well in 6-well plates 20 h prior transfection. One hour prior transfection, cells were rinsed with DPBS and supplemented with 2 mL OptiMEM. pDNA/polymer polyplexes were prepared by mixing 3 μg pDNA with the indicated amounts of the respective polycation stock

solution to achieve the desired N/P ratio in a final volume of 200 μL of aqueous 150 mM NaCl solution. Solutions were vortexed for 10 sec and incubated for 20 min at room temperature to allow polyplex formation. The polyplex suspension (200 μL) was added to the cells and the plates were centrifuged for 5 min at 200 g and placed for 4 h in the incubator. Afterwards, the medium was removed by aspiration, 2 mL of fresh growth medium were added, and the cells were further cultivated for 20 h. For analysis, the cells were harvested by trypsinization and resuspended in DPBS. Dead cells were identified *via* counterstaining with propidium iodide. The relative expression of EGFP fluorescence of 1×10^4 cells was quantified *via* flow cytometry using a Cytomics FC 500 (Beckman Coulter). Group data are reported as mean ± s.d.

MTT Assay. The cytotoxicity of γ-Fe_2O_3@$(PDMAEMA_{590})_{46}$ hybrid NP's was tested using L929 murine fibroblasts according to the norm ISO 10993-5,[69] using 1 mg/mL MTT-stock solution. As non-complexed polymers are considered to be more toxic than the polyplexes, the harsher conditions were tested by applying the hybrid NP's dilutions in a concentration range from 0.001 mg/mL to 5.0 mg/mL in 96-well plates. The cells were seeded at a density of 1×10^4 cells per well 24 h prior to the experiment. As 100% viability control, untreated cells were used. For each dilution step, 8 replicates were used. After dissolving the metabolically formed formazan crystals in isopropanol, the absorbance was measured using a plate reader (Genios Pro, Tecan) at a wavelength of 580 nm. For data evaluation, Origin 6.1 (OriginLab Corporation) software was used, the x-scale was plotted logarithmically and a nonlinear fit was run to obtain the lethal dose 50 (LD_{50}) values. Group data are reported as mean ± s.d.

Magnetic Separation of Cells. CHO-K1 cells were transfected at N/P 10 as described above. 24 h after transfection, the cells were harvested by trypsinization and transferred into PS cuvettes (VWR). The cuvette was then placed in the vicinity of the magnet in the cell culture incubator. After overnight incubation close to the magnet, cells were washed, fixed and stained with Hoechst 33258 (1 μg/mL). Cells growing on side A (wall of the cuvette next to the magnet) and B (wall of the cuvette on the opposite site of the magnet) were analyzed by epifluorescence microscopy (Olympus, BX51TF, Hamburg, Germany).

3.4. Results and Discussion

ATRP initiator-functionalized maghemite NP's (γ-Fe_2O_3@BIBDA). The maghemite (γ-Fe_2O_3) nanoparticles used in this study were synthesized *via* thermal decomposition of $Fe(CO)_5$ and exhibit a well-defined size and narrow size distribution as revealed by transmission electron microscopy (TEM) and dynamic light scattering (DLS) (Supporting Information, Figures S1, S2). TEM image analysis gave a number-average diameter of 9.9 ± 1.8 nm (average over 300 particles). The slightly higher z-averaged hydrodynamic diameter of 13.2 ± 1.2 nm observed by DLS can be attributed to the oleic acid coating of the maghemite nanoparticles. Because of the significantly lower electron density of the oleic acid shell with respect to that of the iron oxide nanoparticle, it is not visible in TEM and thus does not contribute to the measured nanoparticles´ size. The maghemite modification of the synthesized iron oxide nanoparticles was proven by powder diffraction analysis (Supporting Information, Figure S3).

The maghemite NP's were functionalized with a dopamine-based ATRP initiator, 2-bromoisobutyryl dopamide (BIBDA), by ligand exchange reaction in THF (Scheme 1). The composition of the nanoparticles´ surface after functionalization was investigated by energy dispersive X-ray spectroscopy (EDX). The EDX spectrum shows the characteristic signal for bromine at around 1.5 keV indicating a successful attachment of BIBDA onto the surface (Supporting Information, Figure S4). The comparison of the FT-IR spectra of the BIBDA-functionalized NP's (γ-Fe_2O_3@BIBDA) with the spectra of oleic acid stabilized NP's (γ-Fe_2O_3@Oleic acid), pure oleic acid, and pure BIBDA clearly confirms a successful functionalization (Figure 1). In case of γ-Fe_2O_3@Oleic acid, the characteristic stretching vibrations of the aliphatic CH_2 and CH_3 groups at 2900-2800 cm^{-1} and of the carbonyl group at 1700 cm^{-1} of oleic acid are observed. After ligand exchange with BIBDA the maghemite nanoparticles show the specific dopamine bands at 3700-3100 cm^{-1} and 1650 cm^{-1}, corresponding to hydroxyl/amide (-O-H; N-H) and amide I (C=O) bonds, respectively. The pronounced stretching vibrations of the aliphatic CH_2 and CH_3 groups at 2900-2800 cm^{-1} and the small shoulder at 1700 cm^{-1} (carbonyl, C=O) in the IR spectrum of γ-Fe_2O_3@BIBDA indicate that the surface is still covered by remaining oleic acid, *i. e.*, only a partial ligand exchange of the oleic acid with BIBDA occurred. It is noted, that the bands of the molecules attached to the surface of the NP's and especially for the binding groups are slightly shifted compared to the pure substances.

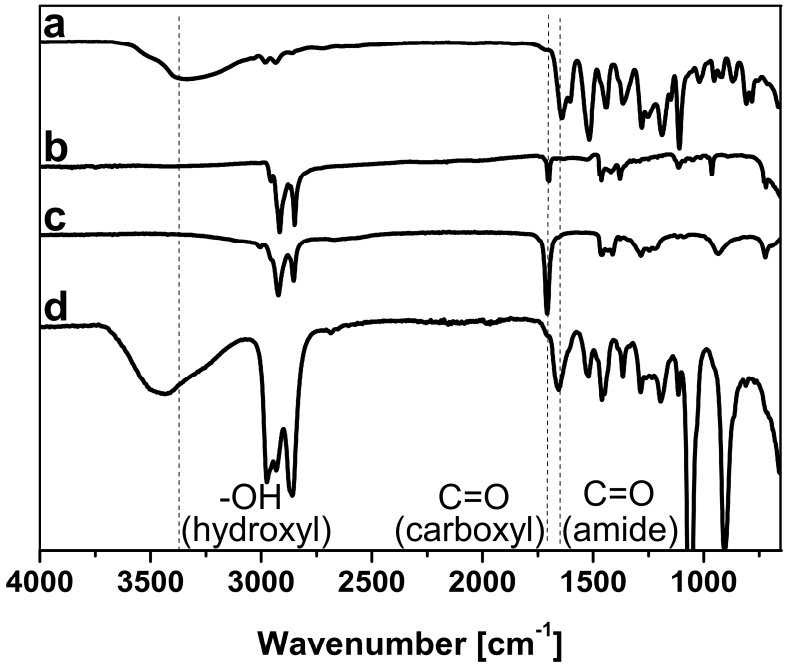

Figure 1. FT-IR spectra of pure BIBDA (a), oleic acid stabilized nanoparticles FT-IR spectra of pure BIBDA (a), oleic acid stabilized nanoparticles γ-Fe_2O_3@Oleic acid (b), pure oleic acid (c) and BIBDA-functionalized nanoparticles γ-Fe_2O_3@BIBDA (d).

Further investigations to quantify the amount of BIBDA on the surface of the NP's were performed by thermogravimetric analysis (TGA). It was found that pure BIBDA shows complete degradation at much higher temperatures compared to oleic acid and exhibits a characteristic degradation step at temperatures above 440 °C, which corresponds to 40% of the total mass loss (Supporting Information, Figure S5). This characteristic degradation beyond 440 °C can also be observed for the BIBDA-functionalized NP's as revealed by comparing the TGA traces of γ-Fe_2O_3@Oleic acid and γ-Fe_2O_3@BIBDA (Figure 2). Thus, this specific weight loss can be used to calculate the weight fraction of the attached BIBDA to 5.7 wt%. This in turn allows to calculate the grafting density according to the procedure described in the Experimental Part, resulting in approx. 350 initiator molecules/nanoparticle. It is noted that the calculated weight fraction of BIBDA is not consistent with the observed weight loss by TGA, which gives an almost threefold higher weight loss of 16.5%. This indicates that just a partial ligand exchange took place and a certain fraction of oleic acid is still remaining on the surface as already observed by FT-IR. We did not evaluate the amount of remaining oleic acid as polar impurities might bind to the nanoparticles' surface, too, and thus would result in an overestimation of the oleic acid content. In addition, the grafting density was determined from the bromine content of 2.13 wt% measured by ion chromatography. The calculated BIBDA content of 8.0 wt% corresponds to a grafting density

of ca. 480 initiator molecules/particle. Both results are in good agreement within the limit of experimental accuracy achieving an average grafting density of ca. 415 initiator molecules/particle.

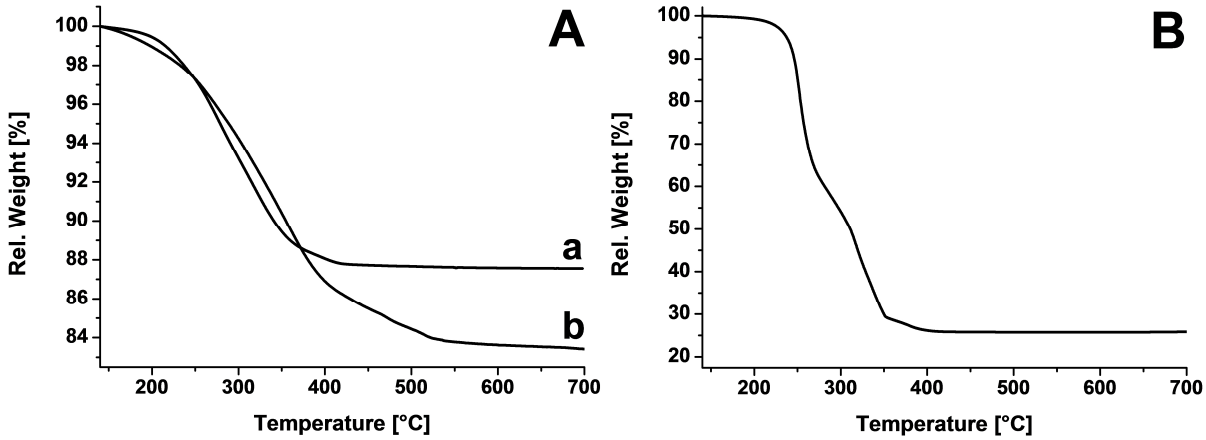

Figure 2. (A) Comparison of the TGA traces of a) γ-Fe_2O_3@Oleic acid and b) γ-Fe_2O_3@BIBDA. (B) TGA trace of γ-Fe_2O_3@$(PDMAEMA_{590})_{46}$.

PDMAEMA-grafted NP's (γ-Fe_2O_3@PDMAEMA). The BIBDA-functionalized particles were further used for the surface-initiated ATRP of 2-(dimethylamino)ethyl methacrylate (DMAEMA) in anisole. Asymmetric flow field-flow fractionation (AF-FFF) was utilized to characterize the crude product obtained after polymerization. In this method low molecular weight fractions elute first. Thus, non-bound PDMAEMA chains are expected to elute at lower elution volumes compared to the PDMAEMA grafted nanoparticles. In Figure 3A the eluograms of the as prepared grafted nanoparticles (γ-Fe_2O_3@PDMAEMA) and the cleaved-off PDMAEMA chains, obtained by acidic hydrolysis of the iron oxide cores, are shown. The grafted nanoparticles show a strong peak at V_e = 15 ml, which corresponds to non-bound PDMAEMA chains as the elution volume is identical to that observed for the cleaved-off PDMAEMA chains. Besides, there is no distinct RI signal detectable for the grafted NP's indicating a large amount of non-bound PDMAEMA chains present in the crude product. Consequently, the resulting PDMAEMA grafted NP's were purified by temperature-induced precipitation in order to remove non-bound PDMAEMA. This method takes advantage of the significantly lower cloud point of the γ-Fe_2O_3@PDMAEMA NP's at high pH with respect to that of non-bound PDMAEMA (see discussion on Figure 5 below). The AF-FFF eluogram of the sample directly after purification shows only an insignificant amount of non-bound polymer (Figure 3A), which allows the determination of the initial grafting density right after purification. For an evaluation of the grafting density by TGA, the molecular weight of the grafted PDMAEMA chains was determined by cleaving the chains from the iron oxide core

via hydrolysis with hydrochloric acid and subsequent SEC analysis, yielding M_n(PDMAEMA) = 93.000 g/mol (PDI = 1.22). The TGA trace of the purified γ-Fe_2O_3@PDMAEMA NP's shows an increased weight loss of about 60.8 % compared to the NP's just carrying the ATRP initiator, indicating the successful grafting of PDMAEMA (Figure 2B). By utilizing eq. 1, the resulting grafting density for the PDMAEMA chains tethered to the surface of the NP's is ca. 46 chains per particle (0.15 chains/nm²). Consequently, the hybrid nanoparticles are denoted as γ-Fe_2O_3@$(PDMAEMA_{590})_{46}$, where the first index corresponds to the number average degree of polymerization of the PDMAEMA chains.

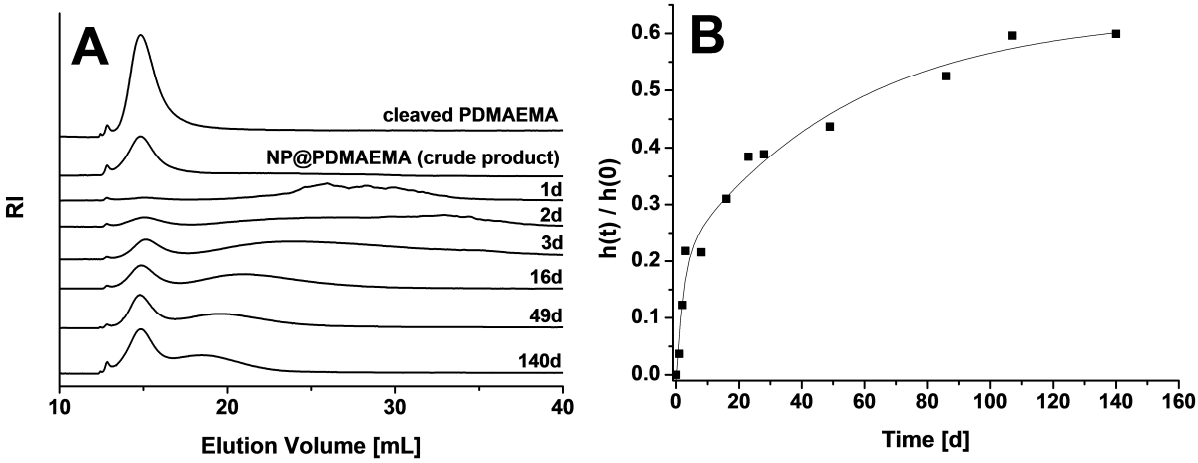

Figure 3. (A) Comparison of AF-FFF eluograms (RI signal, c = 1 g/L) of the cleaved-off PDMAEMA chains, γ-Fe_2O_3@PDMAEMA crude product, and γ-Fe_2O_3@$(PDMAEMA_{590})_{51}$ at various times after purification (eluent: deionized water containing 25 mM $NaNO_3$ and 200 ppm NaN_3).(B) Kinetics of the detachment of PDMAEMA chains.

Stability of γ-Fe_2O_3@PDMAEMA. An AF-FFF study was performed to investigate the stability of the grafted particles. Although the particles are highly stable and well dispersed in aqueous media for months a slow detachment of the dopamine anchoring group was observed. The extent of this effect was investigated by measuring a sample (γ-Fe_2O_3@$(PDMAEMA_{590})_{51}$) right after purification *via* temperature-induced precipitation and further upon storage over several weeks. The AF-FFF eluogram of the sample measured 1 day after purification shows only an insignificant amount of non-bound polymer. However, measurements performed afterwards reveal an increase of the fraction of non-bound PDMAEMA chains with time and thus, a decrease of the grafting density (Figure 3A). The kinetics of the chain detachment were followed by evaluating the height, $h(t)$, of the elution peak at V_e = 15 ml (RI signal) corresponding to non-bound PDMAEMA chains. As a reference, the peak height, $h(0)$, for the sample containing the respective cleaved-off

PDMAEMA chains, only, was used. It is noted, that all measurements were normalized with respect to the PDMAEMA content. Thus, the ratio $h(t)/h(0)$ gives a quantitative measure for the fraction of detached PDMAEMA chains in dependence on time (Figure 3B). A detailed description of the applied procedure can be found in the Experimental Section. The kinetics of this process indicates a fast detachment of polymer chains at the beginning which is already decreasing within the first week and is even more reduced after several weeks. A near-equilibrium state is observed after ca. 110 days indicating that ca. 40% of the initially grafted PDMAEMA chains remain on the particles. During this time a decrease in particle size takes place as revealed by the progressively decreasing elution volume of the grafted particles. The broad distributions observed for the samples shortly after purification are caused by small aggregates, which completely dissolve after one week.

These results are in accordance with the work of Reimhult and co-workers who investigated in detail the stability of dopamine as binding unit.[70, 71] Their studies were based on magnetite nanoparticles modified *via* the grafting-to approach using various dopamine derivatives and end-functionalized poly(ethylene glycol)s. Similar to our results a reversible attachment was found for non-functionalized dopamine.

Despite the reversible binding and the presence of free PDMAEMA chains the polymer-grafted nanoparticles show excellent stability and solubility in aqueous media without agglomeration. γ-Fe_2O_3@$(PDMAEMA_{590})_{46}$ can be stored in deionized water (concentration range 2 – 5 g/L) over time periods of more than 6 months without precipitation. In addition, the long-term stability in buffer solutions was tested for pH 8 – 10. The γ-Fe_2O_3@$(PDMAEMA_{590})_{46}$ solutions (c = 0.5 g/L) were kept for more than 6 months at 3 °C showing no sign of precipitation and the corresponding TEM micrographs show only well dispersed hybrid NP's (Supporting Information, Figure S6).

pH- and Temperature-Responsive Agglomeration. Due to the partial detachment of the PDMAEMA chains with time we used freshly purified NP's bearing 53 $PDMAEMA_{590}$ arms (γ-Fe_2O_3@$(PDMAEMA_{590})_{53}$) to investigate the dual-responsive behavior *via* turbidimetry (Figure 4). The coil-to-globule transitions at the cloud point of the grafted particles were sharp and strongly dependent on pH. At pH 7, the PDMAEMA chains are partially protonated ($pK_a \approx 6.2$),[41] resulting in good solubility in water with a cloud point as high as 80 °C. By increasing the pH the PDMAEMA becomes progressively less charged. Consequently, the cloud point decreases to 28 °C at pH 10. These observations are similar to those for PDMAEMA stars.[41]

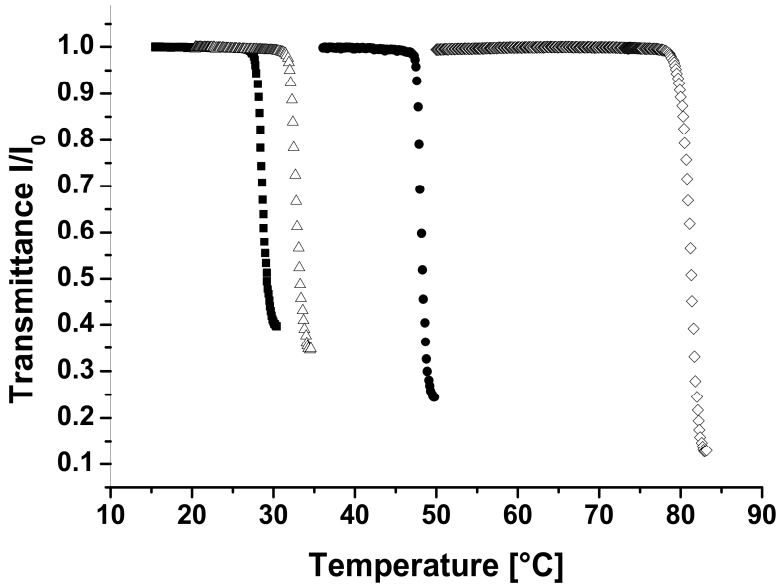

Figure 4. Turbidity measurements of γ-Fe_2O_3@$(PDMAEMA_{590})_{53}$ (c = 0.1 g/L) at different pH: pH 10 (■), pH 9 (△), pH 8 (●), and pH 7 (◇).

In addition, the solution properties of the cleaved-off linear $PDMAEMA_{590}$ chains were also analyzed. Since there is a strong influence of the molecular weight on the cloud point especially at high pH,[41] the cloud point of the PDMAEMA-grafted NP's (having a ca. 50-fold molecular weight) is supposed to be lower than that of the corresponding cleaved-off arms. This is indeed observed (Figure 5). Whereas the cloud points of the γ-Fe_2O_3@$(PDMAEMA_{590})_{53}$ hybrid star and those of a 24-arm PDMAEMA star ($(PDMAEMA_{240})_{24}$) are very close, those of the free arms are higher by about 5 K at pH 10. The reversibility of the temperature induced agglomeration was demonstrated by dispersing the hybrid stars in pH 9 buffer solution (c = 1 g/L; $T_{CP} \approx 33$ °C) and heating above the cloud point up to 45 °C. After 10 cycles of precipitation and redispersion the particles stay still well dispersed in aqueous media.

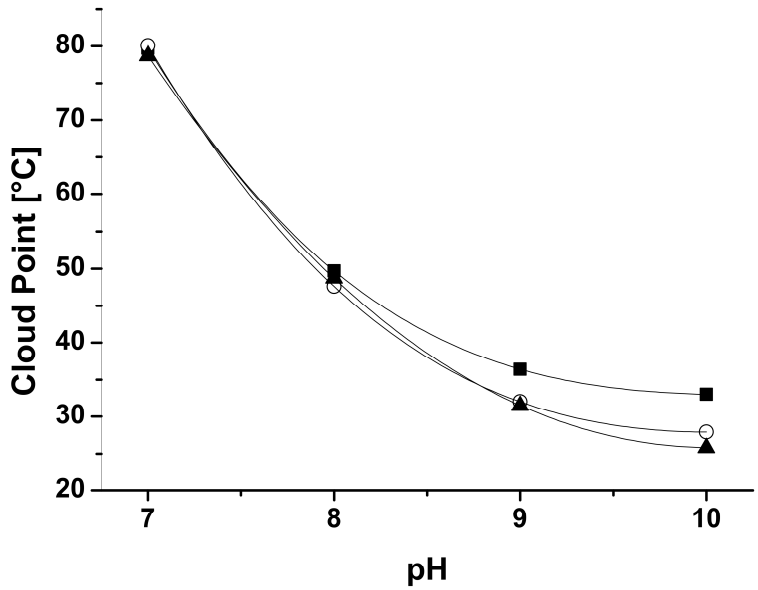

Figure 5. Cloud points in dependence on pH for 0.1 g/L solutions of cleaved $PDMAEMA_{590}$ (■), γ-Fe_2O_3@$(PDMAEMA_{590})_{53}$ (○), and $(PDMAEMA_{240})_{24}$ stars (▲)[41].

Magnetic Properties. Due to steric and electrostatic repulsion of the long PDMAEMA chains (M_n(arm) = 93.000 g/mol) preventing agglomeration, it is impossible to separate the grafted NP's just by applying a magnet. Even by using strong NdFeB magnets (M_r = 1.2 T) the grafted particles stay well-dispersed in solution. This highly stable suspension of the particles causes a motion of the entire liquid in direction of the magnet (Figure 6A). However, above the cloud point only the agglomerated hybrid NP's are attracted by the magnet (Figure 6B). Consequently, for collecting the NP's by applying a magnet they have at first to be precipitated, *e.g.* by heating above the cloud point.

Magnetization measurements carried out *via* vibrating sample magnetometry (VSM) prove the superparamagnetic behavior of the unmodified particles and γ-Fe_2O_3@PDMAEMA (Figure 6C). The normalized graphs of both pure and grafted particles show the typical symmetrical sigmoidal shape without hysteresis indicating that magnetic redistribution takes place *via* internal (Néel) relaxation. No significant difference between the two samples can be observed.

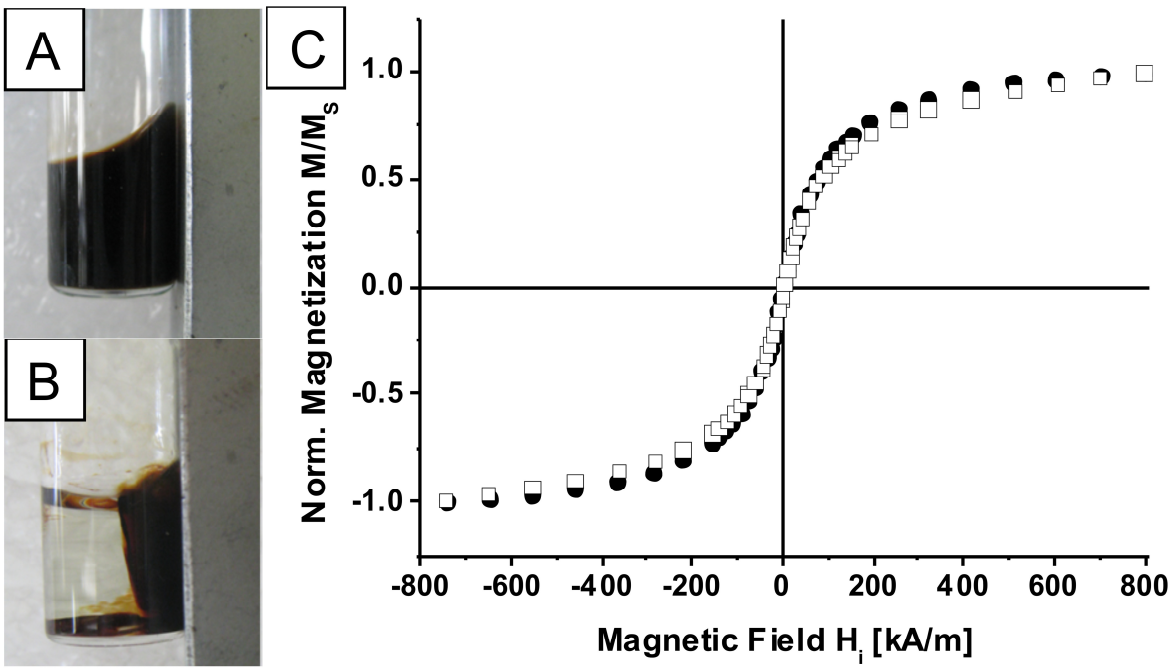

Figure 6. Aqueous γ-Fe_2O_3@PDMAEMA dispersion (50 g/L, pH 10 buffer, cloud point T_{CP} ≈ 27 °C) under influence of a NdFeB magnet below (A) and above the cloud point (B). C) Normalized magnetization curves of γ-Fe_2O_3@Oleic acid (●) and γ-Fe_2O_3@$(PDMAEMA_{590})_{46}$ (□).

Utilization of γ-Fe_2O_3@$(PDMAEMA_{590})_{46}$ hybrid NP's for gene delivery. *Cytotoxicity.* Toxicity is a major issue for non-viral delivery and a rough correlation between toxicity and transfection efficiency has been described in the past for many non-viral delivery agents.[72] For estimation, MTT assays were performed to evaluate the metabolic activity of L929 cells exposed to γ-Fe_2O_3@$(PDMAEMA_{590})_{46}$ hybrid particles and PEI homopolymer under conditions mimicking transfection conditions. In this context, the investigation of the damaging effects of the free, non-bound PDMAEMA chains reflects a worst case setting. γ-Fe_2O_3@$(PDMAEMA_{590})_{46}$ NP's affected the metabolic activity in a concentration dependent manner when it was added in the concentration range 0 to 5 mg/mL to the cells. Under these conditions, the LD_{50} for cells treated with the polycations are 0.09 ± 0.003 mg/mL (γ-Fe_2O_3@$(PDMAEMA_{590})_{46}$) and 0.06 ± 0.004 mg/mL (PEI). These concentration ranges are more than 10-fold above the concentrations utilized for subsequent transfection assays performed at a N/P ratio of 10 to 20. Hence, in contrast to the commonly accepted opinion that cytotoxicity increases as a function of the polycation molecular weight, the γ-Fe_2O_3@$(PDMAEMA_{590})_{46}$ hybrid NP's have clearly a less detrimental effect on cell metabolism despite a molecular weight almost 160-fold higher than the used PEI's.

Transfection. The efficiency of the γ-Fe_2O_3@$(PDMAEMA_{590})_{46}$ hybrid NP's as potential transfection reagents was explored under standard conditions in CHO-K1 cells and the

transfection efficiency was compared to the gold standard PEI. A qualitative analysis of the transfected cells by epifluorescence microscopy revealed that after transfection with γ-Fe_2O_3@$(PDMAEMA_{590})_{46}$ a higher number of EGFP-expressing cells (showing green fluorescence) is seen than for PEI transfection (Figure 7).

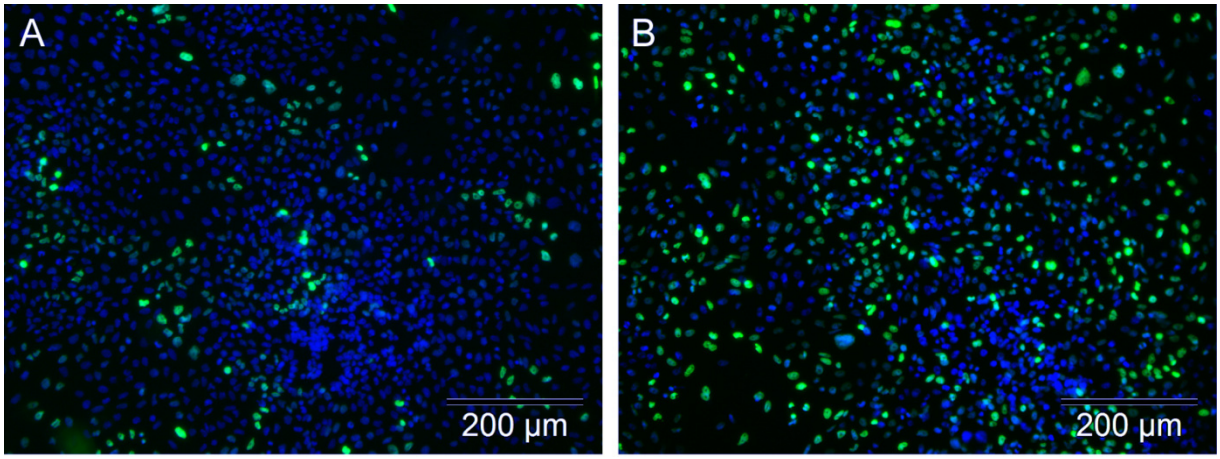

Figure 7. CHO-K1 cells transfected with the indicated polymers and pH2B-EGFP (green) at N/P ratio of 10 in 150 mM NaCl. After transfection cells were washed, fixed, and nuclei are counterstained with Hoechst 33528 (blue). A) PEI, B) γ-Fe_2O_3@$(PDMAEMA_{590})_{46}$.

Additionally, a quantitative analysis was performed by flow cytometry. The results showed that the γ-Fe_2O_3@$(PDMAEMA_{590})_{46}$ led to a high transfection efficiency depending on the N/P ratio and performed best at N/P = 10 - 20 with averaged transfection efficiencies between 53.5 ± 12.4% and 61.4 ± 6.6%. Corresponding experiments with PEI led at most to 27.6 ± 11.2% transfected cells in accordance to data published elsewhere.[63] In all cases, the cell viability was above 75% as measured by counterstaining the dead cells with propidium iodide. It is noted that even a 3 months aged γ-Fe_2O_3@$(PDMAEMA_{590})_{46}$ sample shows no significant decrease of the transfection efficiency compared to a freshly purified one.

Magnetic separation of transfected cells. Despite their superparamagnetic properties in solution, the free γ-Fe_2O_3@$(PDMAEMA_{590})_{46}$ hybrid NP's cannot be separated with a strong permanent magnet (Figure 6A). In a preliminary investigation, we were able to show that a separation with a magnetic field is feasible after polyplex formation, *i.e.*, interaction of γ-Fe_2O_3@$(PDMAEMA_{590})_{46}$ with plasmid DNA. Taking this into consideration, we hypothesized that cells transfected with γ-Fe_2O_3@$(PDMAEMA_{590})_{46}$/pDNA polyplexes might acquire magnetic properties. To verify this hypothesis, CHO-K1 cells were transfected, harvested after 24 h and then incubated overnight in the vicinity of a magnet (Figure 8A). Analysis of the cells localization by epifluorescence microscopy showed that most of the cells,

transfected with γ-Fe_2O_3@$(PDMAEMA_{590})_{46}$, segregated on the wall of the cuvette facing the magnet and thus displayed magnetic properties (Figures 8B, 8C). By comparison, most of the cells transfected with PEI were found to sediment at the bottom of the cuvette. Experimental conditions allowing the magnetic isolation of transfected cells and their further cultivation are currently under investigation.

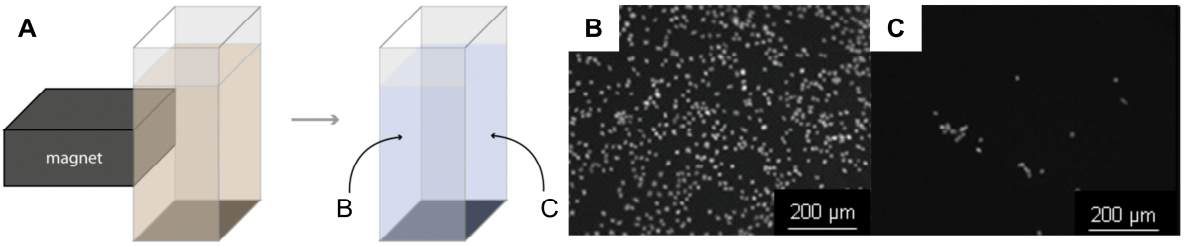

Figure 8. Magnetic separation of cells transfected with γ-Fe_2O_3@$(PDMAEMA_{590})_{46}$/pDNA polyplexes. Separation scheme (A). Fluorescence microscopy pictures of the cells grown on the wall facing the magnet (B) or on the opposite wall (C). The nuclei were counterstained with Hoechst 33258.

3.5. Conclusions

We successfully synthesized dual-responsive magnetic core-shell nanoparticles using a dopamine-functionalized ATRP initiator. The PDMAEMA chains grafted from the maghemite nanoparticles´ surface provide high stability in aqueous media over more than six months, even though a slow detachment of the dopamine anchor and thus of the grafted PDMAEMA chains was observed. The hybrid nanoparticles are able to undergo reversible pH-dependent temperature-induced agglomeration. Nevertheless, a different approach needs to be developed, which enables a permanent covalent attachment of the polymer chains onto the nanoparticles' surface, especially with respect to biotechnological applications.

Despite the reversible binding of the PDMAEMA chains our present approach already provides magnetic core-shell nanoparticles of sufficient solubility and stability in aqueous media. In addition, since PDMAEMA forms polyelectrolyte complexes with pDNA these nanoparticles can be utilized for biotechnological applications. Notably, the hybrid NP's described in this contribution might help solving two major problems of cell line development for production of recombinant proteins in animal cells, *i.e.*, efficient delivery of plasmid DNA into the cells and thereafter selection of the transfected cells. In particular, compared to PEI, which is regarded as one of the best commercially available standard polycationic polymers for non-viral gene transfer, the investigated γ-Fe_2O_3@$(PDMAEMA_{590})_{46}$ NP's offer the great

advantage to combine a high transfection capability (almost twofold higher than PEI) with a low *in vitro* cytotoxicity and should be considered as a good candidate for delivery of plasmid DNA. Most importantly, as opposed to most applications of magnetic nanoparticles for gene delivery (as reviewed by Kami et al.[65]), the improved efficiency in transfections with γ-Fe_2O_3@$(PDMAEMA_{590})_{46}$ NP's does not rely on the application of a magnetic field (*i.e.*, *Magnetofection*™).[73] Furthermore, this contribution is, to the best of our knowledge, the first one describing the magnetic isolation of animal cells without using specific ligands or surface receptors (*i.e.*, magnetic particles linked to specific antibodies). Taking advantage of the magnetic properties of the γ-Fe_2O_3@PDMAEMA/pDNA polyplexes, these NP's provide a tool that allows the identification/isolation of cells containing polyplexes and thus the removal of non-transfected cells. Magnetic cell sorting of transfected cells in turn would also enable a recovery/identification of the magnetic polyplexes trapped inside the cells, which possibly helps investigating the mechanism of transfection. Therefore, the γ-Fe_2O_3@PDMAEMA hybrid NP's might become a useful tool to accelerate the development of production cell lines for the biopharmaceutical industry.

Acknowledgments: This work was supported by the DFG priority program SPP 1259. We thank Melanie Förtsch for performing the TEM experiments, Sandrine Tea and Marietta Böhm for SEC and AF-FFF measurements, Thomas Friedrich for VSM measurements, Thomas Lunkenbein for XRD analysis, Martina Heider for EDX analysis and Dr. Jiayin Yuan for inspiring discussions.

3.6. References

(1) Odenbach, S., *Colloidal magnetic fluids: basics, development and application of ferrofluids*. Springer: Berlin Heidelberg, 2009; Vol. 763, p 430.

(2) Faraji, M.; Yamini, Y.; Rezaee, M. *J. Iran. Chem. Soc.* **2010**, *7*, 1-37.

(3) Behrens, S. *Nanoscale* **2011**, *3*, 877-892.

(4) Hyeon, T.; Lee, S. S.; Park, J.; Chung, Y.; Na, H. B. *J. Am. Chem. Soc.* **2001**, *123*, 12798-12801.

(5) Sun, S.; Zeng, H. *J. Am. Chem. Soc.* **2002**, *124*, 8204-8205.

(6) Park, J.; An, K.; Hwang, Y.; Park, J.-G.; Noh, H.-J.; Kim, J.-Y.; Park, J.-H.; Hwang, N.-M.; Hyeon, T. *Nat. Mater.* **2004**, *3*, 891-895.

(7) Gupta, A. K.; Gupta, M. *Biomaterials* **2005**, *26*, 3995-4021.

(8) Huber, D. L. *Small* **2005**, *1*, 482-501.

(9) Schmidt, A. M. *Colloid Polym. Sci.* **2007**, *285*, 953-966.

(10) Hao, R.; Xing, R.; Xu, Z.; Hou, Y.; Gao, S.; Sun, S. *Adv. Mater.* **2010**, *22*, 2729-2742.

(11) Lutz, J.-F.; Stiller, S.; Hoth, A.; Kaufner, L.; Pison, U.; Cartier, R. *Biomacromolecules* **2006**, *7*, 3132-3138.

(12) White, M. A.; Johnson, J. A.; Koberstein, J. T.; Turro, N. J. *J. Am. Chem. Soc.* **2006**, *128*, 11356-11357.

(13) Nikolic, M. S.; Krack, M.; Aleksandrovic, V.; Kornowski, A.; Förster, S.; Weller, H. *Angew. Chem., Int. Ed.* **2006**, *45*, 6577-6580.

(14) Achilleos, D. S.; Vamvakaki, M. *Materials* **2010**, *3*, 1981-2026.

(15) Gelbrich, T.; Feyen, M.; Schmidt, A. M. *Macromolecules* **2006**, *39*, 3469-3472.

(16) Gravano, S. M.; Dumas, R.; Liu, K.; Patten, T. E. *J. Polym. Sci., Part A: Polym. Chem.* **2005**, *43*, 3675-3688.

(17) Vestal, C. R.; Zhang, Z. J. *J. Am. Chem. Soc.* **2002**, *124*, 14312-14313.

(18) Gu, H.; Xu, K.; Yang, Z.; Chang, C. K.; Xu, B. *Chem. Commun.* **2005**, 4270-4272.

(19) Nagesha, D. K.; Plouffe, B. D.; Phan, M.; Lewis, L. H.; Sridhar, S.; Murthy, S. K. *J. Appl. Phys.* **2009**, *105*, 07B317/1-07B317/3.

(20) Peng, S.; Wang, C.; Xie, J.; Sun, S. *J. Am. Chem. Soc.* **2006**, *128*, 10676-10677.

(21) Xu, C.; Xu, K.; Gu, H.; Zheng, R.; Liu, H.; Zhang, X.; Guo, Z.; Xu, B. *J. Am. Chem. Soc.* **2004**, *126*, 9938-9939.

(22) Goldmann, A. S.; Schödel, C.; Walther, A.; Yuan, J.; Loos, K.; Müller, A. H. E. *Macromol. Rapid Commun.* **2010**, *31*, 1608-1615.

(23) Araujo, P. Z.; Morando, P. J.; Blesa, M. A. *Langmuir* **2005**, *21*, 3470-3474.

(24) Dalsin, J. L.; Hu, B.-H.; Lee, B. P.; Messersmith, P. B. *J. Am. Chem. Soc.* **2003**, *125*, 4253-4258.

(25) Dalsin, J. L.; Lin, L.; Tosatti, S.; Vörös, J.; Textor, M.; Messersmith, P. B. *Langmuir* **2005**, *21*, 640-646.

(26) Fan, X.; Lin, L.; Dalsin, J. L.; Messersmith, P. B. *J. Am. Chem. Soc.* **2005**, *127*, 15843-15847.

(27)Hong, R.; Fischer, N. O.; Emrick, T.; Rotello, V. M. *Chem. Mater.* **2005**, *17*, 4617-4621.

(28) Rodríguez, R.; Blesa, M. A.; Regazzoni, A. E. *J. Colloid Interface Sci.* **1996**, *177*, 122-131.

(29) Ye, Q.; Wang, X.; Hu, H.; Wang, D.; Li, S.; Zhou, F. *J. Phys. Chem. C* **2009**, *113*, 7677-7683.

(30) Ye, Q.; Wang, X.; Li, S.; Zhou, F. *Macromolecules* **2010**, *43*, 5554-5560.

(31) Mistlberger, G.; Koren, K.; Scheucher, E.; Aigner, D.; Borisov, S. M.; Zankel, A.; Pölt, P.; Klimant, I. *Adv. Funct. Mater.* **2010**, *20*, 1842-1851.

(32) Sheparovych, R.; Sahoo, Y.; Motornov, M.; Wang, S.; Luo, H.; Prasad, P. N.; Sokolov, I.; Minko, S. *Chem. Mater.* **2006**, *18*, 591-593.

(33) Niu, D.; Li, Y.; Ma, Z.; Diao, H.; Gu, J.; Chen, H.; Zhao, W.; Ruan, M.; Zhang, Y.; Shi, J. *Adv. Funct. Mater.* **2010**, *20*, 773-780.

(34) Zhu, J.; Hayward, R. C. *J. Am. Chem. Soc.* **2008**, *130*, 7496-7502.

(35) Reinicke, S.; Döhler, S.; Tea, S.; Krekhova, M.; Messing, R.; Schmidt, A. M.; Schmalz, H. *Soft Matter* **2010**, *6*, 2760-2773.

(36) Neoh, K. G.; Kang, E. T. *Polym. Chem.* **2011**, *2*, 747-759.

(37) Medeiros, S. F.; Santos, A. M.; Fessi, H.; Elaissari, A. *Int. J. Pharm.* **2011**, *403*, 139-161.

(38) Chanana, M.; Jahn, S.; Georgieva, R.; Lutz, J.-F.; Bäumler, H.; Wang, D. *Chem. Mater.* **2009**, *21*, 1906-1914.

(39) Gelbrich, T.; Reinartz, M.; Schmidt, A. M. *Biomacromolecules* **2010**, *11*, 635-642.

(40) Schmalz, A.; Hanisch, M.; Schmalz, H.; Müller, A. H. E. *Polymer* **2010**, *51*, 1213-1217.

(41) Plamper, F. A.; Ruppel, M.; Schmalz, A.; Borisov, O.; Ballauff, M.; Müller, A. H. E. *Macromolecules* **2007**, *40*, 8361-8366.

(42) Üzgün, S.; Akdemir, Ö.; Hasenpusch, G.; Maucksch, C.; Golas, M. M.; Sander, B.; Stark, H.; Imker, R.; Lutz, J.-F.; Rudolph, C. *Biomacromolecules* **2010**, *11*, 39-50.

(43) Boyer, C.; Priyanto, P.; Davis, T. P.; Pissuwan, D.; Bulmus, V.; Kavallaris, M.; Teoh, W. Y.; Amal, R.; Carroll, M.; Woodward, R.; St Pierre, T. *J. Mater. Chem.* **2010**, *20*, 255-265.

(44) Namgung, R.; Singha, K.; Yu, M. K.; Jon, S.; Kim, Y. S.; Ahn, Y.; Park, I.-K.; Kim, W. J. *Biomaterials* **2010**, *31*, 4204-4213.

(45) Babič, M.; Horák, D.; Jendelová, P.; Glogarová, K.; Herynek, V.; Trchová, M.; Likavčanová, K.; Lesný, P.; Pollert, E.; Hájek, M.; Syková, E. *Bioconjugate Chem.* **2009**, *20*, 283-294.

(46) Al-Deen, F. N.; Ho, J.; Selomulya, C.; Ma, C.; Coppel, R. *Langmuir* **2011**, *27*, 3703-3712.

(47) van de Wetering, P.; Cherng, J.-Y.; Talsma, H.; Crommelin, D. J. A.; Hennink, W. E. *J. Control. Release* **1998**, *53*, 145-153.

(48) Cherng, J.-Y.; van de Wetering, P.; Talsma, H.; Crommelin, D. J. A.; Hennink, W. E. *Pharm. Res.* **1996**, *13*, 1038-1042.

(49) van de Wetering, P.; Cherng, J.-Y.; Talsma, H.; Hennink, W. E. *J. Control. Release* **1997**, *49*, 59-69.

(50) Deshpande, M. C.; Davies, M. C.; Garnett, M. C.; Williams, P. M.; Armitage, D.; Bailey, L.; Vamvakaki, M.; Armes, S. P.; Stolnik, S. *J. Control. Release* **2004**, *97*, 143-156.

(51) Deshpande, M. C.; Garnett, M. C.; Vamvakaki, M.; Bailey, L.; Armes, S. P.; Stolnik, S. *J. Control. Release* **2002**, *81*, 185-199.

(52) Rungsardthong, U.; Deshpande, M.; Bailey, L.; Vamvakaki, M.; Armes, S. P.; Garnett, M. C.; Stolnik, S. *J. Control. Release* **2001**, *73*, 359-380.

(53) Lam, J. K. W.; Ma, Y.; Armes, S. P.; Lewis, A. L.; Baldwin, T.; Stolnik, S. *J. Control. Release* **2004**, *100*, 293-312.

(54) He, C.-X.; Tabata, Y.; Gao, J.-Q. *Int. J. Pharm.* **2010**, *386*, 232-242.

(55) Grigsby, C. L.; Leong, K. W. *J. R. Soc. Interface* **2010**, S67-S82.

(56) Üzgün, S.; Nica, G.; Pfeifer, C.; Bosinco, M.; Michaelis, K.; Lutz, J.-F.; Schneider, M.; Rosenecker, J.; Rudolph, C. *Pharm. Res.* **2011**, *28*, 2223-2232.

(57) Uchida, E.; Mizuguchi, H.; Ishii-Watabe, A.; Hayakawa, T. *Biol. Pharm. Bull.* **2002**, *25*, 891-897.

(58) Plank, C.; Scherer, F.; Schillinger, U.; Anton, M. *J. Gene Med.* **2000**, *2 (Suppl)*, 24.

(59) Plank, C.; Zelphati, O.; Mykhaylyk, O. *Adv. Drug Delivery Rev.* **2011**, *63*, 1300-1331.

(60) Corchero, J. L.; Villaverde, A. *Trends Biotechnol.* **2009**, *27*, 468-476.

(61) Guo, X.; Huang, L. *Acc. Chem. Res.* **2011**, *In press*.

(62) McBain, S. C.; Yiu, H. H. P.; Dobson, J. *Int. J. Nanomed.* **2008** *3*,169-180.

(63) Schallon, A.; Jérôme, V.; Walther, A.; Synatschke, C. V.; Müller, A. H. E.; Freitag, R. *React. Funct. Polym.* **2010**, *70*, 1-10.

(64) Synatschke, C. V.; Schallon, A.; Jérôme, V.; Freitag, R.; Müller, A. H. E. *Biomacromolecules* **2011**, *12*, 4247-4255.

(65) Kami, D.; Takeda, S.; Itakura, Y.; Gojo, S.; Watanabe, M.; Toyoda, M. *Int. J. Mol. Sci.* **2011**, *12*, 3705-3722.

(66) Plamper, F. A.; Becker, H.; Lanzendörfer, M.; Patel, M.; Wittemann, A.; Ballauff, M.; Müller, A. H. E. *Macromol. Chem. Phys.* **2005**, *206*, 1813-1825.

(67) Kanda, T.; Sullivan, K. F.; Wahl, G. M. *Curr. Biol.* **1998**, *8*, 377-385.

(68)Anthony, J. W.; Bideaux, R. A.; Bladh, K. W.; Nichols, M. C., *Handbook of mineralogy, volume III: halides, hydroxides, oxides*. Mineralogical Society of America: Chantilly, 1997; p 628.

(69) ISO 10993-5:2009 Biological evaluation of medical devices part 5: tests for *in vitro* cytotoxicity. Edition: 3, Stage: 60.60 - TC 194 - ICS: 11.100.20.

(70) Amstad, E.; Gehring, A. U.; Fischer, H.; Nagaiyanallur, V. V.; Hähner, G.; Textor, M.; Reimhult, E. *J. Phys. Chem. C* **2011**, *115*, 683-691.

(71) Amstad, E.; Gillich, T.; Bilecka, I.; Textor, M.; Reimhult, E. *Nano Lett.* **2009**, *9*, 4042-4048.

(72) Godbey, W. T.; Mikos, A. G. *J. Control. Release* **2001**, *72*, 115-125.

(73) Scherer, F.; Anton, M.; Schillinger, U.; Henke, J.; Bergemann, C.; Krüger, A.; Gänsbacher, B.; Plank, C. *Gene Ther.* **2002**, *9*, 102-109.

3.7. Supporting Information

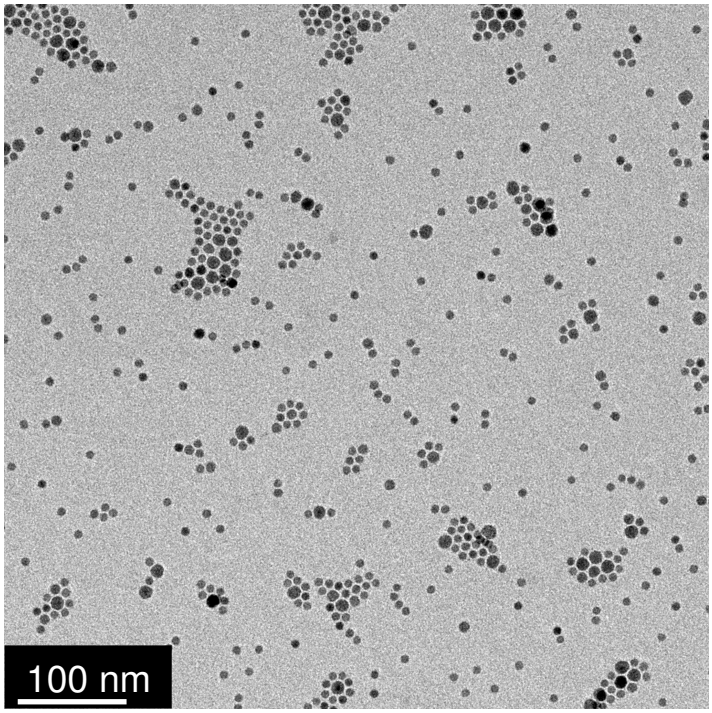

Figure S1. TEM micrograph of oleic acid stabilized γ-Fe_2O_3 nanoparticles (γ-Fe_2O_3@oleic acid). The sample was prepared by drop-coating a toluene dispersion of the nanoparticles (c < 0.1 g/L) on a carbon-coated copper grid.

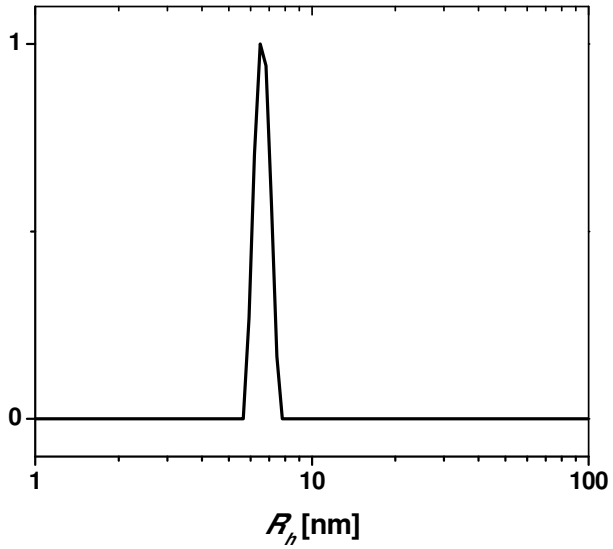

Figure S2. Hydrodynamic radii distribution of γ-Fe_2O_3@oleic acid in toluene obtained from DLS data applying the CONTIN algorithm (c = 0.5 g/L, θ = 90°).

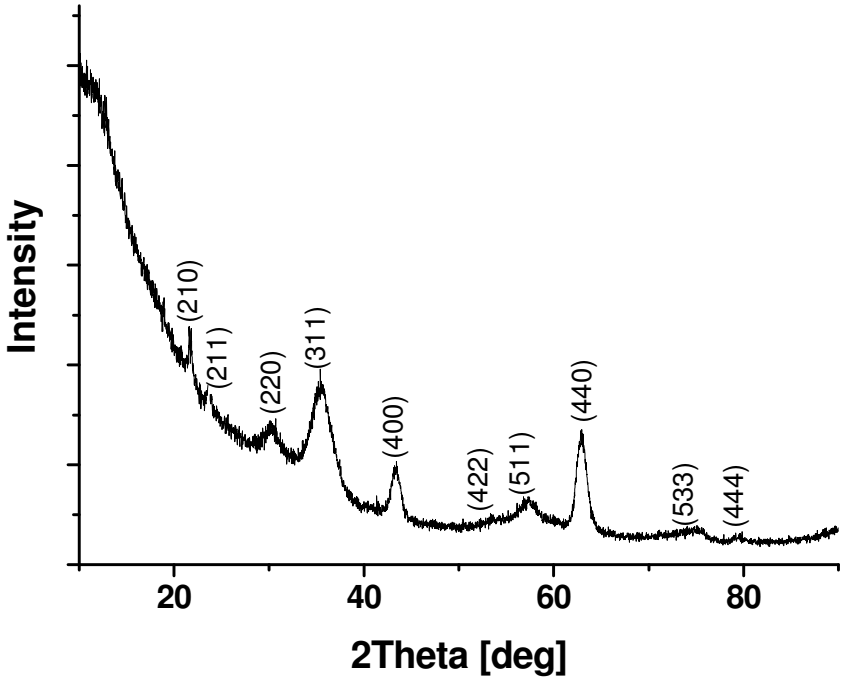

Figure S3. XRD pattern of γ-Fe_2O_3@oleic acid.

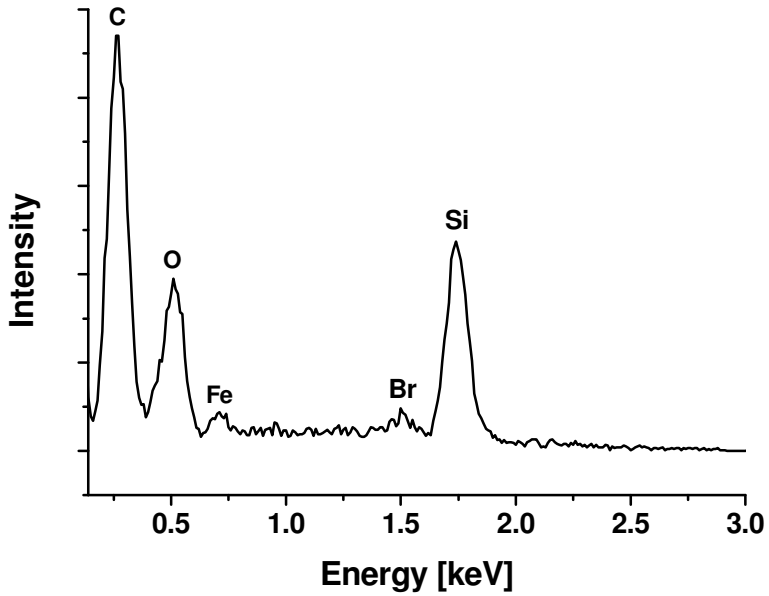

Figure S4. EDX spectrum of γ-Fe_2O_3@BIBDA initiator showing the characteristic signal for bromine at 1.5 keV. Because of the high carbon and oxygen content and hence, the high signal intensity for both elements, the signal for nitrogen with its signal at values < 0.5 keV is completely covered.

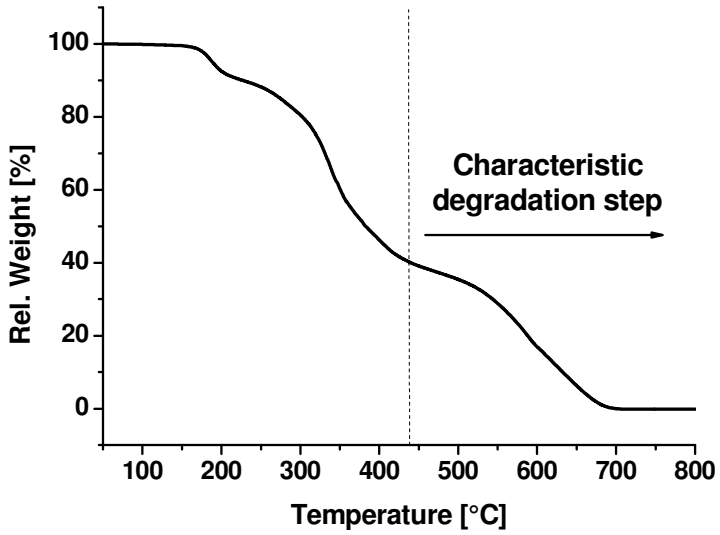

Figure S5. TGA trace of pure dopamine based ATRP initiator (BIBDA).

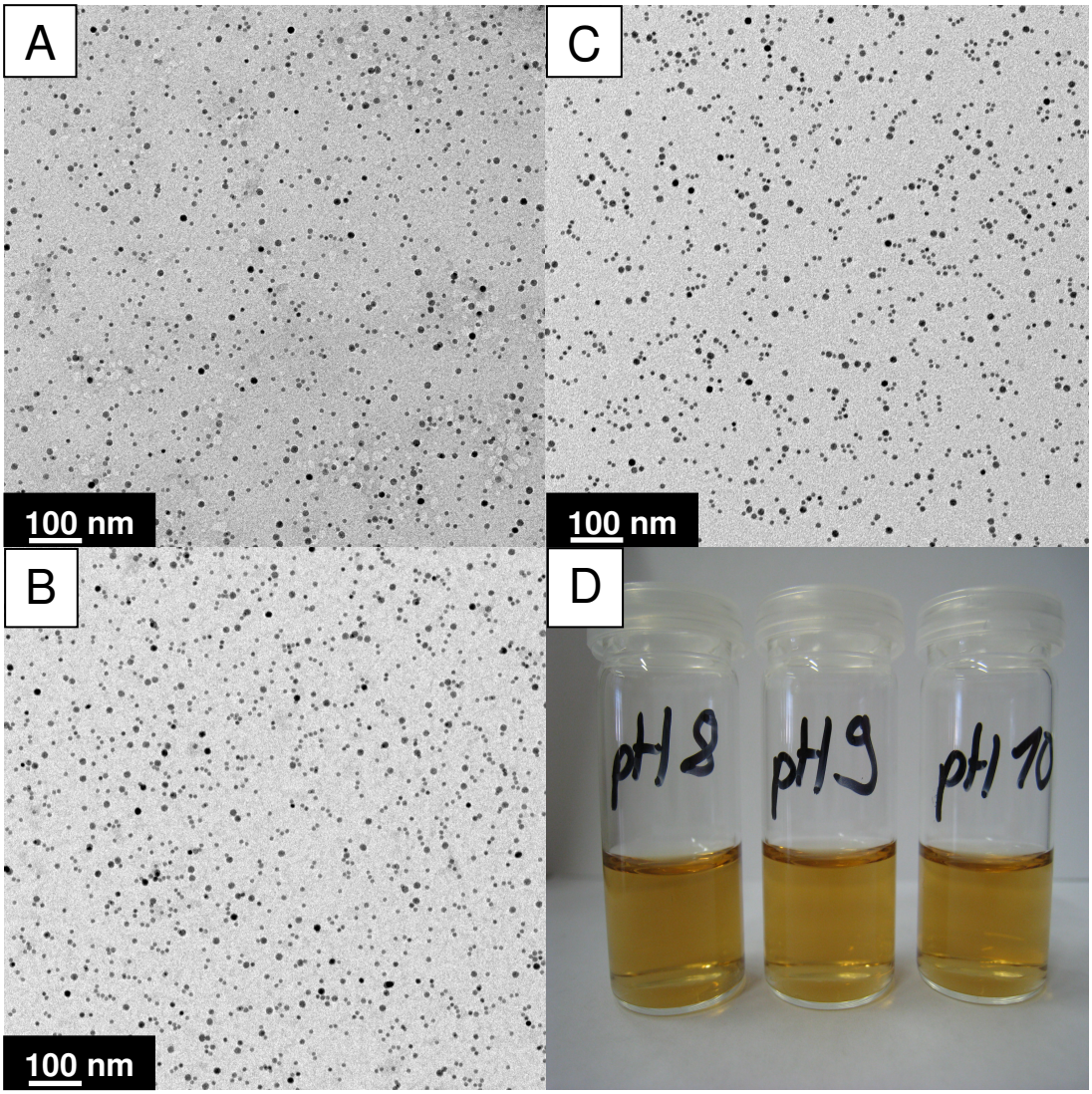

Figure S6. TEM micrographs of γ-Fe_2O_3@$(PDMAEMA_{590})_{46}$ in pH 8 buffer solution (A), pH 9 buffer solution (B) and pH 10 buffer solution (C) prepared by drop-coating from water (c = 0.5 g/L) on a hydrophilized carbon-coated copper grid after more than 6 month storage at 3 °C. D) The photographs of γ-Fe_2O_3@$(PDMAEMA_{590})_{46}$ dispersions in different buffer solutions (pH 8 – 10) taken after 6 month storage do not show any sign of nanoparticle agglomeration or precipitation.

Chapter 4

PDMAEMA-Grafted Core-Shell-Corona Particles for Non-Viral Gene Delivery and Magnetic Cell Separation

Alexander P. Majewski[1], Ullrich Stahlschmidt[2], Valérie Jérôme[2], Ruth Freitag[2,*], Axel H. E. Müller[1,3*] and Holger Schmalz[1,*]

[1]Makromolekulare Chemie II and [2]Bioprozesstechnik, Universität Bayreuth, 95440 Bayreuth, Germany; Fax: +49 921553393; [3]new address: Institute of Organic Chemistry, Johannes Gutenberg-Universität Mainz, D-55099 Mainz, Germany.

E-Mail: ruth.freitag@uni-bayreuth.de; holger.schmalz@uni-bayreuth.de; axel.mueller@uni-mainz.de

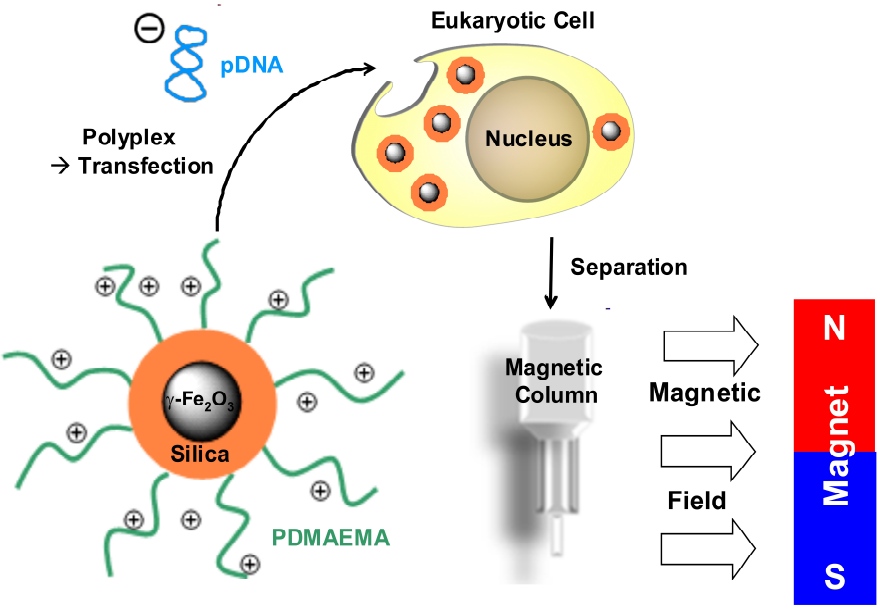

Reprinted with permission from Majewski, A.P.; Stahlschmidt, U.; Jérôme, V.; Freitag, R.; Müller, A.H.E.; Schmalz, H. *Biomacromolecules* **2013**, 14, 3081-3090.

4.1. Abstract

Monodisperse, magnetic nanoparticles as vectors for gene delivery were successfully synthesized *via* the grafting-from approach. First, oleic acid stabilized maghemite nanoparticles (γ-Fe_2O_3) were encapsulated with silica utilizing a reverse microemulsion process with simultaneous functionalization with initiating sites for atom transfer radical polymerization (ATRP). Polymerization of 2-(dimethylamino)ethyl methacrylate (DMAEMA) from the core-shell nanoparticles led to core-shell-corona hybrid nanoparticles (γ-Fe_2O_3@silica@PDMAEMA) with an average grafting density of 91 polymer chains of DP_n = 540 ($PDMAEMA_{540}$) per particle. The permanent attachment of the arms was verified by field-flow fractionation. The dual-responsive behavior (pH and temperature) was confirmed by dynamic light scattering (DLS) and turbidity measurements. The interaction of the hybrid nanoparticles with plasmid DNA at various N/P ratios (polymer nitrogen / DNA phosphorous) was investigated by DLS and zeta-potential measurements, indicating that for N/P $\geq$ 7.5 the complexes bear a positive net charge and do not undergo secondary aggregation. The hybrids were tested as transfection agents under standard conditions in CHO-K1 and L929 cells, revealing transfection efficiencies > 50 % and low cytotoxicity at N/P ratios of 10 and 15, respectively. Due to the magnetic properties of the hybrid gene vector it is possible to collect most of the cells that have incorporated a sufficient amount of magnetic material by using a magnetic activated cell sorting system (MACS™). Afterwards cells were further cultivated and displayed a transfection efficiency of ca. 60 % together with a high viability.

4.2. Introduction

The combination of biotechnology and polymer chemistry offers great potential for optimizing and developing new gene vectors. Especially non-viral gene delivery using polycationic systems represents an interesting class of gene vectors due to their facile synthesis and the possibility to tailor their functionality and architecture.[1,2] Besides other established materials for gene delivery, such as polyethyleneimine (PEI), chitosan, poly(L-lysine) or even dendrimers, methacrylate-based gene vectors, such as poly(2-(dimethylamino)ethyl methacrylate (PDMAEMA), show high potential.[3] Initial studies by the groups of Hennink and Armes/Stolnik pioneered PDMAEMA for *in vitro* gene transfection.[4, 5] It was found that the transfection efficiency of linear PDMAEMA can be increased by applying higher molecular weights. However, this simultaneously increases the cytotoxicity.[6] Since then a large variety of different systems based on PDMAEMA as potential gene delivery agents were developed.[7] Thereby, the development of a star-like architecture, as pioneered by the group of Patrickios,[8-10] was shown to be a promising candidate showing high *in vitro* transfection efficiencies by simultaneously keeping cytotoxicity at a low level.[11-13] This concept was confirmed by using micelles as related star-like structures.[13, 14]

Magnetic gene vectors allow for additional manipulation by external magnetic fields. They can be obtained by grafting cationic polymers on magnetic nanoparticles (NPs). The synthesis of magnetic NPs is well-established resulting in a large variety of different synthesis methods and elemental compositions.[15] In particular, magnetic NPs consisting of maghemite (γ-Fe_2O_3) and magnetite (Fe_3O_4) have gained considerable attention for biotechnical applications due to the accepted biocompatibility and synthesis methods yielding monodisperse NPs in large quantities.[16-18] The functionalization of iron oxide NPs is commonly performed *via* ligand exchange reactions resulting in a physical attachment of the functional molecule, e.g., an initiator moiety or a polymer. In particular, amine-, carboxylic acid-, phosphoric acid- or catechol-functionalized initiators and polymers are well suited and have been frequently used.[19-24] Plank and co-workers performed initial studies utilizing the magnetic properties of nanoparticles for gene delivery (Magnetofection™) and recently reviewed the progress of this method.[25, 26] In magnetofection, a magnetic particle carrying polycationic chains is loaded with DNA and a magnetic field is applied to speed up the movement of the structures into the cells, which are grown on a surface and placed on top of a magnet. Recently, we synthesized a star-shaped hybrid polymer based on PDMAEMA-grafted γ-Fe_2O_3 NPs by surface-initiated polymerization from a physically bound dopamine-based ATRP initiator.[23] These superparamagnetic NPs revealed high capability to deliver pDNA to mammalian cells without

applying an external magnetic field. Thus, the principle of the transfection leading to the observed high transfection efficiency is based on a standard polyfection and not on magnetofection. Preliminary experiments revealed that the cells could be even separated *via* a laboratory magnet after uptake of the magnetic gene vector. However, one problem arose: due to the used dopamine anchor group the polymer chains were only physisorbed to the NP surface, resulting in a partial detachment of the grafted chains over weeks.[23, 27, 28] Various approaches can be envisioned for improving this situation. For instance, silane end-functionalized molecules have been applied, which are able to coordinate to the particle surface and subsequently undergo a self-condensation reaction forming a stable polysiloxane coating around the nanoparticle.[29-32] Another way is encapsulating the particles by cross-linking the polymer corona.[33] Alternatively, micelle formation taking advantage of hydrophobic or electrostatic interactions between a suitable (block) copolymer and the particles can be applied for trapping the NPs inside the micellar core. However, as a result poor control over the amount of the captured NPs and consequently, a significant increase of the micellar core size was obtained.[34-37] Covering the NPs with a thin silica shell is a smart and effective route. Several ways for encapsulating small particles with a silica shell exist.[38-40] A reverse microemulsion approach was developed for encapsulating single NPs while controlling simultaneously the thickness of the silica layer.[41-43] Further advantages of this approach are the biocompatibility of silica and the well investigated methods for its surface modification, which in turn offers stable chemical bonds between the core and the attached molecules.[44-49]

Here, we describe the synthesis of PDMAEMA-grafted γ-Fe_2O_3@silica core shell NPs and their utilization for gene transfection and magnetic cell separation. The maghemite NPs were obtained *via* thermal decomposition of $Fe(CO)_5$ and encapsulated with a thin silica layer bearing an ATRP initiator. A subsequent polymerization of DMAEMA *via* a grafting-from approach resulted in γ-Fe_2O_3@silica@PDMAEMA core-shell-corona NPs (Scheme 1). In contrast to our previous work,[23] the PDMAEMA chains are covalently and, thus, permanently attached to the NP preventing a partial detachment over time. The hybrid particles were characterized according to their physical properties, grafting density and stability. Moreover, the complexation behavior with plasmid DNA was investigated by determining the zeta potentials and hydrodynamic radii at different N/P ratios. The hybrid NPs were further tested as transfection agents for CHO-K1 and L929 cells under standard conditions and the magnetic property of the γ-Fe_2O_3@silica@PDMAEMA gene vector was used for separating cells after transfection.

Scheme 1. Synthesis of PDMAEMA grafted core-shell-corona nanoparticles.

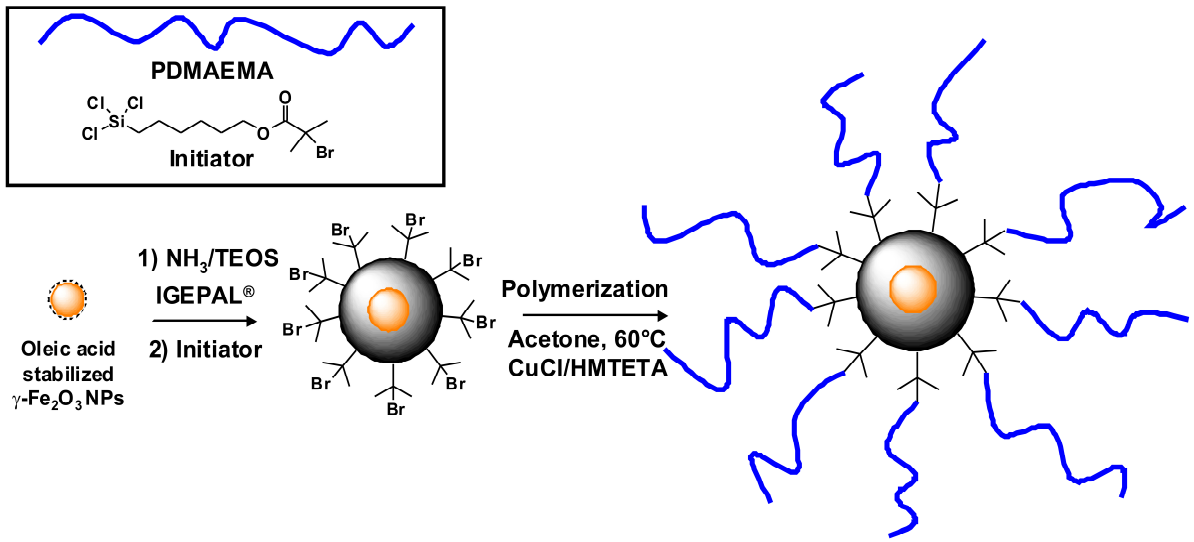

4.3. Experimental Part

Materials. Acetone (p.a. grade, VWR), ammonium hydroxide (28% in H_2O, Sigma-Aldrich), AVS buffer solution pH 7-10 (Titrinorm™, VWR), 2-bromoisobutyryl bromide (98%, Sigma-Aldrich), chloroplatinic acid (H_2PtCl_6, Sigma-Aldrich), cyclohexane (p.a. grade, VWR), dimethoxyethane (≥99.9%, Acros Organics), 2-(dimethylamino)ethyl methacrylate (DMAEMA, 99%, Sigma-Aldrich), dioctyl ether (99%, Sigma-Aldrich), dichloromethane (anhydrous, ≥99.9%, Merck), ethanol (99.8%, VWR), 1,1,4,7,10,10-hexamethyl triethylenetetramine (HMTETA, 97%, Sigma-Aldrich), 5-hexen-1-ol (98%, Sigma Aldrich), hydrofluoric acid (HF, 40%, Merck), iron(0) pentacarbonyl (99.9%, Sigma-Aldrich), oleic acid (90%, Fluka), polyoxyethylene(5)nonylphenylether (Igepal® CO 520, Sigma-Aldrich), tetraethylorthosilicate (TEOS, >98%, Acros Organics), toluene (anhydrous, 99.,8%, Sigma-Aldrich), trichlorosilane (99%, Sigma-Aldrich), triethylamine (99 %, Grüssing GmbH) were used as received. Copper(I) chloride was purified according to literature[50] and the monomers were destabilized by passing through a basic aluminum oxide column. For dialysis a regenerated cellulose tube (ZelluTrans, Roth) with a MWCO of 6-8 kDa was utilized. The applied NdFeB magnets were purchased at Fehrenkemper Magnetsysteme (dimensions: D = 25 mm, H = 16 mm (disc); L = 63 mm, W = 36 mm, H = 10 mm (block)). The synthesis of the ATRP initiator 6-(trichlorosilyl)hexyl 2-bromoisobutyrate (BIBSI) was performed as described elsewhere.[51] 3-(4,5-Dimethylthyazolyl-2)-2,5-diphenyl tetrazolium bromide (MTT), was purchased from Sigma-Aldrich. Cell culture materials, media and solutions were from

PAA Laboratories. Serum reduced medium OptiMEM was from Invitrogen. Plasmid DNA was prepared by using the EndoFree Plasmid Kit from Qiagen. Ultrapure deionized water was used for the preparation of all aqueous solutions and for dialysis. Plasmid pEGFP-N1 (4.7 kbp; Clontech) encoding the enhanced green fluorescent protein (EGFP) driven by the cytomegalovirus immediate early promoter was used in all transfection experiments. The plasmid was amplified in *E. coli* DH5 alpha strain in LB medium to sufficient quantities by using standard molecular biology techniques, including harvesting and purification via Qiagen's Giga-Prep kits. Plasmid DNA (pDNA) concentration and quality were determined by A_{260}/A_{280} ratio and by agarose gel electrophoresis. For magnetic sorting of the cells, LS columns and a MidiMACS™ separator both from Miltenyi Biotec were used.

Synthesis of Hybrid Nanoparticles

Synthesis of Oleic Acid Stabilized Maghemite Nanoparticles (γ-Fe_2O_3@oleic acid). The synthesis of the γ-Fe_2O_3 nanoparticles was adapted from our previous publication.[23] Briefly, $Fe(CO)_5$ was added to a degassed reaction mixture of dioctyl ether and oleic acid at 100 °C and refluxed for 1.5 h under nitrogen atmosphere until the color of the solution turned black. The oxidation of the yielded iron nanoparticles to γ-Fe_2O_3 took place while stirring the reaction mixture under air at room temperature. The nanoparticles were precipitated with ethanol and collected by an NdFeB magnet. After decantation of the supernatant, the nanoparticles were immediately redispersed and stored in toluene. Further purification was performed by precipitating in ethanol, collecting with an NdFeB magnet and subsequent redispersion in cyclohexane. This purification process was repeated three times before redispersing the iron oxide nanoparticles in a final cyclohexane stock-solution containing 8 g/L γ-Fe_2O_3@oleic acid.

Synthesis of Initiator-Functionalized Silica Coated Maghemite Nanoparticles (γ-Fe_2O_3@silica@BIBSI). This approach was adapted from Ruhland *et. al.*[43] yielding thinner silica shells, which are already functionalized with an ATRP initiator in one single reaction step. The synthesis was typically carried out in a 500 mL round-bottom flask charged with 8.2 g Igepal® CO-520 (polyoxyethylene(5)nonylphenyl ether, 18.6 mmol) and 250 mL cyclohexane. The reaction mixture was treated 10 min with ultrasound for dissolving the Igepal® CO-520. Subsequently, 6.25 mL of the γ-Fe_2O_3@oleic acid stock solution (8 g/L in cyclohexane) were dispersed followed by the addition of 1.43 mL of a 28 % aqueous ammonia solution to the reaction mixture forming a reverse brownish microemulsion. The reaction was started by adding 0.36 mL TEOS (1.6 mmol). The reaction mixture was shaken

in an incubatic shaker at 100 rpm for 48 h at ambient temperature. The functionalization was performed by a subsequent addition of 70 µL of 2-bromoisobutyryl 6-(trichlorosilyl)hexanoate (BIBSI, 16 mol% solution in toluene) and further shaking for 24 h. After the functionalization step the cyclohexane was removed by using a rotary evaporator and the particles were purified by centrifugation for removing the surfactant. For this purpose, the particles were precipitated with methanol prior to the centrifugation and additionally rinsed twice with methanol before redispersion in acetone. Finally, the functionalized particles were further purified by dialyzing against acetone, the solvent applied for ATRP of DMAEMA.

Synthesis of PDMAEMA Grafted Core-Shell-Corona Nanoparticles (γ-Fe_2O_3@silica@PDMAEMA). A 250 mL screw cap glass equipped with a septum was charged with 330 mg ATRP initiator functionalized nanoparticles dispersed in 150 mL acetone, 70 mL DMAEMA (65.3 g, 415.5 mmol) and 3 mg $CuCl_2$ (0.03 mmol). The mixture was purged with nitrogen for 30 min before adding 8 µL degassed HMTETA (7 mg, 0.03 mmol) dissolved in 2 mL acetone. The reaction mixture was heated to 60 °C for 8 h. After cooling down to room temperature the reaction was terminated by exposing the mixture to air under stirring for 10 min. The crude product was purified by several cycles of centrifugation with 4000 rpm and redispersion in methanol to remove the copper catalyst and remaining monomer. The grafted hybrid particles were finally redispersed and dialyzed against deionized water. The obtained stock solution of the hybrid particles in deionized water (c = 1.75 g/L) was stored at 3 °C.

Cleavage of PDMAEMA from γ-Fe_2O_3@silica@PDMAEMA Nanoparticles. The grafted PDMAEMA chains were cleaved from the inorganic core by adding 8-10 drops of hydrofluoric acid (3 wt%) to the dispersion of γ-Fe_2O_3@silica@PDMAEMA in ca. 5 mL deionized water (polymer content ca. 5-10 mg). Subsequently, the resulting clear solution was dialyzed for 3 days against pH 10 water before freeze-drying. The detached polymer chains were characterized by DMAc-SEC using a PDMAEMA calibration, which revealed a number average molecular weight of M_n(PDMAEMA) = 85.000 g/mol and a PDI of 1.36.

Characterization. *Asymmetric Flow Field-Flow Fractionation (AF-FFF)* was performed on a Wyatt Technology Eclipse 2 separation system equipped with an RI detector. The flow channel was equipped with a 30 kDa regenerated cellulose membrane and a 490 μm thickness spacer. Degassed and filtered deionized water containing $NaNO_3$ (25 mM) and NaN_3 (200 ppm) was used as the carrier solvent. The flow profile was 1 min of an initial focusing step, 20 μL sample injection into the flow channel over 2 min, followed by a sample focusing step

of 5 min. The volumetric channel flow rate was set at 1.5 mL/min and the constant cross-flow rate at 0.4 mL/min for 90 minutes. The sample concentration was 1 g/L.

Size Exclusion Chromatography (SEC) was performed on a system based on GRAM columns (7 μm particle diameter) with 10^2 and 10^3 Å pore diameter (Polymer Standards Service) equipped with a RI- and UV-detector from Agilent 1200 Series. N,N-Dimethylacetamide (DMAc) with 0.05% lithium bromide was used as eluent at a flow rate of 0.8 mL/min. The measurements were conducted at 60 °C. For data evaluation a calibration with linear PDMAEMA standards was applied.

Fourier Transform Infrared Spectroscopy (FT-IR) was carried out on a Spectrum 100 FT-IR spectrometer (Perkin Elmer) using an U-ATR unit. The measurements were performed by placing the dried samples directly on top of the U-ATR unit.

Vibrating Sample Magnetometry (VSM). Magnetization curves at room temperature were recorded with an Lake Shore Vibrating Sample Magnetometer Model 7404 applying field strengths up to 1.4 T. Samples were measured in sealed Kel-F vessels, placed on a fiber glass sample holder between two poles of an electromagnet, and vibrated at a frequency of 82 Hz.

Transmission Electron Microscopy (TEM) images were taken with a Zeiss EM922 OMEGA (EFTEM) electron microscope. Samples were prepared by placing one drop of the solution onto carbon-coated copper grids. Afterwards the remaining solvent was removed by blotting with a filter paper. Zero-loss filtered images (ΔE = 0 eV) were taken at an accelerating voltage of 200 kV. All images were registered digitally by a bottom mounted CCD camera system (Ultrascan 1000, Gatan), combined and processed with a digital imaging processing system (Gatan Digital Micrograph Suite GMS 1.8). The hydrophilization of the TEM grids was performed for 30 s under air utilizing a Solarius 950 Advance Plasma System from Gatan.

Dynamic Light Scattering (DLS) was carried out on an ALV DLS/SLS-SP 5022F compact goniometer system with an ALV 5000/E correlator and a He-Ne laser (λ = 632.8 nm). The measurements were performed for 10-30 min (non-grafted particles) and 120 sec (PDMAEMA grafted particles), respectively, at a scattering angle of 90°. The samples (c = 0.1-0.5 g/L) were filtrated through a 0.2 µm PTFE-filter (non-grafted particles) or 5 µm Nylon-filter (PDMAEMA grafted particles) prior to the measurement. The data were analyzed using the CONTIN algorithm, which yields an intensity-weighted distribution of relaxation times, τ, after an inverse Laplace transformation of the intensity auto-correlation function.

These relaxation times were transformed into translational diffusion coefficients and further into hydrodynamic radii using the Stokes-Einstein equation.

Thermogravimetric Analysis (TGA) was carried out using a Mettler Toledo TGA/SDTA 85 at a heating rate of 10 K/min between 30 and 1000 °C under an air-flow of 60 mL/min. The typical sample weight was between 8 and 15 mg. For determining the grafting densities, ρ_{graft}, of the functionalized maghemite-silica core-shell nanoparticles the weight loss determined by TGA was used to calculate the amount of molecules per nm^2 according to eq. 1:

$$\rho_{graft} = \frac{\Delta m / M}{\mathrm{Q} \cdot A_{NP}} \cdot N_A , \qquad (1)$$

$$\mathrm{Q} = \left(m_0 - \Delta m\right) / m_{NP} , \qquad (2)$$

where m_0, Δm and m_{NP} correspond to the initial sample weight, the weight of the grafted molecules or polymer determined by TGA, and the mass of a single nanoparticle, respectively. M is the molecular weight of BIBSI (384.6 g/mol) or M_n of the grafted polymer (85 kg/mol), respectively. N_A is Avogadro's number and A_{NP} corresponds to the surface of one nanoparticle. For the calculation the iron oxide NPs and the silica coated NPs were assumed to be monodisperse in size with a spherical shape and an average diameter of 15.0 nm and 28.8 nm, respectively, as determined by TEM and DLS. This results in an average surface area of A_{NP} = 2605 nm² and an average NP volume of V_{NP} = 12507 nm^3 for a single silica coated iron oxide nanoparticle. The mass of such a single NP (m_{NP} = $3.2 \cdot 10^{-17}$ g) was obtained by considering the density of maghemite (ρ = 4.9 g/cm³) and a silica shell thickness of 6.9 nm (ρ = 1.9 g/cm³).[52, 53]

Turbidity Measurements were performed using a titrator (Titrando 809, Metrohm, Herisau, Switzerland) equipped with a turbidity probe (λ_0 = 523 nm, Spectrosense, Metrohm) and a temperature sensor (Pt 1000, Metrohm). The temperature program (1 K/min) was run by a thermostat (LAUDA RE 306 and Wintherm_Plus software), using a home-made thermostatable vessel. The cloud points were determined from the intersection of the two tangents applied to the two linear regimes of the transmittance curve at the onset of turbidity.

Zeta Potential and Dynamic Light Scattering Measurements of the polyplexes were performed on a Zetasizer Nano ZS (Malvern). The conditions for the polyplex formation are identical to the transfection protocol. The zeta potentials were accessed *via* Laser Doppler Micro-Electrophoresis applying the laser interferometric technique M3-PALS (Phase Analysis Light Scattering). The final results were generated by averaging over 2-3 zeta

potential measurements. The size of the formed polyplexes was determined by Non-Invasive Back Scatter technology (NIBS) utilizing a He-Ne laser (λ = 633 nm, max. 5 mW). All experiments were performed at 25 °C.

Cell Transfection Experiments

Mammalian Cell Lines and Culture Conditions. The CHO-K1 (CCL-61, ATCC) and L929 (CCL-1, ATCC) cell lines were used in the transfection and cytotoxicity experiments. The cell lines were maintained in RPMI 1640 (CHO-K1) and MEM (L929) cell culture media supplemented with 10% fetal calf serum (FCS), 100 µg/mL streptomycin, 100 IU/mL penicillin, and 2 - 4 mM L-glutamine (as recommended by ATCC; "growth medium"). Cells were cultivated at 37 °C in a humidified 5% CO_2 atmosphere.

Transfection. For transfection, the cells were seeded at a density of 3×10^5 cells/well in six-well plates 20 h prior to transfection. One hour prior to transfection, cells were rinsed with DPBS and supplemented with 1 mL OptiMEM. pDNA/polymer polyplexes were prepared by first mixing 1 µg pDNA in a final volume of 50 µL of aqueous 150 mM NaCl solution and then adding 1 mL OptiMEM. Thereafter, suitable amounts of the polycation stock solution were added in a single drop to achieve the desired N/P ratio. Solutions were vortexed for 10 s and incubated for 30 min at room temperature to allow polyplex formation. The polyplex suspension (1 mL) was added to the cells and the plates were centrifuged for 5 min at *200 g* and placed for 4 h in the incubator. Afterward, the medium was removed by aspiration, 2 mL of fresh growth medium were added, and the cells were further cultivated for 20 h. For analysis, the cells were harvested by trypsinization and resuspended in DPBS. The relative expression of EGFP fluorescence of 1×10^4 cells was quantified via flow cytometry using a Cytomics FC 500 (Beckman Coulter). The transfection efficiency data represent the percentage of cells expressing EGFP in the non-apoptotic cell population defined by scatter properties as determined by flow cytometry analysis. For determination of the viability, dead cells were identified via counterstaining with propidium iodide. Group data are reported as mean ± s.d.

MTT Assay. The cytotoxicity of γ-Fe_2O_3@silica@$(PDMAEMA_{540})_{91}$ hybrid NPs was tested using L929 murine fibroblasts and the CHO-K1 cells according to the norm ISO 10993-5 as it is (L929) and slightly modified (CHO-K1) using 1 mg/mL MTT-stock solution. As non-complexed polymers are considered to be more toxic than the polyplexes, the harsher conditions were tested by applying the hybrid NP dilutions in a concentration range from 0.002 up to 1.0 mg/mL in 96-well plates. The cells were seeded at a density of 1×10^4 cells

(L929) or 1.5 × 10^4 cells (CHO-K1) per well in their respective growth media 24 h prior to the experiment. As 100% viability control, untreated cells were used. For each dilution step, eight replicates were used. After dissolving the metabolically formed formazan crystals in isopropanol, the absorbance was measured using a plate reader (Genios Pro, Tecan) at a wavelength of 580 nm. For data evaluation, Origin 6.1 (OriginLab Corporation) software was used, the x-scale was plotted logarithmically, and a nonlinear fit was run to obtain the lethal dose 50 (LD_{50}) values. Group data are reported as mean ± s.d.

Magnetic Separation of Cells. CHO-K1 cells were transfected at N/P 7.5, as described above. 24 h after transfection, the cells were harvested by trypsinization and rinsed twice with growth medium. The cells were then resuspended at a cell density of 14 x 10^6 cells/mL in DPBS - 0.5% FCS - 2mM EDTA ("sorting buffer"). Under sterile conditions, 0.5 mL of the cell suspension was then loaded on a Miltenyi Biotec's LS separation column and sorted using a MidiMACS™ separator according to the manufacturer's instructions (Miltenyi Biotec's). The "unbound" (flow-through plus wash) and the "bound" fractions were collected and stored on ice for further analysis. The cells density in each fraction was measured in a Vi-Cell cell counter (Beckmann Coulter). To assess the outcome of the transfection in the collected cells, 5 x 10^5 cells of each fraction were plated per well of a 6-well plate in a total volume of 2 mL suitable "growth medium" and the cells were further cultivated for at least 20 h. For analysis, the cells were treated as described above (*Transfection*).

4.4. Results and Discussion

ATRP Initiator-Functionalized Core-Shell Maghemite Nanoparticles (γ-Fe_2O_3@silica@BIBSI). Oleic acid stabilized maghemite nanoparticles (γ-Fe_2O_3@oleic acid) were synthesized *via* thermal decomposition according to our previous publication yielding well defined NPs with a narrow size distribution.[23] The particles were characterized by transmission electron microscopy (TEM) and dynamic light scattering (DLS) revealing an average radius of 7.5 ± 0.8 nm determined by TEM image analysis (300 counts), which is in good agreement with the narrow size distribution determined by DLS revealing a hydrodynamic radius of 7.9 ± 0.4 nm (Figure 1A). Subsequently, the maghemite nanoparticles were covered by a thin silica shell bearing initiating sites for atom transfer radical polymerization (ATRP) using a microemulsion approach adopted from Ruhland et al.[43] Furthermore, we accessed the initiator-functionalized core-shell NPs in just one step by first completely consuming the applied TEOS (2 days of reaction) before adding 6-

(trichlorosilyl)hexyl 2-bromoisobutyrate (BIBSI) directly to the reaction mixture for functionalizing the outer silica shell with the ATRP initiator.

After the encapsulation of the iron oxide NPs with silica, DLS revealed a significant change in the hydrodynamic radius from 7.9 to 14.4 nm achieving a monomodal and narrow size distribution (D.I. = 0.09) of the core-shell nanoparticles (Figure 1A). The TEM micrograph of the ATRP initiator-grafted particles shows monodisperse silica-encapsulated iron oxide NPs (γ-Fe_2O_3@silica@BIBSI) each bearing one single iron oxide NP (Figure 1B).

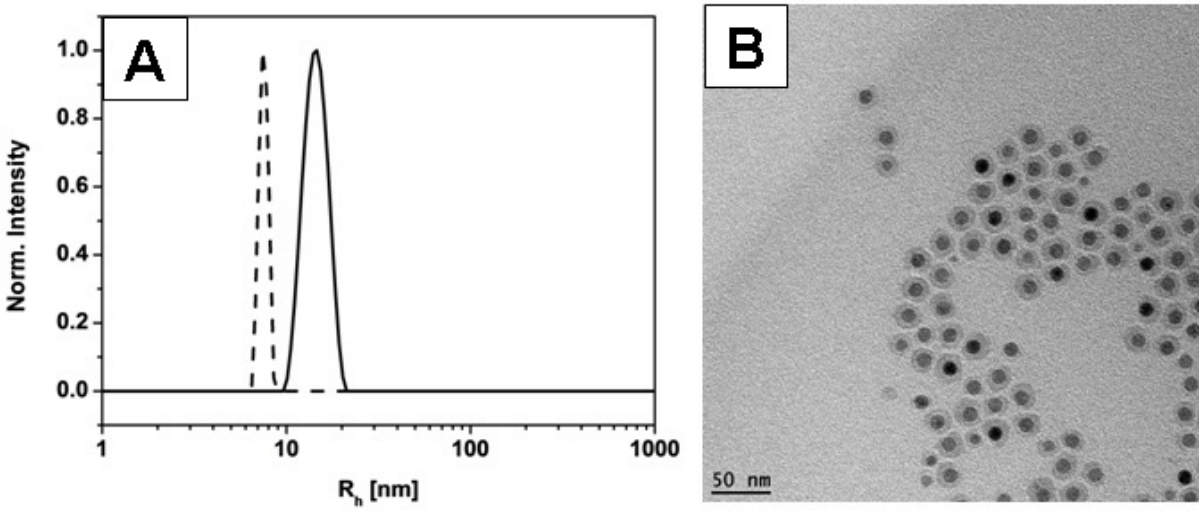

Figure 1. A) Hydrodynamic radii distribution of γ-Fe_2O_3@oleic acid (dashed line; $\theta = 90°$; $c = 0.5$ g/L) and γ-Fe_2O_3@silica (solid line; $\theta = 90°$; $c = 0.1$ g/L) in cyclohexane. B) TEM micrograph of γ-Fe_2O_3@silica@BIBSI nanoparticles. The sample was prepared by drop-coating a cyclohexane dispersion of the nanoparticles ($c < 0.1$ g/L) on a carbon-coated copper grid.

Investigation *via* FT-IR reveals the development of the silica shell as well as the functionalization with the ATRP initiator (Figure 2A). After covering the oleic acid stabilized NPs with silica all characteristic stretching vibrations of the oleic acid at 2900–2800 cm^{-1} (CH_3, CH_2) and 1700 cm^{-1} (C=O) disappear completely. Instead, a broad absorption band occurs at 3700–3100 cm^{-1}, which can be assigned to the presence of hydroxyl groups (-OH). Due to the formed silica shell strong stretching vibrations occur ranging from 1290–740 cm^{-1}, which are attributed to the asymmetric stretching vibrations at 1050 cm^{-1} (Si-O) and 950 cm^{-1} (Si-OH) as well as the symmetric stretching at 795 cm^{-1} (Si-O). The purified particles bearing the ATRP initiator (γ-Fe_2O_3@silica@BIBSI) show an additional weak signal at 1700 cm^{-1} (C=O) confirming the successful attachment of the initiator (Figure 2B).

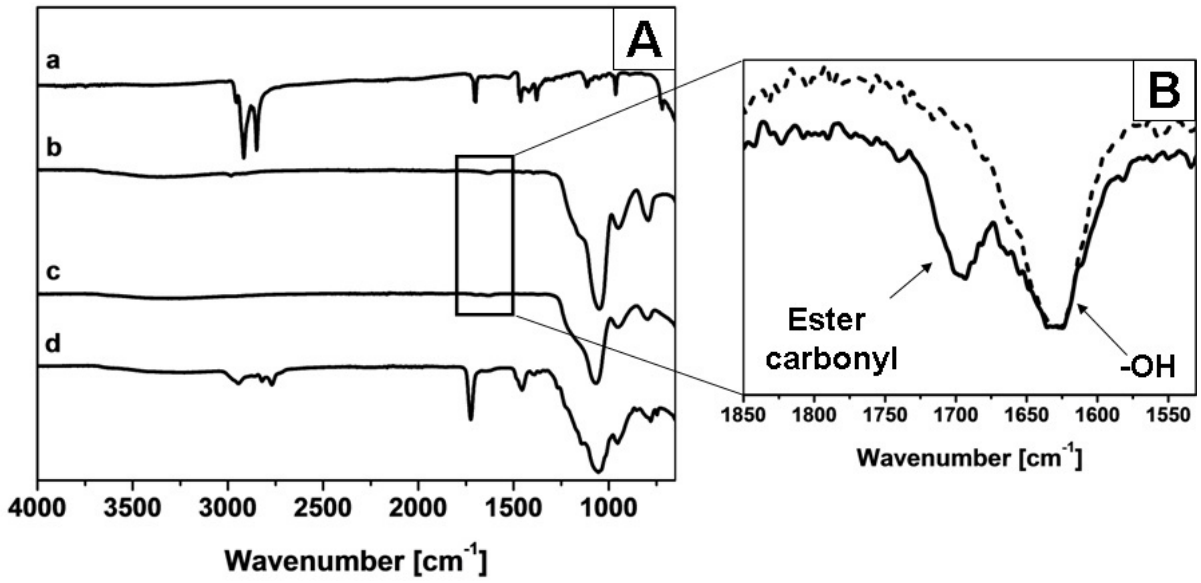

Figure 2. A) FT-IR of γ-Fe_2O_3@oleic acid (a), γ-Fe_2O_3@silica (b), γ-Fe_2O_3@silica@BIBSI (c) and γ-Fe_2O_3@silica@PDMAEMA (d). B) Magnification of the γ-Fe_2O_3@silica (dashed line) and γ-Fe_2O_3@silica@BIBSI (solid line) spectra.

The comparison of the thermograms of γ-Fe_2O_3@silica and γ-Fe_2O_3@silica@BIBSI obtained by thermogravimetric analysis (TGA) shows an additional weight loss of 2.7 % after grafting the ATRP-initiator (Figure 3A). Since the molecular weight of the initiator is known the grafting density of γ-Fe_2O_3@silica@BIBSI can be estimated directly from the TGA traces according to eq. 1 (Experimental Section). Consequently, each γ-Fe_2O_3@silica@BIBSI particle bears about 1360 initiator molecules resulting in a grafting density of 0.52 molecules / nm².

Synthesis of PDMAEMA-Grafted Core-Shell-Corona Nanoparticles (γ-Fe_2O_3@silica@PDMAEMA). The ATRP initiator-functionalized NPs (γ-Fe_2O_3@silica@BIBSI) were further utilized for the polymerization of DMAEMA *via* the grafting-from approach. The obtained PDMAEMA-grafted core-shell-corona NPs (γ-Fe_2O_3@silica@PDMAEMA) were easily purified by centrifugation removing residual monomer, catalyst and free, non-bound PDMAEMA. Although the γ-Fe_2O_3@silica@BIBSI NPs were purified by dialysis a certain amount of free polymer occurred after polymerization. We assume that during functionalization with the ATRP initiator also some hydrolyzed non-covalently bound initiator is adsorbed on the nanoparticles´ surface, as the reaction was conducted in one step directly in the microemulsion without isolating the core-shell γ-Fe_2O_3@silica NPs. Thus, PDMAEMA chains growing from physically bound initiating sites upon subsequent polymerization are detached resulting in free polymer chains. It is relevant to

note that a further detachment of polymer while storing the particles in aqueous solution was not observed, as confirmed by Asymmetric Flow Field-Flow Fractionation (AF-FFF) measurements after purification (Figure S1). If free polymer would appear after purification a bimodal distribution would be expected, as demonstrated in our previous publication.[23] However, even after three weeks the distribution is still monomodal, indicating stable, covalently bound polymer chains on the nanoparticles´ surface.

The successful polymerization of DMAEMA is demonstrated by FT-IR, TGA and size exclusion chromatography (SEC) investigations. The purified γ-Fe_2O_3@silica@PDMAEMA hybrid NPs show the characteristic stretching vibrations at 2900-2800 cm^{-1} indicating the presence of aliphatic CH_2 and CH_3 groups of PDMAEMA. Additionally, a significant increase of the stretching vibration at 1700 cm^{-1} (C=O) compared to γ-Fe_2O_3@silica@BIBSI is observed (Figure 2A). The TGA trace of the polymer grafted particles reveals a weight loss of 36.5 % and, thus, an additional weight loss of about 24.6 % as compared to γ-Fe_2O_3@silica@BIBSI (Figure 3A). The M_n of the grafted PDMAEMA chains was determined by first cleaving the grafted polymer chains from the core by etching the silica shell and dissolving the iron oxide nanoparticles with hydrofluoric acid, followed by SEC analysis, yielding M_n (PDMAEMA) = 85.000 g/mol (DP_n = 540; *PDI* = 1.36; Figure S2). Furthermore, the grafting density was determined by applying the results of TGA and SEC and taking the particle diameter into account. The performed calculations are described in detail in the Experimental Section. As a result, the grafted core-shell-corona particles carry ca. 91 PDMAEMA chains (0.04 chains/nm²) with a DP_n of 540 and are denoted as γ-Fe_2O_3@silica@$(PDMAEMA_{540})_{91}$. Notably, the polymer corona of the hybrid particles has a total molecular weight of ca. 7.7 MDa.

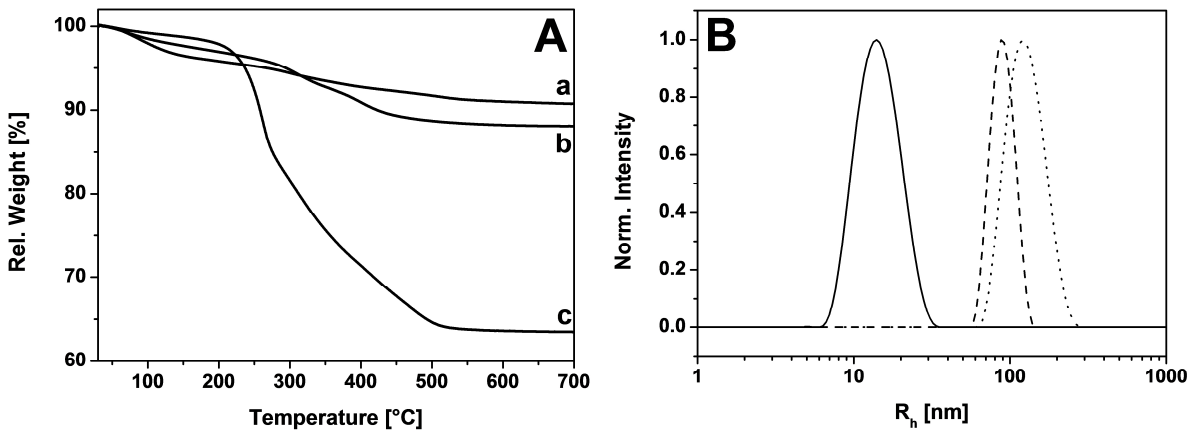

Figure 3. A) Comparison of the TGA traces of γ-Fe_2O_3@silica (a), γ-Fe_2O_3@silica@BIBSI (b) and γ-Fe_2O_3@silica@$(PDMAEMA_{540})_{91}$ (c). B) Hydrodynamic radii distribution ($\theta = 90°$; c = 0.1 g/L) of γ-Fe_2O_3@Silica@BIBSI in cyclohexane (solid line), γ-Fe_2O_3@silica@$(PDMAEMA_{540})_{91}$ in pH 10 buffer solution (dashed line) and in pH 4 buffer solution (dotted line).

pH- and Temperature-Responsive Agglomeration and Stability. The pH- and temperature-responsive behavior of the hybrid NPs was investigated by turbidity and DLS measurements. PDMAEMA is known for being responsive to both temperature and pH. The core-shell-corona particles show a pH-dependent Lower Critical Solution Temperature (LCST). The cloud points determined by turbitimetry are consistent with those of high molecular weight PDMAEMA star polymers reported by Plamper *et al.* and γ-Fe_2O_3@$(PDMAEMA_{590})_{53}$ hybrid NPs studied in our previous publication (Figures S3, S4).[23, 54] DLS shows that the hydrodynamic radius of the hybrid particles undergoes a significant increase by switching the pH from 10 to 4, due to protonation of the amino groups (Figure 3B). The hybrid NPs agglomerate above the cloud point and this process is fully reversible (Figure S5). Furthermore, these hybrid particles show an excellent long-term stability. After one year of storage at 3 °C in deionized water the particles remained stable showing no sign of sedimentation (Figure S6).

Magnetic Properties. The magnetization curve of γ-Fe_2O_3@silica@$(PDMAEMA_{540})_{91}$ was recorded *via* vibrating sample magnetometry (VSM). It exhibits the characteristic sigmoidal shape without hysteresis, which is typical for superparamagnetic particles (Figure 4). Thus, the magnetic redistribution takes place via internal (Neél) relaxation leading to the conclusion that the silica-encapsulation and subsequent polymerization has no significant influence on the superparamagnetic behavior.

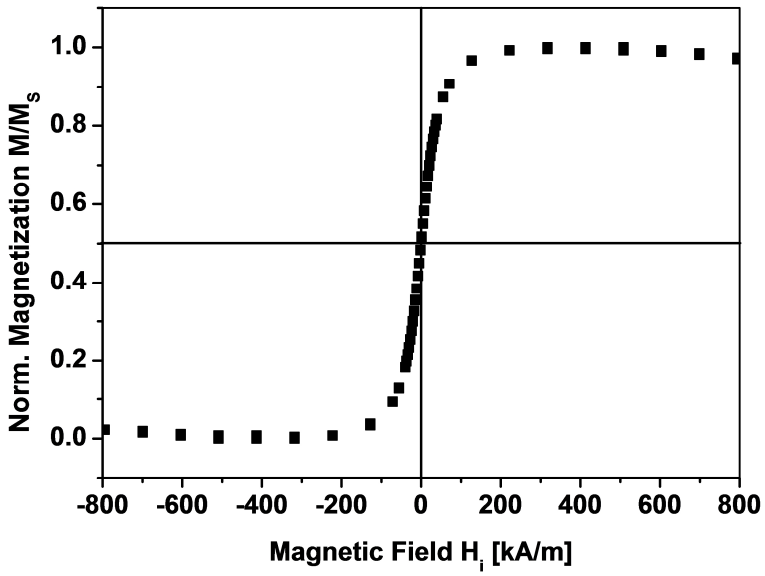

Figure 4. Normalized magnetization curve of γ-Fe_2O_3@silica@$(PDMAEMA_{540})_{91}$ (c = 1.75 g/L) in deionized water.

Polyplex Formation with pDNA. The polyplex formation of the cationic γ-Fe_2O_3@ silica@$(PDMAEMA_{540})_{91}$ particles and pDNA was investigated by determining zeta potentials and hydrodynamic radii of the formed polyplexes as a function of the N/P ratio buffered at pH 7.8. The polyplexes were prepared identically to the protocol used for our transfection experiments (*vide infra*) and measured with a zetasizer. The average hydrodynamic radii of the pure pDNA (N/P = 0) and of the pure hybrid particles in the transfection medium are 50 nm (D.I. = 0.2) and 160 nm (D.I. = 0.15), respectively. The grafted PDMAEMA chains are assumed to be rather stretched at pH 7.8 due to the repulsive interactions of the protonated tertiary amine groups (degree of protonation > 90 %[54]). Here a theoretical estimation of the NP size, which takes a NP radius of 7.2 nm and the contour length of a polyvinyl chain of DP = 540 (≈ 135 nm) into account, results in a NP radius of 142 nm, which is in good agreement with the experimental data.

At high ratios of PDMAEMA nitrogen to DNA phosphorous (N/P ≥ 7.5) we observe hydrodynamic radii close to the pure hybrid particles and low polydispersity (Figure 5A). This indicates that the DNA molecules are complexed with single nanoparticles. Due to the excess of the polycations the zeta potentials are positive (Figure 5B). However, at N/P = 5 the zeta potential measurements indicate nearly uncharged complexes and hydrodynamic radius and dispersity index double. The lack of necessary charges for stabilizing the polyplexes apparently leads to aggregation. A further decrease of the N/P ratio causes charge reversal and a slight decrease of hydrodynamic radius and polydispersity at N/P = 3. These aggregates are

still almost twice as large as the pure hybrid particles and a strongly negative potential was observed, which is close to that of pure pDNA. We assume bridging of two hybrid particles, bound to one single pDNA molecule resulting in an elevated hydrodynamic radius.

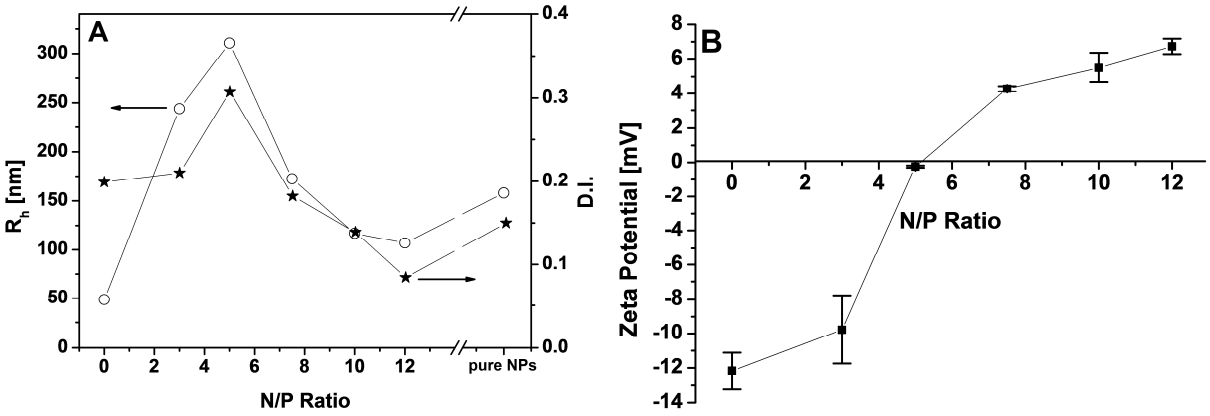

Figure 5. A) Average hydrodynamic radii (○) and dispersity indices (★) at different N/P ratios of the γ-Fe_2O_3@silica@$(PDMAEMA_{540})_{91}$/pDNA polyplexes; pH ~ 7.8. B) Zeta potentials of the γ-Fe_2O_3@silica@$(PDMAEMA_{540})_{91}$/pDNA polyplexes at different N/P ratios. The lines in both graphs are guides to the eye.

Utilization of Hybrid NPs for Gene Delivery and Cell Sorting.

Cytotoxicity. Toxicity is a major issue for non-viral delivery as reviewed by Rodíguez-Gascón *et al.* and Al-Dosari *et al.*[55, 56] The influence of γ-Fe_2O_3@silica@$(PDMAEMA_{540})_{91}$ on the metabolic activity of L929 and CHO-K1 cells was tested by MTT assay under conditions mimicking transfection conditions (4 h incubation time). In this context, the investigation of the damaging effects of the free, non-bound PDMAEMA chains reflects a worst-case setting. The NPs affected the metabolic activity in a concentration-dependent manner when they were added in the concentration range 0 to 1 mg/mL to the cells. Under these conditions, the LD_{50} for cells treated with the hybrid NPs is 0.010 ± 0.001 mg/mL (CHO-K1) and 0.030 ± 0.003 mg/mL (L929) indicating a slightly lower cytotoxicity of the nanoparticles in the L929 cells. Hence, the LD_{50} of this core-shell nanoparticle is in L929 3.6-fold lower than values previously measured for structurally similar NPs with a dopamine anchor instead of a functionalized silica shell (γ-Fe_2O_3@$(PDMAEMA_{590})_{46;}$ LD_{50} = 0.09 ± 0.003 mg/mL; total M_n of PDMAEMA shell = 4.3 MDa).[23] A doubling of the arms density on the NPs and the concomitantly doubling of the molecular weight (7.7 MDa) might be responsible for the observed increase in cytotoxicity.

Transfection. Previous work in our group showed that star-shaped polycationic structures with high molecular weight are very efficient carriers for gene delivery, independent of the chemistry of the core.[13, 23] Therefore, the efficiency of the γ-Fe_2O_3@silica@ $(PDMAEMA_{540})_{91}$ NPs as potential transfection agent was explored under standard conditions in CHO-K1 followed by a quantitative analysis of the EGFP expression by flow cytometry. Preliminary transfection tests revealed an unacceptable cytotoxicity of the polyplexes indicating that an adaptation of our former protocol was necessary.[23] In particular, we found that increasing the incubation volume for the polyplex formation step in the transfection protocol drastically reduced the cytotoxicity. Using this adapted protocol, we showed that the γ-Fe_2O_3@silica@$(PDMAEMA_{540})_{91}$ NPs led to high transfection efficiency in CHO-K1 cells depending on the N/P ratio and performed best at N/P = 7.5 to 10 with averaged transfection efficiencies (in %) of 40.9 ± 10.3 and 52.5 ± 3.7, respectively (Table 1). In addition, the efficiency of the γ-Fe_2O_3@silica@ $(PDMAEMA_{540})_{91}$ NPs as transfection agent was also investigated in L929 cells. In that case, similarly to CHO-K1, high transfection efficiency (up to 58.8%) could be achieved provided that higher N/P ratios (N/P ≥ 12) were used. This result showed that PDMAEMA-based polycations are suitable agents for the transfection of L929 cells, as also recently published by Zhang and co-workers.[57] The cell viability of both cell lines at the tested N/P ratio was always above 85%, as measured by counterstaining the dead cells with propidium iodide. The transfection experiments were repeated in CHO-K1 cells with NPs that had been stored in solution for a year. The measured transfection efficiencies were in the range of the ones displayed in Table 1 indicating a high stability of the NPs over the time.

Table 1. Transfection efficiency (TE) and cell viability after transfection with polyplexes based on γ-Fe_2O_3@silica@$(PDMAEMA_{540})_{91}$

	N/P ratio	TE (%)	Viability (%)
CHO-K1	3	1.8 ± 0.2	82.4 ± 3.0
	5	16.9 ± 0.6	89.1 ± 1.8
	7.5	40.9 ± 10.3	98.7 ± 1.4
	10	52.5 ± 3.7	99.5 ± 0.4
	12	36.9 ± 1.4	95.9 ± 1.3
L929	3	0.2 ± 0.1	99.0 ± 0.3
	5	0.3 ± 0.1	94.3 ± 3.2
	7.5	0.5 ± 0.2	90.2 ± 2.3
	10	9.4 ± 1.7	90.2 ±2.5
	12	36.8 ± 4.1	90.3 ± 1.5
	15	58.8 ± 1.1	89.7 ± 0.6

The cells were transfected with pEGFP-N1 (EGFP expression plasmid). The EGFP expression was measured 24 h after transfection by flow cytometry and analyzed as described in the materials and methods section. Data represent mean ± s.e.m., n ≥ 3.

The transfection results correlate well with the zeta-potential data (Figure 5B). At N/P = 3 the polyplexes present a negative net charge and therefore cannot interact with the negatively charged plasma membrane and as a consequence almost no transfection occurs. At higher charge ratio (N/P ≥ 7.5) increasing the amount of polymer leads to a decrease in complex aggregation and to an increase of the overall charge, which promotes cellular uptake and in the end gene expression (i. e., greater transfection efficiency). At N/P = 5 however the polyplexes are almost uncharged (Figure 5B). Yet approximately 17 % of the CHO-K1 cells but only 0.3% of the L929 cells are transfected. An efficient transfection of the L929 cells only occurs when the polyplexes displayed a positive net charge ≥ +5 mV. These results suggest that depending on the cell line a net positive charge of the polyplexes is not absolutely necessary for transfection, possibly due to fluctuations in the composition of the polyplexes. However, it can at present not be excluded that a cell specific interaction / uptake occurs by mechanisms not requiring positive net charges of the polyplexes. For example, given the size of the polyplexes macropinocytosis should still be possible.[58] Interestingly, polyplexes formed at N/P 5 also show the highest hydrodynamic radius (> 300 nm) and the highest D.I. (0.34) (Figure 5A). The comparatively low transfection efficiency of only 17% in CHO-K1 suggests

that additional factors, such as nuclease sensitivity and reduced stability of the polyplexes / DNA, in the intracellular compartment may influence the overall transfection outcome.

Magnetic separation of transfected cells. In our recent contribution, using a simple experimental setting, we showed that the uptake of maghemite core-shell nanoparticles-based polyplexes confers CHO-K1 cells magnetic properties.[23] Here, we implemented experimental conditions allowing the isolation and further cultivation of cells that have taken up the polyplexes to assess the level of EGFP expression within the sorted cell population. CHO-K1 cells were transfected with γ-Fe_2O_3@silica@$(PDMAEMA_{540})_{91}$/pDNA at N/P = 7.5, harvested after 24 h and sorted using the magnetic activated cell sorting system (MACS™). In order to calculate the recovery yield, the cell density was determined before magnetic separation and directly afterwards. After separation, the expression of the EGFP protein in the various fractions was analyzed and the cells exhibiting magnetic properties were further cultivated to follow the development of the EGFP expression.

Table 2. Recovery and transfection efficiency in the various cell fractions after magnetic separation of transfected cells.

Fraction	**Recovery (%)**	**EGFP expression**		
		0 h	24 h	48 h
		expressing cells (%)	expressing cells (%)	expressing cells (%)
Control	-	31.2 ± 5.0	58.3 ± 9.4	59.7 ± 5.7
Unbound	12 ± 0.6	8.1 ± 0.0	49 ± 0.0	47.4 ± 0.5
Bound	82.0 ± 10.1	31.8 ± 5.2	57.5 ± 9.5	57.6 ± 11.3

CHO-K1 cells were transfected with pEGFP-N1 (EGFP expression plasmid). The magnetic separation was performed 22 h after transfection. EGFP expression was analyzed on the day of the separation (0 h), 24 , and 48 hours after the cells were put back in culture by flow cytometry as described in the materials and methods section. In all cases the viability was ≥ 90%. Data represent mean ± s.e.m., n ≥ 3. Control: transfected cells that were not submitted to magnetic separation but otherwise similarly treated. Unbound: pool of cells which did not bind to the column and were collected in the wash fraction (i.e, fraction without magnetic properties). Bound: cells that were retained and then eluted by removing the magnet (i.e, fraction with magnetic properties). When non-transfected CHO cells were submitted to the magnetic separation 99.6% of the cells were recovered in the unbound fraction.

The data presented in Table 2 show that more than 80% of the cells transfected with the γ-Fe_2O_3@silica@$(PDMAEMA_{540})_{91}$/pDNA polyplexes can be separated via MACS (magnetic

activated cell sorting) technique and can be further cultivated after sorting. The transfection efficiencies for the "bound fraction" and for the control cells are comparable. Thus, the amount of polymer, taken up by the cells, is not fully associated with an efficient delivery of DNA to the nucleus as only ~32 % (0 h) to 58 % (48 h) of the cells expresses the transgene. Therefore, we conclude a strong influence of cytoplasmic events involved in the breakdown of the complex and playing a crucial role in efficient gene delivery. Among the cells recovered in the unbound fraction (12 %), eight percent express the transgene on the day of sorting indicating that some polyplexes have been taken up and that some plasmid reached the nucleus. Moreover, the transfection efficiency rises up to almost 50% when these cells were further cultivated. Since these cells were not retained in the magnetic field one can argue that the quantity of polyplexes engulfed by the cells was too low to provide magnetic properties but high enough to allow transgene expression.

4.5. Conclusions

The studies on the γ-Fe_2O_3@silica@$(PDMAEMA_{540})_{91}$ gene delivery system showed a significant improvement compared to our previous approach based on physically attached polymer chains. The encapsulation of single iron oxide NPs by silica provided a convenient basis for the irreversible attachment of PDMAEMA chains onto the nanoparticle surface. Consequently, an unpredictable influence of free polymer chains can be excluded and the performance as gene vector can be fully attributed to the hybrid material. The produced core-shell-corona NPs remain stable for more than a year in aqueous media without showing precipitation/sedimentation while keeping excellent performance in transfection experiments. Thus, this approach provides highly stable hybrid particles with a precisely determined amount of polymer, which allows now a systematic investigation of the transfection efficiency and cytotoxicity as a function of the grafting density and chain length of the polymer. A library of hybrid particles with different polymer contents has already been prepared and is currently under investigation. The γ-Fe_2O_3@silica@$(PDMAEMA_{540})_{91}$ NPs investigated in this study offer the great advantage of combining a high transfection efficiency with a very low *in vitro* cytotoxicity and is therefore a good candidate for delivery of plasmid DNA, as shown here with two representative cell lines. Even though the overall molecular weight of the polymer corona of the individual NPs has almost doubled (7.7 MDa) as compared to our previous system, the performance as gene vector remains similar. Thus, we could confirm that the influence of the architecture plays a crucial role in non-viral gene

delivery revealing enhanced transfection results for star-like structures. Most importantly, as opposed to most applications using magnetic nanoparticles for gene delivery,[59] the improved efficiency in transfections with γ-Fe_2O_3@silica@$(PDMAEMA_{540})_{91}$ NPs does not rely on the application of a magnetic field (*i.e.*, Magnetofection™).[26] Here, the magnetic properties of the hybrid material were exploited for cell separation showing that a high amount of cells could be magnetically isolated. Interestingly, although all these cells must have engulfed the polyplexes, only a fraction expresses the transgene. The coexistence of expressing and non-expressing cells within the separated population illustrates and simultaneously highlights the not yet understood complexity of the intracellular trafficking of the polyplexes and nuclear uptake of the pDNA. The superparamagnetic γ-Fe_2O_3@silica@ $(PDMAEMA_{540})_{91}$ NPs might be therefore a helpful tool in the future to understand these intracellular mechanisms and in the end optimize the transfection of mammalian cells.

Acknowledgments: The authors would like to thank Prof. Stephan Förster (Bayreuth Center for Colloids and Interfaces) for access to the zetasizer. We thank Melanie Förtsch for performing the TEM experiments, Marietta Böhm for SEC and AF-FFF measurements, Thomas Friedrich for VSM measurements and Thomas Ruhland for helpful discussions on the synthesis of the NPs.

4.6. References

(1) Uchida, E.; Mizuguchi, H.; Ishii-Watabe, A.; Hayakawa, T. *Biol. Pharm. Bull.* **2002**, *25*, 891-897.

(2) Yue, Y.; Wu, C. *Biomater. Sci.* **2013**, *1*, 152-170.

(3) Mintzer, M. A.; Simanek, E. E. *Chem. Rev.* **2008**, *109*, 259-302.

(4) Cherng, J.-Y.; van de Wetering, P.; Talsma, H.; Crommelin, D. J. A.; Hennink, W. E. *Pharm. Res.* **1996**, *13*, 1038-1042.

(5) Rungsardthong, U.; Deshpande, M.; Bailey, L.; Vamvakaki, M.; Armes, S. P.; Garnett, M. C.; Stolnik, S. *J. Control. Release* **2001**, *73*, 359-380.

(6) van de Wetering, P.; Cherng, J.-Y.; Talsma, H.; Hennink, W. E. *J. Control. Release* **1997**, *49*, 59-69.

(7) Agarwal, S.; Zhang, Y.; Maji, S.; Greiner, A. *Mater. Today* **2012**, *15*, 388-393.

(8) Georgiou, T. K.; Vamvakaki, M.; Patrickios, C. S.; Yamasaki, E. N.; Phylactou, L. A. *Biomacromolecules* **2004**, *5*, 2221-2229.

(9) Georgiou, T. K.; Vamvakaki, M.; Phylactou, L. A.; Patrickios, C. S. *Biomacromolecules* **2005**, *6*, 2990-2997.

(10) Georgiou, T. K.; Phylactou, L. A.; Patrickios, C. S. *Biomacromolecules* **2006**, *7*, 3505-3512.

(11) Schallon, A.; Jérôme, V.; Walther, A.; Synatschke, C. V.; Müller, A. H. E.; Freitag, R. *React. Funct. Polym.* **2010**, *70*, 1-10.

(12) Synatschke, C. V.; Schallon, A.; Jérôme, V.; Freitag, R.; Müller, A. H. E. *Biomacromolecules* **2011**, *12*, 4247-4255.

(13) Schallon, A.; Synatschke, C. V.; Jérôme, V.; Müller, A. H. E.; Freitag, R. *Biomacromolecules* **2012**, *13*, 3463-3474.

(14) Gary, D. J.; Lee, H.; Sharma, R.; Lee, J.-S.; Kim, Y.; Cui, Z. Y.; Jia, D.; Bowman, V. D.; Chipman, P. R.; Wan, L.; Zou, Y.; Mao, G.; Park, K.; Herbert, B.-S.; Konieczny, S. F.; Won, Y.-Y. *ACS Nano* **2011**, *5*, 3493-3505.

(15) Behrens, S. *Nanoscale* **2011**, *3*, 877-892.

(16) Reddy, L. H.; Arias, J. L.; Nicolas, J.; Couvreur, P. *Chem. Rev.* **2012**, *112*, 5818-5878.

(17) Hyeon, T.; Lee, S. S.; Park, J.; Chung, Y.; Na, H. B. *J. Am. Chem. Soc.* **2001**, *123*, 12798-12801.

(18) Park, J.; An, K.; Hwang, Y.; Park, J.-G.; Noh, H.-J.; Kim, J.-Y.; Park, J.-H.; Hwang, N.-M.; Hyeon, T. *Nat. Mater.* **2004**, *3*, 891-895.

(19) Dong, H.; Huang, J.; Koepsel, R. R.; Ye, P.; Russell, A. J.; Matyjaszewski, K. *Biomacromolecules* **2011**, *12*, 1305-1311.

(20) Gillich, T.; Acikgöz, C.; Isa, L.; Schlüter, A. D.; Spencer, N. D.; Textor, M. *ACS Nano* **2013**, *7*, 316-329.

(21) Yuan, Y.; Rende, D.; Altan, C. L.; Bucak, S.; Ozisik, R.; Borca-Tasciuc, D.-A. *Langmuir* **2012**, *28*, 13051-13059.

(22) Lutz, J.-F.; Stiller, S.; Hoth, A.; Kaufner, L.; Pison, U.; Cartier, R. *Biomacromolecules* **2006**, *7*, 3132-3138.

(23) Majewski, A. P.; Schallon, A.; Jérôme, V.; Freitag, R.; Müller, A. H. E.; Schmalz, H. *Biomacromolecules* **2012**, *13*, 857-866.

(24) Goldmann, A. S.; Schödel, C.; Walther, A.; Yuan, J.; Loos, K.; Müller, A. H. E. *Macromol. Rapid Commun.* **2010**, *31*, 1608-1615.

(25) Plank, C.; Scherer, F.; Schillinger, U.; Anton, M. *J. Gene Med.* **2000**, *2 (Suppl)*, 24.

(26) Plank, C.; Zelphati, O.; Mykhaylyk, O. *Adv. Drug Delivery Rev.* **2011**, *63*, 1300-1331.

(27) Amstad, E.; Gehring, A. U.; Fischer, H.; Nagaiyanallur, V. V.; Hähner, G.; Textor, M.; Reimhult, E. *J. Phys. Chem. C* **2011**, *115*, 683-691.

(28) Amstad, E.; Gillich, T.; Bilecka, I.; Textor, M.; Reimhult, E. *Nano Lett.* **2009**, *9*, 4042-4048.

(29) Tchoul, M. N.; Dalton, M.; Tan, L.-S.; Dong, H.; Hui, C. M.; Matyjaszewski, K.; Vaia, R. A. *Polymer* **2012**, *53*, 79-86.

(30) Gelbrich, T.; Reinartz, M.; Schmidt, A. M. *Biomacromolecules* **2010**, *11*, 635-642.

(31) Flesch, C.; Delaite, C.; Dumas, P.; Bourgeat-Lami, E.; Duguet, E. *J. Polym. Sci., Part A: Polym. Chem.* **2004**, *42*, 6011-6020.

(32) Frickel, N.; Messing, R.; Gelbrich, T.; Schmidt, A. M. *Langmuir* **2009**, *26*, 2839-2846.

(33) Messing, R.; Frickel, N.; Belkoura, L.; Strey, R.; Rahn, H.; Odenbach, S.; Schmidt, A. M. *Macromolecules* **2011**, *44*, 2990-2999.

(34) Talelli, M.; Rijcken, C. J. F.; Lammers, T.; Seevinck, P. R.; Storm, G.; van Nostrum, C. F.; Hennink, W. E. *Langmuir* **2009**, *25*, 2060-2067.

(35) Reinicke, S.; Döhler, S.; Tea, S.; Krekhova, M.; Messing, R.; Schmidt, A. M.; Schmalz, H. *Soft Matter* **2010**, *6*, 2760-2773.

(36) Mistlberger, G.; Koren, K.; Scheucher, E.; Aigner, D.; Borisov, S. M.; Zankel, A.; Pölt, P.; Klimant, I. *Adv. Funct. Mater.* **2010**, *20*, 1842-1851.

(37) Niu, D.; Li, Y.; Ma, Z.; Diao, H.; Gu, J.; Chen, H.; Zhao, W.; Ruan, M.; Zhang, Y.; Shi, J. *Adv. Funct. Mater.* **2010**, *20*, 773-780.

(38) Laurenti, M.; Guardia, P.; Contreras-Cáceres, R.; Pérez-Juste, J.; Fernandez-Barbero, A.; Lopez-Cabarcos, E.; Rubio-Retama, J. *Langmuir* **2011**, *27*, 10484-10491.

(39) Li, Q.; Zhang, L.; Bai, L.; Zhang, Z.; Zhu, J.; Zhou, N.; Cheng, Z.; Zhu, X. *Soft Matter* **2011**, *7*, 6958-6966.

(40) Deng, Y. H.; Yang, W. L.; Wang, C. C.; Fu, S. K. *Adv. Mater.* **2003**, *15*, 1729-1732.

(41) Yi, D. K.; Lee, S. S.; Papaefthymiou, G. C.; Ying, J. Y. *Chem. Mater.* **2006**, *18*, 614-619.

(42) Yi, D. K.; Selvan, S. T.; Lee, S. S.; Papaefthymiou, G. C.; Kundaliya, D.; Ying, J. Y. *J. Am. Chem. Soc.* **2005**, *127*, 4990-4991.

(43) Ruhland, T. M.; Reichstein, P. M.; Majewski, A. P.; Walther, A.; Müller, A. H. E. *J. Colloid Interface Sci.* **2012**, *374*, 45-53.

(44) Yanes, R. E.; Tamanoi, F. *Ther. Deliv.* **2012**, *3*, 389-404.

(45) Vivero-Escoto, J. L.; Huxford-Phillips, R. C.; Lin, W. *Chem. Soc. Rev.* **2012**, *41*, 2673-2685.

(46)Mori, H.; Chan Seng, D.; Zhang, M.; Müller, A. H. E. *Prog. Coll. Polym. Sci.* **2004**, *126*, 40-43.

(47) Cao, L.; Man, T.; Zhuang, J.; Kruk, M. *J. Mater. Chem.* **2012**, *22*, 6939-6946.

(48) Zhu, Y.; Fang, Y.; Borchardt, L.; Kaskel, S. *Microporous Mesoporous Mater.* **2011**, *141*, 199-206.

(49) Huang, Y.; Liu, Q.; Zhou, X.; Perrier, S.; Zhao, Y. *Macromolecules* **2009**, *42*, 5509-5517.

(50) Plamper, F. A.; Becker, H.; Lanzendörfer, M.; Patel, M.; Wittemann, A.; Ballauff, M.; Müller, A. H. E. *Macromol. Chem. Phys.* **2005**, *206*, 1813-1825.

(51) Mori, H.; Seng, D. C.; Zhang, M.; Müller, A. H. E. *Langmuir* **2002**, *18*, 3682-3693.

(52) Green, D. L.; Lin, J. S.; Lam, Y.-F.; Hu, M. Z. C.; Schaefer, D. W.; Harris, M. T. *J. Colloid Interface Sci.* **2003**, *266*, 346-358.

(53)Anthony, J. W.; Bideaux, R. A.; Bladh, K. W.; Nichols, M. C., *Handbook of mineralogy, volume III: halides, hydroxides, oxides*. Mineralogical Society of America: Chantilly, 1997; p 628.

(54) Plamper, F. A.; Ruppel, M.; Schmalz, A.; Borisov, O.; Ballauff, M.; Müller, A. H. E. *Macromolecules* **2007**, *40*, 8361-8366.

(55) Al-Dosari, M. S.; Gao, X. *AAPS J.* **2009**, *11*, 671-681.

(56) Rodríguez-Gascón, A.; del Pozo-Rodríguez, A.; Ángeles-Solinís, M., In *Gene Therapy - Tools and Potential Applications*, Molina, F. M., Ed. InTech: Riejka, 2013; pp 3-33;

http://www.intechopen.com/books/gene-therapy-tools-and-potential-applications/non-viral-delivery-systems-in-gene-therapy.

(57) Zhang, Y.; Zheng, M.; Kissel, T.; Agarwal, S. *Biomacromolecules* **2012**, *13*, 313-322.

(58) Conner, S. D.; Schmid, S. L. *Nature* **2003**, *422*, 37-44.

(59) Schwerdt, J. I.; Goya, G. F.; Calatayud, M. P.; Herenu, C. B.; Reggiani, P. C.; Goya, R. G. *Curr. Gene Ther.* **2012**, *12*, 116-126.

4.7. Supporting Information

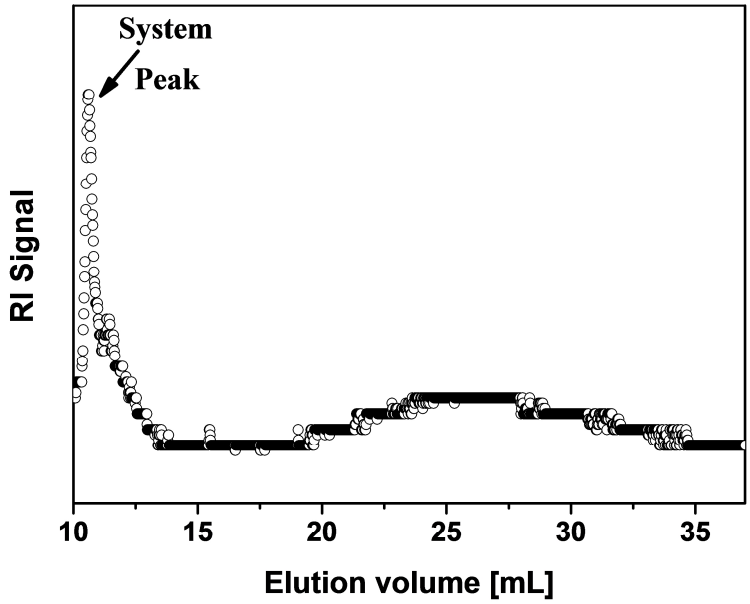

Figure S1. AF-FFF eluogram (RI signal, c = 1 g/L) of γ-Fe_2O_3@Silica@$(PDMAEMA_{540})_{91}$ 3 weeks after purification showing a monomodal distribution of the sample (eluent: deionized water containing 25 mM $NaNO_3$ and 200 ppm NaN_3).

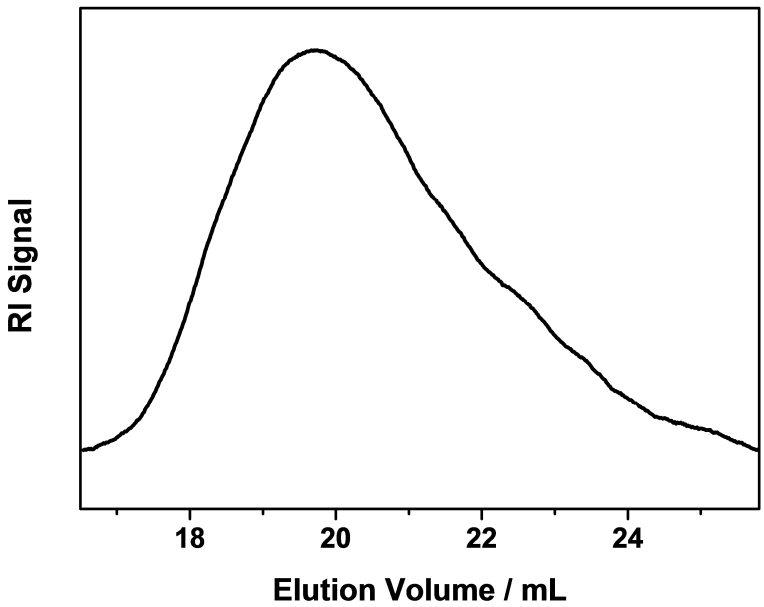

Figure S2. SEC trace of the cleaved PDMAEMA chains.

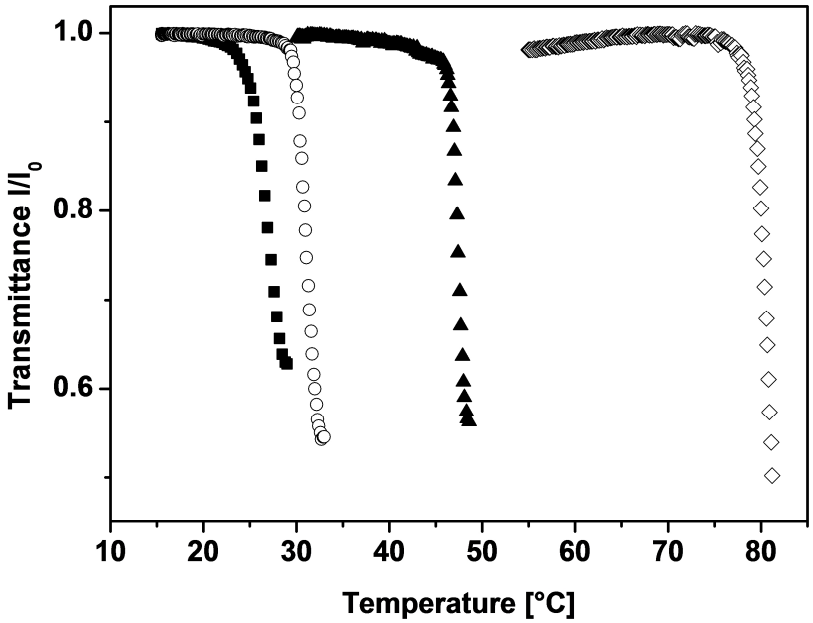

Figure S3. Turbidity measurements of γ-Fe_2O_3@Silica@$(PDMAEMA_{540})_{91}$ (c = 0.1 g/L) at different pH: pH 10 (■), pH 9 (○), pH 8 (▲), pH 7 (◇).

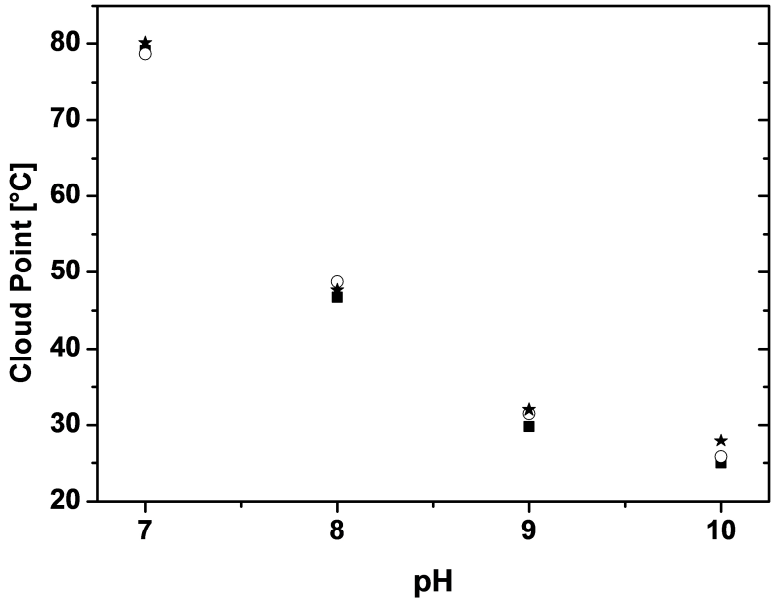

Figure S4. Cloud points in dependence on pH for 0.1 g/L solutions of γ-Fe_2O_3@Silica@$(PDMAEMA_{540})_{91}$ (■), γ-Fe_2O_3@$(PDMAEMA_{590})_{53}$ (★),[1] and $(PDMAEMA_{240})_{24}$ stars (○).[2]

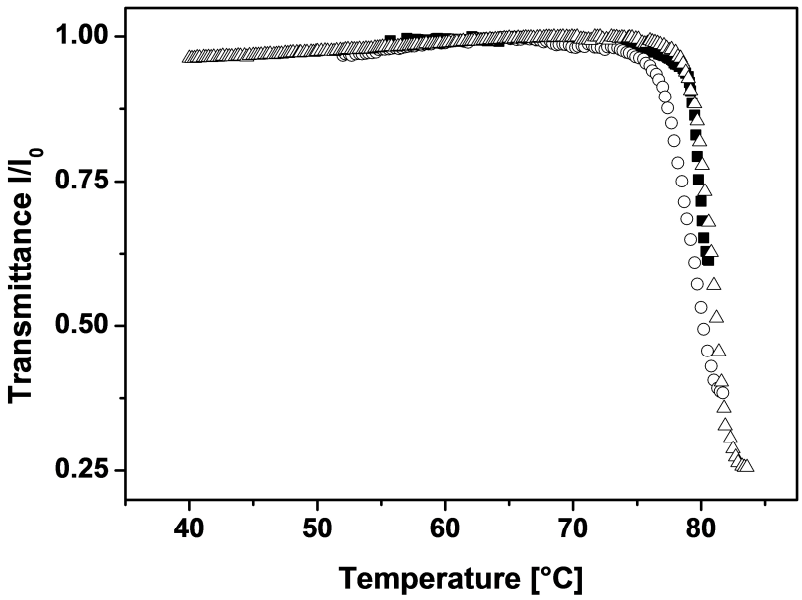

Figure S5. Three cylces of turbidity measurements of γ-Fe_2O_3@Silica@$(PDMAEMA_{540})_{91}$ at pH 7 (c = 0.1 g/L): cycle 1 (■), cycle 2 (○), cycle 3 (Δ).

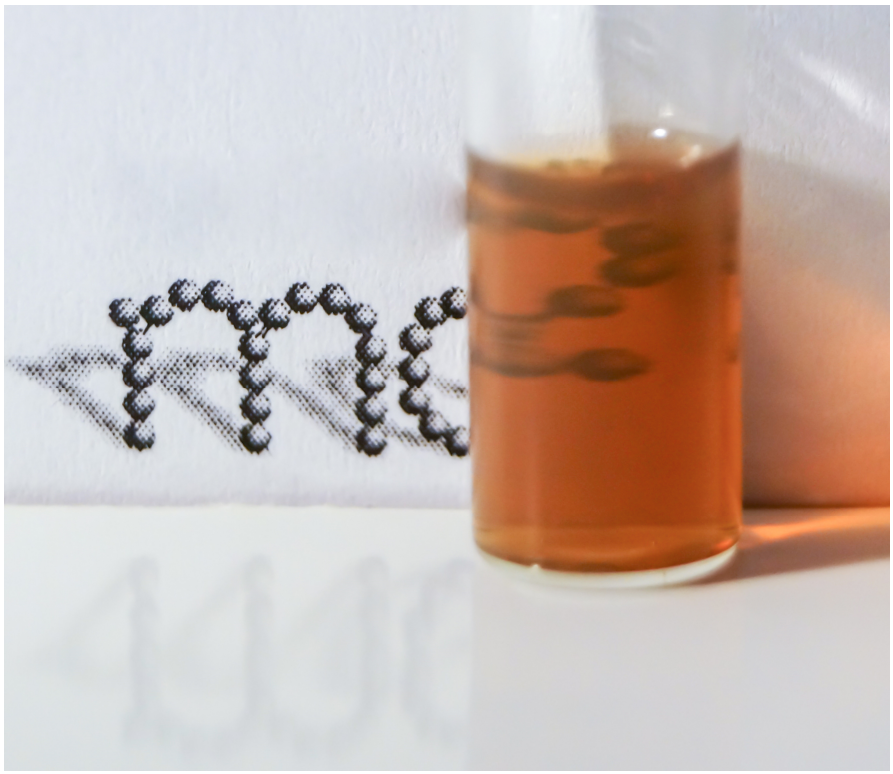

Figure S6. The photograph of a clear γ-Fe_2O_3@Silica@$(PDMAEMA_{540})_{91}$ dispersion in deionized water (pH 5.5) taken after 1 year storage do not show any sign of nanoparticle agglomeration or precipitation.

References

(1) Majewski, A. P.; Schallon, A.; Jérôme, V.; Freitag, R.; Müller, A. H. E.; Schmalz, H. *Biomacromolecules* **2012**, *13*, 857-866.

(2) Plamper, F. A.; Ruppel, M.; Schmalz, A.; Borisov, O.; Ballauff, M.; Müller, A. H. E. *Macromolecules* **2007**, *40*, 8361-8366.

Chapter 5

Double Responsive Pentablock Terpolymers: Self-Assembly and Gelation Behavior

Alexander P. Majewski[1], Tina Borke[1], Andreas Hanisch[1], Axel H. E. Müller[1,2,*] and Holger Schmalz[1,*]

[1]Makromolekulare Chemie II Universität Bayreuth, D-95440 Bayreuth, Germany; Fax: +49 921553393; [2]new address: Institute of Organic Chemistry, Johannes Gutenberg Universität Mainz, D-55099 Mainz, Germany.

E-Mail: holger.schmalz@uni-bayreuth.de; axel.mueller@uni-mainz.de

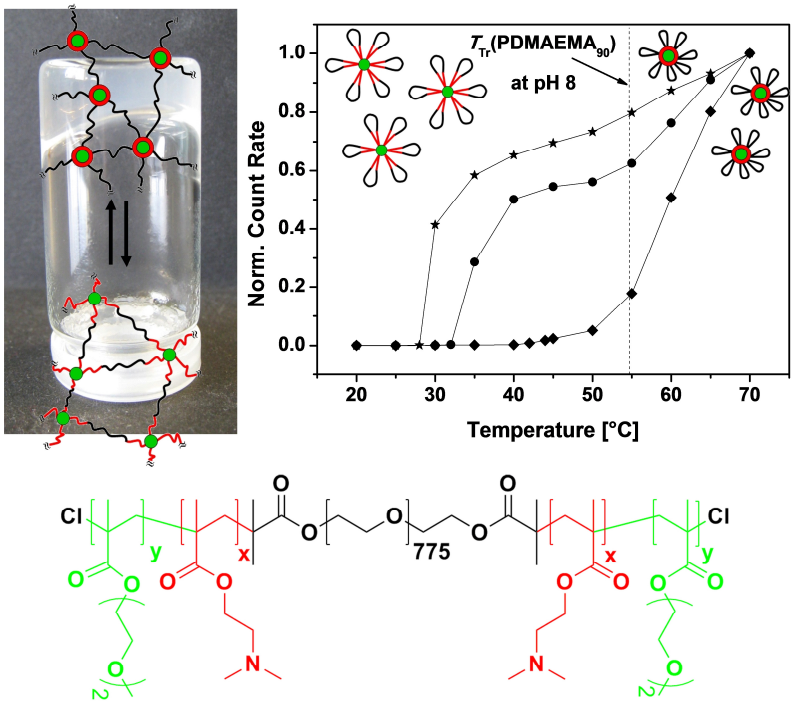

5.1. Abstract

Double responsive ABCBA pentablock terpolymers were successfully synthesized utilizing a bifunctional poly(ethylene oxide) (PEO) macroinitiator and sequential atom transfer radical polymerization (ATRP) of 2-(dimethylamino)ethyl methacrylate (DMAEMA) to form dual-responsive (temperature/pH) B-blocks and di(ethylene glycol) methyl ether methacrylate (DEGMA) for thermo-sensitive A-blocks. Besides the ABCBA structure, the PDMAEMA-*b*-PEO-*b*-PDMAEMA (ABA) triblock copolymer intermediates were investigated in dilute solution *via* dynamic light scattering (DLS) in dependence of temperature and pH. The temperature-dependent aggregation behavior of the ABCBA pentablock terpolymers with different PDEGMA block lengths (11 – 43 repeating units) revealed thereby two separated coil-to-globule phase transitions. The first phase transition at low temperatures could be attributed to the thermo-sensitive PDEGMA leading to the formation of flower-like micelles, which consist of a collapsed PDEGMA core and a looped PDMAEMA-*b*-PEO-*b*-PDMAEMA corona. Furthermore, the phase transition temperatures of the second contraction of the PDMAEMA blocks, which are integrated in the ABCBA corona, were shown to be dependent on pH. Due to their bifunctional character, concentrated solutions of both the ABA intermediates and the ABCBA pentablock terpolymers showed reversible formation of physically cross-linked hydrogels. Here, a DMAEMA molar fraction of at least 0.19 is needed for the ABA intermediates to form strong gels at elevated pH (≥ 10) and high concentrations (20 wt%). Lower DEGMA molar fractions (< 0.1) for the ABCBA already decreased the sol-gel transition by 8-10 °C in comparison to the ABA counterpart. Interestingly, the two individually switchable transitions accessed *via* DLS and µDSC are invisible in the rheology measurements. These results may indicate that the low DEGMA molar fractions of the investigated ABCBA pentablock terpolymers have no sufficient impact on the gelation behavior for a distinct separation of the different stimuli with respect to the mechanical properties.

5.2. Introduction

The synthesis and characterization of smart hydrogels is a fast developing field in polymer chemistry. Here, the term "smart" refers to polymers, which respond to external stimuli by undergoing reversible sharp phase transitions (*e.g.* coil-to-globule) caused by small changes of physical and/or chemical parameters in the environment. These phase transitions are typically based on hydrogen bonding, hydrophobic or electrostatic interactions.[1, 2] Since these water-based multipurpose materials reveal interesting properties such as temperature and pH responsiveness, they are frequently used for applications in medicine and biotechnology.[3-5] This broad field of polymeric hydrogels can be roughly categorized as either synthetic or biopolymeric systems, which are either physically/reversibly or chemically/covalently cross-linked.[6, 7]

A physically cross-linked hydrogel network, formed by applying an external stimulus (*e.g.* temperature, pH, etc.), has the advantage of full reversibility back into the liquid state, in contrast to chemically cross-linked systems. For this purpose, typically AB/ABA, BAB or $(AB)_x$ block copolymers with water-soluble A-blocks and stimuli-responsive B-blocks are frequently used. In AB/ABA block copolymer hydrogels micelle formation takes place by switching the B-block water-insoluble, which causes hydrogel formation from closely packed micelles upon exceeding the critical gelation concentration (c_{cgc}).[8-11] Conversely, the hydrogel formation in BAB systems takes place by causing a phase transition of the B-blocks leading to flower-like micelles with a looped hydrophilic middle block. Due to bridging of the micelles at the c_{cgc} a hydrogel network is formed.[12-15] $(AB)_x$ diblock copolymer stars show as well high potential for forming physically cross-linked hydrogels *via* an open association at the c_{cgc} caused by their architecture, which provides multiple connection sites for each molecule.[16-19]

In general, block copolymer systems rely on temperature or pH for triggering the phase transition. Here, for integrating a pH switch in the hydrogel ionic polymers such as poly(acrylic acid) (PAA) and poly(2/4-vinylpyridine) (P2VP/P4VP) are potential candidates.[20-22] Thermo-responsive polymers, which are typically applied for hydrogels, show generally a Lower Critical Solution Temperature (LCST). Among these thermosensitive polymers is poly(N-isopropylacrylamide) (PNIPAAm) probably the most investigated material for hydrogels, due to its coil-to-globule transition around body temperature.[23-26] Another example for thermo-responsive polymers are poly(oligo(ethylene glycol) methyl ether methacrylate)s (POEGMAs) carrying 2 – 10 ethylene oxide units in their side chains.

The coil-to-globule transition of these polymers can be easily varied *via* copolymerization of POEGMAs with different side chain lengths resulting in an adjustable cloud point between 26 °C (pure poly(di(ethylene glycol) methyl ether methacrylate) (PDEGMA)) and 90 °C (pure POEGMA bearing 8 – 9 ethylene oxide units).[27-30] An outstanding class of responsive polymers are PDMAEMA and PDEAEMA showing both, responsiveness to temperature and pH.[31-33] Due to protonation of the pendant tertiary amine side groups this polymer is highly charged at low pH, which drastically increases the solubility. Conversely, at high pH the polymer is completely deprotonated causing a coil-to-globule phase transition, even at lower temperatures. Thus, the transition temperatures can vary, *e.g.* for $PDMAEMA_{133}$ (subscript denotes the average degree of polymerization), from 40.5 °C at pH 10 to 78.7 °C at pH 7 and below pH 7 does the LCST completely disappear.[33]

Hydrogels that undergo two separate phase transitions, however, are much less investigated due to their complexity in synthesis and characterization. The advantage of these systems is not only the formation of a hydrogel network triggered *via* external stimuli, but also the possibility to alter the gelation behavior caused by a second separate phase transition. Reported double responsive block copolymer hydrogel systems are made either from ABA[22, 34] and $(AB)_x$[35, 36] block copolymers where both blocks are stimuli-responsive or ABC triblock copolymers,[37-39] which bear a hydrophilic B-block and two independently switchable A- and C-blocks. Further examples of hydrogel formation *via* self-assembly of bis- or tris-hydrophilic block copolymers based on methacrylates were recently reviewed in detail by Madsen and Armes.[40]

Even more sophisticated structures for double responsive hydrogels are ABCBA pentablock terpolymers. Here, typically two of the three different blocks provoke a phase transition under different environmental conditions. A frequently used method is the modification of the commercially available Pluronics® polymers (BASF), which are water-soluble triblock copolymers consisting of two poly(ethylene oxide) (PEO) end blocks and a thermo-responsive poly(propylene oxide) (PPO) middle block.[41, 42] These PEO-*b*-PPO-*b*-PEO triblock copolymers can easily be end-capped with ATRP initiating sites resulting in bifunctional ATRP-macroinitiators. A subsequent polymerization of stimuli-responsive outer blocks yields double responsive ABCBA pentablock terpolymers containing the Pluronics® polymer as the inner BCB core. This approach was applied using stimuli responsive polymers such as PNIPAAm, PDEAEMA and PAA as A-blocks, obtaining interesting materials for hydrogel formation and biotechnological applications.[43-45] Generally, studies of pentablock terpolymers are rare and there exist even less examples of pentablock terpolymers used for

hydrogels. For instance, the group of Lee investigated dual-responsive ABCBA pentablock terpolymers consisting of a thermo-responsive PEO-based biodegradable polyester block copolymer BCB inner segment (poly(ε-caprolactone-*co*-lactide)-*b*-PEO-*b*-poly(ε-caprolactone-*co*-lactide) (PCLA-PEO-PCLA) or poly(ε-caprolactone-*co*-glycolide)-*b*-PEO-*b*-poly(ε-caprolactone-*co*-glycolide) (PCGA-PEO-PCGA)) and pH-sensitive oligomeric sulfomethazine (OSM) A-blocks.[46-48] Hydrogels from ABCBA pentablock terpolymers with two permanently hydrophobic poly(methyl methacrylate) (PMMA) A-blocks and a polyampholyte BCB triblock as potential bridging middle chain (PMMA-*b*-PAA-*b*-P2VP-*b*-PAA-*b*-PMMA) were reported by Tsitsilianis *et al.*[49]

Here, we describe the synthesis and self-assembly of tris-hydrophilic ABCBA pentablock terpolymers consisting of a PEO C-block, two PDMAEMA B-blocks as well as two PDEGMA A-blocks. The non-responsive PEO middle block was chosen to enhance the stability of the system and is merely responsible for the water-solubility. The PDMAEMA blocks show responsiveness to both temperature and pH. Since the A-block of our system should be triggered first, the PDEGMA block should undergo a coil-to-globule phase transition prior to the PDMAEMA B-block. The aggregation behavior of the ABCBA pentablock terpolymers and PDMAEMA-*b*-PEO-*b*-PDMAEMA triblock copolymer intermediates in dilute and concentrated solutions were investigated primarily via dynamic light scattering (DLS) and rheology measurements, respectively. It has to be mentioned, that one study about similar ABCBA pentablock terpolymers already exists.[50] There is, however, no detailed characterization about the block length dependence given and the investigation of the self-assembly in dilute solution is insufficiently discussed in comparison to our detailed study on these ABCBA systems. In addition, we investigated concentrated solutions for potential applications as hydrogels.

The proposed self-assembly behavior of the pentablock terpolymer is shown in Scheme 1. At low concentrations the polymer forms flower-like micelles consistent with the collapse of the PDEGMA A-block at low temperatures. The resulting micelles are stabilized by a looped PDMAEMA-*b*-PEO-*b*-PDMAEMA corona. The PDMAEMA is now located between the collapsed PDEGMA core and the outer PEO shell. A second coil-to-globule phase transition caused by the PDMAEMA can be triggered and occurs consistently at higher temperatures in comparison to the PDEGMA block independent of pH. At concentrations above the critical gelation concentration, c_{cgc}, the collapsing PDEGMA blocks form physically cross-linked junctions of the hydrogel network. Here, the bridging segments consist of the hydrophilic PDMAEMA-*b*-PEO-*b*-PDMAEMA blocks (BCB) of the ABCBA pentablock terpolymer,

where the PDMAEMA blocks are located next to the collapsed PDEGMA core. The second contraction of the PDMAEMA should lead to a significant change in the mechanical properties, while the PEO middle block prevents a total collapse of the system.

Scheme 1. Self-assembly of ABCBA pentablock terpolymers.

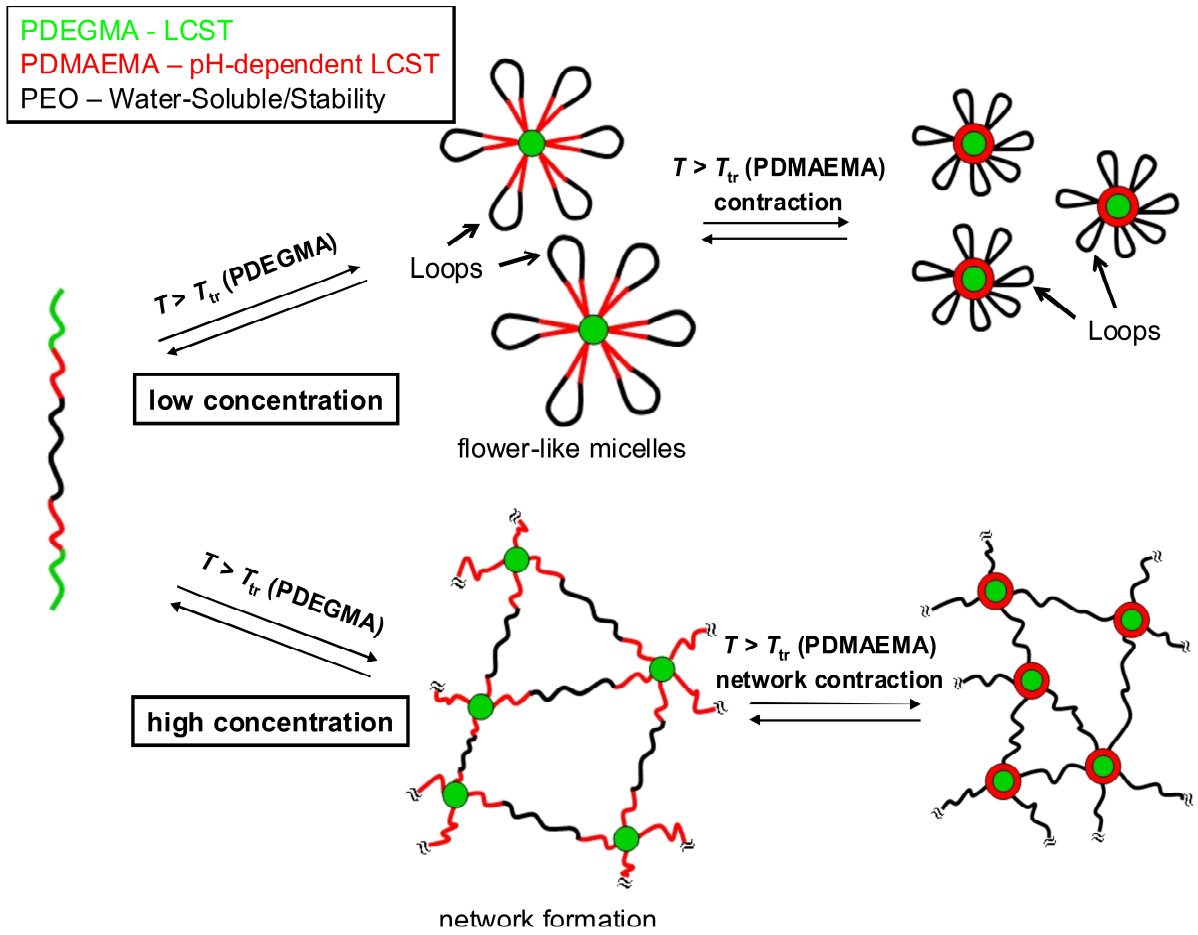

5.3. Experimental Part

Materials. AVS buffer solutions pH 3, 8-10 (Titrinorm™, VWR), 2-bromoisobutyric acid (98%, Sigma-Aldrich), *N,N*'-dicyclohexylcarbodiimide (DCC, 99%, Sigma-Aldrich), 4-(dimethylamino)pyridine (DMAP, 99%, Sigma-Aldrich), dichloromethane (DCM, p.a., Sigma-Aldrich), 1,1,4,7,10,10-hexamethyltriethylenetetramine (HMTETA, 97%, Sigma-Aldrich) and HO-PEG_{32k}-OH (Sigma-Aldrich, M_n = 32 kg/mol, PDI = 1.08) were used as received. 1,1,4,7,7-pentamethyldiethylenetriamine (PMDETA) was purchased from Sigma-Aldrich and distilled and degassed by purging with nitrogen. Copper(I) chloride and copper(I) bromide were purified according to literature.[51] The monomers di(ethylene glycol) methyl ether methacrylate (DEGMA, 95%, Sigma-Aldrich), 2-(dimethylamino)ethyl methacrylate (DMAEMA, 99%, Sigma-Aldrich) were destabilized by passing over a column of basic

aluminum oxide. For dialysis a regenerated cellulose tube (ZelluTrans, Roth) with a MWCO of 6-8 kDa was used. If not stated elsewhere, all other chemicals were purchased in analytical grade and used as received.

Synthesis of the PEO-macroinitiator. HO-PEO_{32k}-OH (50 g, 1.6 mmol), 4-(dimethylamino)pyridine (38 mg, 0.31 mol) and *N,N*'-dicyclohexylcarbodiimide (1.6 g, 7.8 mmol) were dissolved in 300 mL dichloromethane (DCM) before adding dropwise a solution of 2-bromoisobutyric acid (1.5 g, 8.9 mmol, dissolved in 10 mL DCM) under nitrogen atmosphere. The reaction mixture was stirred for two days at room temperature. Subsequently, the reaction mixture was filtered and the solvent was then rotary evaporated. The residue was recrystallized three times from ethanol before freeze-drying.

Synthesis of 2-propynyl benzoate. Benzoic acid (2.00 g, 16.4 mmol), 4-(dimethylamino)-pyridine (0.24 g, 2.0 mmol) and 2-propyn-1-ol (1.01 g, 18.0 mmol) were dissolved in 30 mL DCM and cooled down to 0 °C before adding dicyclohexylcarbodiimide (3.70 g, 17.9 mmol) under nitrogen atmosphere. The reaction mixture was stirred over night at room temperature. The solvent was then rotary evaporated and the residue was purified by column chromatography on silica gel with petroleum ether/diethyl ether (7:3 v/v).

Synthesis of the UV-labeled PEO derivative. 250 mg PEO-macroinitiator ($7.8 \cdot 10^{-3}$ mmol) was dissolved in dimethylformamide (DMF) and sodium azide (10.2 mg, 0.16 mmol) was added before stirring the reaction mixture for 5 days at room temperature. The resulting azide-terminated PEO was precipitated in cold diethyl ether and filtered, before being redissolved in chloroform, extracted with water (3 times) and subsequently dried over anhydrous magnesium sulphate. The azide-terminated PEO (400 mg, 0.026 mmol), 2-propynyl benzoate (10.6 mg, 0.063 mmol) and copper(I) bromide (3.6 mg, 0.026 mmol) were dissolved in THF and degassed with nitrogen. PMDETA (4.5 µL, 0.026 mmol) was added in order to initiate the reaction which was allowed to proceed for 3 days under stirring before being terminated by exposing the mixture to air and stirring for 10 min at room temperature. The crude product was purified by dialysis against methanol in order to remove the copper catalyst, PMDETA and residual 2-propynyl benzoate.

Synthesis of PDMAEMA-b-PEO-b-PDMAEMA triblock copolymers. A typical reaction was carried out in a 25 mL screw cap flask equipped with a septum and charged with PEO-macroinitiator (0.5 g, 0.015 mmol) dissolved in 1 mL anisole, DMAEMA (2.4 mL, 14.25 mmol) and CuCl (2.2 mg, 0.02 mmol). The mixture was purged with nitrogen for 10 min before adding degassed HMTETA (6.3 µL, 0.02 mmol) dissolved in 1 mL anisole. The

polymerization was conducted at 90 °C and the conversion was monitored *via* ^{1}H-NMR. The reaction was terminated by exposing the mixture to air with stirring for 10 min at room temperature. The crude product was purified by dialysis against methanol in order to remove the copper catalyst, HMTETA, monomer and anisole.

Synthesis of PDEGMA-b-PDMAEMA-b-PEO-b-PDMAEMA-b-PDEGMA pentablock terpolymers. A typical reaction was carried out in a 50 mL screw cap flask equipped with a septum and charged with ABA-macroinitiator ($PDMAEMA_{90}$-*b*-PEO_{775}-*b*-$PDMAEMA_{90}$, 1.0 g, 0.017 mmol) dissolved in 10 mL acetonitrile, DEGMA (11.0 mL, 59.6 mmol) and CuCl (2.5 mg, 0.025 mmol). The mixture was purged with nitrogen for 10 min before adding degassed HMTETA (6.8 µL, 0.025 mmol) dissolved in 1 mL acetonitrile. The polymerization was conducted at 60 °C and the conversion was monitored *via* ^{1}H-NMR. The reaction was terminated by exposing the mixture to air with stirring for 10 min at room temperature. The crude product was purified by dialysis against methanol in order to remove the copper catalyst, HMTETA, monomer and acetonitrile.

Characterization. *^{1}H-NMR spectroscopy* was performed with a Bruker Avance 300 spectrometer using deuterated chloroform or deuterium oxide as solvent. The NMR spectra were used to determine the block lengths of the ABA and ABCBA block copolymers, applying a M_n of ... g/mol for the PEO block, as determined by SEC, for internal signal calibration. The block lengths of the ABA block copolymers were calculated by comparison of the PEO signal at 3.65 ppm with the signal at 2.3 ppm, which corresponds to the $–N(CH_3)_2$ group of the PDMAEMA (Figure S1). The block lengths of the ABCBA pentablock terpolymer were similarly determined by comparison of the signals at 2.3 and 3.4 ppm, which correspond to the $–N(CH_3)_2$ (PDMAEMA) and $–OCH_3$ groups (PDEGMA), respectively (Figure S2).

Rheology measurements were conducted using a Physica MCR 301 rheometer with a cone-and-plate shear cell geometry (D = 50 mm, cone angle = 1°). The temperature was controlled by a Peltier element. For the temperature-dependent measurements in this study a frequency of 1 Hz, a heating rate of 0.5 K/min and a strain of 1%, which is inside the linear viscoelastic regime, were used. The polymers were dissolved in deionized water for 1 – 2 days at 3 °C until a clear solution was obtained, the pH adjusted with NaOH (1 mol/L) to pH = 9 or 10, and the solutions were stored at 3 °C until use.

Size Exclusion Chromatography (SEC) was performed on a system based on GRAM columns (7 μm particle diameter) with 10^2 and 10^3 Å pore diameter (Polymer Standards

Service) equipped with Agilent 1200 Series RI- and UV-detectors. N,N-Dimethylacetamide (DMAc) with 0.05% lithium bromide was used as eluent at a flow rate of 0.8 mL/min and a temperature of 60 °C was applied. For data evaluation a calibration with linear PDMAEMA or PEO standards was used.

Dynamic Light Scattering (DLS) was carried out on an ALV DLS/SLS-SP 5022F compact goniometer system with an ALV 5000/E correlator and a He-Ne laser (λ = 632.8 nm) at a scattering angle of 90°. All samples were dissolved in buffer solutions (c = 2 g/L; pH 8, 9 and 10) and filtrated through a 0.2 μm Nylon filter prior to measurement.. The samples were then placed in a decaline bath and the temperature was controlled by using a LAUDA Proline RP 845 thermostat. For temperature-dependent measurements, the samples were equilibrated for 10 min at each temperature before performing three consecutive measurements of 120 sec. The given results represent the average count rate over three measurements. The data were analyzed using the CONTIN algorithm which yields an intensity-weighted distribution of relaxation times (τ) after an inverse Laplace transformation of the intensity auto-correlation function. These relaxation times were transformed into translational diffusion coefficients and further into hydrodynamic radii using the Stokes-Einstein equation. The transition temperatures were determined from the intersection of the two tangents applied to the two linear regimes of the count rate progression at the onset of the coil-to-globule phase transition.

Micro-Differential Scanning Calorimetry (μDSC) measurements were performed with a Setaram μDSC III using closed "batch" cells at a scanning rate of 0.5 K/min. Deionized water was used as reference.

5.4. Results and Discussion

Synthesis of PDMAEMA-*b*-PEO-*b*-PDMAEMA (ABA) Triblock Copolymers. The ABA triblock copolymer intermediates consisting of poly(2-(dimethylamino)ethyl methacrylate) (PDMAEMA) A-blocks and a PEO_{775} (subscript denotes the average degree of polymerization) middle block were synthesized under standard ATRP conditions (Scheme 2). The bifunctional PEO macroinitiator bearing two ATRP initiating sites was obtained *via* a Steglich esterfication of HO-PEO_{775}-OH with 2-bromoisobutyric acid. First, the bifunctionality of the PEO macroinitiator was verified by introducing benzoic acid moieties as UV-labels to the macroinitiator *via* Huisgen azide-alkyne cylcoaddition ("click" reaction). For this purpose, the bromine end groups of the macroinitiator were replaced with azide groups by a substitution reaction and subsequently "clicked" to 2-propynyl benzoate (Figure S3).

UV-/Vis analysis reveals a degree of functionalization of 1.66 by comparison of the UV-labeled PEO-macroinitiator with 2-propynyl benzoate at the same concentration (Figure S4), which is close to the expected value of 2 for a bifunctional macroinitiator. Since the PEO macroinitiator has a considerably high molecular weight the "click"-reaction might not be quantitative for long PEO chains resulting in an even higher degree of functionalization than that determined by UV-/Vis analysis.

Scheme 2. Synthesis of PDEGMA-*b*-PDMAEMA-*b*-PEO-*b*-PDMAEMA-*b*-PDEGMA (ABCBA) pentablock terpolymers.

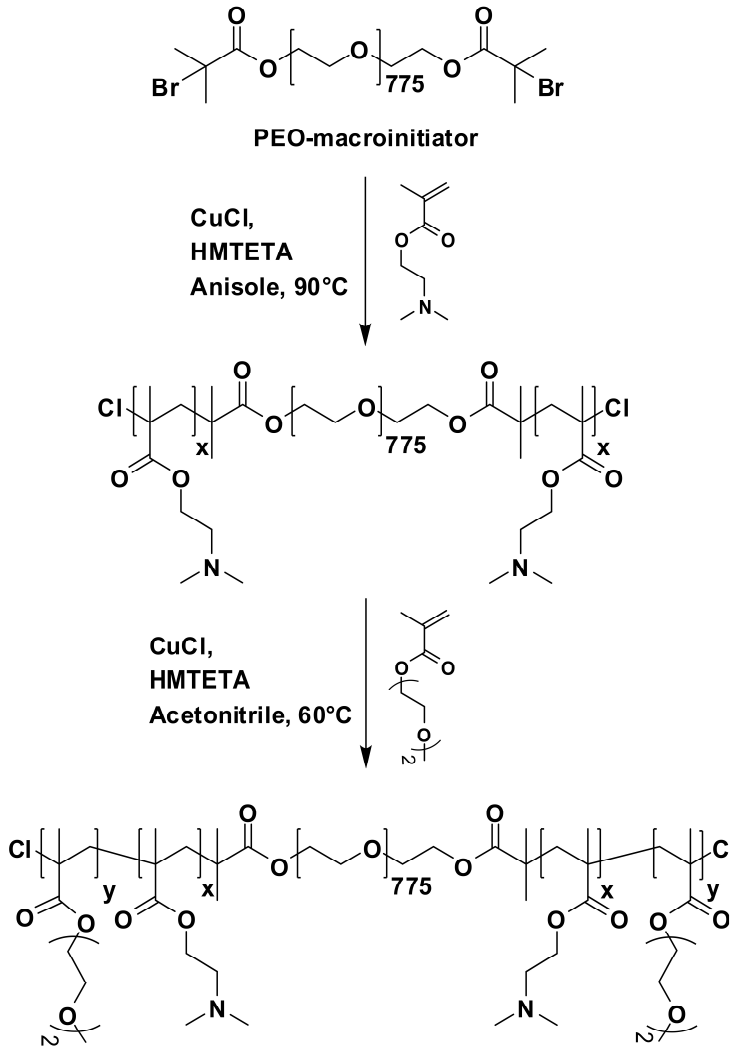

The molecular characteristics of the synthesized PDMAEMA-*b*-PEO-*b*-PDMAEMA triblock copolymers, denoted as ABA-x (x = number average degree of polymerisation of PDMAEMA block) in the following, are listed in Table 1. From this data it can be seen that the PDI of the copolymers increases with increasing molecular weight of the PDMAEMA

block. A narrow molecular weight distribution could be obtained for ABA triblock copolymers up to 90 repeating units per PDMAEMA block (ABA-90, Figure 1).

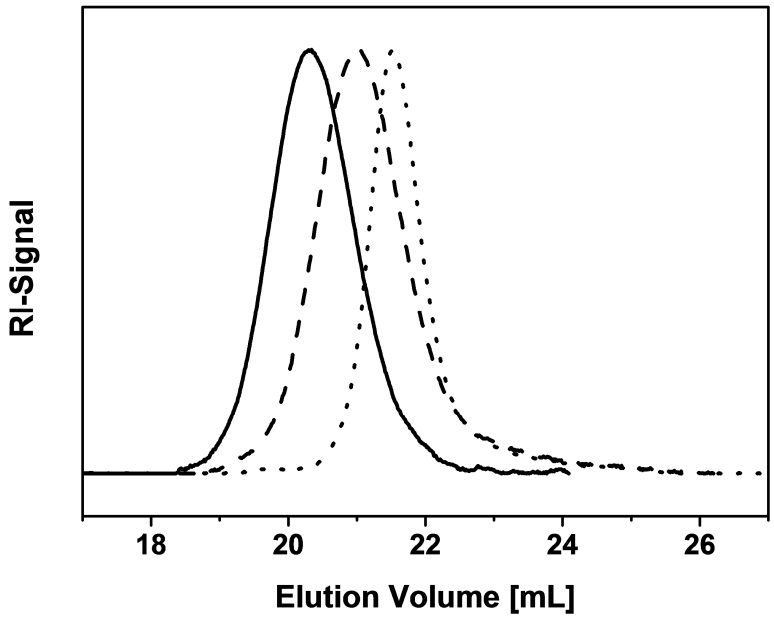

Figure 1. DMAc-SEC traces of the PEO precursor (dotted line), ABA-90 triblock copolymer (dashed line) and ABCBA-25 pentablock terpolymer (solid line).

The corresponding SEC traces for ABA-188 and ABA-255 shown in the Supplementary Information reveal a shoulder at the low molecular weight side (higher elution volume) of the eluogram (Figure S5). This shoulder, which becomes progressively more pronounced with an increasing degree of polymerization of the PDMAEMA blocks, corresponds to a lower molecular weight with respect to that of the PEO-macroinitiator. This leads to the conclusion that it is caused by PDMAEMA homopolymer produced by transfer reactions during the polymerization. This results in the termination of active end groups of the ABA triblock copolymers and consequently in a reduced degree of functionalization with respect to the ATRP initiating sites. Since these intermediates should be used as ATRP-macroinitiators for the subsequent polymerization of DEGMA the ABA-90 triblock copolymer represented a suitable candidate due to no sign of transfer reactions as well as a low PDI.

Table 1. Molecular characteristics and phase transitions of PDMAEMA-*b*-PEO-*b*-PDMAEMA triblock copolymers.

					T_{tr}(PDMAEMA) [°C][f]		
Sample[a]	f_{DMAEMA}[b]	M_n(PDMAEMA) [g/mol][c]	PDI[d]	Gelation[e]	pH 8	pH 9	pH 10
ABA-70	0.15	11 000	1.15	no	54	44	39
ABA-90	0.19	14 000	1.13	no	55	42	40
ABA-188	0.33	29 500	1.25	yes	50	39	37
ABA-255	0.40	40 000	1.45	yes	50	39	34

a) A-block: PDMAEMA, B-block: PEO_{775}; subscript denotes the number-average degree of polymerization of the A-block. b) Molar fraction of DMAEMA units. c) Determined by ^{1}H-NMR. d) Determined by DMAc-SEC applying a PDMAEMA calibration. e) Gelation behavior for a 10 wt% polymer solution at pH ≈ 8.7. f) Phase transition temperatures T_{tr} determined by temperature-dependent dynamic light scattering.

Synthesis of PDEGMA-*b*-PDMAEMA-*b*-PEO-*b*-PDMAEMA-*b*-PDEGMA (ABCBA) pentablock terpolymers. The ABA triblock copolymer with the lowest PDI (ABA-90) was used for further synthesis of ABCBA pentablock terpolymers *via* ATRP, carrying PDEGMA as outer A-block (Scheme 2). Similar to the ABA triblock copolymers, the synthesized PDEGMA-*b*-PDMAEMA-*b*-PEO-*b*-PDMAEMA-*b*-PDEGMA pentablock terpolymers are denoted as ABCBA-y (y = number average degree of polymerisation of PDEGMA block) and the molecular characteristics of the pentablock terpolymers are summarized in Table 2. Monomodal SEC traces indicate a homogeneous growth of PDEGMA on both ends of the corresponding ABA triblock copolymer (Figure 1). It is noted that higher degrees of polymerization for the PDEGMA blocks (> 50 repeating units) lead to considerably broad molecular weight distributions and in order to investigate well-defined polymers are only PDEGMA block lengths up to 43 repeating units presented in this study. Here, the attempt to polymerize longer PDEGMA block lengths led as well to partial termination of the active end groups as a result of chain transfer reactions.

Table 2. Molecular characteristics and phase transitions of PDEGMA-*b*-PDMAEMA-*b*-PEO-*b*-PDMAEMA-*b*-PDEGMA pentablock terpolymers.

Sample[a]	f_{DEGMA}[b]	M_n(PDEGMA) [g/mol][c]	PDI[d]	T_{tr}(PDEGMA) [°C][e]
ABCBA-11	0.02	2 100	1.05	45
ABCBA-25	0.05	4 800	1.05	33
ABCBA-43	0.08	8 100	1.13	29

a) A-block: PDEGMA, B-block: $PDMAEMA_{90}$, C-block: PEO_{775}; subscripts give the number-average degree of polymerization of the respective block. b) Molar fraction of DEGMA units. c) Determined by ^{1}H-NMR. d) Determined by DMAc-SEC applying a PDMAEMA calibration. e) Phase transition temperatures T_{tr} determined by temperature-dependent dynamic light scattering at pH 8.

Aggregation behavior of the ABA triblock copolymers in dilute solution. Due to the protonatable tertiary amine group, the PDMAEMA block shows a pH-dependent coil-to-globule transition upon heating, herein denoted as phase transition temperature (T_{tr}) of the PDMAEMA block. At low pH PDMAEMA is positively charged ($pK_a \approx 6.2$),[33] resulting in an enhanced solubility and high coil-to-globule transition temperatures. Conversely, high pH leads to deprotonation of the PDMAEMA, causing a significant decrease in the transition temperature (T_{tr}). The dependence of T_{tr} on the architecture and molecular weight of PDMAEMA homopolymers has already been investigated by Plamper *et al*.[33] Here, we show *via* temperature-dependent dynamic light scattering (DLS) experiments of dilute samples (c = 2 g/L) that this effect still remains even though the PDMAEMA is connected to a long hydrophilic PEO block, which may be expected to influence the solubility behavior of the PDMAEMA blocks in the ABA triblock copolymers. The collapse of the PDMAEMA blocks causes self-assembly into flower-like micelles, which can be detected by a significant increase of the count rate during a temperature-dependent DLS measurement (Figure S6). Since DLS reveals a much higher sensitivity than common turbidity measurements, it may give slightly lower transition temperatures compared to those obtained from turbidimetry. The transition temperatures decrease with increasing pH and block length of the PDMAEMA (Figure 2A, Table 1). It is noted that the transition points determined in this study are in good agreement with the established cloud points of PDMAEMA, even though the long hydrophilic PEO middle block would be expected to cause an increase in the transition temperature.[33]

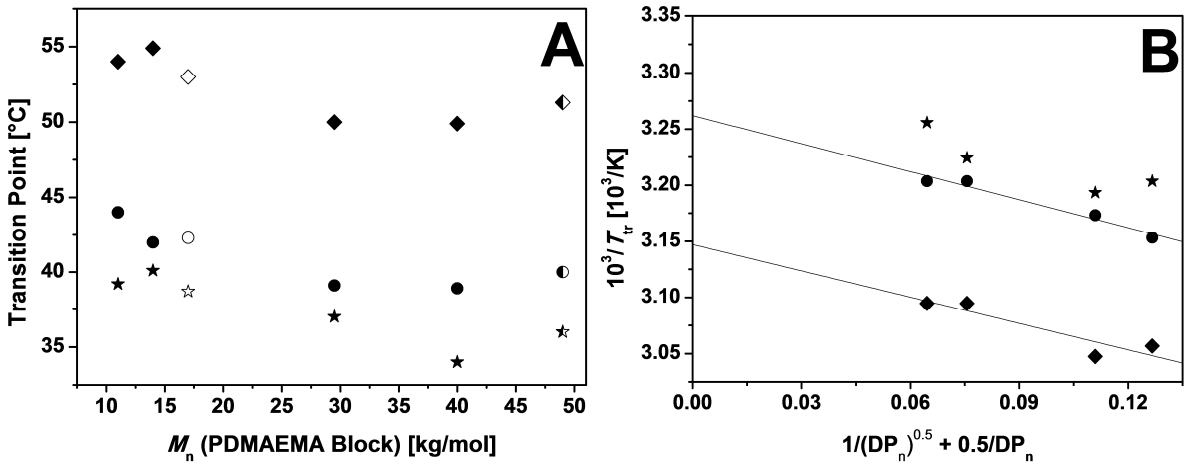

Figure 2. A) pH-dependent phase transitions of ABA block copolymers with varying PDMAEMA block lengths, determined by DLS (c = 2 g/L, θ = 90°): pH 8 (◆), pH 9 (●), pH 10 (★). Phase transitions of linear $PDMAEMA_{108}$ (pH 8 (◇), pH 9 (○), pH 10 (☆)) and $PDMAEMA_{100})_{3.1}$ stars (pH 8 (◈), pH 9 (◐), pH 10 (✯)) were determined by turbidimetry and taken from reference 33. B) Plot of inverse transition points according to Flory-Huggins theory (**Eq. 1**) using the number-average degree of polymerization DP_n of the PDMAEMA-blocks: pH 8 (◆), pH 9 (●), pH 10 (★).

These results were also compared to the Flory-Huggins theory, which describes the dependence of T_{tr} on the degree of polymerization (DP) for linear polymers (Equation 1).[52]

$$\frac{1}{T_{Tr}} = \frac{1}{\theta} + \frac{1}{\theta\psi} \cdot \left(\frac{1}{2 \cdot \mathrm{DP}} + \frac{1}{\sqrt{\mathrm{DP}}} \right) \qquad \textbf{(1)}$$

Here, θ is the transition temperature for infinite DP and ψ is related to the entropy part of the Flory-Huggins parameter, χ. The plot according to Eq. 1 reveals a straight line for pH = 8 and 9, which is in good agreement with the Flory-Huggins theory (Figure 2B). At pH = 10, however, small deviations are observed. This may be attributed to the low molecular weight PDMAEMA blocks, since Plamper *et al.* also noticed deviations for short linear PDMAEMA.[33] It is very interesting, however, that at pH 8 or 9 the T_{tr} can be shown to depend on PDMAEMA block lengths, even for an ABA block copolymer containing a long hydrophilic PEO middle block.

Self-assembly of ABCBA pentablock terpolymers in dilute solution. After the introduction of an additional temperature-responsive PDEGMA block, a significant change in the aggregation behavior occurred. PDEGMA is known to be only responsive to temperature,

showing a coil-to-globule transition at approximately 26 °C independent of the pH.[30] This temperature is significantly lower as compared to the observed phase transition temperatures of the PDMAEMA block in the ABA triblock copolymers within the investigated pH range of 8 – 10 (Table 1). Thus, the PDEGMA outer block should collapse first, initiating the formation of flower-like micelles consisting of a collapsed PDEGMA core with looped PDMAEMA-*b*-PDEGMA-*b*-PDMAEMA block segments as corona before the PDMAEMA B-block undergoes the second phase transition (Scheme 1).

Consequently, the significant increase of the count rate at low temperatures can be attributed to the phase transition of the PDEGMA blocks of ABCBA-25 and -43, which leads to the formation of flower-like micelles (Figure 3). The PDEGMA phase transition of ABCBA-11 (the pentablock terpolymer with the shortest PDEGMA blocks), however, revealed only a weak impact on the count rate at 45 °C for pH = 8 and could not be determined for higher pH as a result of T_{tr}(PDEGMA) > T_{tr}(PDMAEMA) for pH > 8 (Tables 1, 2). Due to the pH independence of the T_{tr} of PDEGMA, the transition temperature was indeed be shown to be similar for ABCBA pentablock terpolymers regardless of pH and as expected, the introduced PDEGMA A-blocks with suitable bock lengths (ABCBA-25 and -43) undergo a coil-to-globule transition at lower temperatures for any investigated pH in comparison to the PDMAEMA B-blocks of ABA-90 (Tables 1, 2), which was used as the ATRP-macroinitiator for the ABCBA pentablock terpolymers.

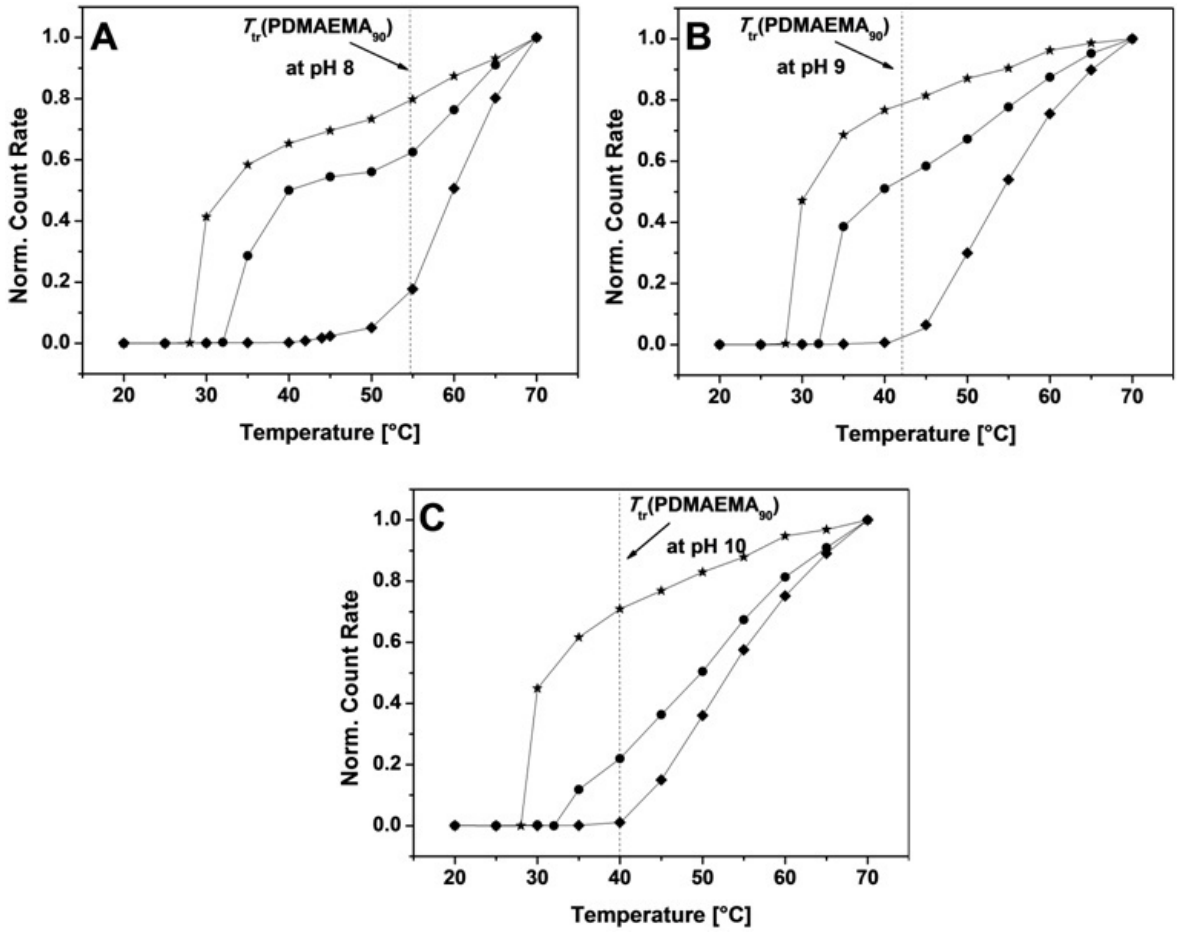

Figure 3. Temperature-dependent scattering intensities at θ = 90° for ABCBA pentablock copolymers in different buffer solutions (c = 2 g/L) at A) pH 8, B) pH 9 and C) pH 10 (ABCBA-11 (◆), ABCBA-25 (●) and ABCBA-43 (★)); the dashed line indicates the T_{tr} of the PDMAEMA block in ABA-90 at the respective pH.

The determined transition points for the PDEGMA blocks showed a strong dependence on the molecular weight in the investigated molecular weight range (2000 – 8000 g/mol) (Figure 4A). This trend could further be confirmed by applying the Flory-Huggins equation for linear polymers (Eq. 1), again showing that all transition points lie on a straight line (Figure 4B). Consequently, polymers with short PDEGMA blocks show significantly higher transition temperatures than their high molecular weight counterparts. Hence, the typical transition temperature found in literature (T_{tr} = 26 °C) is only accurate for PDEGMA block lengths of more than 50 repeating units. Another reason for the elevated transition temperatures for the short PDEGMA blocks may be the influence of the long hydrophilic PEO and PDMAEMA blocks of the ABCBA pentablock terpolymers. Such an effect, for instance, has been already observed for the thermosensitive poly(glycidyl methyl ether-*co*-ethyl glycidyl ether) P(GME-*co*-EGE), which was included in a P2VP-*b*-PEO-*b*-P(GME-*co*-EGE) triblock terpolymer.[20] A decrease of the transition temperature for higher PDEGMA block lengths might then be

explained by the increase of the molar fraction of DEGMA units resulting in a diminished effect of the hydrophilic segments.

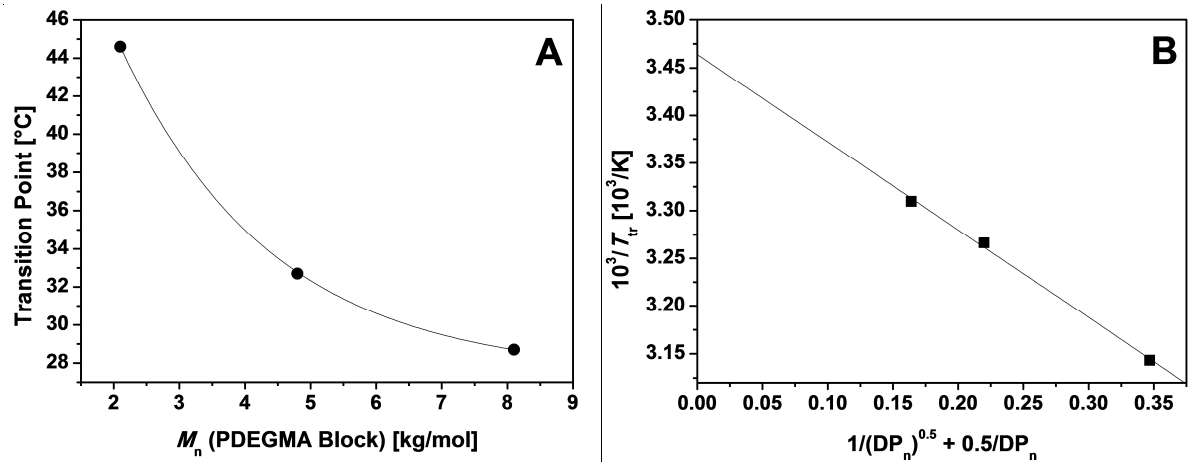

Figure 4. A) Dependence of the phase transitions of ABCBA pentablock terpolymers on PDEGMA block length, determined *via* DLS (pH = 8, c = 2 g/L, θ = 90°). B) Plot of inverse transition points according to the Flory-Huggins theory (Eq. 1), calculated using the number-average degree of polymerization DP_n of the PDEGMA blocks.

Since the phase transitions of the PDMAEMA and PDEGMA blocks start to merge for pH ≥ 9, the second transition of the PDMAEMA blocks can be only clearly determined for the samples at pH = 8 (Figure 3A). At this pH both ABCBA-25 as well as ABCBA-43 reveal a sharp phase transition of the PDEGMA, as indicated by the strong increase of the count rate, at 33 °C and 29 °C, respectively. The count rate levels then off into a plateau before at 55 °C the phase transition of the PDMAEMA block causes a second significant increase of the count rate. This behavior can be explained by the micelle formation initiated by the collapsing PDEGMA block, which results in an initial increase of the count rate. The second transition attributable to the collapse of the PDMAEMA block should result in a shrinkage of the micelles (Scheme 1) and thus in a decreasing count rate. However, a significant increase of the count rate was observed, which indicates higher aggregation numbers of the micelles for temperatures above T_{tr}(PDMAEMA). Due to only slight changes in the count rate caused by the PDEGMA phase transition of ABCBA-11 (T_{tr} = 45 °C) at pH = 8 the second phase transition of the PDMAEMA at 55 °C showed a significantly more pronounced impact on the count rate (Figure 3A). Notably, the considerably higher PDEGMA transition temperature leads to an overlap with the transition points of the PDMAEMA B-blocks at a pH ≥ 9 (Figure 3B, C, Table 1) and, thus, a further separation of the two different phase transitions is impossible for ABCBA-11.

Hydrogel formation of ABA block copolymers. At sufficiently high concentrations of the PDMAEMA-*b*-PEO-*b*-PDMAEMA triblock copolymers, *i.e.*, above the critical gelation concentration (cgc), a reversible gelation is expected due to the PDMAEMA blocks becoming insoluble upon heating above their respective phase transition temperature (T_{tr}). Here, the physical crosslinking points are formed by the collapsed PDMAEMA blocks, which are connected by the water-soluble PEO middle block.

First, the gelation behavior of 10 wt% solutions of the ABA triblock copolymers at pH ≈ 9 were investigated *via* a tube inversion test (Table 1). The results indicate that a block length of the PDMAEMA block above about 90 repeating units (molar fraction of DMAEMA units $f_{DMAEMA} > 0.19$) is required to form freestanding hydrogels. Thus, a certain chain length, which corresponds to a certain molar fraction of the thermo-responsive DMAEMA units in the copolymer, has to be reached before the chain ends are able to form stable network junctions after PDMAEMA insolubilization. Previous studies of Peng *et al.* found a similar behavior for a $PDMAEMA_{35}$-*b*-PEO_{90}-*b*-$PDMAEMA_{35}$ triblock copolymer with considerably smaller PDMAEMA block lengths.[53] In this case, gel formation only occurred under a combination of comparatively harsh conditions, namely, at a concentration of 25 wt%, pH 14, and temperatures of 80 °C.

Another possible mechanism of gel formation is based on a close packing of micelles, which occurs with AB diblock copolymers. Thus, this mechanism might be active in the case that an insufficient blocking in the ABA triblock copolymer synthesis takes place, resulting in a significant amount of AB diblock copolymer. A hydrogel formed by close packing of AB diblock copolymer micelles is unstable and will dissolve upon dilution. However, a hydrogel formed by open association of an ABA triblock copolymer will be stable. Consequently, we tested the stability of ABA-255 based hydrogels against dilution (Figure S7). This particular triblock copolymer was chosen because it bears the longest PDMAEMA blocks and exhibits the highest PDI, arising from a considerable amount of homopolymer impurities due to transfer reactions during the polymerization (*vide supra*). For this purpose, a 20 wt% solution of ABA-255 (pH ≈ 8.7, $T_{SG} \approx 34$ °C) was heated above the gelation temperature and an excess amount of preheated water ($T \approx 45$ °C) was added and equilibrated for 30 minutes at 45 °C. The tube inversion test clearly shows that the hydrogel is stable against dilution and, thus, proves a sufficient bifunctionality of the ABA triblock copolymers.

Since ABA-70 does not form hydrogels even at concentrations above 10 wt% and ABA-255 exhibits a rather high PDI caused by transfer reactions, only the rheological properties of

hydrogels based on ABA-90 and ABA-188 were investigated in detail. Due to the high transition temperatures of PDMAEMA at pH 8 ($T_{tr} \geq 50$ °C, Table 1) the investigated pH range was limited to pH 9 and 10. All samples were prepared by dissolving the polymer at the desired concentration (10 and 20 wt%) in deionized water and equilibrated at 3 °C for 1-2 days until a clear solution was obtained followed by a subsequent adjustment of the pH. For the rheological studies an oscillatory stress was applied to the sample using a cone-and-plate shear cell geometry. Regimes where the storage modulus (G') exceeds the loss modulus (G'') are referred to as gel state with respect to the common definitions and $G' \geq 1$ kPa is taken as a characteristic value for strong freestanding gels.[54-56] Accordingly, $G' < G''$ is defined as sol state. The temperature at which the G' and G'' traces intersect upon heating is taken as the sol-gel transition temperature (T_{SG}).

Figure 5A shows the temperature-dependent storage and loss modulus for a 20 wt% solution of ABA-90 at pH = 9. At room temperature G'' exceeds G' and, thus, the solution is in the sol state. Upon increasing temperature the moduli increase slightly with a pronounced increase of G'' close to the transition temperature of the PDMAEMA blocks of T_{tr} = 42 °C (Table 1), going along with an increase in viscosity. However, the solution is still in the sol state and does not form a hydrogel. Only at about 80 °C, *i.e.*, under conditions where the PEO block already starts to loose some of the bound water,[57, 58] G' crosses G'' and a very weak gel is formed. Consequently, even at a concentration of 20 wt% the ABA-90 triblock copolymer does not form stable freestanding gels at pH = 9, probably due to the low fraction of DMAEMA units (f_{DMAEMA} = 0.19) resulting in an insufficient amount of stable network junctions.

In contrast, ABA-188 forms stable hydrogels at pH 9 and concentrations of 10 and 20 wt% (Figure 5B). Here, both G' and G'' show a strong increase upon approaching the phase transition temperature of the PDMAEMA block (T_{tr} = 39 °C) and the sol-gel transition, *i.e.*, the crossover of the G' and G'' traces, occurs already at 59 °C and 45 °C for the 10 and 20 wt% sample (Table 3), respectively. The sol-gel transition is shifted to lower temperatures and the gel strength, characterized by the plateau modulus at 75 °C ($G'_{plateau}$, Table 3) increases with increasing concentration of the solution. This can be attributed to the higher concentration resulting in an increased concentration of physical crosslinking sites.

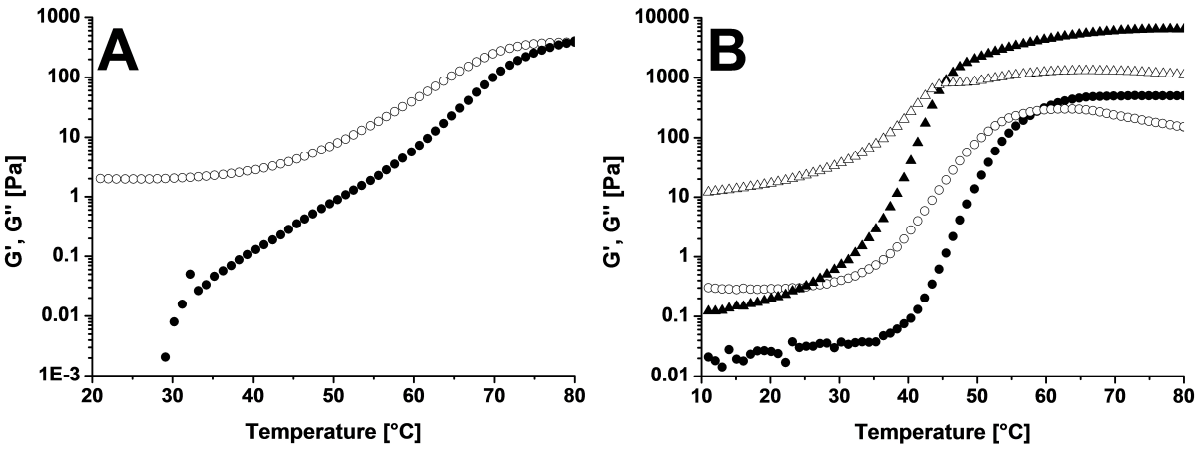

Figure 5. Temperature-dependent storage and loss moduli for A) a 20 wt% solution of ABA-90 at pH = 9 (*G*' (●), *G*'' (○)) and B) for ABA-188 at pH 9 and a concentration of 10 wt% (*G*' (●), *G*'' (○)) and 20 wt% (*G*' (▲), *G*'' (△)), respectively.

Results from all rheology measurements are summarized in Table 3. The corresponding graphs of the temperature-dependent storage and loss moduli (*G*', *G*'') can be found in Figures 5, 6 for the ABA triblock copolymers. The results reveal that the molar fraction of DMAEMA units (f_{DMAEMA}) plays a crucial role for the ABA hydrogel formation. ABA-90 exhibits a f_{DMAEMA} of 0.19, which is close to the limit for forming gels under suitable conditions. A doubling of the block length, however, results in significant higher gel strengths by simultaneously reducing the sol-gel transition temperature T_{SG}.

Table 3. Gelation behavior of ABA and ABCBA copolymers.

ABA Triblock Copolymer				
Sample	f_{DMAEMA}[a]	pH[b]	T_{SG} [°C][c]	$G'_{Plateau}$ [kPa][d]
10 wt%				
ABA-90	0.19	9.0	-	-
ABA-90	0.19	10.2	73	0.11
ABA-188	0.33	9.1	59	0.49
ABA-188	0.33	9.8	54	0.96
20 wt%				
ABA-90	0.19	9.0	79	0.40[e]
ABA-90	0.19	10.1	58	2.5
ABA-188	0.33	9.3	45	6.4
ABA-188	0.33	10.0	46	6.9
ABCBA Pentablock Terpolymer				
Sample	f_{DEGMA}[f]	pH[b]	T_{SG} [°C][c]	$G'_{Plateau}$ [kPa][d]
10 wt%				
ABCBA-25	0.05	9.8	63	0.17
20 wt%				
ABCBA-25	0.05	9.8	50	2.8
ABCBA-43	0.08	10.1	51	2.3

a) Molar fraction of DMAEMA units. b) pH of the solution applied for rheology measurements. c) Sol-gel transition temperature, defined as the crossover of G' and G''. d) Value of G' in the plateau region taken at 75 °C, which is taken as a measure of the gel strength. e) Value of G' at 80°C since the plateau could not be reached within the investigated temperature range. f) Molar fraction of DEGMA units.

Figure 6 shows that at a pH of 10 both triblock copolymers, ABA-90 and ABA-188, form hydrogels at concentrations of 10 and 20 wt%. The most prominent change in the gelation behavior occurs for ABA-90 (Figure 6A). Here, already the 10 wt% solution of ABA-90 is able to form hydrogels, which did not form hydrogels at pH = 9. However, the sol-gel transition temperature is still comparably high and only a very soft hydrogel ($G'_{plateau}$ = 0.11 kPa) is formed. For the 20 wt% sample T_{SG} shifts significantly by about 20 °C to lower temperatures compared to the sample at pH 9 and the formed hydrogel exhibits a considerably higher gel strength ($G'_{plateau}$ = 2.5 kPa at pH 10, compared to $G'_{plateau}$ = 0.40 kPa at pH 9, which represents the value for G' at 80 °C since no plateau is reached within the investigated temperature range). Concerning the gelation behavior of ABA-188 solutions at pH = 10 a decrease of the sol-gel transition temperature was observed for the 10 wt% solution, whereas for 20 wt% T_{SG} does not change significantly (Figure 6B, Table 3). For both concentrations (10 and 20 wt%) an increase in gel strength was detected with respect to the hydrogels formed at pH = 9. This might be attributed to the PDMAEMA block being more hydrophobic at high

pH, which strengthens the hydrophobic interactions upon collapse of the PDMAEMA blocks resulting in stronger crosslinking points.

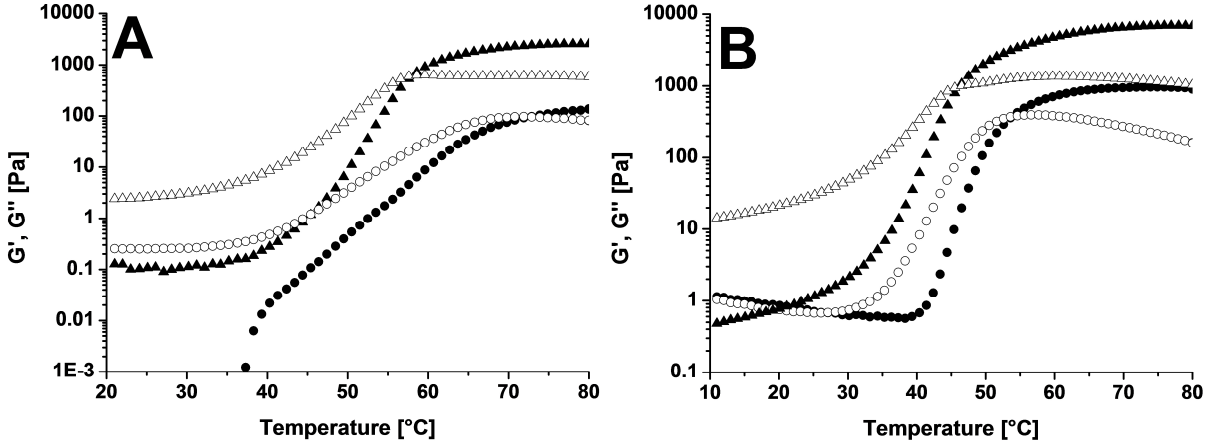

Figure 6. Temperature-dependent storage and loss moduli for A) ABA-90 at pH 10 and a concentration of 10 wt% (*G*' (●), *G*'' (○)) and 20 wt% (*G*' (▲), *G*'' (△)), respectively and B) for ABA-188 at pH 10 and a concentrion of 10 wt% (*G*' (●), *G*'' (○)) and 20 wt% (*G*' (▲), *G*'' (△)), respectively.

In general, ABA-188 solutions (f_{DMAEMA} = 0.33) exhibit lower sol-gel transition temperatures and higher gel strengths compared to ABA-90 (f_{DMAEMA} = 0.19) at comparable pH and concentration. Furthermore, for ABA-90 freestanding gels ($G' \geq 1$ kPa) could only be achieved for pH = 10 and the highest concentration studied (20 wt%). Consequently, the molar fraction of DMAEMA units (f_{DMAEMA}) plays a decisive role in the gelation behavior of PDMAEMA-*b*-PEO-*b*-PDMAEMA triblock copolymers, which is consistent with the results obtained by tube inversion tests.

The phase transition of the PDMAEMA block was further investigated by µDSC (Figure 7). Here, the desolvation of the PDMAEMA blocks in ABA-90 leads to a broad endothermic transition, which is similar to studies about PDMAEMA containing $(AB)_x$ hydrogels by Schmalz *et al.*[35] The onset of the PDMAEMA phase transition revealed by µDSC at pH 10 is in good agreement with the T_{tr}(PDMAEMA) determined from DLS measurements. The sol-gel transition, however, overlaps perfectly with the minimum of the endothermic phase transition in the corresponding µDSC heating trace.

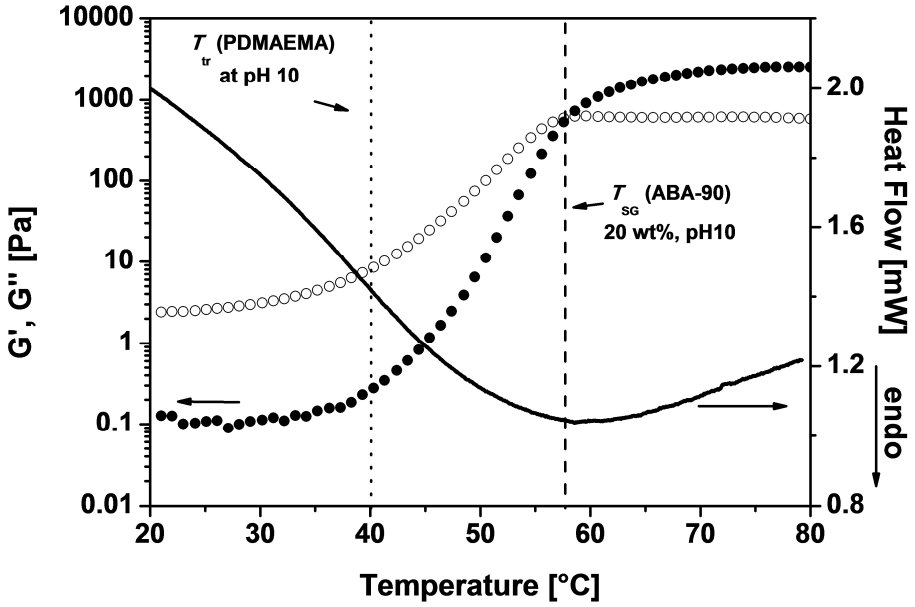

Figure 7. Temperature-dependent storage and loss moduli for a 20 wt% solution of ABA-90 at pH = 10 (G' (●), G'' (○)) and the corresponding μDSC heating trace recorded at a scanning rate of 0.5 K/min (solid trace).

Hydrogel formation of ABCBA pentablock terpolymers. Since ABA-90 only forms considerably strong hydrogels at pH = 10 we studied the gelation behavior of the corresponding ABCBA pentablock terpolymers at pH 10, too. At this pH the outer PDEGMA blocks of the PDEGMA-*b*-PDMAEMA-*b*-PEO-*b*-PDMAEMA-*b*-PDEGMA pentablock terpolymers with a molar fraction of DEGMA units of $f_{DEGMA} > 0.02$ should collapse first upon heating due to the lower phase transition temperature with respect to that of the PDMAEMA blocks (Tables 1, 2; Scheme 1). The 10 and 20 wt% solutions of ABCBA-25 show a similar rheological behavior except that the sol-gel transition temperatures are reduced by 8-10 °C and the gel strength ($G'_{plateau}$) is slightly increased compared to the ABA-90 precursor (Figure 8, Table 3). Due to the significantly lower phase transition of the PDEGMA block (T_{tr} = 29 – 33 °C) in dilute solution compared to PDMAEMA (T_{tr} = 40 °C) the sol-gel transition was expected to occur at even lower temperatures around T_{tr}(PDEGMA). This in turn would have caused a gelation at low temperatures initiated by the collapsing PDEGMA A-blocks followed by a clearly separated phase transition of the PDMAEMA B-blocks at higher temperatures as depicted in Scheme 1. As a result, the hydrogel network would undergo a contraction as soon as the PDMAEMA blocks become water-insoluble leading to a significant change in the mechanical properties (probably softening) of the gel. Instead of that proposed gelation behavior, however, only a pronounced increase of the dynamic moduli was observed around T_{tr}(PDEGMA) and G' could exceed G'' only at elevated temperatures when

the PDMAEMA blocks start to desolvate leading to an overlap of the two phase transitions. The reason for this gelation behavior of ABCBA-25 may be attributed to the low molar fraction of DEGMA units (f_{DEGMA} = 0.05), *i.e.*, the collapse of the PDEGMA blocks is not sufficient to form stable hydrogel junctions by its own and gelation occurs only at the point, where the PDMAEMA block is already considerably destabilized.

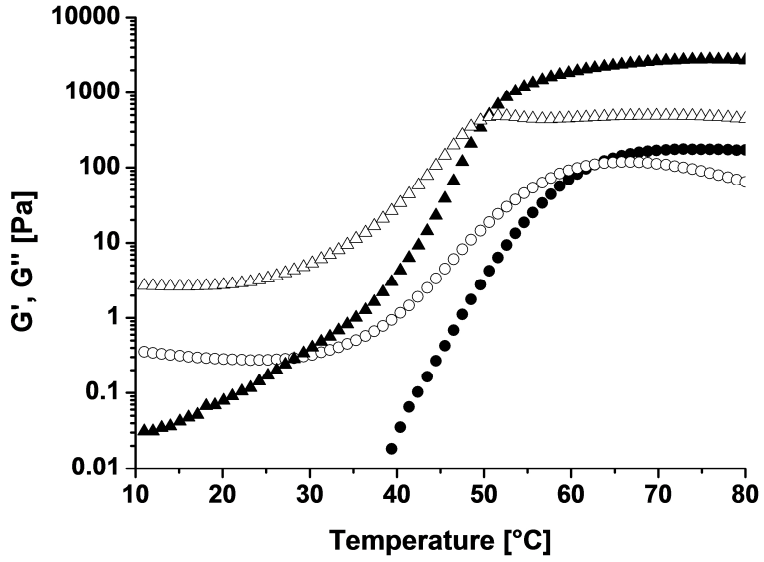

Figure 8. Temperature-dependent storage and loss moduli for ABCBA-25 at pH 10 and a concentration of 10 wt% (*G*' (●), *G*'' (○)) and 20 wt% (*G*' (▲), *G*'' (△)), respectively.

The specific data from the ABCBA rheology measurements, which correspond to Figure 8 and 9, can be found in Table 3. These results reveal that already small molar fractions of PDEGMA units (f_{DEGMA}) ≤ 0.08 of the ABCBA hydrogels lead to a considerable decrease of T_{SG} in comparison to its primary ABA-90 intermediate structure. Notably, no significant influence on the gel strengths could be observed.

ABCBA-43 was then investigated in order to verify whether two clearly separated phase transition of the A- and B-blocks can be detected as the fraction of DEGMA units (f_{DEGMA} = 0.08) is almost doubled. The higher PDEGMA block length, however, brings no further improvement to this system and the sol-gel transition temperature as well as the mechanical properties of the gel remain nearly constant (Table 3, Figure 9). For this reason, the ABCBA-25 and ABCBA-43 pentablock terpolymers were further studied *via* µDSC in order to show that the two phase transitions can be triggered separately as indicated by the DLS experiments on dilute solutions. In consistency with the µDSC results for the ABA-90 triblock copolymer precursor (Figure 7), a broad phase transition for the PDMAEMA blocks was observed for

ABCBA-43 (Figure 9). A second transition occurred, however, at lower temperatures of about 30 °C, which corresponds to the phase transition temperature of the PDEGMA block (T_{tr} = 29 °C at pH 10, Table 2). A similar transition was observed for ABCBA-25, which shows a significant weaker transition for the PDEGMA block in comparison to ABCBA-43 due to the lower molar fraction of DEGMA units (Figure S8). The broad and indistinct phase transition of PDMAEMA leads to a partial overlap with the phase transition of PDEGMA. Notably, the temperature of the phase transition of PDEGMA by µDSC is in good agreement with the phase transition determined *via* DLS.

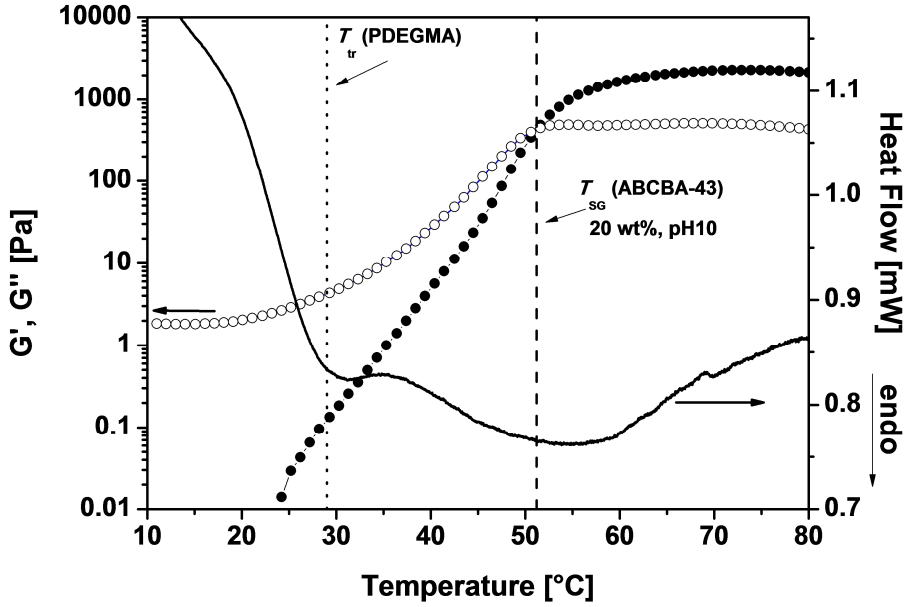

Figure 9. Temperature-dependent storage and loss moduli for a 20 wt% solution of ABCBA-43 at pH = 10 (G' (●), G'' (○)) and the corresponding µDSC heating trace recorded at a scanning rate of 0.5 K/min (solid trace).

This leads to the conclusion that the low molar fractions of DEGMA units of ABCBA-25 and ABCBA-43 (f_{DEGMA}(ABCBA-25) = 0.05 and f_{DEGMA}(ABCBA-43) = 0.08) have no sufficient impact on the gelation behavior, besides the fact that the phase transitions of both PDEGMA and PDMAEMA can be triggered independently as revealed by DLS and µDSC. After passing the crossover of G' and G'' both samples reach a plateau without showing any further changes in the mechanical properties over the whole remaining temperature range up to 80 °C. We assume that this might be attributed to the long PEO block being able to compensate for the collapse of the PDMAEMA blocks, which prevents an expected reduction of the plateau modulus at the phase transition temperature of PDMAEMA. Here, even longer block lengths of the PDEGMA blocks would have been the key for a clear separation of the two phase

transitions in rheology, which, however, was limited due to the synthetic complications in achieving high degrees of polymerization. This strong dependence on f_{DEGMA} is consistent with recent findings from Schmalz *et al.*[35] The investigated (PDMAEMA-*b*-PDEGMA)$_x$ hydrogels in this study revealed a sol-gel transition at low temperatures caused by the PDEGMA block only for relatively high f_{DEGMA} and in addition, an influence on the mechanical properties could be only observed for weak gels.

5.5. Conclusions

Dual-responsive PDEGMA-*b*-PDMAEMA-*b*-PEO-*b*-PDMAEMA-*b*-PDEGMA (ABCBA) pentablock terpolymers were successfully synthesized *via* sequential atom transfer radical polymerization (ATRP) utilizing a bifunctional PEO macroinitiator. The self-assembly behavior of the intermediate PDMAEMA-*b*-PEO-*b*-PDMAEMA (ABA) triblock copolymers and the ABCBA pentablock terpolymers in dilute solutions strongly depends on the block lengths. All these systems were shown to form flower-like micelles upon heating caused by the collapsing outer A-blocks. Thus, the ABA triblock copolymers are stabilized by looped PEO middle blocks and the ABCBA pentablock terpolymers by looped PDMAEMA-*b*-PEO-*b*-PDMAEMA (BCB) segments, respectively. Furthermore, the ABCBA pentablock terpolymers revealed a second phase transition at higher temperatures caused by the collapse of the PDMAEMA blocks in the corona of the corresponding flower-like micelles. Interestingly, the long hydrophilic PEO middle block does not have a significant impact on the transition temperatures of the PDMAEMA blocks, which are in good agreement with literature values. Furthermore, the PDEGMA A-blocks of the pentablock terpolymers reveal a significant lower phase transition at any investigated pH as compared to the corresponding PDMAEMA blocks for molar fractions of DEGMA units (f_{DEGMA}) > 0.02. This results in two distinct phase transitions upon heating for the ABCBA systems.

In addition, these systems were shown to form hydrogels at sufficiently high concentrations. A minimum molar fraction of DMAEMA units (f_{DMAEMA}) of 0.19 in the ABA triblock copolymers is necessary to form strong freestanding gels. The sol-gel transition temperature (T_{SG}) decreases significantly with increasing concentration and the gel strength increases. Similar effects were observed by increasing the pH from 9 to 10 which can be attributed to the pH-dependence of the PDMAEMA phase transition. Further introduction of short thermo-responsive PDEGMA outer blocks, which are switchable at lower temperatures than the PDMAEMA B-blocks, could reduce the sol-gel transition of the ABCBA pentablock

terpolymers by 8-10 °C while simultaneously slightly increasing the gel strength at a given concentration. Since both phase transitions can be independently triggered, as shown by DLS and μDSC measurements, we expected the gelation of the system at the phase transition of the PDEGMA blocks (T_{tr}(PDEGMA) in dilute solution followed by a softening of the hydrogel caused by the second contraction of the PDMAEMA. However, a significant change of the mechanical properties of the hydrogel could not be observed, perhaps due to the long PEO middle block, which may compensate for the second collapse of the PDMAEMA. Consequently, an increase of the DEGMA weight fractions might be necessary to shift the sol-gel transitions of the ABCBA hydrogels to lower temperatures close to T_{tr}(PDEGMA) and, in addition, to realize two clearly separated phase transitions with a sufficient impact on the mechanical properties of the hydrogel at the point where PDMAEMA starts to collapse.

Despite potential applications in stimuli-responsive hydrogels the ABCBA pentablock terpolymer might be interesting as a smart gene vector for gene delivery. Recent studies showed PDMAEMA-based micelles as effective gene vector.[59, 60] The ABCBA pentablock terpolymers form flower-like core-shell-corona micelles with a collapsed PDEGMA core, a cationic PDMAEMA shell and a PEO corona at temperatures slightly above room temperature. Thus, the cationic PDMAEMA shell of the micelles might be utilized to form polyplexes with pDNA at physiological conditions while the biocompatible PEO corona provides sufficient shielding of the polyplex.

Acknowledgments: The authors would like to thank N. Aksel and H. Lutz (Applied Mechanics and Fluid Dynamics, University of Bayreuth) as well as R. Richter (Experimental Physics V, University of Bayreuth) for access to the rheometer. We thank M. Böhm for SEC measurements and M. Krekhova for helpful discussions on the rheology experiments.

5.6. References

(1) Ahn, S.-K.; Kasi, R. M.; Kim, S.-C.; Sharma, N.; Zhou, Y. *Soft Matter* **2008**, *4*, 1151-1157.

(2) Tsitsilianis, C. *Soft Matter* **2010**, *6*, 2372-2388.

(3) Seliktar, D. *Science* **2012**, *336*, 1124-1128.

(4) Bermudez, J. M.; Quinteros, D.; Grau, R.; Allemandi, D.; Palma, S. *Drug Deliv. Lett.* **2011**, *1*, 135-149.

(5) Samchenko, Y.; Ulberg, Z.; Korotych, O. *Adv. Colloid Interface Sci.* **2011**, *168*, 247-262.

(6) Van Vlierberghe, S.; Dubruel, P.; Schacht, E. *Biomacromolecules* **2011**, *12*, 1387-1408.

(7) Patel, A.; Mequanint, K., Hydrogel Biomaterials. In *Biomedical Engineering - Frontiers and Challenges*, Fazel, R., Ed. InTech: Rijeka, 2011; pp 275-296.

(8) Choi, B. G.; Sohn, Y. S.; Jeong, B. *J. Phys. Chem. B* **2007**, *111*, 7715-7718.

(9) Chen, C. F.; Lin, C. T. Y.; Chu, I. M. *Polym. Int.* **2010**, *59*, 1428-1435.

(10) Scalfani, V. F.; Bailey, T. S. *Macromolecules* **2011**, *44*, 6557-6567.

(11) Hamley, I. W.; Cheng, G.; Castelletto, V. *Macromol. Biosci.* **2011**, *11*, 1068-1078.

(12) Ma, Y.; Tang, Y.; Billingham, N. C.; Armes, S. P.; Lewis, A. L. *Biomacromolecules* **2003**, *4*, 864-868.

(13) Castelletto, V.; Hamley, I. W.; Ma, Y.; Bories-Azeau, X.; Armes, S. P.; Lewis, A. L. *Langmuir* **2004**, *20*, 4306-4309.

(14) Vermonden, T.; Besseling, N. A. M.; van Steenbergen, M. J.; Hennink, W. E. *Langmuir* **2006**, *22*, 10180-10184.

(15) Fechler, N.; Badi, N.; Schade, K.; Pfeifer, S.; Lutz, J.-F. *Macromolecules* **2009**, *42*, 33-36.

(16) Lin, H.-H.; Cheng, Y.-L. *Macromolecules* **2001**, *34*, 3710-3715.

(17) Zhang, H.; Yan, Q.; Kang, Y.; Zhou, L.; Zhou, H.; Yuan, J.; Wu, S. *Polymer* **2012**, *53*, 3719-3725.

(18) Cao, Z.; Liu, W.; Ye, G.; Zhao, X.; Lin, X.; Gao, P.; Yao, K. *Macromol. Chem. Phys.* **2006**, *207*, 2329-2335.

(19) Li, Y.; Tang, Y.; Narain, R.; Lewis, A. L.; Armes, S. P. *Langmuir* **2005**, *21*, 9946-9954.

(20) Reinicke, S.; Schmelz, J.; Lapp, A.; Karg, M.; Hellweg, T.; Schmalz, H. *Soft Matter* **2009**, *5*, 2648-2657.

(21) Reinicke, S.; Karg, M.; Lapp, A.; Heymann, L.; Hellweg, T.; Schmalz, H. *Macromolecules* **2010**, *43*, 10045-10054.

(22) Angelopoulos, S. A.; Tsitsilianis, C. *Macromol. Chem. Phys.* **2006**, *207*, 2188-2194.

(23) Jeong, B.; Kim, S. W.; Bae, Y. H. *Adv. Drug Delivery Rev.* **2002**, *54*, 37-51.

(24) Schwartz, V. B.; Thétiot, F.; Ritz, S.; Pütz, S.; Choritz, L.; Lappas, A.; Förch, R.; Landfester, K.; Jonas, U. *Adv. Funct. Mater.* **2012**, *22*, 2376-2386.

(25) Cong, H.; Li, L.; Zheng, S. *Polymer* **2013**, *54*, 1370-1380.

(26) Kikuchi, A.; Okano, T. *Prog. Polym. Sci.* **2002**, *27*, 1165-1193.

(27) Reinicke, S.; Schmalz, H. *Colloid Polym. Sci.* **2011**, *289*, 497-512.

(28) Munoz-Bonilla, A.; Fernandez-Garcia, M.; Haddleton, D. M. *Soft Matter* **2007**, *3*, 725-731.

(29) Han, D.; Tong, X.; Boissière, O.; Zhao, Y. *ACS Macro Letters* **2011**, *1*, 57-61.

(30) Lutz, J.-F.; Hoth, A. *Macromolecules* **2005**, *39*, 893-896.

(31) Schmalz, A.; Hanisch, M.; Schmalz, H.; Müller, A. H. E. *Polymer* **2010**, *51*, 1213-1217.

(32) Plamper, F. A.; Schmalz, A.; Müller, A. H. E. *J. Am. Chem. Soc.* **2007**, *129*, 14538-14539.

(33) Plamper, F. A.; Ruppel, M.; Schmalz, A.; Borisov, O.; Ballauff, M.; Müller, A. H. E. *Macromolecules* **2007**, *40*, 8361-8366.

(34) O'Lenick, T. G.; Jin, N.; Woodcock, J. W.; Zhao, B. *J. Phys. Chem. B* **2011**, *115*, 2870-2881.

(35) Schmalz, A.; Schmalz, H.; Müller, A. H. E. *Soft Matter* **2012**, *8*, 9436-9445.

(36) Schmalz, A.; Schmalz, H.; Müller, A. H. E. *Z. Phys. Chem.* **2012**, *226*, 695-709.

(37) Sugihara, S.; Kanaoka, S.; Aoshima, S. *J. Polym. Sci., Part A: Polym. Chem.* **2004**, *42*, 2601-2611.

(38) Li, C.; Buurma, N. J.; Haq, I.; Turner, C.; Armes, S. P.; Castelletto, V.; Hamley, I. W.; Lewis, A. L. *Langmuir* **2005**, *21*, 11026-11033.

(39) Reinicke, S.; Döhler, S.; Tea, S.; Krekhova, M.; Messing, R.; Schmidt, A. M.; Schmalz, H. *Soft Matter* **2010**, *6*, 2760-2773.

(40) Madsen, J.; Armes, S. P. *Soft Matter* **2012**, *8*, 592-605.

(41) Parmar, A.; Parekh, P.; Bahadur, P. *J. Solution Chem.* **2013**, *42*, 80-101.

(42) Nakashima, K.; Bahadur, P. *Adv. Colloid Interface Sci.* **2006**, *123-126*, 75-96.

(43) Determan, M. D.; Cox, J. P.; Seifert, S.; Thiyagarajan, P.; Mallapragada, S. K. *Polymer* **2005**, *46*, 6933-6946.

(44) Mei, A.; Guo, X.; Ding, Y.; Zhang, X.; Xu, J.; Fan, Z.; Du, B. *Macromolecules* **2010**, *43*, 7312-7320.

(45) Choo, E. S. G.; Yu, B.; Xue, J. *J. Colloid Interface Sci.* **2011**, *358*, 462-470.

(46) Shim, W. S.; Yoo, J. S.; Bae, Y. H.; Lee, D. S. *Biomacromolecules* **2005**, *6*, 2930-2934.

(47) Shim, W. S.; Kim, S. W.; Lee, D. S. *Biomacromolecules* **2006**, *7*, 1935-1941.

(48) Huynh, D. P.; Shim, W. S.; Kim, J. H.; Lee, D. S. *Polymer* **2006**, *47*, 7918-7926.

(49) Tsitsilianis, C.; Stavrouli, N.; Bocharova, V.; Angelopoulos, S.; Kiriy, A.; Katsampas, I.; Stamm, M. *Polymer* **2008**, *49*, 2996-3006.

(50) Ren, T.; Lei, X.; Yuan, W. *Mater. Lett.* **2012**, *67*, 383-386.

(51) Plamper, F. A.; Becker, H.; Lanzendörfer, M.; Patel, M.; Wittemann, A.; Ballauff, M.; Müller, A. H. E. *Macromol. Chem. Phys.* **2005**, *206*, 1813-1825.

(52) Shultz, A. R.; Flory, P. J. *J. Am. Chem. Soc.* **1952**, *74*, 4760-4767.

(53) Peng, Z.; Li, G.; Liu, X.; Tong, Z. *J. Polym. Sci., Part A: Polym. Chem.* **2008**, *46*, 5869-5878.

(54) Nishinari, K. *Prog. Colloid Polym. Sci.* **2009**, *136*, 87-94.

(55) Winter, H. H.; Mours, M. *Adv. Polym. Sci.* **1997**, *134*, 165-234.

(56) Chambon, F.; Winter, H. H. *Polym. Bull.* **1985**, *13*, 499-503.

(57) Castelletto, V.; Hamley, I. W.; English, R. J.; Mingvanish, W. *Langmuir* **2003**, *19*, 3229-3235.

(58) Li, H.; Yu, G.-E.; Price, C.; Booth, C.; Hecht, E.; Hoffmann, H. *Macromolecules* **1997**, *30*, 1347-1354.

(59) Schallon, A.; Synatschke, C. V.; Jérôme, V.; Müller, A. H. E.; Freitag, R. *Biomacromolecules* **2012**, *13*, 3463-3474.

(60) Gary, D. J.; Lee, H.; Sharma, R.; Lee, J.-S.; Kim, Y.; Cui, Z. Y.; Jia, D.; Bowman, V. D.; Chipman, P. R.; Wan, L.; Zou, Y.; Mao, G.; Park, K.; Herbert, B.-S.; Konieczny, S. F.; Won, Y.-Y. *ACS Nano* **2011**, *5*, 3493-3505.

5.7. Supporting Information

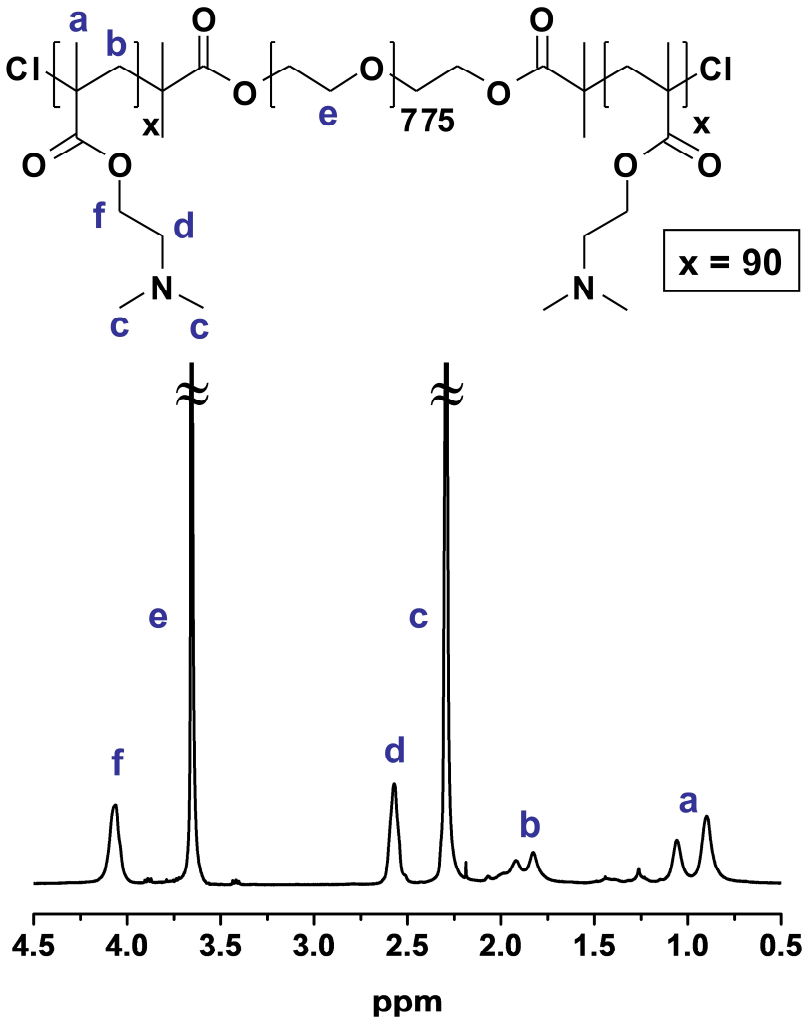

Figure S1. ^{1}H-NMR spectrum of ABA-90 in $CDCl_3$.

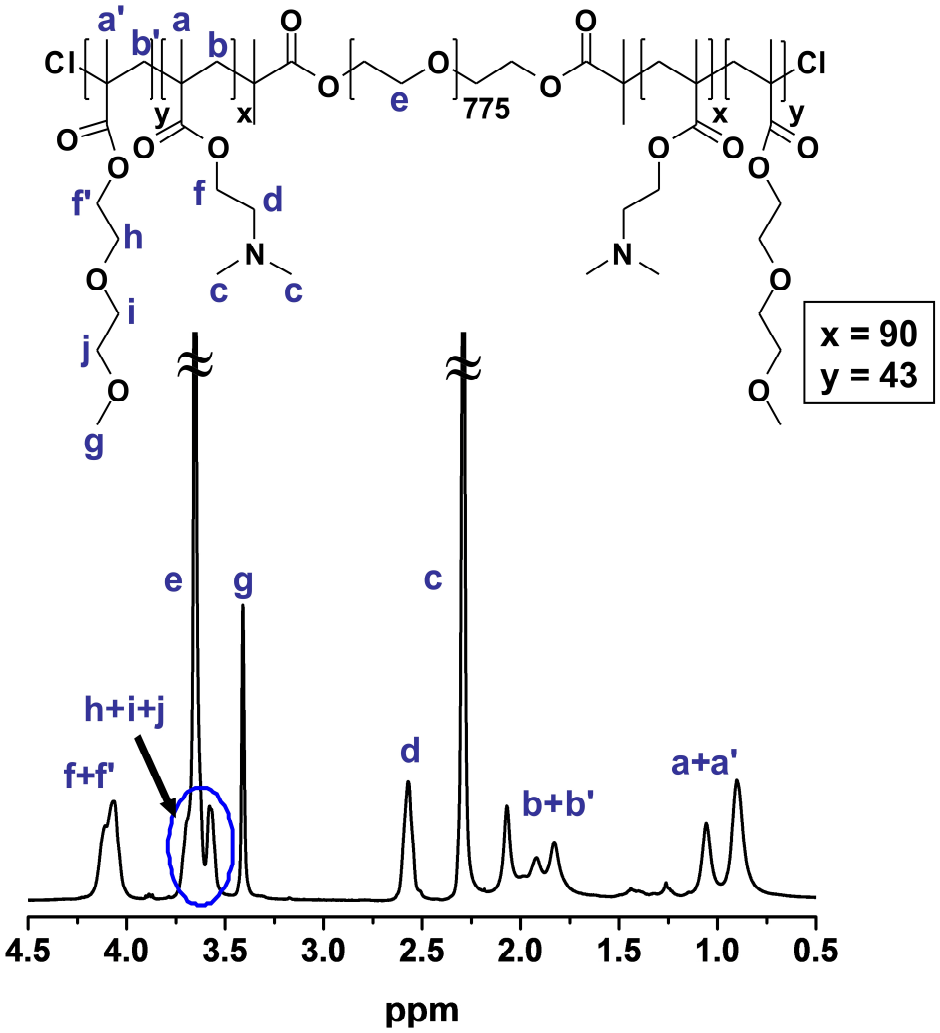

Figure S2. ^{1}H-NMR spectrum of ABCBA-43 in $CDCl_3$.

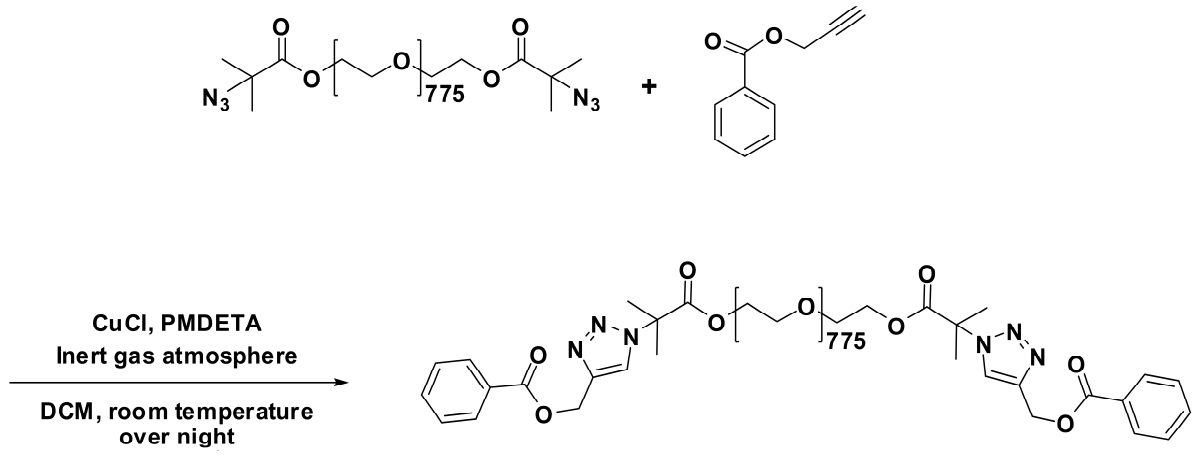

Figure S3. Synthesis of UV-labeled PEO *via* azide-alkyne Huisgen cycloaddition ("click-reaction").

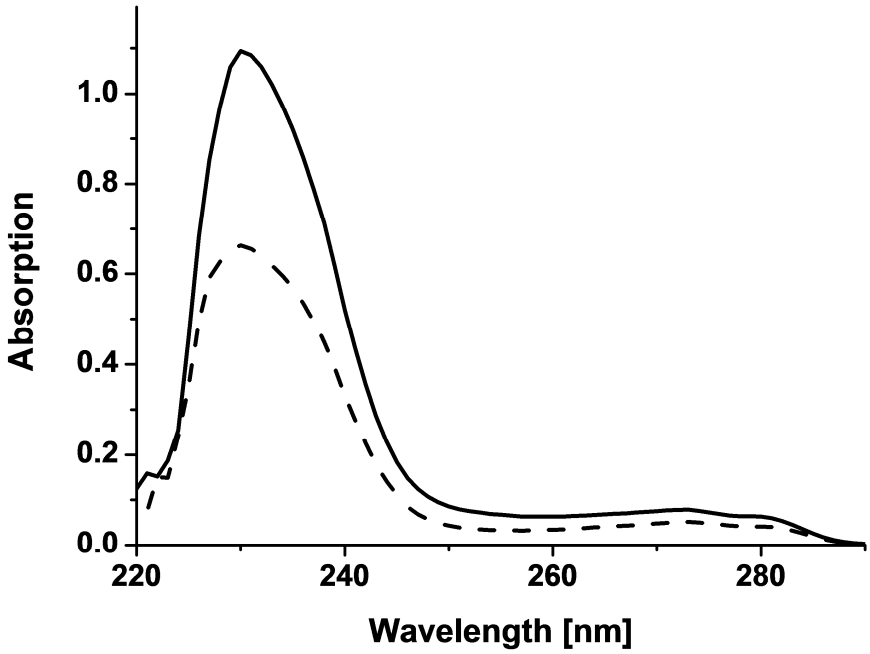

Figure S4. UV/Vis spectra of 2-proynyl benzoate (dashed line) and the UV-labeled PEO (solid line) dissolved in chloroform at $1 \cdot 10^{-4}$ mol/L.

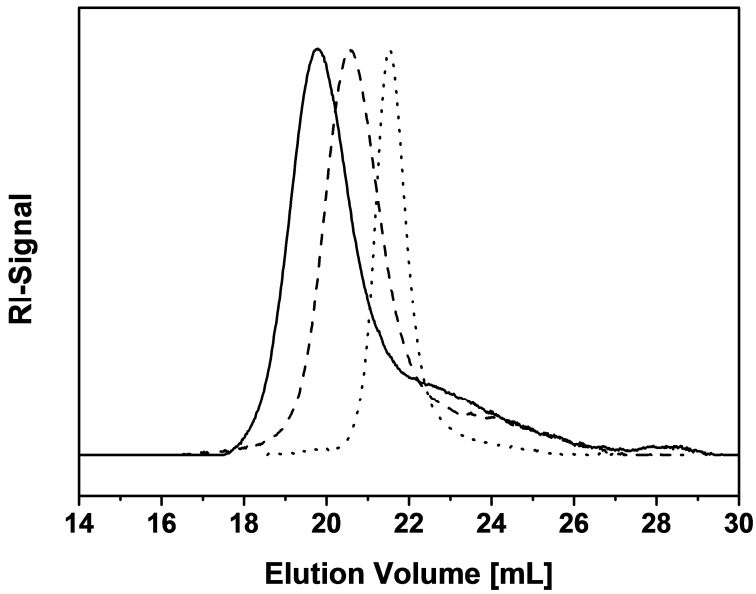

Figure S5. DMAc-SEC traces of the PEO-macroinitiator (dotted line), ABA-188 (dashed line) and ABA-255 (solid line).

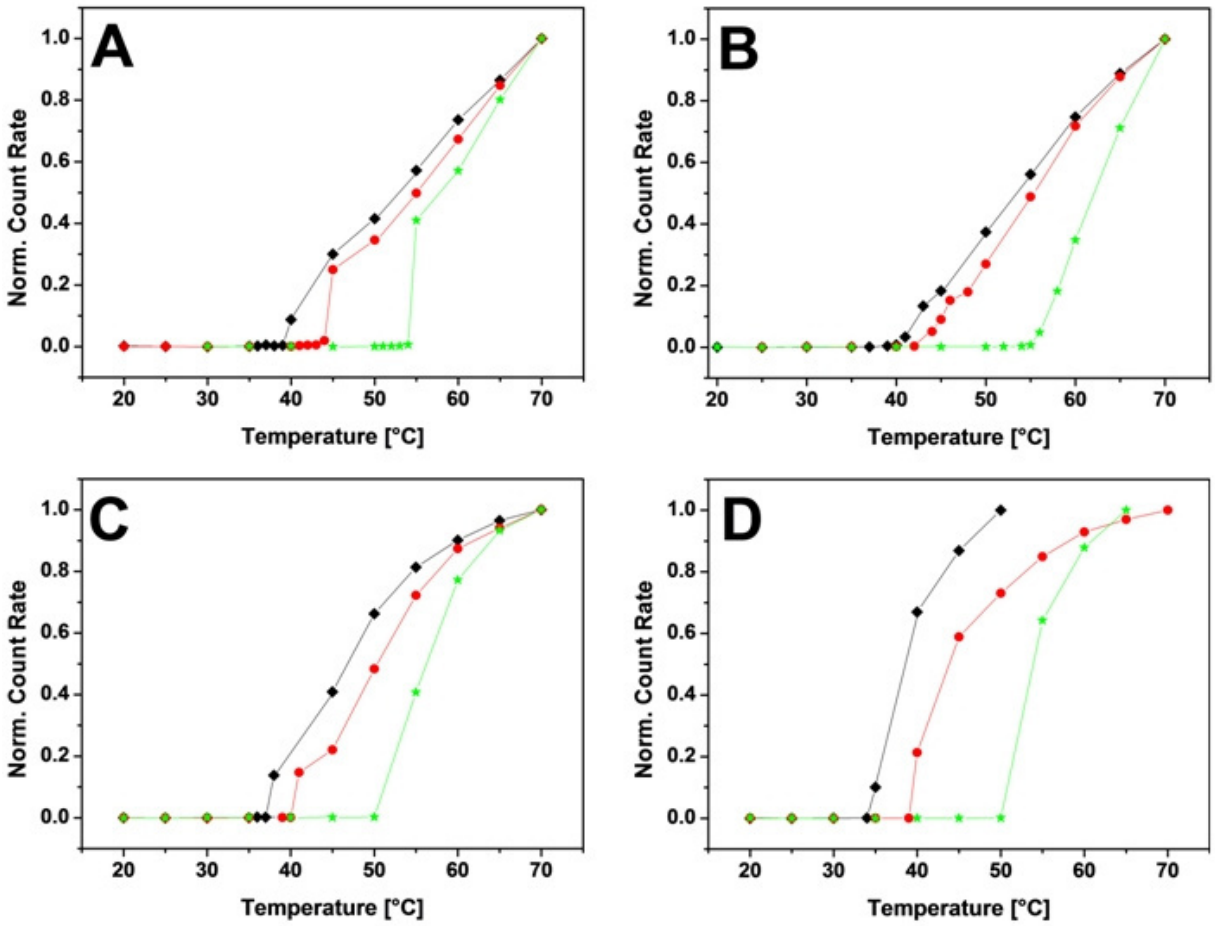

Figure S6. Scattering intensity at θ = 90° in dependence of temperature for ABA block copolymers in different buffer solutions (pH = 8 (★), 9 (●) and 10 (◆); c = 2 g/L) for A) ABA-70, B) ABA-90, C) ABA-188 and D) ABA-255.

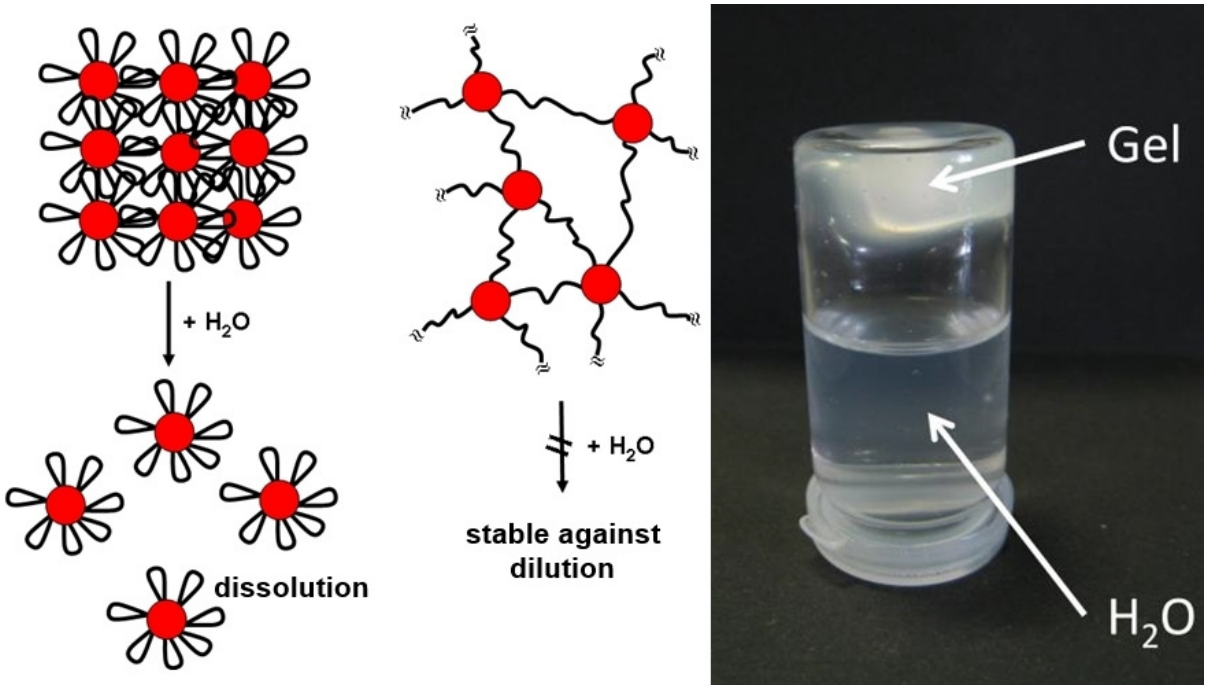

Figure S7. Schematic illustration of a densely packed micellar gel and a physically cross-linked hydrogel upon adding an excess of water (left). The photograph of the hydrogel formed by ABA-255 (20 wt%, pH ≈ 9) at elevated temperatures (gel state) after adding an excess of deionized water shows that the hydrogel is stable against dilution due to physical crosslinks.

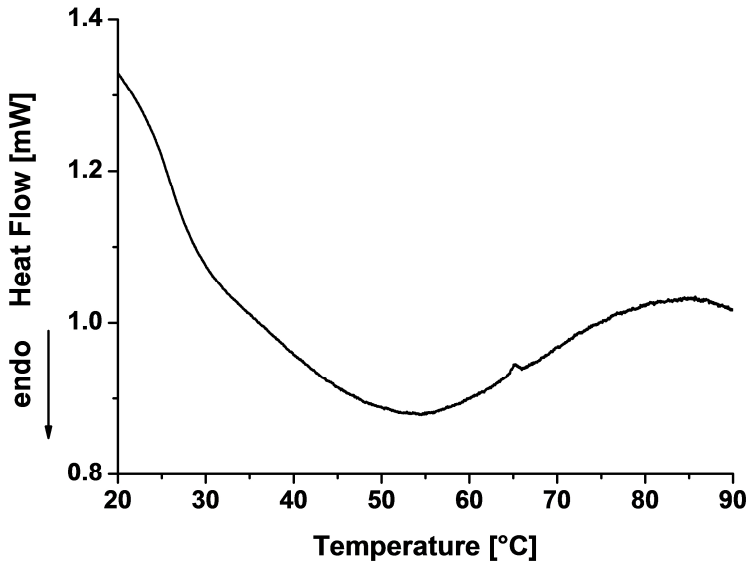

Figure S8. µDSC heating trace of a 20 wt% polymer solution of ABCBA-25 at pH 9.8 recorded at a heating rate of 0.5 K/min.

List of Publications & Patents

Publications

- **Majewski, A.P.**; Borke, T.; Hanisch, A.; Müller, A.H.E.; Schmalz, H. *Double Responsive Pentablock Terpolymers: Self-Assembly and Gelation Behavior*, to be submitted.
- **Majewski, A.P.**; Stahlschmidt, U.; Jérôme, V.; Freitag, R.; Müller, A.H.E.; Schmalz, H. *PDMAEMA Grafted Core-Shell-Corona Particles for Non-Viral Gene Delivery and Magnetic Cell Separation,* submitted to Biomacromolecules.
- **Majewski, A.P.**; Schallon, A.; Jérôme, V.; Freitag, R.; Müller, A.H.E.; Schmalz, H. *Dual-Responsive Magnetic Core-Shell Nanoparticles for Non-Viral Gene Delivery and Cell Separation,* Polym. Prepr. (Am. Chem. Soc., Div. Polym. Chem.) **2012**, 53, 595.
- **Majewski, A.P.**; Schallon, A.; Jérôme, V.; Freitag, R.; Müller, A.H.E.; Schmalz, H. *Dual-Responsive Magnetic Core-Shell Nanoparticles for Non-Viral Gene Delivery and Cell Separation,* Biomacromolecules **2012**, 13, 857.
- Ruhland, T.; Reichstein, P.; **Majewski, A.P.**; Walther, A.; Müller, A.H.E., S*uperparamagnetic and fluorescent thermo-responsive core-shell-corona hybrid nanogels with a protective silica shell*, J. Coll. Interf. Sci. **2012**, 374, 45.
- Pfaff, A.; Schallon, A.; Ruhland, T.; **Majewski, A.P.**; Schmalz, H.; Freitag, R.; Müller, A.H.E., *Magnetic and Fluorescent Glycopolymer Hybrid Nanoparticles for Intranuclear Optical Imaging,* Biomacromolecules **2011**, 12, 3805.
- Müller, A.H.E.; **Majewski, A.P.**; Reinicke, S.; Schmalz, A.; Schmalz, H., *New Block Copolymers, Stars, and Hybrid Particles for Smart Hydrogels,* Polym. Prepr. (Am. Chem. Soc., Div. Polym. Chem.) **2011**, 52, 800.

Patents

- Freitag, R.; Jérôme, V.; Müller, A.H.E.; Schmalz, H.; Schallon, A.; Synatschke, C.V.; **Majewski, A.P.**, *Nonviral Transfection Systems*, WO 2012/156058 A1, **2012**.
- Freitag, R.; Jérôme, V.; Müller, A.H.E.; Schmalz, H.; Schallon, A.; Synatschke, C.V.; **Majewski, A.P.**, *Utilization of Magnetic Nanoparticles as Intracellular Pull-Down System*, WO 2012/156059 A1, **2012**.

Acknowledgments & Danksagung

Zunächst möchte ich mich bei meinem Doktorvater Prof. Dr. A. H. E. Müller für die Aufnahme in die MC² Familie herzlich bedanken. Damit verbunden war eine tolle Betreuung, gekennzeichnet durch viele hilfreiche Tipps und Verbesserungsvorschlägen bei der Ausarbeitung der hier vorgestellten Manuskripte. Bessere Arbeitsbedingungen als hier in der MC² lassen sich schwer vorstellen. Dies schließt nicht nur eine einzigartige tolle Arbeitsatmosphäre mit einer Vielzahl von netten und kreativen Leuten, sondern auch die Möglichkeit sich selbst zu entfalten und eigene Ideen auszuprobieren mit ein. Zudem möchte ich mich für auch für die Organisation meines 6-monatigen Auslandsaufenthalt in Südkorea bedanken, auch wenn dies den Zeitraum kurz vor den Antritt meiner Promotion betrifft. Erwähnenswert sind auch die Besuche der Konferenzen in Freiburg, Schottland, Schweden und USA, in denen mir u.a. die Chance gegeben wurde meine Arbeit einem internationalen Publikum zu präsentieren. Auch hierfür ein herzliches Dankeschön. Alles in allem war es eine unvergessliche Zeit in Bayreuth, welche ich mit Freude in Erinnerung behalten werde.

Ein besonderer Dank geht auch an Dr. Holger Schmalz für die hervorragende Betreuung. Sprich, immer einen guten Ratschlag für jedes x-beliebiges Problem und eine Vielzahl an Verbesserungsvorschlägen für die Manuskripte parat zu haben. Des Weiteren geht auch ein dickes Dankeschön an Alex Schmalz, der mich schon seit Diplomarbeitszeiten in die Geheimnisse der PDMAEMA-Polymerisation eingewiesen und auch mit allen anderen für mich wichtigen Geräten vertraut gemacht hat. Ich möchte mich auch bei meinem anderen Laborpartner - Andreas Hanisch - für die tolle Atmosphäre und Diskussionen über arbeitsrelevante und sonstige Themen während meiner Zeit am Lehrstuhl herzlich bedanken. Und nicht zu vergessen, Thomas Ruhland von der Janus – Nanopartikel Crew, der immer für ein konstruktives Gespräch bei einer Tasse Kaffee zu haben war.

Ein herzliches Dankeschön auch an den Lehrstuhl von Prof. Dr. R. Freitag. In den letzten 3 Jahren konnten wir durch eine harmonisierende Zusammenarbeit mehrere exzellente Ergebnisse erzielen. Dafür möchte ich mich besonders bei Dr. Anja Schallon und Ullrich Stahlschmidt für alles Rund um die Zelltests und bei Dr. Valérie Jérôme und Prof. Dr. R. Freitag für das Schreiben bzw. Korrigieren der biologischen Teile der Manuskripte bedanken.

An dieser Stelle möchte ich mich bei all denjenigen bedanken, die Messungen für mich durchgeführt haben, ohne die ein reibungsloser Ablauf meiner Dissertation nicht möglich gewesen wäre. Bedanken möchte ich mich bei: Melanie Förtsch/Annika Pfaffenberger für

unzählige TEM-Aufnahmen, Marietta Böhm für GPC und AF4 Messungen, Thomas Lunkenbein für XRD Messungen meiner γ-Fe_2O_3 Nanopartikel, Thomas Friedrich für VSM Messungen, Martina Heider für EDX Messungen und Dr. Marina Krekhova für die Unterweisung und Hilfestellungen bei den Rheologiemessungen. Natürlich gilt auch ein herzlicher Dank an Thomas Gegenhuber für seine herausragende Arbeit während seiner Bachelorarbeit und meinen fleißigen Praktikanten: Tina Borke, Jonas Schubert, Christian Stelling und Samuel Shehata. Natürlich möchte ich mich auch bei allen anderen bedanken, welche zu der einzigartigen Atmosphäre in der MC² beigetragen haben. Das wären vor allem: Christopher Synatschke, Tina Löbling, Eva Betthausen, Stephan Weiß, Andrea Wolf, Zhicheng Zheng, Francesca Bennet, Markus Drechsler, Anja Goldmann, André Gröschel, Markus Müllner, André Pfaff, Stefan Reinicke, Fleix Schacher, Joachim Schmelz, Sandrine Tea, Ramón Novoa-Carballal und Lourdes Pastor-Pérez.

Ein ganz besonderer Dank geht an meine Familie, die mein Vorhaben immer unterstützte und immer, egal ob Kleinigkeiten oder größeren Anliegen, mit Rat und Tat beiseite stand. Besonders möchte ich aber meine Frau Songyi und Sohn Aaron hervorheben, bei denen ich mich für die Geduld mit mir, vor allem während der Endphase der Promotion, ganz herzlich bedanke.

Erklärung

Die vorliegende Arbeit wurde von mir selbstständig verfasst und ich habe dabei keine anderen als die angegebenen Hilfsmittel und Quellen benutzt.

Ferner habe ich nicht versucht, anderweitig mit oder ohne Erfolg eine Dissertation einzureichen oder mich einer Doktorprüfung zu unterziehen.

Bayreuth, den 14.06.2013

Alexander P. Majewski